

**SANTA CLARA UNIVERSITY**  
Department of Mechanical Engineering  
Department of Computer Science & Engineering  
Department of General Engineering

I HEREBY RECOMMEND THAT THE THESIS  
PREPARED UNDER MY SUPERVISION BY

Sam Carhart, David Cooper, Luis Gaitan, Michael Kaliterna,  
Sami Lama, Paul Rogel-Herrera, and Yuya Yabe

ENTITLED  
**Heavy Lift Drone**

BE ACCEPTED IN PARTIAL FULFILLMENT OF THE REQUIREMENTS  
FOR THE DEGREES OF  
**BACHELOR OF SCIENCE**  
IN  
**MECHANICAL ENGINEERING, COMPUTER SCIENCE & ENGINEERING, AND**  
**GENERAL ENGINEERING**

---

Dr. Christopher Kitts, Thesis Advisor                      Date

---

Dr. Drazen Fabris, Department Chair Mechanical Engineering                      Date

---

Dr. Mark Godfrey Mungal, Thesis Advisor                      Date

---

Dr. Jessica Kuczenski, Department Chair General Engineering                      Date

---

Dr. Michael Taylor, Thesis Advisor                      Date

---

Dr. Nam Ling, Department Chair Computer Science & Engineering                      Date

# **Heavy Lift Drone**

By

Sam Carhart, David Cooper, Luis Gaitan, Michael Kaliterna,  
Sami Lama, Paul Rogel-Herrera, and Yuya Yabe

## **SENIOR DESIGN PROJECT REPORT**

Submitted to the Department of Mechanical Engineering,  
Computer Science & Engineering, and General Engineering

of

SANTA CLARA UNIVERSITY

in Partial Fulfillment of the Requirements for the  
Degree of Bachelor of Science in  
Mechanical Engineering, Computer Science & Engineering, and General Engineering

Santa Clara, California

2020

# **Heavy Lift Drone**

Sam Carhart, David Cooper, Luis Gaitan, Michael Kaliterna,  
Sami Lama, Paul Rogel-Herrera, and Yuya Yabe

Department of Mechanical Engineering

Department of Computer Science and Engineering

Department of General Engineering

Santa Clara University

Santa Clara, California

2020

## **ABSTRACT**

Despite the rapid rise in the number of drones in the past few years, there has been little work done to produce a drone that is optimized for the FAA's 55 lb upper takeoff limit. This gap in the market is one that the Heavy Lift Drone (HLD) fills - a light-weight, higher payload capability, and inexpensive drone to be used in commercial applications - most notably irrigation monitoring. The HLD is a contra-rotating hexagonal configuration system featuring two levels of propellers that allow for larger propeller diameter and generate greater lift. After performing extensive finite element analyses and material testing, as well as the design, assembly, and flight test of a quadcopter prototype, the equipment, electronics, and components to be used on the final HLD were chosen. The four individual subsystems - mechanical, aerospace, electronics, and software - were each addressed and analyzed separately. It was found that the inclusion of the ducts (shrouds) around the propellers does indeed increase the lift of the drone by a factor of 14.7%. Additionally, the final projected cost for the drone, including labor and volume production, was significantly lower than that of our direct competitors, standing at \$13,921. This is nearly 8.5% lower than the nearest comparable drone available for sale, while also featuring a higher projected payload to weight ratio of 0.5, as opposed to 0.4 for the competition. Finally, the HLD utilized multiple software applications that were implemented for effective flight planning, automated image stitching, and analysis of the IR photos taken during flight operation in order to generate a new flight plan.

## Acknowledgements

Thank you to the Robotic Systems Lab for their endless support throughout the duration of the project. We also want to thank the Maker Lab and Anne Mahacek specifically - without their aid in 3D printing, material cutting, and providing helpful tools, the Heavy Lift Drone would not be in the state we see it today. We'd also like to thank Dr. Marks for his assistance in material testing as it identified what materials we should move forward with early on in the project's progress. Moreover, the support of the Mechanical Engineering department at Santa Clara University is appreciated on many accounts. Furthermore, we wanted to thank our advisers, Dr. Kitts, Dr. Mungal, Dr. Taylor, and Dr. Kuczenski who always provided valuable and constructive guidance and feedback. Additional thanks to Dr. Riccomini and Dr. Restivo who served as the Honors thesis mentor and reader. Lastly, to our families and friends who have supported us during the entirety of the project, the Heavy Lift Drone was realized due to your support!

# Table of Contents

<b>1. Introduction</b>	1
<b>2. Background</b>	3
2.1 - Literature Review	3
2.2 - Drones and their Main Components	4
2.3 - Market Comparison	12
<b>3. Customer Research &amp; System Definition</b>	15
3.1 - Customer Needs	15
3.2 - Product Specifications	17
3.3 - Product Overview	21
<b>4. Concept Selection Analysis</b>	27
4.1 - Arm Design Generation	27
4.2 - Chassis and Full Assembly Design Generation	32
4.3 - Undercarriage Design Generation	38
<b>5. Material and Component Analysis</b>	41
5.1 - Material Screening and Selection	41
5.2 - Motor Selection	47
<b>6. Aerodynamic and Mechanical Analysis</b>	50
6.1 - Operating Conditions for Analysis	50
6.2 - Aerodynamics Subsystem	50
6.3 - Mechanical Subsystem	71
<b>7. Electrical Subsystem</b>	78
7.1 - Propulsion Substructure	78
7.2 - Communication and Control Substructure	82
7.3 - Subsystem Design and Implementation	86

7.4 - Integration, Testing, and Validation	93
<b>8. Software Subsystem</b>	100
8.1 - Generation of the Mow-the-Lawn Flight Plans	100
8.2 - IR Image Analysis	104
<b>9. Hardware</b>	108
9.1 - Budget	108
9.2 - Physical Testing Accomplishments and Documentation	109
9.3 - Completed Hardware	113
<b>10. Professional Issues</b>	118
10.1 - Ethics	118
10.2 - Safety and Legal Framework	118
10.3 - Economics and Sustainability	119
<b>11. Conclusion</b>	121
11.1 - Summary	121
11.2 - Future Work	122
<b>References</b>	125
<b>Appendix</b>	127
A - Airflight Research	127
B - Customer Needs Q&A	130
C - Component Diagrams and Additional Concept Generation	140
D - Design Matrix Tables	182
E - Material Testing Specimen Results	184
F - Additional Solidworks Simulations	187
G - Electrical	189
H - Software	194

## List of Figures

Figure 1: Drones Built for More Commercial-like Applications	4
Figure 2: Examples of Brushless Motors	5
Figure 3: Examples of Propellers	6
Figure 4: Examples of Electronic Speed Controllers	7
Figure 5: Examples of Power Distribution Boards	8
Figure 6: A Pixhawk 2.4.8 Flight Controller	9
Figure 7: Coupled Telemetry Radio Modules	10
Figure 8: Mission Planner, by Ardupilot	11
Figure 9: Comparison of Drone Characteristics	19
Figure 10: System Level Sketch of Dodecacopter	21
Figure 11: Concept of Operations Diagram	22
Figure 12: Subsystem Layout of Dodecacopter	24
Figure 13: Electrical Component Subsystem Diagram	25
Figure 14: Software Subsystem Control Block Diagram	26
Figure 15: Exploded view for Structural Assembly	27
Figure 16: First Concept of the Arms	28
Figure 17: Second Concept of the Arms	28
Figure 18: Third Concept of the Arms	29
Figure 19: Fourth Concept of the Arms	29
Figure 20: Arm Component Diagram	32
Figure 21: Renderings for Assembly Design 1 and Design 2	33
Figure 22: Rendering for Assembly Design 3	34
Figure 23: Rendering for Assembly Design 4	35
Figure 24: Rendering for Assembly Design 5	36
Figure 25: Scoring Matrix for Physical Properties	37
Figure 26: Scoring Matrix for Total Properties	38

Figure 27: Model for Design 1 of the Undercarriage	39
Figure 28: Models for Design 2 and Design 3 of the Undercarriage	40
Figure 29: Various Polymers Density and Yield Strength	42
Figure 30: Various Metal Density and Yield Strength	42
Figure 31: Tensile Test Specimen	43
Figure 32: Stress Plotted Against Strain for Three Different Materials	44
Figure 33: Bending Test Specimen	45
Figure 34: Combined Bending Behavior for Three Different Specimens	46
Figure 35: Thrust Comparison Between Motor Model	48
Figure 36: Plot for Comparing Potential Thrust	49
Figure 37: Rough Sketch of the Duct	55
Figure 38: Cylindrical 29" Diameter Duct	56
Figure 39: Linear Converging/Diverging 29" Duct	56
Figure 40: Implementation of Parabolic Leading Edge on a Duct	56
Figure 41: STAR CCM+ Simulations of Duct	57
Figure 42: Model of Bump Featured Duct	57
Figure 43: Model of Lip Featured Duct	58
Figure 44: Rod Attached to Back of Duct	58
Figure 45: Simulated Duct and Arm System	59
Figure 46: T-Motor's 28" Carbon Fiber Propeller	61
Figure 47: More Accurate Propeller Design	62
Figure 48: Single Propeller Model	64
Figure 49: Single Propeller Cut Plot	64
Figure 50: Contra Rotating Propellers Model	65
Figure 51: Contra Rotating Propellers Cut Plot	66
Figure 52: Contra Rotating Propellers Particle Flow Plot	66
Figure 53: Ducted Contra Rotating Propellers Models	67

Figure 54: Ducted Contra Rotating Propellers Cut Plot	68
Figure 55: Ducted Contra Rotating Propellers Particle Flow Plot	68
Figure 56: Complete Ducted Contra Rotating Propeller Model	69
Figure 57: Subsystem Configuration for Arm	71
Figure 58: Updated Subsystem Configuration for Arm	71
Figure 59: Free Body Diagram of Arm	72
Figure 60: Hand Calculations for Stress in the Arm	73
Figure 61: FEA for the Arm in Bending	74
Figure 62: Subsystem Configuration of the Undercarriage	75
Figure 63: Simplified Configuration of the Undercarriage	76
Figure 64: FEA Results for the Undercarriage during a Drop Test	77
Figure 65: U8-II Motor that the HLD used	79
Figure 66: ESC that the HLD used	80
Figure 67: PDB that the HLD used	81
Figure 68: Tattu LiPo Battery	82
Figure 69: The PixHawk4 Flight Controller	83
Figure 70: The PixHawk4 GPS Module	84
Figure 71: The Flysky FS-i6X Transmitter	84
Figure 72: The Flysky FS-iA6B 6-channel receiver	85
Figure 73: Pulse Position Modulation (PPM) Encoder	85
Figure 74: Holybro Telemetry Kit	86
Figure 75: QGroundControl Drone Overview	86
Figure 76: Propulsion System Component Block Diagram	87
Figure 77: Propulsion Substructure showing Utilized Electronics	88
Figure 78: Communications Component Block Diagram	89
Figure 79: Main components necessary for semi-autonomous flight	89
Figure 80: Main components necessary for autonomous flight	90

Figure 81: Video Assistance Component Block Diagram	90
Figure 82: Camera and Monitor with integrated 5.8 GHz transmitter and receiver	91
Figure 83: Various Electronic Components of Communication Substructure	92
Figure 84: Prototype of the camera trigger Arduino-Pixhawk system	93
Figure 85: Prototype of Electrical Subsystem for the initial Quadcopter	93
Figure 86: Roll, Pitch, Yaw, and Throttle on the Transmitter	94
Figure 87: Electrical system incorporated onto the Quadcopter	95
Figure 88: I/O of Transmitter-Motor Relationship	96
Figure 89: Quadcopter During Autonomous Flight Path Test	97
Figure 90: QGroundControl Drone Configuration Selection	98
Figure 91: The Hexacopter Test Setup	98
Figure 92: Mow-the-Law Approach	100
Figure 93: How a single image can cover a calculated area	101
Figure 94: Calculation for Area of Coverage	101
Figure 95: Test Area for Mow-the-Law Approach	103
Figure 96: Test Area for Mow-the-Law Approach with Travel Path Implemented	103
Figure 97: QGroundControl's Survey Feature with FLIR-Duo R Configuration	104
Figure 98: Screenshot of Agisoft Metashape with Active IR Stitch	105
Figure 99: An Input IR Image	105
Figure 100: Extracted Regions of Interest via Color Filter	106
Figure 101: Applied K-means Algorithm	106
Figure 102: New Generated Flight Plan from IR Image	107
Figure 103: Velocity Test Stand	110
Figure 104: Configuration for Quadcopter Prototype	111
Figure 105: Hover Test for Quadcopter Prototype	112
Figure 106: Conceptual Design and Achieved Design for the Chassis	114
Figure 107: Conceptual Design and Achieved Design for the Arms	114

Figure 108: Conceptual Design and Achieved Design for the Undercarriage

115

Figure 109: Conceptual Design and Achieved Design for Full Drone Assembly

116

## List of Tables

Table 1. Similar Products to the Heavy Lifting Drone (HLD)	12
Table 2. Customers Interviewed	15
Table 3. Customer Needs Matrix Abridged	16
Table 4. Metrics, Importance, and Units	18
Table 5. Anticipated Range for Current Specifications	20
Table 6. Legend for System Components in Figure 10	22
Table 7. Design Matrix for Comparing Four Arms Designs	30
Table 8. Comparison of Various Cross Sectional Properties	31
Table 9. Positives and Negatives for Design 1	33
Table 10. Positives and Negatives for Design 2	33
Table 11. Summary of Tensile Tests	45
Table 12. Summary of Bending Tests	47
Table 13. Comparison of Hand Calculations to FEA for Arm Analysis	74
Table 14. Income for the Drone	108
Table 15. Expenses for the Drone	108
Table 16. The Purpose and Expected Outcomes of Aerodynamic Tests	110
Table 17. Descriptions for Two Test Stands	111

# 1. Introduction

When drones were first created, they were designed to be vehicles that did not explicitly require a pilot physically operating them. Due to the versatility of these unmanned vehicles, drones have become an important tool in robotics, avionics, and aquatic environments. Since these tools are unmanned, drones are designed with great flexibility so that their tasks can be carried out in the most efficient manner. Drones' rise in popularity has been coupled with the development of their constituent technologies, such as high density batteries, advancements in brushless motors, and refinement of control systems. Although the breadth of applications available for these systems is extensive, the primary field of interest for the heavy lift drone project and thesis is the Unmanned Aerial Vehicles (UAVs) sector.

There exist many tasks an aerial drone can carry out. For example, a UAV can be used to take overhead video in an area of interest while also accomplishing payload delivery. Current manned aerial vehicles, such as bi-planes, are used in crop surveying/pesticide dispersal. Using drones to carry out these tasks is a far less expensive endeavor that can accomplish the mission in a similar time frame without putting lives at risk. Additionally, while a person can deliver packages with relative ease, they are often slower and more susceptible to failure than a drone. A drone could also be utilized for important tasks such as immediate medical supply deliveries. It is evident that there is a need in the drone market for a UAV system that can accomplish heavy lifting activities while achieving comparable range to existing drones.

The goal of this project is to build a drone with the ability to lift a total system weight of 55 lbs (due to a legal weight limit dictated by Federal Aviation Administration (FAA) Small Unmanned Aircraft Rule, Part 107) [1]. It should also be able to maintain flight for 20-30 minutes, which translates into a considerable range (which can vary depending on external conditions). The drone will be primarily used in agricultural settings, largely irrigation monitoring applications. Potential uses in package delivery and industrial videography were also explored along with consolidated package flow, fertilizer delivery, hazard management, and building surveying. The aim of this thesis is to document the various design choices made in this project, and whether or not these design choices were the most optimal design choices for creating a drone that can accomplish our requirements. This thesis serves as a guide to future teams who wish to improve on, or otherwise modify the Heavy Lift Drone. Although the

progress we made was in line with the schedule we outlined at the beginning of the year, the COVID-19 pandemic either delayed or resulted in the cancellation of some of the drone's features. Some of these changes include: cancellation of testing beyond prototype hover testing, increasing the number and quality of simulations and analyses, as well as changing some of the materials used for constructing the drone. However, the team developed several well documented testing procedures that can be performed by anyone with the proper qualifications and approval.

The complexity of the Heavy Lift Drone (HLD) warrants highly detailed descriptions that delve into every aspect of the drone, something that this thesis explains. This introduction lays out the ground details such as the conceptual design and implementation of the Heavy Lift Drone (HLD) - whereas the majority of the finer details are covered in later chapters, most notably the market competition, specific subsystem implementation, iteration, and analysis, as well as the budget and other miscellaneous items.

Current market solutions for heavy lifting drones require advanced and expensive drone licenses to operate. These licenses are based on the total system weight, and weights exceeding 55 lbs require a \$30,000 license, the flight applications of which often do not justify the exorbitant costs [1]. The HLD bridges the gap between a drone light enough to operate without advanced licenses, affordable enough to be purchased by individuals, safer than existing models, while simultaneously boasting a high payload-to-weight ratio.

The drone features six pairs of contra-rotating propellers in a hexagonal configuration. Each of these propellers are over two feet in length (28 inch diameter) in order to supply sufficient amounts of lift. Originally, the planned airframe of the drone consisted of carbon fiber. However due to complications in material acquisition due to COVID-19, the material was altered to plywood. Additionally, the 3D printed parts making up the airframe connectors are made of PETG, along with the ducts that encapsulate the carbon fiber propellers. The plastic ducts are present in order to focus air flow downwards through the sweeping area of the propellers which increases lift efficiency while also improving the safety of the system by preventing contact with the propellers. This results as a lightweight drone with excellent material properties and high impact resistance.

## 2. Background

### 2.1 - Literature Review

Several journals and papers regarding aeronautics yielded helpful information regarding duct design and fluid flow. The first publication, *Computational Aerodynamic Modeling of Small Quadcopter Vehicles* was conducted by NASA researchers. They looked into several factors: propeller orientation, propeller thrust, and efficiency between the two [2]. The useful aspects of this particular report were the data related to efficiency and thrust. It was demonstrated that orientation of the propeller in proximity to the center of the drone body does in fact impact the efficiency to generate a given thrust. Since the heavy lift drone should maximize thrust while minimizing power consumption (so that the target time of flight can be reached), initial designs of the drone can be constructed to match the best orientation of the propellers. Orientation data can also be found in Appendix A.2 through Appendix A.5, and the drone designs can be found later in this report.

The next article had information pertaining to ducted propellers, which allowed for the first iterations of the duct to be created. The publication, *Propeller shrouding influence on lift force of mini unmanned quadcopter*, specifically pointed out how varying the height and widths (relative to the propeller) changes the force generated by the spinning propeller. The study also found that as the height of the duct increases there is initially a decrease in the force, and then an increase until it levels out at a force that is 95% of the force without a duct [3]. When the gap between the propeller and the duct wall increases, the force increases but remains less than the force generated by a non-ducted propeller. This conflicts with up-to-date information regarding fluid flow in a ducted environment, namely the fact that ducted propellers increase fluid flow [4]. Evidence to support this can be seen on turbojet engines, where the ducts are designed to help force low pressure air through the cavity and aid in the propeller efficiency. In the original study the ducts had flat walls which have been shown to have a very little impact on the outlet velocity. Slowing of the outlet velocity was ultimately achieved in this set up due to the shearing of the fluid and development of the boundary layer on the sides, decreasing the mass flow rate substantially.

The next two articles, *Computation of Incompressible Viscous - Flow Around a Ducted Propeller Using a RANS Equation Solver and Quadcopter Body Frame model Analysis* shows

simulations of propellers - the first one is meant to look at the differences between simulation (which represent theoretical values) and experimental values [4]. The results demonstrated that the simulation data can accurately model the real world, (as expected) and as such using a similar program to run simulations is a feasible option for testing. Likewise the last article shows quadcopters simulations, and from this it provides a template to look at the mechanical stresses and aeronautical flows during flight [5]. This would be helpful during analysis to look into the transition of inward fluid flow and how that translates into propulsion.

## 2.2 - Drones and their Main Components

Drones, also known as unmanned aerial vehicles (UAVs), can be divided into three categories: fixed wing, single-rotor, or multirotor [6]. Fixed wing vehicles rely on affixed (static) wings to generate lift. Single-rotor vehicles, like helicopters, use a single shaft to rotate propellers in order to generate lift. Multirotors, also called multicopters, use three or more propellers to generate enough lift to take off. The Heavy Lift Drone uses twelve motors, placing it in the multirotor category of UAVs. Drones are typically composed of three substructures: propulsion, communication/control, and chassis [6]. A standard drone is shown in Figure 1 below:



**Figure 1:** Drones built for more commercial-like applications, like this photography drone, have similar characteristics to the Heavy Lift Drone. (Public Domain)

### 2.2.1 - Propulsion Substructure

The propulsion system is responsible for generating the lift that a drone needs to fly. The components selected for this system determine the vehicle's payload capacity and time of flight.

This one in particular is composed of motors, speed controllers, batteries, and a power distribution board which activate the propulsive substructure.

### 2.2.1.1 - Motors

Motors are an essential component to drone flight in which at least three or more are required for these systems to take off. Brushed direct current (DC) motors are common motors in the industry with two wires, voltage and ground, though they are not the best choice for aerial operations as they are less efficient in power consumption. Brushless motors gain mechanical simplicity at the expense of control complexity. Each of the four motors in a brushless quadcopter setup needs to have its own microprocessor where the back current is evaluated by unused coils. This determines the position that the motor is in as well as adjustment of the current to other coils which achieves the speed set by the central flight controller. This synchronization of powering certain coils high and low based on hall sensors is called electronic commutation. In the market, one of the most popular motor manufacturing companies is T-Motor - which specializes in both hobby level and industry level motors and propellers. T-Motor has many different motors available for consumers specialized for rotations per minute (RPM), weight, etc. In a later section, more detail is given on which specific brushless motor was selected and why.



*Figure 2: Examples of brushless motors.*

### 2.2.1.2 - Propellers

Typical materials that are generally used for propellers are metal, glass fiber and carbon fiber. For heavier drones, since carbon fiber tends to be stronger, more rigid, and can withstand

more tensile and bending forces while being very light, it tends to be more commonly used. Likewise, in the event of a crash, it has a higher likelihood of surviving. Due to these characteristics, for a high-performance and heavy payload drone such as ours, this selection is the ideal choice.



*Figure 3: Examples of propellers.*

#### **2.2.1.3 - Ducts**

Ducted systems can serve two purposes: one is to increase the lift efficiency that a propeller can produce and the other is to restrict a particular fluid flow so that the propeller can operate in a protected manner. When the propeller rotates airflow inside the inlet flows faster than the air outside the inlet which creates a lower pressure inside the inlet according to Bernoulli's Principle[7]. As such, this lower pressure creates additional thrust[7]. With this in mind, the ducts on the drone were meant to allow for additional thrust for a given speed of the propellers. As a secondary effect the ducts would alter the noise that is emitted from the propellers, which has been recorded to be above 90 decibels. Finally the ducts act as a safety measure to help prevent people who fly the drone or operate near the drone from being seriously hurt by contact with the spinning propellers.

#### **2.2.1.4 - Electronics Speed Controllers**

Each motor is controlled by an Electronic Speed Controller (ESC). The ESC controls the rotational speed of the motor via a pulse width modulation (PWM) signal and electronic commutation. This electronic commutation is implemented through the use of hall sensors in the brushless motor and a six MOSFET bridge in the ESC. The ESC receives a PWM signal from

the flight controller and translates this signal into three voltage signals that go to the brushless motor. These ESCs play an important role in controlling the lift and movement of the drone, and without them the drone would not be able to make the fine adjustments in pitch, altitude, and physical position.



*Figure 4: Examples of electronic speed controllers.*

#### 2.2.1.5 - Batteries

Of the several battery types that were considered, LiPo batteries were the most readily available and had the highest energy density, and as such they were chosen over other types such as NiCd batteries. There are three main components of a LiPo battery: main cable, feedback, and capacity cable. LiPos "...don't like to be left fully charged for long but don't want to be stored completely empty either. Treat them wrong and it is pretty easy to ruin them, or worse." [8] The battery's capacity is typically defined by the number of cells and the milliamperere hours (mAh), where each cell contains a nominal voltage of 3.7V and a maximum voltage of 4.2V. Another important specification to consider is the discharge rate, measured in coulombs (C). Batteries are limited in the amount of charge that they can deliver over a given period of time. The discharge rate helps engineers determine whether the battery can handle the electrical needs of the system being powered. Without the batteries as the power source, the system would need another source of energy - which would imply a tethered power source or an alternative fuel system which overcomplicates and limits the design. Though the implementation of a battery in the drone system is trivial, the battery size and amperage is important because the motors/control system

can only take so much load before failure. This failure can mean that the wires “melt” or the electrical components that receive the charge shorts the circuit. Likewise, the opposite could also occur where there isn’t enough power left in the batteries for the system to perform. This issue is a primary concern if the drone is already in flight. If the system is underpowered during takeoff - the flight can be cancelled to prevent any damage until a fully charged battery can be swapped.

### 2.2.1.6 - Power Distribution Board

The purpose of the power distribution board (PDB) is to provide power from the battery to the rest of the system. These boards typically also include power ports that can be used to power peripherals. For the dodecacopter configuration, there are two PDBs, with each board supplying six motors with power. If the voltage at a port is too high or too low, a buck converter or a boost converter can be used, respectively.

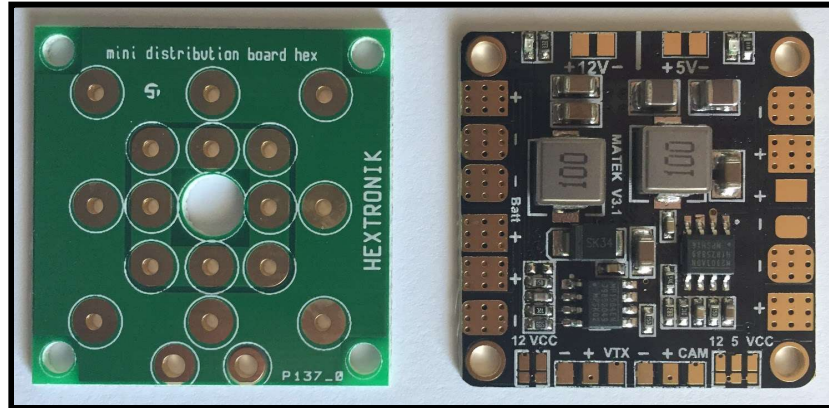


*Figure 5: Examples of power distribution boards.*

### 2.2.2 - Communication and Control Substructure

To have the system perform nominal behaviors (i.e. not flying off or spinning wildly), a controller is required. Nearly all flight controllers have basic sensors such as gyroscopes and accelerometers. Some flight controllers might include more advanced sensors such as barometers and magnetometers. Our system is composed of the Pixhawk 4 flight controller which includes many of the aforementioned peripherals. This, paired with the individual ESCs , each motor is used in order for nominal flight to occur to correct any sudden changes to movement and prevent erratic flight. In addition to a transmitter, a receiver is also needed for the system to perform functions correctly. The receiver reads the inputs from the transmitter (usually a controller of

some sort) and relays this information to the flight controller. The receiver and transmitter have a limited range so if the drone travels outside of that range, the pilot may lose control of the drone.

### 2.2.2.1 - Flight Controller

The flight controller is responsible for translating pilot commands into signals that communicate with the rest of the vehicle. These commands include flight directions from the pilot via a controller or a telemetry kit. The flight controllers have a variety of sensors such as an internal gyroscope, accelerometer, magnetometer, and barometer that allow it to take input from the surroundings and make control decisions, such as stabilizations, for the drone [9].



*Figure 6: A Pixhawk 2.4.8 flight controller*

### 2.2.2.2 - Transmitter and Receiver

A transmitter is used by the pilot to send flight commands to a receiver which is mounted to the drone. That information is then passed to the flight controller which then changes the throttle, pitch, yaw, or roll accordingly. This form of flight where a pilot controls the movement of the drone directly through a transmitter-receiver combination is known as semi-autonomous flight. Transmitters typically interface with several joysticks and switches and this whole assembly is known as a controller. The x and y movement of the joysticks and each of the switches is connected to a channel. Different transmitters have a different number of channels available to the pilot. Each of these channels outputs a PWM signal. Transmitters usually have 4-12 channels. Four of these channels are reserved for the drone's throttle, yaw, pitch, and roll

control. Channels can also be mapped to landing gears and any other peripherals attached to the drone that require PWM signals for control. Channels can also be attached to commands that are setup in the ground control station software. The receiver needs to be able to accept an equal number of channels or more than the transmitter is outputting. For RC communication a pulse position modulation (PPM) encoder may need to be connected between the receiver and the flight controller in order to generate a signal that the flight controller can read. This PPM encoder can encode multiple PWM signals into one signal transmitted over a servo cable to the flight controller. The most common frequencies to use for drone transmitters and receivers are 2.4GHz and 5.8GHz frequencies. Generally speaking 5.8GHz is used for FPV drone racing and 2.4GHz is used for longer range communication.

#### 2.2.2.3 - Telemetry Kit

Telemetry modules, as shown in Figure 7 below, allow the user to receive live data from the drone during its flight and send flight commands through the ground control station while the drone is airborne. Flight plans can also be specified in the ground control station software prior to takeoff. Drone parameters can also be tuned mid-flight through the ground control station. This form of flight is known as autonomous flight. The telemetry kit is composed of two transceivers or modules. One is attached to the flight controller and the other is attached to a laptop with the ground control station software.



*Figure 7: Coupled telemetry radio modules.*

#### 2.2.2.4 - Ground Control Station

The ground control station allows the pilot to see live flight data being transmitted from the flight controller through the telemetry modules. The ground control station is composed of a laptop, telemetry module, and software. The software for the ground control station allows the user to calibrate the flight controller's sensors, change different parameters of the vehicle, and map out flight paths for autonomous flight.

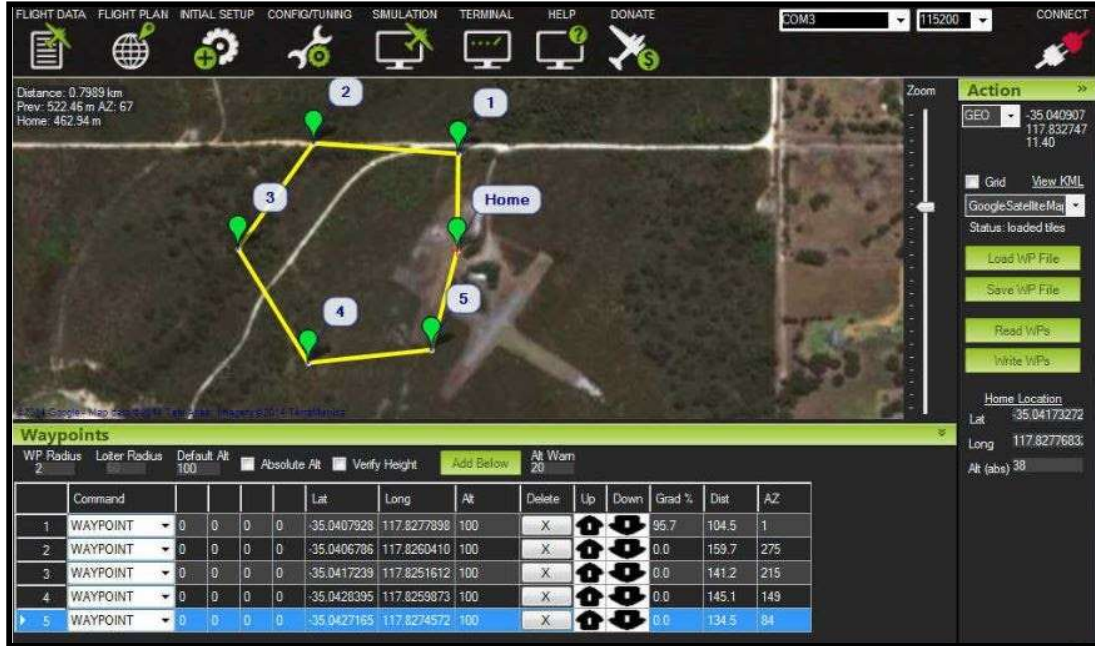


**Figure 8:** Mission Planner, by ArduPilot, is an example of a popular ground control station software.

#### 2.2.3 - Chassis and Material Composition

When it comes to designing aerial vehicles, the material has to be sturdy and rigid enough to survive basic flight and light enough so that flight can occur. For the many components that are needed for flight, a chassis is required to hold all the necessary devices. Two typical materials used are glass fiber and carbon fiber. Carbon fiber tends to be stronger, more rigid, and can withstand more tensile and bending forces. Carbon fiber is also one of the lightest composite materials produced, so high-performance small drones may opt for this material. Likewise in the event of a crash, it has a higher likelihood of surviving the crash compared to the other materials that were considered.

Our system utilizes PETG in 3D prints so that the drone components can be assembled in a desired configuration. Another major material used in the final model of the drone was aluminum, which comprises the appendages of the drone. This material is very light, and has the strength to survive flight even in commercial aircrafts, making this selection appropriate for use in far less harsh conditions. Additionally, polycarbonate was to be used for the bulk of the chassis, due to it being strong and relatively lightweight, however, due to COVID-19 this material choice could not be met (due to the fact that places that could make this product closed as a result of the pandemic).

## 2.3 - Market Comparison

There are several existing models on the market that are comparable to the Heavy Lift Drone project. These systems vary greatly in price and lifting capabilities from those that can lift 200 lbs to others that can lift 20 lbs. The following table outlines drones that have performance specs closest to what the Heavy Lift Drone aims to achieve. Quantities such as similar payload-to-weight ratios, time-of-flight, and lift are examined as well. Table 1 outlines and characterizes products similar to the HLD.

*Table 1: Similar Products to the Heavy Lift Drone (HLD)*

Name:		Price (\$):	Lift (kg):	Time of Flight (min):	Payload-to-Weight Ratio
Heavy Lift Drone (Projected)		13,921	25 (55 lbs)	20-30	0.5
X-Fold Dragon-12 <sup>[10]</sup>		32,000	44 (97 lbs)	10	0.62

Big Hexy <sup>[11]</sup>		15,000	25 (55 lbs)	20	0.4
Scorpion <sup>[12]</sup>		10,000	10 (22 lbs)	15	0.4
OnyxStar Hydra-12 <sup>[13]</sup>		36,000	12 (26 lbs)	15	0.42
Vulcan UAV Airlift <sup>[14]</sup>		27,000	25 (55 lbs)	10	0.45

The payload-to-weight ratio (PWR) is one of the most critical aspects when assessing the efficiency of a drone. Based on existing products' low payload-to-weight ratio (meaning that the bulk of the total weight is taken up by the drone itself), it may be useful to explore a potential product that optimizes weight to allow for much higher ratios. This is the gap in the market that our heavy lift drone fills. It is both light enough to accommodate a high payload, and inexpensive enough to be used in agricultural applications. As seen in Table 1 above, the heavy lift drone has a PWR of 0.5, meaning that half of the takeoff weight is taken up by the payload. In comparison, the other drones on the market have PWR's that are 20% lower, with the exception of the "X-Fold Dragon". However, the "X-Fold Dragon" which has a PWR of 0.62, can only fly for 10 minutes and requires a light aircraft license from the FAA, whereas our drone only requires a drone license, which is much easier to obtain.

Regarding safety for multi-rotor aircraft, the Federal Aviation Administration (FAA) has a set of guidelines for piloting such devices. All controllers must have a certified drone license if the drone is to be piloted in a public or outdoor setting. Once in flight the drone must fly below an elevation of 400 feet in the air and fly within visual line of sight of the controller. Moreover, the controller must be aware of certain airspace requirements such as restricted flights near airports, restricted flights directly over schools or hospitals, and other requirements. Considering

flight safety, a duct system surrounding each propeller was designed so that safety near the physical system was maintained - serving both as a barrier to touching the propellers as well as an increase in lift efficiency (which will be discussed extensively in the analysis section of Chapter 6).

### **3. Customer Research and System Definition**

#### **3.1 - Customer Needs**

Interviews were conducted with those with an interest in drones and/or who are involved in the related fields that the drone would operate in (such as agriculture or delivery). These people have a significant impact on the final design of the drone. The names and roles of these potential customers are listed in Table 2 below:

*Table 2: Customers Interviewed*

Name	Role
John Cugini	Packaging and Delivery Director at Phoenix Controls
Chris Shay	VP of Operations at SCU
Nina Shami	Agricultural Developer
Kevin Fontana	Assistant Director to Facilities and Operations
Mike Rasay	Research Associate at the Robotics Systems Lab

Each of these potential customers has some interest in a heavy lifting drone - for instance the Agricultural Developer can use it for irrigation monitoring (ie. the relative temperature gradient of the soil), and the Packaging and Delivery Director can use it for transporting payloads rapidly and effectively.

The questions and answers for all the conducted interviews can be found in Table A1 located in the Appendix. Based on the answers provided by the customers, the following table, Table 3, was created to list some of the requested needs and features:

**Table 3: Customer Needs Matrix Abridged** (see also section B in the Appendix where a score of 5 is the highest importance).

Component	Need	Importance
The drone	Is easy to assemble/disassemble	4
The drone	Is not too noisy	2
The drone	Is safe to handle and manipulate	5
The drone	Can sustain flight for 30 minutes	3
The drone	Can carry a large load	4
The drone	Is controlled through an app	1
The drone	Stored in a convenient way	5
The drone	Is less expensive than competitors	4
The chassis	Is sturdy and does not flex too much	5
The landing gear	Is able to land on uneven surfaces	2
The ducts	Protect the drone from minor collisions	4

The most important requirements for the drone include a robust design and safety. In terms of robustness, the drone should be able to handle weather conditions such as rain, snow, heavy wind, etc. The next important factor is safety - as such, both mechanical and electrical safety systems are implemented both in terms of testing and in terms of flight tests. The propellers in particular are a primary concern, as the high RPM the blades achieve can easily cut through skin. The ducts not only act as a way to increase flow but also act as a barrier/shroud to protect against rogue propeller projectiles. The programming of the drone implements certain safety measures so that if an issue does occur - for instance: low battery, collision, fast descent - the code will ensure it will land quickly and safely so that the drone and its controller will be safe

during an emergency landing. Without this, the ability of the drone to perform certain tasks becomes a liability.

Quantities such as time of flight, which should be a minimum of 20 minutes, and a vertical take off acceleration of  $1.25 \text{ m/s}^2$  are other attributes that the project is striving toward. While agricultural and package delivery purposes would benefit from a long time of flight in conjunction with the weight specification, the capability to lift heavy loads is also an important focus. In terms of speed, all that is required is that the drone can quickly respond to location/height input. The speed at which the drone can fly would also allow for greater ranges of travel, although that is also not as critical as the aforementioned requirements.

### **3.2 - Product Specifications**

From the interviews conducted with the customers, the following metrics were formulated with the intention of minimizing weight while maximizing performance and safety. Additionally, project requirements such as those set by the FAA and the safety guidelines set forth by the Santa Clara School of Engineering were also considered in Table 4. Highlighted metrics indicate that they are considered crucial ones. After outlining the importance of these metrics, a comparison was made between our drone and the competition regarding important customer needs. This comparison can be seen in Figures 9a and 9b following the table.

There are a few reasons why some of the particular ideal values, shown in Table 5, were chosen. For instance, 55 lbs maximum takeoff weight is an FAA requirement, and the chassis and payload weights are a result of our aforementioned PWR ratio. A vertical acceleration limit of  $1.25 \text{ m/s}^2$  was selected in order to maximize acceleration while maintaining structural stability of the chassis. Additionally, a flight time of 30 minutes was found to be a satisfactory time for most applications, as well as a noise level of 80 db maximum at 10 ft away. The duct diameter ranges were chosen based on the diameter of the propellers. Lastly the temperature range was chosen for optimal motor operation so that overheating would be avoided.

**Table 4: Metrics, Importance, and Units**

Metric #	Need #'s (seen in Appendix Table B.1)	Metric	Importance	Units
1	10, 12	Total Weight	5	lbs
2	12	Chassis Weight	4	lbs
3	10	Payload Weight	4	lbs
4	4, 11	Ascent Acceleration	4	s
5	4	Lateral Acceleration	3	m/s^2
6	2	Noise level at 10 ft away	1	dB
7	7, 18	Maximum Cost	4	\$
8	9, 25, 29	2 Year Guaranteed Lifespan	4	Years
9	13, 20	Instills Pride and is Aesthetically pleasing	3	Subj
10	1, 14, 17	Assembly/Disassembly	4	N/A
11	3,5,21,23,26	Overall Safety	5	N/A
12	16	Temperature Range (0-120F)	3	°F
13	14,27,28,30	Maintenance Accessibility	3	N/A
14	15,29	Remote Accessibility	2	N/A
15	23, 24	Duct Diameter Size	3	in
16	6	Flight Time	2	s
17	19, 21	Material Factor of Safety	4	ksi/ksi

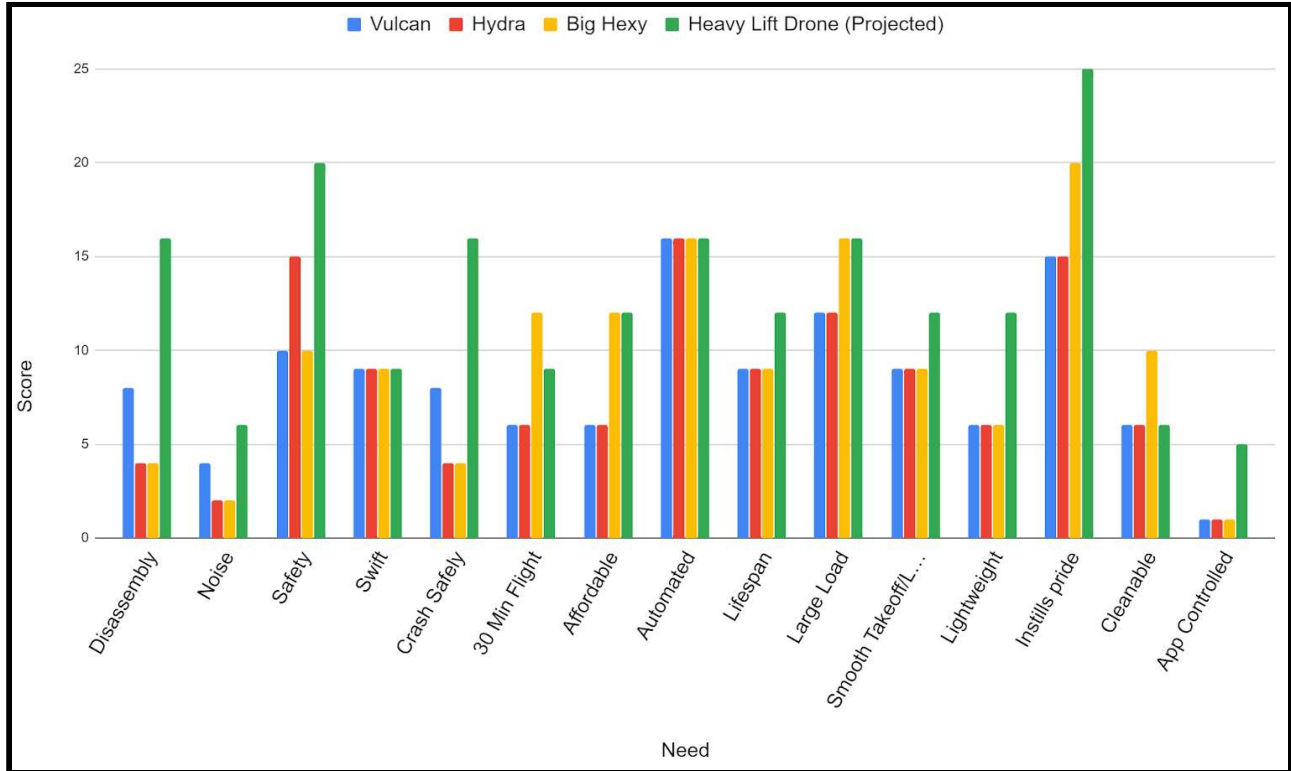


**Figure 9a:** Comparison of Drone Characteristics

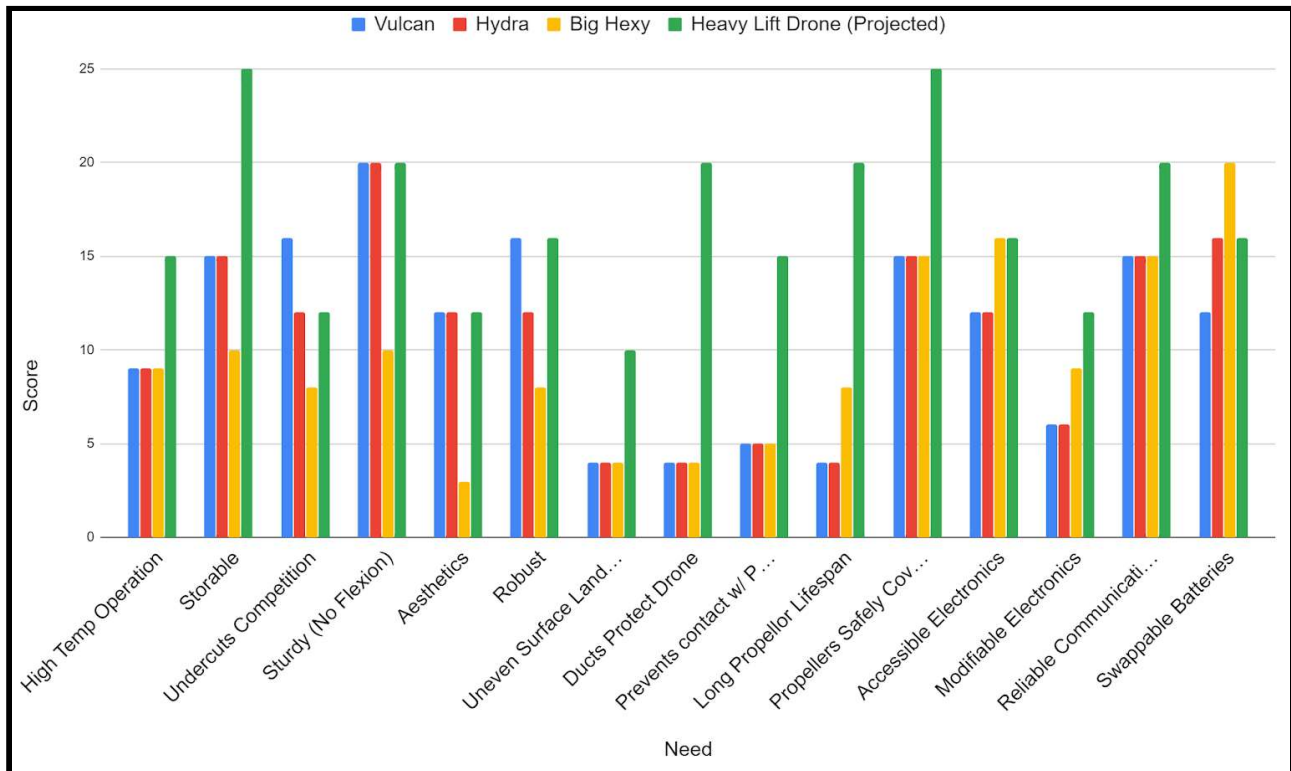


**Figure 9b:** Comparison of Drone Characteristics

This data was then formulated into Table 5 below with the marginal and ideal values for the Heavy Lift Drone specifications.

**Table 5: Anticipated range for current specifications**

#	Metric	Units	Marginal Values	Ideal Values
1	Total Weight	lbs	50-55	55
2	Chassis Weight	lbs	35-40	35
3	Payload Weight	lbs	15-20	20
4	Vertical Acceleration	$\frac{m}{s^2}$	1.00-1.25	1.25
5	Lateral Acceleration	$\frac{m}{s^2}$	1.50-2.00	2.00
6	Noise at 10 ft	dB	85-90	80
7	Maximum Cost	\$	17,000	14,000
8	Lifespan	Years	1	2
9	Flight Time	Minutes	20	30
10	Duct (Outer) Diameter	in	N/A	30
11	Duct (Inner) Diameter	in	N/A	28
12	Temperature Range	°F	32-95	0-120
13	Factor of Safety	ksi/ksi	1.5	2.5

### 3.3 - Product Overview

#### 3.3.1 - System Level Sketch

By consolidating these customer needs and specifications, a more detailed picture for the development of the product can be created. The HLD will be constructed to feature twelve propellers in contra-rotating pairs. The central chassis will protect the essential electronic components while ducts will surround each pair of propellers to provide protection and improve performance. The major subsystems are broken down into four sections: Mechanical, Aerodynamics, Electrical, and Software. The physical layout for the structure of the drone is organized and presented in Figure 10 which shows the component layout diagram of the drone.

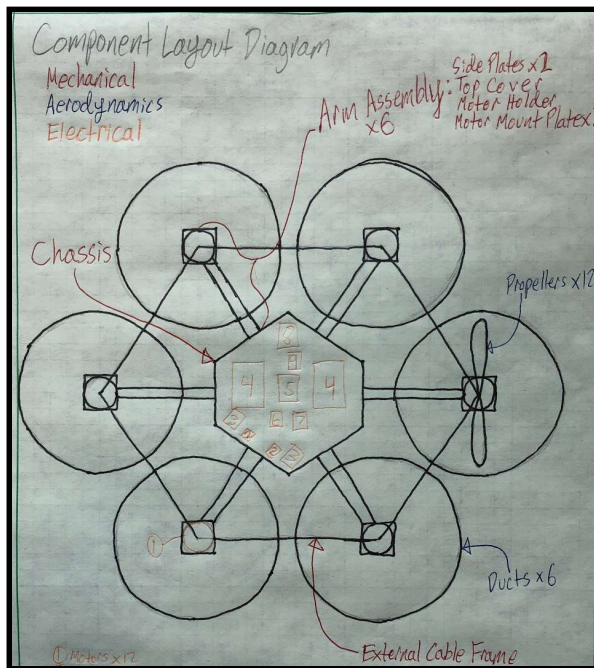


**Figure 10:** System level sketch of dodecacopter with electrical components (in orange)

This sketch was informed by customer needs, development of product specifications, and through research of common configurations for existing drone designs. The sketch also displays which parts are assigned to each subgroup and subsystem. Additionally, it lists the basic materials and components needed for the design of the drone. Below is Table 6, breaking down the necessary electrical components for the drone, along with their corresponding number on Figure 10.

**Table 6:** Legend for system components in Figure 10 (see orange labels)

Label Number	Electrical Component
1	Motors x12
2	ESCs x12
3	Power Distribution Board x2
4	Batteries x2
5	Pixhawk 4 Flight Controller
6	GPS Module
7	PPM Encoder + Receiver
8	Video Camera + Transmitter
9	Radio Telemetry Air Module

### 3.3.2 - Concept of Operations Diagram

The Concept of Operations details the process for a typical mission that the drone would follow, including the various stages at which important actions take place. The concept of operations, as shown in Figure 11 below, follows a mission plan, which for this project was set to be agricultural surveying.

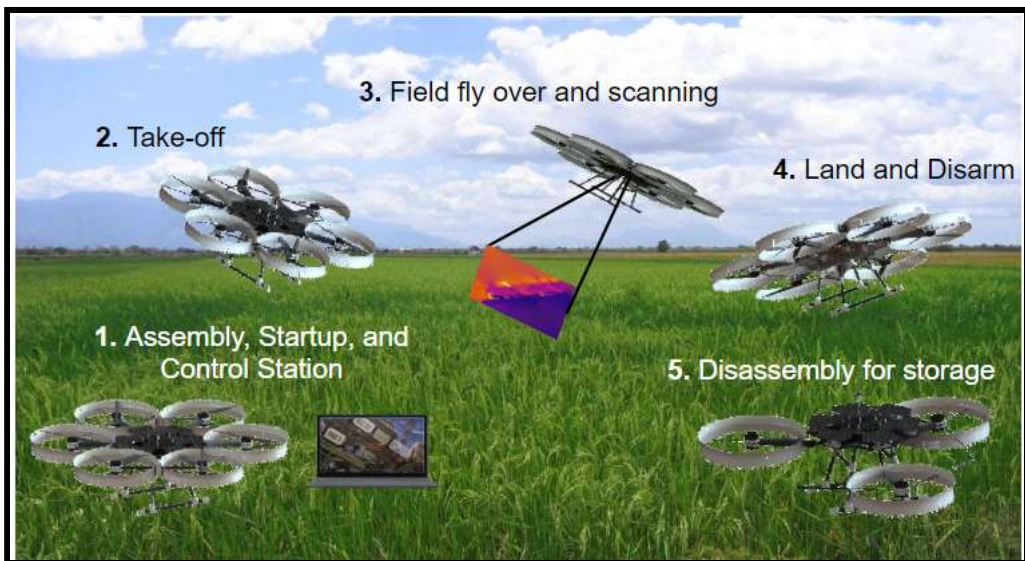


**Figure 11:** Concept of Operations Diagram for the drone's assembly and activity in the field

The mission starts with the assembly of the drone. Conceptually the drone had most of the chassis and arms preassembled, and the landing system already mounted on the underbelly. With that in the mind, the ducts and arms need to be attached to the chassis.

Once assembled, initiation of communication and start up sequences is performed so that take-off can commence. The start-up sequences include the physical testing of the components to ensure functionality of all parts on the drone. Additionally a flight plan is generated for an autonomous flight operation to scan the field with a thermal camera. When those are completed the drone can finally start its tasks, with the pilot carefully taking off.

After the take off, the mission is performed by following the flight plan. This plan is typically outlined by the flightpath and by what task it is set to do. Although for this project it is just surveying. Once the mission is completed or low battery levels are reached, landing and disarming of the system is performed. Any photos taken during the flight operation can be analyzed to identify regions of interest and then to generate a new flight plan to visit all points of interest.

Once all flight operations at the field is done, the system can be disassembled for storage. In most cases this disassembly process means that certain appendages of the drone will not be fully dismantled and merely returned to the state they were in prior to the mission.

### **3.3.3 - Subsystem Layout Diagram**

The features and components shown in the initial sketch of Figure 10 were maintained to show the breakdown for the subsystems in this project. As the design was finalized, a render was color coded to show the involvement of the different subsystems in the physical implementation of the design. In Figure 12, features of the design are highlighted in red to note the mechanical subsystem, in blue for the aerodynamics subsystem, and in yellow for the electrical subsystem. Not physically pictured is the software subsystem which would be indicated in green.

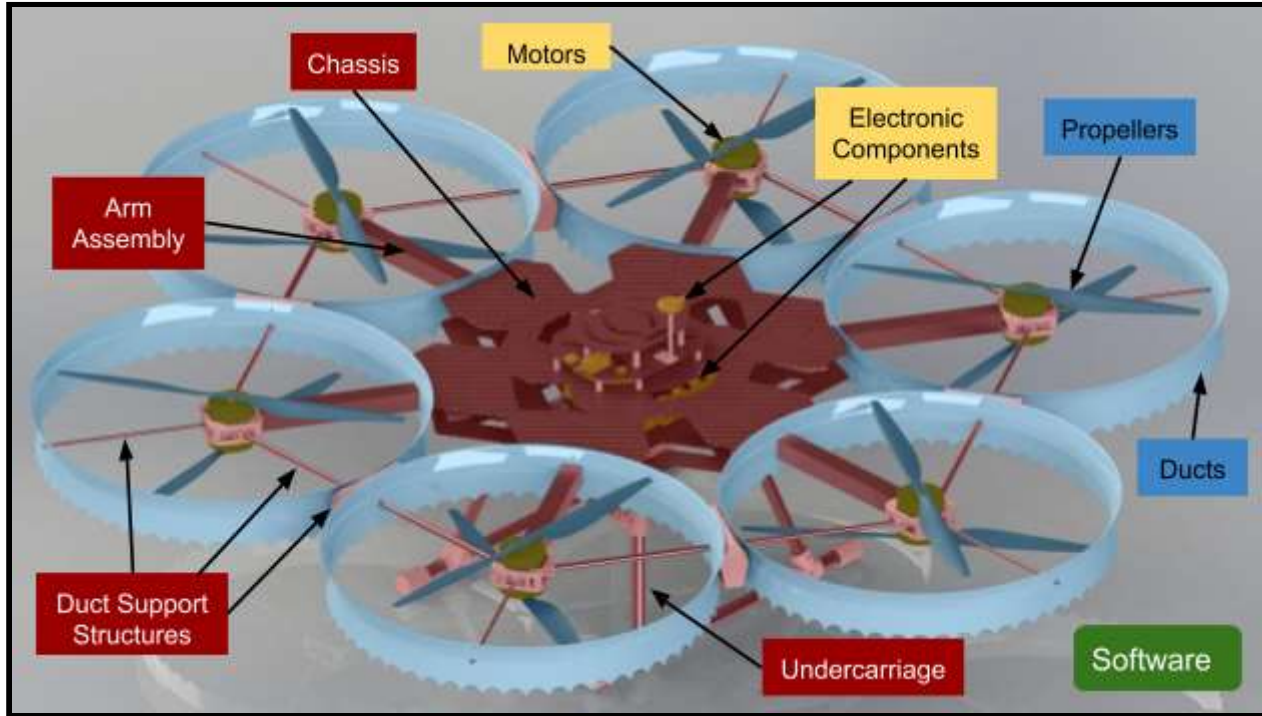


**Figure 12:** Subsystem Layout of Dodecacopter. Mechanical subsystem is Red, Aerodynamics subsystem is Blue, Electrical subsystem is Yellow, and Software subsystem is Green.

This diagram includes essential features of the structural assembly of the drone including the primary mechanical subassemblies, the location of the main electronic components, and the configuration for the ducts and propellers. While software is not physically represented, the diagram notes that the subsystem is coded in green which will be the consistent system in further system diagrams.

### 3.3.4 - Electrical Component Subsystem Diagram

The next main subsystem of interest is the electrical subsystem which bridges the requirements of the propulsion system and the communication system in order to ensure that the physical components of the drone can successfully perform the tasks programmed by the software. Figure 13 shows the entire electrical system and how all the components of the propulsion system interact with the control and communication components to form a cohesive system that the drone uses for flight. What is also shown is where the components are attached to and whether the pilot or vehicle uses them for its part of the electrical system.

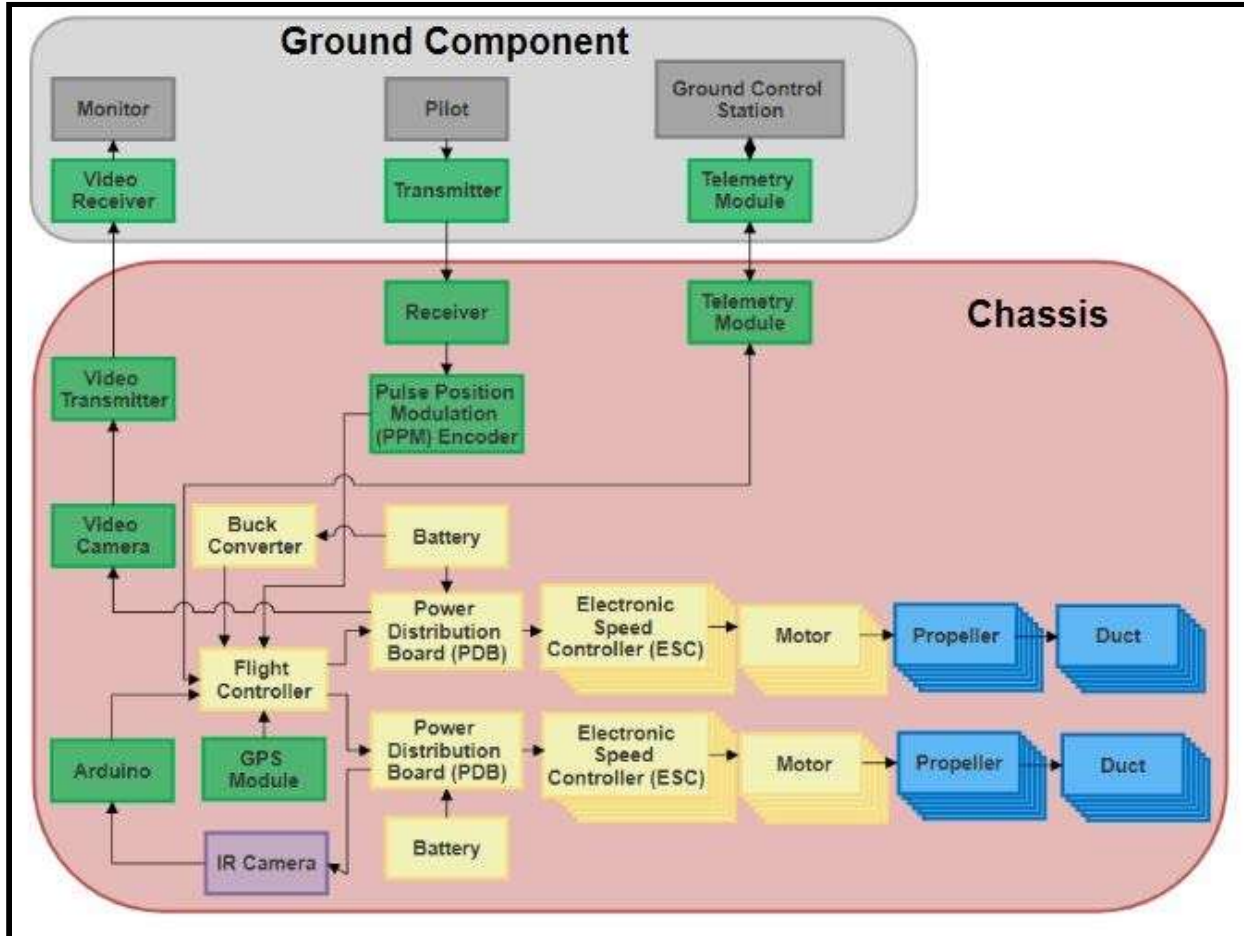


**Figure 13:** Electrical Component Subsystem Diagram. Displays how components are related. The propulsion components are yellow and the communications and control components are green.

As shown in this diagram, the color code from the Subsystem Layout Diagram in Figure 12 is carried forward by showing the location of various components. The component blocks in green show the components involved in the software analysis and communication, while the electrical components are shown in yellow. The components in blue including the ducts and propellers are from the aerodynamics subsystem, while everything contained in the large red block notes that those components are secured in the structure of the drone.

### 3.3.5 - Software Subsystem Block Diagram

The next subsystem diagram is the Software Block diagram which details the flow for autonomous flight and the communication between the drone, its image processing system, and

the web app associated with generating flight plans and communicating with the flight controller. The software block diagram is presented in Figure 14 below.

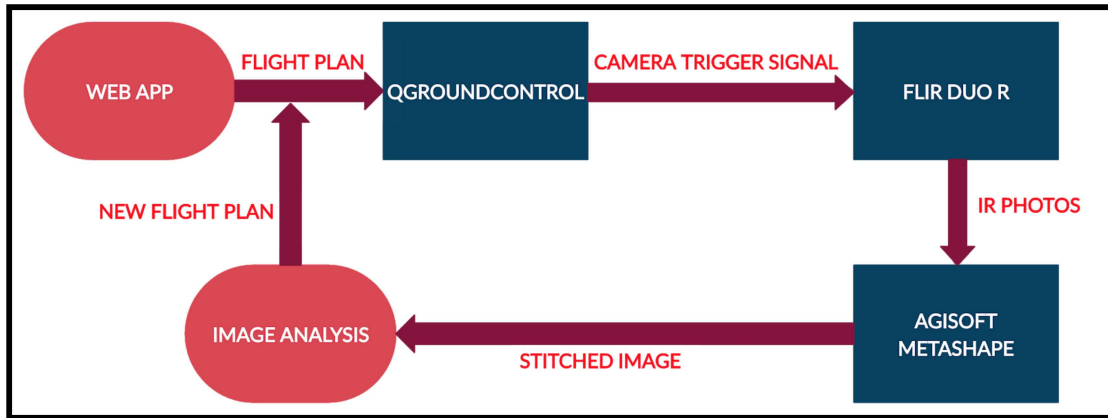


**Figure 14:** Software Subsystem Control Block Diagram. All code is archived in SVN within the RSL.

The red components represent what was implemented and the blue components represent what was utilized in the process of development.

## 4. Concept Selection Analysis

During the conceptual design generation for the system, several mechanical subassemblies were examined and expanded upon in order to determine their strengths and weaknesses. Feasibility for implementation into the design was also evaluated in these analyses. Initially, hand sketches were created for various configurations of the drone's propellers, some of which are presented in the appendix of this report as well. In addition, the final component diagrams for each of the designs in the assembly are presented in full all entries in Appendix C. The design process for some of the subassemblies are described in detail, primarily the arms, the undercarriage, and the chassis. These are the primary structural subassemblies which make up the construction of the drone, so several iterations and improvements were made throughout the course of developing the final design of this project. The exploded configuration for the overall assembly is presented in Figure 15, which includes labels for the previously mentioned subassemblies as well as some additional features such as the duct connector assembly.

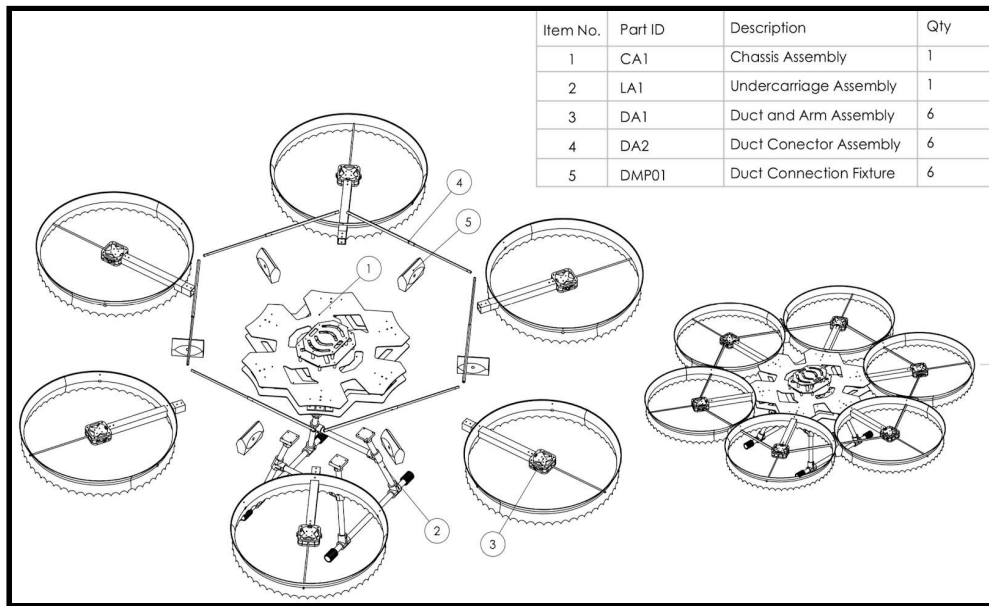


**Figure 15:** Exploded view for Structural Assembly of the drone showing major subassemblies

### 4.1 - Arm Design Generation

Three initial designs for the assembly of the arms are compared in the models, starting with Figure 13 below. These designs were developed and compared primarily based on weight and feasibility of manufacturing. The first design incorporates various 3D printed segments which would be connected together; however, this design would be very heavy. Additionally,

having many segmented parts would cause it to be prone to separation and/or unnecessary dynamic conditions.

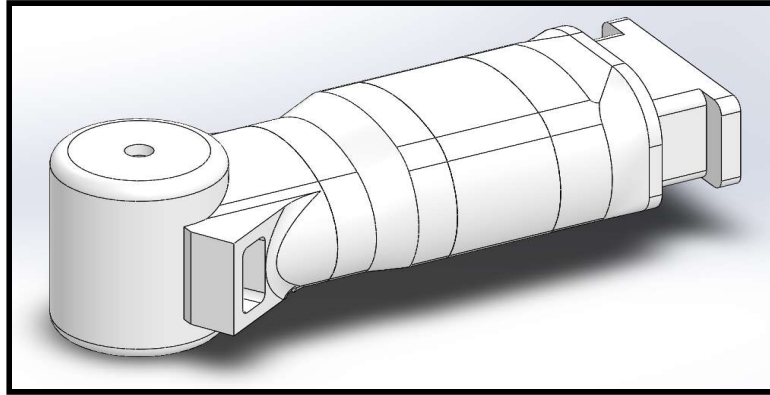


**Figure 16:** Solidworks model for the first arm concept of the drone assembly through various 3D printed segments

The second design was intended to be more lightweight while maintaining structural integrity by using sheet metal truss structures connected by a 3D printed frame. While this second design would be lighter and have a smaller volume compared to the first design shown above, it may not be as simple to manufacture. The 3D printed structure on top was made to be very lightweight, though printing such geometries would be unnecessarily complex to construct. In addition to that, the mount for the motors at the end of the arms were designed as one solid piece, making it heavy and less modular to account for affixing the motors after each flight.

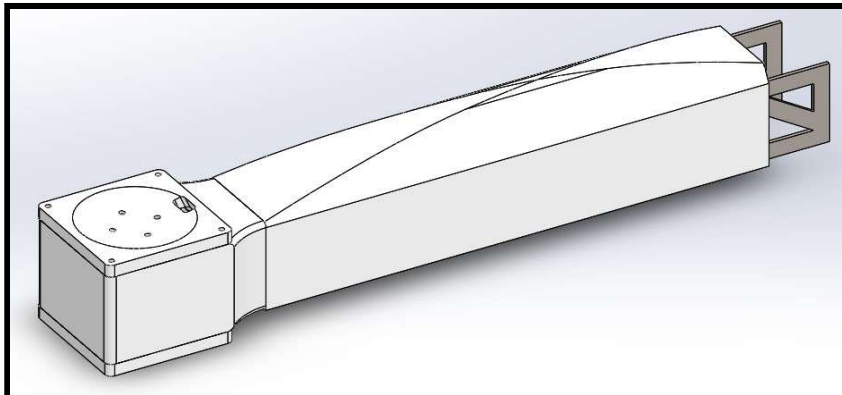


**Figure 17:** Solidworks model for the second arm concept of the drone using sheet metal trusses and 3D printed structures.

The third design focused on improving the strengths from the second iteration in terms of weight and manufacturability. This would result in increasing the effectiveness of the structure

along with making it easier to manufacture. This design utilizes a 1.5" square tubing made of aluminum as the primary geometry where the end on the right shown in Figure 18 below is fixed via brackets to the chassis in the final design. Similar to the previous design, motor mounts on the opposing end were improved so that removal of such parts could be done easily. This design resulted in several strengths, particularly its low weight, low cost, and ease of manufacturing.

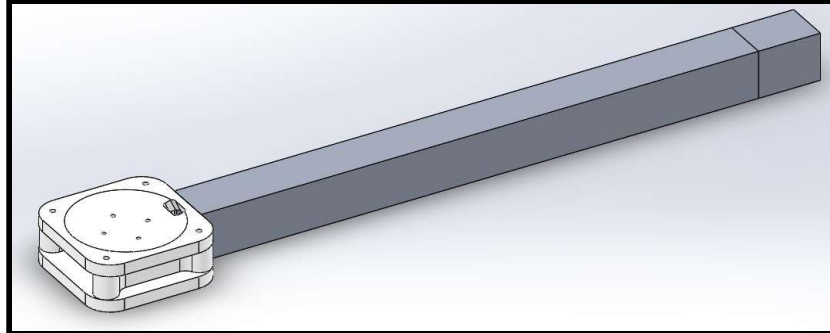


**Figure 18:** Solidworks model for the third arm concept of the drone using square aluminum tubing and 3D printed structures.

In the fourth design iteration, the third design was iterated on and optimized to reduce the weight, material cost, and stability of the previous design. In this final version, the length of the arm was shortened in order to coincide with changes to the design of the chassis, which will be discussed in a later section. In addition, the design of the 3D printed motor mount at the end of the arm was optimized using finite element analysis (FEA) in order to reduce the weight and improve airflow as shown in Appendix F.1 and Appendix F.2

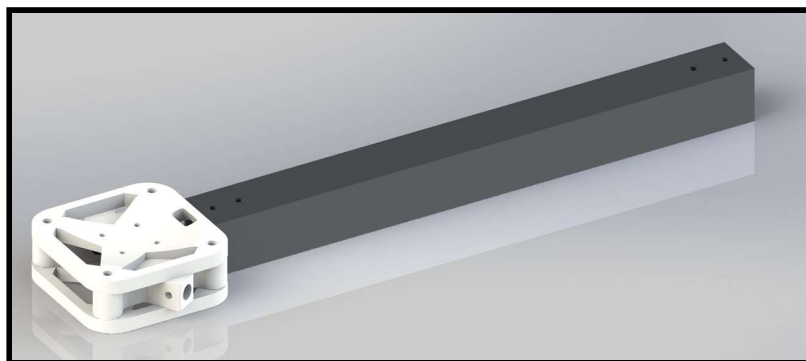


**Figure 19:** Solidworks model for the fourth design iteration of the arms of the drone using square aluminum tubing and 3D printed structures.

Each of these four designs was compared using the following design matrix in Table 7, which gives a relative comparison of the most important qualities of the design including the

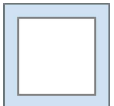
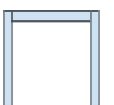
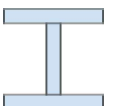
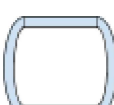
weight, the ease of assembly, the aerodynamics, and the ability to contain and access electronic components. As shown by these comparisons, the final design ranks the highest overall and has the greatest improvements of any other design.

**Table 7:** Design Matrix comparing the four design iterations for the arm assembly based on various relative qualities where 1 is poor and 5 is best.

Ranking (1 = poor) (5 = best)	Mass	Assembly	Aerodynamics	Electronics Housing	Total
<b>Design 1</b>	1	2	2	4	9
<b>Design 2</b>	3	3	3	3	12
<b>Design 3</b>	4	4	4	3	15
<b>Design 4</b>	5	4	5	5	19

In addition, the design was further examined by comparing different cross sectional shapes from the same 6063 Aluminum material. These various cross sections were compared based on the moment of inertia that the arm would experience when bending about the y-axis, as well as the estimated weight, cost, and manufacturability for an arm of each shape. The square tube was eventually chosen.

**Table 8:** Comparison of various cross sectional properties and shapes that could be utilized for the aluminum structure of the arms.

Cross Sectional Shape	Moment of Inertia (y-axis)	Estimated weight (for 20 inches)	Cost of Material	Manufacturability- Required Machining
Square tube: 1.5" ( $\frac{1}{8}$ " wall) 	0.22 in <sup>4</sup>	1.39 lbs	\$54	As Manufactured - Cut to length
3 Sided Channel: W1.25" L1.25" 	0.11 in <sup>4</sup>	0.89 lbs	\$36	As Manufactured - Cut to length
I-beam: 2.5" x 3" (.33" wall) 	0.89 in <sup>4</sup>	1.84 lbs	\$230	As Manufactured - Cut to length
Circular Tube: 1.5" ( $\frac{1}{8}$ " wall) 	0.13 in <sup>4</sup>	1.05 lbs	\$176	As Manufactured - Cut to length
Elliptical Sided Rectangle: 1.5"x2" ( $\frac{1}{8}$ "wall) 	0.67 in <sup>4</sup>	1.95 lbs	\$60	Manufactured rectangle - Cut to length - Deform to create shape

The assembly of the arm is constructed from five components, with the aluminum tubing and two designs which were 3D printed. The assembly requires two copies of each 3D printed component since each arm has two motors in order to build the contra-rotating configuration. The configuration shown previously from Figure 19 is presented in the exploded assembly view in the design diagram in Figure 20. The legend in the top right points out the component names and their quantity in the assembly.

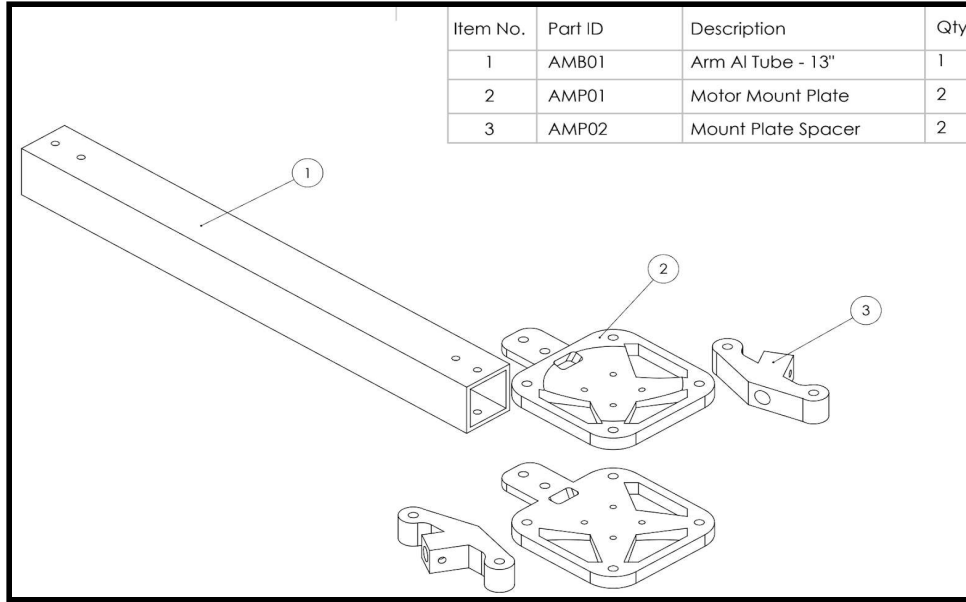


**Figure 20:** Arm Component Diagram showing the exploded view for the assembly of the arm.

The components shown here which secure to the arm are designed to be 3D printed and bolted together. The design designated with part ID AMP01 is the fixture which the motors are secured to. This component is designed to have an indented bowl shape which matches the curve of the motor in order to securely hold it in place and prevent any unwanted movement. In addition, there are sections which were removed in order to allow the wires to pass through the mount and be protected in the hollow aluminum tubing of the arm, as well as sections which were removed to optimize for weight reduction and airflow. The design designated AMP02 is a spacer which secures the two motor mounts together. In addition, these each have ports where

## 4.2 - Chassis and Full Assembly Design Generation

For the development of the design of the drone, initial models were developed using Solidworks for the overall assembly of the drone. As hinted at in the arm design generation, the

first design developed in Solidworks was focused on being robust and strong enough to resist strain from the weight carried by the drone. This initial design contains much larger features such as the wider arms and a thicker chassis. When looking at this design more critically, it became clear that it would not be feasible to construct it while remaining under the 55 lbs weight limit. This design then had to be dramatically altered in order to reduce the weight.

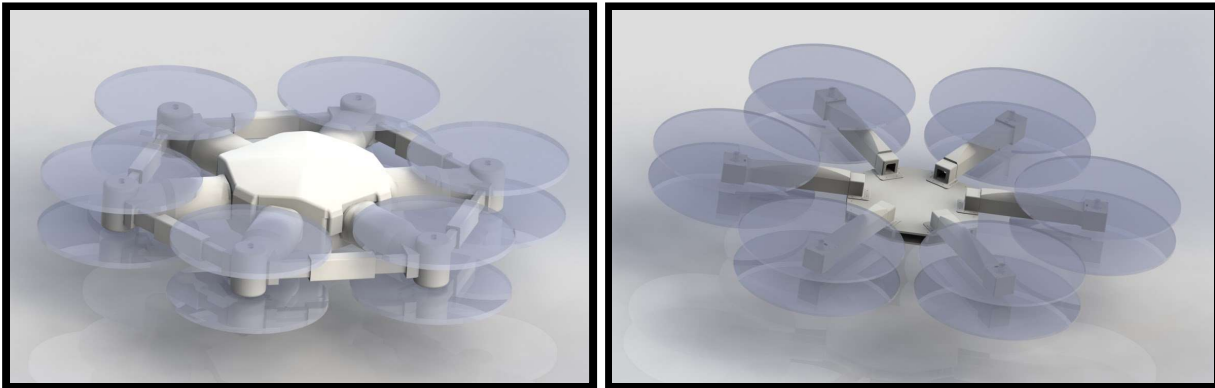


**Figure 21:** Solidworks renderings for preliminary Design 1 (left) and Design 2 (right) of the assembly of the drone. In these figures, transparent features are shown to represent the swept area of the propellers.

**Table 9:** Positives and negatives for the first design of the drone

Positives	Negatives
<ul style="list-style-type: none"> <li>• Safe</li> <li>• Sturdy</li> </ul>	<ul style="list-style-type: none"> <li>• Unstreamlined design</li> <li>• High mass</li> <li>• Difficult to assemble</li> </ul>

**Table 10:** Positives and negatives for the second design of the drone

Positives	Negatives
<ul style="list-style-type: none"> <li>• Lower Mass</li> <li>• More Streamlined</li> <li>• Less difficult to assemble</li> </ul>	<ul style="list-style-type: none"> <li>• Electronics prone to weather damage</li> <li>• High mass</li> </ul>

The second design used much smaller features in order to maintain a lighter overall weight. The thick structure of the chassis was replaced by sheets of plastic used to provide enough volume and strength to hold the electronic components and support the weight. This

design featured the second iteration of the design for the arms as previously discussed. As this design was further examined, it was iterated upon to reduce more weight to continue its goal of being lightweight while still attaining a certain level of strength and ease in manufacturing.

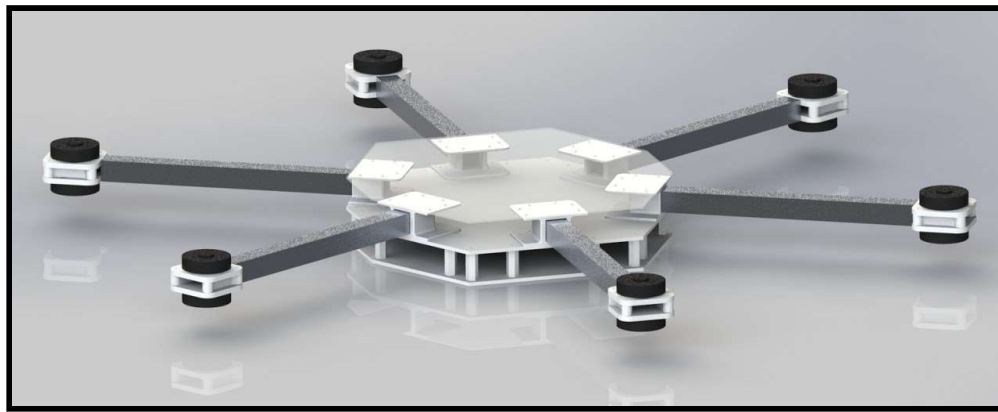


*Figure 22: Solidworks rendering for Design 3 of the assembly of the drone.*

The third conceptual design (presented in Figure 22 above) created for the assembly of the drone was a larger improvement from the previous design where qualities like weight, manufacturability, and cost were kept in focus. This iteration in particular implemented a multilayered chassis in order to keep all of the electrical components secured and protected from elements like wind or moisture. This most recent iteration of the HLD conceptual design represents the last major changes in the geometry - future changes were mostly small. In addition to the chassis and arms, this model also includes the legs that are mounted on the final design. This landing gear system will be discussed later in this chapter.

In addition to these changes, specific components such as the motors, electronic speed controllers, and power distribution boards were added in order to establish a more accurate representation for the physical layout of the system. These are displayed in Figure 23 below which also includes the Pixhawk flight controller, and the receiver antenna to connect to the controller.



**Figure 23:** Solidworks rendering for Design 4 in the conceptual design generation process of the drone.

The fourth conceptual design (presented in Figure 23 above) implemented the fixed landing gear into the design. While this makes the system weigh more, it would mean that the system would be able to more safely take off and land before and after a mission. This also allows the design to handle the possibility of an undercarriage to carry objects, and also allows space for the batteries to be stored.

Although the drone and its various appendages would handle a typical flight (discussed later using FEA in Chapter 6), there was potential for the ducts that attach to the system to be damaged, which can be seen in Figure 44. To help mitigate this the design two primary features were added in order to provide far more support to the ducts. These changes included crossing support tubes that attached from arm-to-arm in order to improve the overall rigidity of the system and prevent deflection between the arms. The next change was to add another support member which extends from the end of the arm to the outermost point of the duct in order to prevent it from deflecting around the end of the structure. These features are displayed in Figure 24 below, along with some of the other features that will be discussed about the fifth and final iteration.



**Figure 24:** Solidworks rendering for Design 5 in the conceptual design generation process of the drone.

In this design, the chassis was enlarged to cover a wider area in between the points where the propellers would attach, and as such the length of the arms was decreased. This change was intended to minimize the area that the drone takes up in addition to improving the stability of the chassis by having a shorter cantilevered length for the arms. By making this adjustment, the weight of the aluminum for the arms was traded for the lighter weight carbon fiber of the chassis. In addition, this larger area led to an increased examination of internal cut-outs through which airflow could pass through the chassis.

The most accurate estimation for the weight of the system can be made from this Solidworks model as well. By assigning the material properties and masses of the various components (these material selections will be elaborated on in Chapter 5), the total mass was estimated to be 33 lbs. This weight represents only the structural components of the drone, but by factoring for the weight of the components added to the model, the total weight is estimated at 37 lbs.

In order to document the concept selection process throughout the various iterations described in this section, a concept scoring matrix was constructed to represent the most important qualities addressed by the different designs. This scoring matrix is presented in Figure

25 below, which includes a holistic rating from 1-5 for a variety of qualities where 1 is a poor rating and 5 is the most optimal rating. These qualities are additionally assigned a weight based on how crucial they are in the consideration for each design. Certain justifications for these weights are further detailed below in Figure 26 as well.

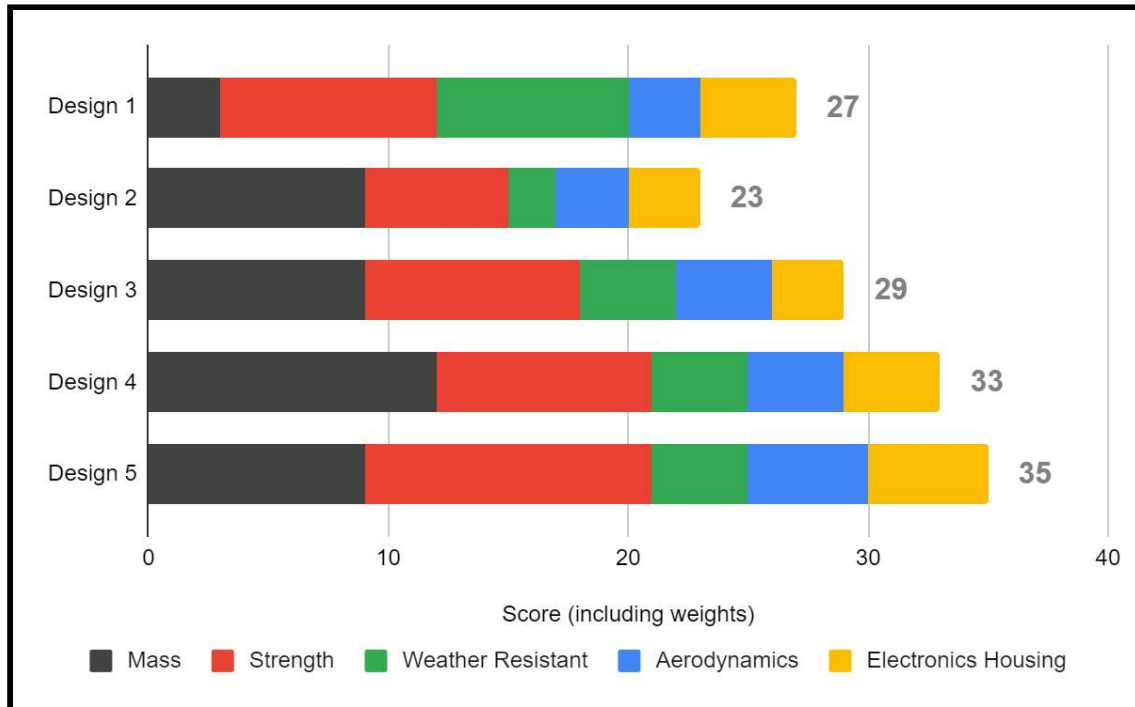


**Figure 25:** Scoring Matrix for Physical Properties. Criteria were assigned weights pertaining to their importance. Mass and Strength were most important so they were given weights of 3, Weather Resistance had a weight of 2, Aerodynamics and Electronics Housing had a weight of 1.

The scoring was split into two tables: one that looked at how well the theoretical drone could perform and another to take into account the difficulty associated with manufacturing the drone and certain parts. Table C.1 and Table C.2 in the Appendix represents both Figure 25 and Figure 26.

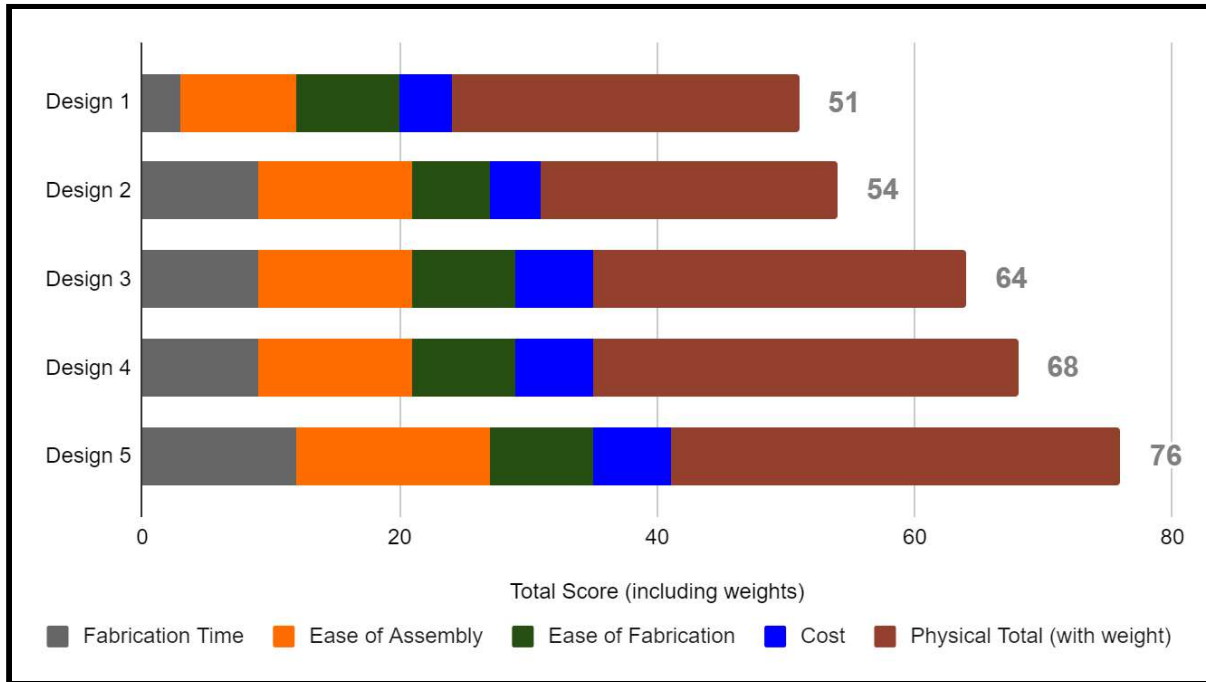


**Figure 26:** Scoring Matrix for Total Properties. Criteria were assigned weights pertaining to their importance. Fabrication Time and Ease of Assembly were given weights of 3, Ease of Fabrication and Cost were assigned weights of 2, and the Physical Total had a weight of 1.

Mass and ease of assembly were chosen to be the most important factors in our design. This is due to the hard limit of 55 lbs takeoff weight set by the FAA, as well as the fact that, during a future flight, this drone will likely be assembled on site and thus must be simple enough to do so. Weather resistance was also an important consideration, as the motors require wires running down the arms to the power distribution boards located on the main chassis, thus exposing them to the elements. In order to accommodate these wires, later designs feature a bore going through the length of the arms in which the wires are housed in. The cost was not a huge factor as we are already well under the market competitions' price points, so any increase in cost, if necessary, can be justified. Additionally, the aerodynamics of the arms, though important, are not critical, as the majority of the drag originates from the central chassis which houses the electronics, and not the arms themselves.

### 4.3 - Undercarriage Design Generation

The next subassembly to be discussed is the concept generation for the HLD undercarriage. The first concept, shown in Figure 27, is designed to have 3 identical legs,

diverging from the center of the chassis by the single connection with two branches that would each attach to one of the arms of the drone. While this design was intended to make the drone as stable as possible to prevent it from tipping, it was quickly determined that this design would impede the motion of the lower set of propellers.

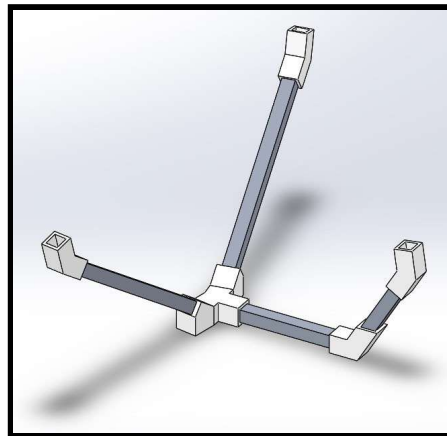


**Figure 27:** A Solidworks model for Design 1 undercarriage generated for the drone.

The second design was focused on being easier to manufacture and assemble along with being less intrusive to the functions of the drone. This design featured two identical legs which would extend downward from the center of the chassis. Each one was designed to form an A-frame-like configuration in order to provide greater structural support. While this design, as presented in Figure 28 below on the left side, would be simpler to manufacture, it was considered less structurally stable if the two sections were not additionally interconnected.



**Figure 28:** Solidworks models for Design 2 (left) and Design 3 (right) of the undercarriage as constructed from aluminum tubing and 3D printed connections.

The third conceptual design then improved on this stability issue as seen in Figure 28 on the right side where the two legs are connected. This design features an A-Frame structure in both directions in order to improve the stability and weight distribution of the structure. Some design additions for this sub assembly include a customizable payload attachment. This means a custom payload can be attached and secured to the undercarriage; these payloads could include geometries such as a structure to carry payloads, supports to attach a gyroscopic camera rig, or a way to secure additional devices.

## **5. Material and Component Analysis**

### **5.1 - Material Screening and Selection**

As mentioned earlier in the text, material selection for the HLD system was critical as weight was to be optimized while still maintaining strength. Therefore, material testing procedures were formulated for this project in order to analyze several different 3D printed polymers. This would allow for optimal material decisions to be made which would be used in many of the drone's structure components. For such decisions, material selections were made based on the findings of these tests with an emphasis on selecting the material with the most beneficial balance between strength, weight, manufacturability, and cost. This section discusses the analysis, conclusions, and applications that can be drawn from the material testing that was performed.

#### **5.1.1 - Materials**

In selecting materials for the motor fixtures and ducts in the system, focus toward balancing weight with strength was important as our system needs to lift payloads successfully. The materials selected for these tests were primarily 3D printed polymers as this is the intended manufacturing method for many of the structural components of the HLD. Several characteristics of the 3D printing manufacturing process were considered, including the infill volume, the external wall thickness, and the support structure.

To begin this process, a screening selection was created using CES EduPack in order to identify a wider variety of materials and ensure that our selection was geared towards weight reduction while maintaining strength. Using CES, various mechanical and thermal parameters such as glass point and melting point were utilized as input filters to obtain viable results. Figure 29 and Figure 30 show the material screening selection that was conducted for the polymer used in the 3D printed components and the metal used for the structure of the arms.

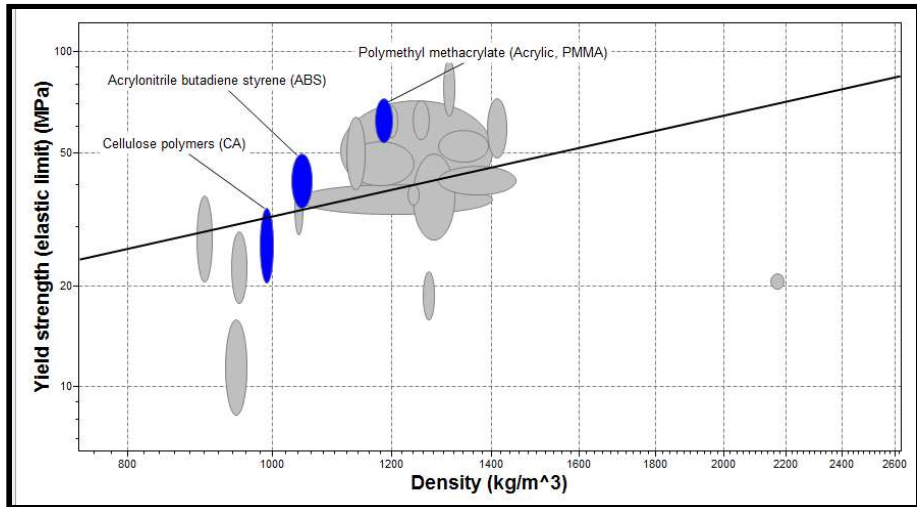


**Figure 29:** Various Polymers Density and Yield Strength. Plots generated in CES Edupack

In both Figure 29 and Figure 30, the greyed out ellipses indicate that these materials do not satisfy the required conditions, meaning that the yield strength - density line crosses through some part of these ellipses.

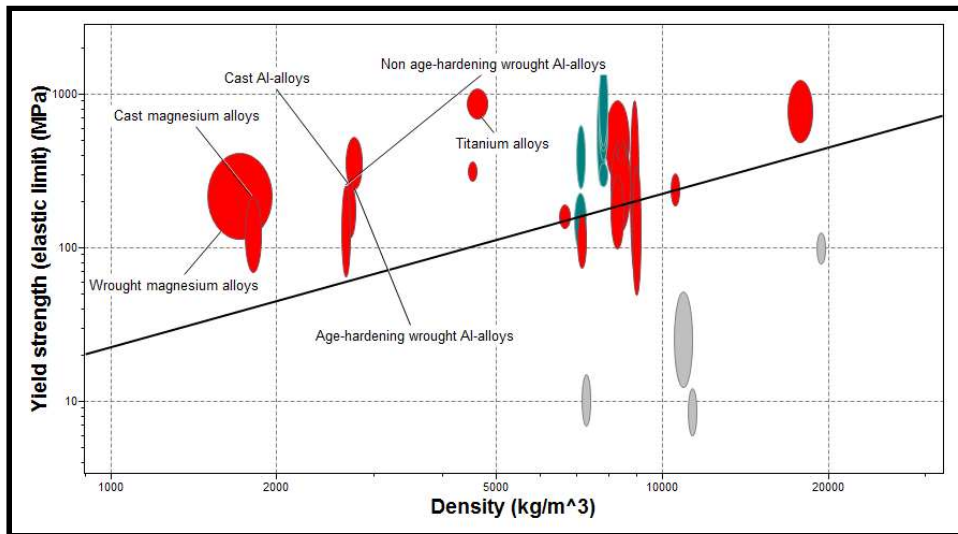


**Figure 30:** Various Metals Density and Yield Strength. Plots generated in CES Edupack

Based on the material screening process and the guidance of members from the Santa Clara University Maker Lab, several materials were chosen to examine further for 3D printed filaments. The materials that were selected for testing are:

- Carbon Fiber Filament - ColorFabb XT-CF20
- PETG Black Filament - Prusa PETG
- ABS Black Filament

With each specimen created for these material tests, an examination of the density was conducted based on the mass using different materials produced at different volume infills. This density was compared between the different trials to determine a ratio between strength and density.

### 5.1.2 - Tensile Tests

Tensile tests were conducted using 3D printed specimens that were formed in the geometry shown in Figure 31. Because these 3D printed specimens had different infill properties, their material properties were slightly different compared to the typically reported values for these materials. The tensile test was conducted using the Instron Low Force Universal Testing System in the Santa Clara material testing lab using displacement control. Each specimen was placed in tensile loading until failure of the part occurred where fractures were evident.

Because of the potential for brittle layers to separate in 3D printed parts, one common cause for failure was splitting along layer boundaries followed by a transverse fracture across the specimen. At higher density, such as the PETG with 50% volume infill, the specimen exhibited a cleaner fracture pattern, where it split evenly across the cross section of the specimen. Some detailed images of the fractured state of these specimens are presented in all entries of Appendix E. These specimens were tested in order to determine their material properties including yield strength and ultimate tensile strength.

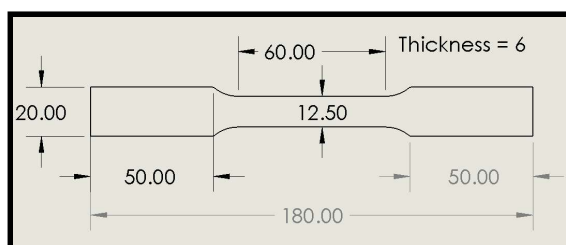


**Figure 31:** The tensile test specimen was created using 3D printing. All dimensions in mm.

This information could be utilized to determine the factor of safety for predicted loading conditions to a greater degree of accuracy compared to Solidworks materials simulations. This could be more accurate since standard values for polymers are limited in the solidworks library, and they all assume that parts are solid. A stress-strain plot of such tensile tests is shown in Figure 32, where the three materials are pictured.

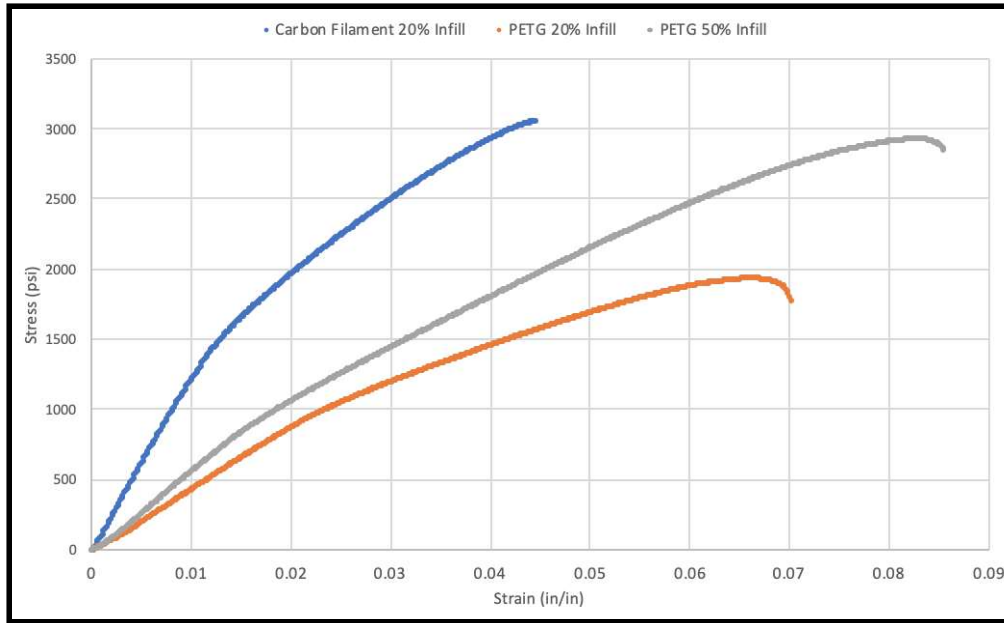


*Figure 32: Stress plotted against strain for three different materials.*

The results of these tensile tests prompted discussions about the optimal material to be selected for the construction of the drone's components. The carbon polymer filament was the leading candidate as it was supposed to have a higher strength than other polymer filaments while staying very lightweight, and this tensile test confirmed that. Although the carbon polymer had a higher strength, the PETG had a higher overall toughness which means it would be more suitable. The most essential results of these tensile tests and the conclusions that can be made from them are presented in Table 11.

**Table 11:** Summary of the purpose, results, and conclusions for the tensile tests.

Purpose	Results	Learning Outcome
To measure the strength and toughness of various polymers	Carbon Filament has highest yield strength	PETG has a higher toughness but Carbon Filament may be stronger at lower infills - i.e. lower strength to density ratio

### 5.1.3 - Bending Tests

In addition, bending tests were conducted using 3D printed specimens in the dimensional layout shown below in Figure 33. As with the tensile tests, these specimens were printed from Carbon Fiber filament at 20% volume infill, and PETG filament at 20% and 50% volume infill.

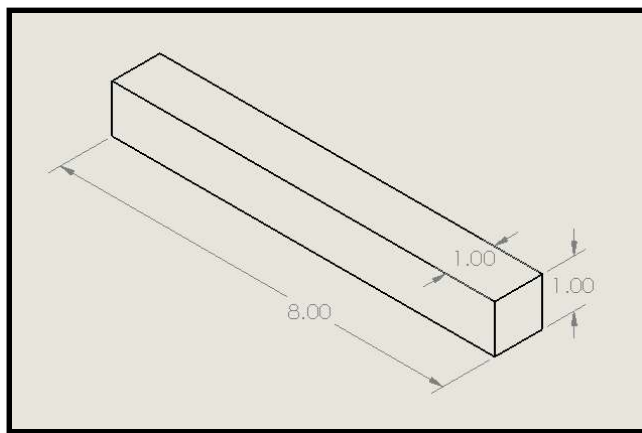


**Figure 33:** The bending test specimen was created using 3D printing. All dimensions in inches.

The bending test was conducted using the MTS Landmark Servohydraulic Test System in the Santa Clara material testing lab. This was performed as a four point bending test with the high strength bend fixture. The tests were conducted using displacement control, following a prescribed speed up to a maximum limit of 20 mm of displacement, however the test was typically stopped when failure occurred, which was characterized by notable deformation in the specimen or evidence of layer separation. Additional images of the testing configuration as well as the failure conditions of the parts are presented in all entries of Appendix E.

The combined results of these bending tests are presented in Figure 34 below so that comparisons could be made between the three specimens. In this figure, the bending behavior of the carbon polymer filament can be compared with that of two different samples of PETG at varying levels of infill.

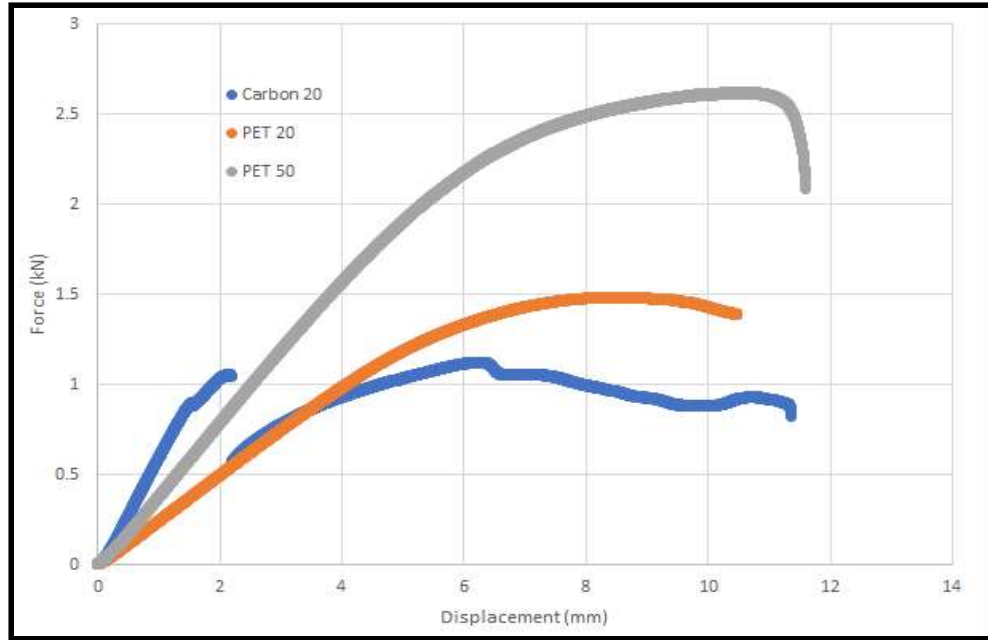


**Figure 34:** Combined bending behavior (force vs. displacement) resulting from the tests with each of the three specimens.

From these results, greater insight into the behavior of these polymers was revealed. While previously the carbon polymer was more favorable for its tensile strength, the specimen ultimately reacted very poorly in bending. The carbon polymer (represented by the series in blue) had initial layer separations from the 3D printing process (using a Prusa 3D printer) where multiple samples had similar notable errors from printing as well. The potential problem is still vague, though it was hypothesized that a proper extrusion speed and extrusion tip temperature among other unforeseen variables could be optimized to produce better prints with the carbon polymer. As reflected in the testing summary table, Table 12, presented below, the conclusion can be drawn that a more consistent material should be selected instead of the carbon polymer, despite its good strength and density properties.

**Table 12:** Summary of the purpose, results, and conclusions for the bending tests of these polymer specimens.

Purpose	Result	Learning Outcome
To measure the bending strength	PETG 50% Infill performed bent the least.	3D Printed Carbon Polymer has layer separation issues and thus cannot be used.

#### 5.1.4 - Material Testing Conclusions

Based on the findings from the material screening and the results of the material testing, several decisions were made for the subassembly designs of the drone. The initial benefits seen in using the carbon polymer filament were its higher strength and lower mass. However, due to the unreliability in the printing process with this material, it was found to have too many issues such as layer separation when subjected to bending. These findings lead to the decision to use PETG, a different polymer than ABS that also has good strength properties while maintaining a very high reliability in manufacturing. This was identified through CES and expanded upon in further tensile/bending tests.

In addition, the screening process conducted for a variety of metal materials guided the selection to choose an aluminum alloy for the metal components of the drone due to its balance of high strength and low weight. This aluminum was a 6063 Al alloy, and it comprised the arms and legs of the final product to ensure best performance.

#### 5.2 - Motor Selection

In addition to the selection process for the HLD materials, a great deal of consideration went into the process of selecting the best components to use for the functionality of the drone. One such process was the selection of the optimal motors that would be used to allow flight to occur where control was also considered.

The manufacturer selected for the motor is a company called T-Motor, one of the leading companies in making small scale multicopter motors for larger systems such as heavy lifting drones. While there were many selections available, a primary screening process was conducted to show which motors could meet the thrust requirements of lifting 55 lbs at approximately 70% throttle. This comparison is presented in Figure 35 below, in which the thrust and throttle information for ten different models are compared.

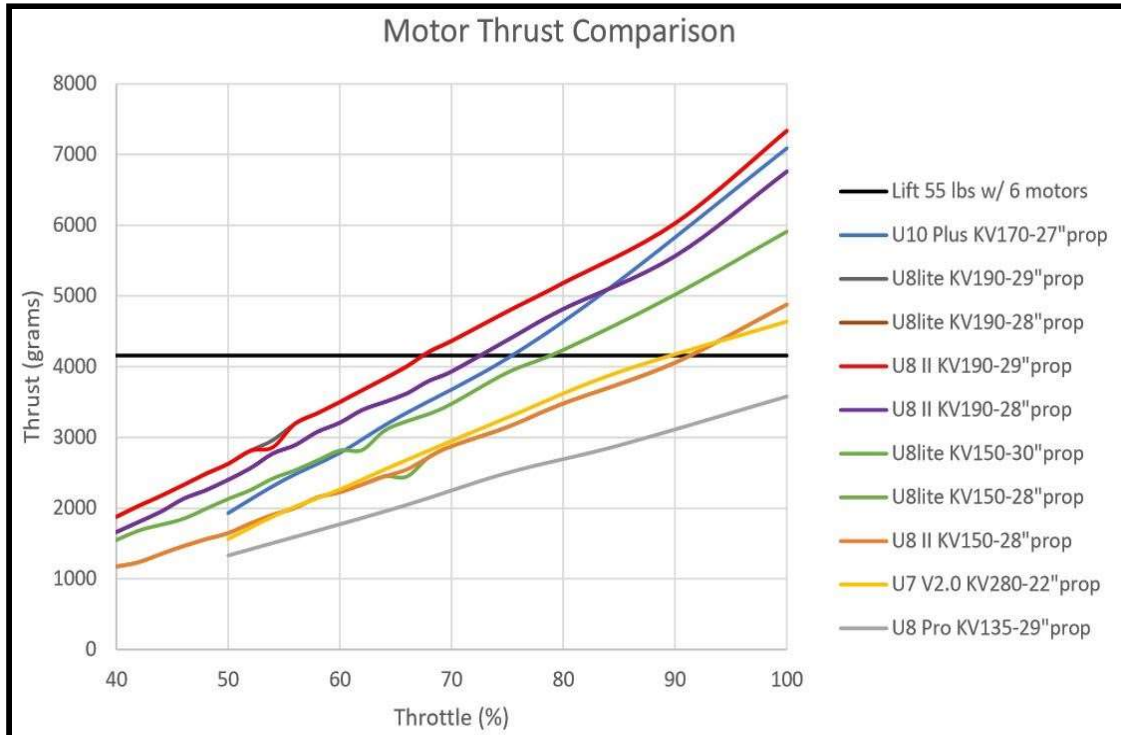


**Figure 35:** Thrust comparison between ten motor models from T-Motor based on thrust at different levels of throttle.

Considering this initial screening process, several models rose to the top of the list for consideration. These motors were selected based on their ability to generate the thrust required to lift a 55 lbs system at a reasonable throttle percentage of 70%, to avoid overheating the motor and damaging the electrical and mechanical components. The initial selections considered from this screening process were then narrowed to two models: the U10 Plus KV170 and the U8 II KV190. The deciding factor that went into the selection between these two models was the weight of each. While the U10 Plus KV170 had the potential for a lower throttle rate for take off, its mass (511 grams) was almost double that of the U8 II KV190 (277 grams). Ultimately, the decision was made to use the U8 II KV190 motors due to its weight and its potential for a takeoff

thrust around 70% throttle. The characteristics of this particular motor are presented in Figure 36 below in order to highlight its behavior.

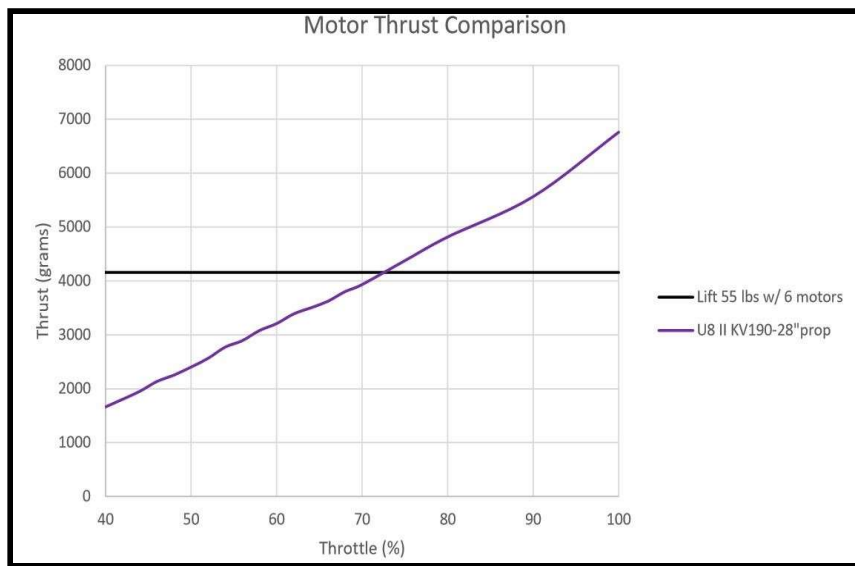


**Figure 36:** Plot for comparing potential thrust at different levels of throttle for the selected motor: U8 II KV190.

## **6. Aerodynamic and Mechanical Analysis**

### **6.1 Operating Conditions for Analysis**

To meet the primary goal of creating a drone capable of lifting a total system mass of 55 lbs for a 20-30 minute flight duration, it was critical to model the most vulnerable parts of this system - those that experience the highest stresses. This included key parts and subassemblies in the aeronautical and mechanical subsystems of the drone. In addition, the aerodynamics of the systems' propellers and ducts were critically examined to identify simulated values versus commercially reported values and to determine how optimal the ducts work to increase air flow.

The ideal environment under which these subsystems would operate is characterized by minimal wind speed, standard temperature and pressure conditions, no precipitation, a level surface on which the drone lands upon, as well as an obstacle free airspace. With a level surface, an equally distributed force on the landing gear ensures the system does not undergo shearing or concentrated forcing.

### **6.2 Aerodynamics Subsystem**

The main purpose for the implementation of ducts is to cause a faster airflow to be developed by the 28 in. propellers. This is explored in ducted propeller theory where air flow in a ducted environment flows at a quicker velocity than an unducted system. The other benefit is that noise is reduced (that is not a part of this analysis and will be saved for future testings and implementations of the project). Before simulations were created, a few calculations regarding the aerodynamics of the system were completed to consider what thrust is needed for the system and whether turbulent flow was achieved within the ducts. These calculations can be found in a Section 6.2.4 which lay out the minimum flow speed the system needs to achieve for turbulent flow.

#### **6.2.1 - Propulsion Calculations**

For the ducted system, Bernoulli's equation was used in order to determine the necessary velocity [15]. This was used to justify the use of a duct (i.e. ensure turbulent flow in the system), as shown in equation 1 below:

$$\frac{P}{\rho} + \frac{v^2}{2} + gh = const \quad (\text{Eq. 1})[15]$$

where P is the pressure at a specific point,  $\rho$  is the density of the fluid, v is the velocity at a specific point, g is the gravitational acceleration, and h is the elevation at which the specific point is located. All of this assumes a region where steady flow is occurring while the density of the fluid remains constant, no friction is imposed on the fluid, the flow is along a streamline, and no heat/work is generated [16]. Since the flow is most likely turbulent due to the propellers contained in the system that stir the air rapidly, many of these rules break down, hence the conservation of linear momentum must be applied.

For the thrust, the force was based on the weight needed for each arm to lift (9.2 lbs), and the velocity of the propellers needed to achieve that thrust. A Reynold's flow calculation determined whether turbulent or laminar characteristics were present along with what the minimum speed for turbulence is. The ducts' corrugated edges serve the purpose of "tripping" the boundary layer and ensuring that turbulent air flow is achieved.

Given standard sea level conditions:  $\rho = 1.225 \text{ kg/m}^3$  and  $\mu = 1.77 \times 10^{-5} \text{ kg s/m}$ . The minimum speed to ensure turbulent flow needs to be found so that the propeller rotation meets that minimum. For turbulent flow the Reynold's number, Re, should be at least 4000. Where

$$Re = \frac{\rho V D}{\mu} \quad (\text{Eq. 2})[16]$$

To meet that minimum Reynold's number, the equation is modified where  $D = 0.7112 \text{ m}$ .

$$\frac{\mu Re}{\rho D} = V \quad (\text{Eq. 3})[16]$$

The velocity V is then equal to  $0.08214 \text{ m/s}$  which is far slower than the speed of the propellers (being  $92 \text{ m/s}$ ). After proving the system is turbulent, computations can then be conducted with this assumption.

Using Reynolds Transport Theorem in order to evaluate the fluid for the conservation of linear momentum, the flow in the y-direction can be mathematically modeled as:

$$\Sigma F_{applied,y} = \frac{d}{dt} \int_{cv} v_y \rho dV + \int_{cs} v_y \rho v_{rel} dA \quad (\text{Eq. 4})[16]$$

where the applied force  $F$  is considered the thrust imposed by the propellers. Additionally, the control volume integral encompasses the product of the velocities in the  $y$  direction and the density of the fluid medium (being air in this application). Furthermore, the control surface integral also includes the same product as the control volume integral along with the inclusion of relative velocities in the  $y$ -direction. The expression can be simplified as the following expression relating the mass flow rate and velocity to thrust:

$$\Sigma F_{applied,y} = m_e V_e - m_o V_o \quad (\text{Eq. 5})[16]$$

where  $m_o$  is the entering mass flow rate,  $V_o$  is the entering velocity,  $V_e$  is the exiting velocity, and  $m_e$  the exiting mass flow rate. This equation only requires an inertial frame of reference to be declared along with the summation of all the applied forces in  $y$ -direction to form the total applied force in the system. Since the thrust of the propellers is already predetermined to be a value equal to or greater than 11.25 lbs each, along with the density of the air which is known at sea level and the velocity of the air coming into the ducted system roughly equal to 3 m/s (10 mph), the output velocity  $V_e$  is to be determined in order to satisfy the equation 3.

The system uses 55 lbs as the weight requirement which is equivalent to 25 kg. That is lifted by six arms so each arm-propeller system will lift 4.167 kg which can be converted into a force via Newton's Second Law:

$$F = ma \quad (\text{Eq. 6})[17]$$

For this equation,  $m = 4.167$  kg and  $a = 9.81\text{m/s}^2$  so each arm system must provide 40.88 N of lifting force. This can be used to find the necessary mass flow rate to find the speed of the fluid to develop this force.

$$\begin{aligned} mV &= F \\ \rho VA &= m \\ \rho V^2 A &= F \end{aligned} \quad (\text{Eq. 7})[17]$$

The density, is equal to  $1.225 \text{ kg/m}^3$ ,  $A$  is equal to the area of a circle:

$$\frac{\pi d^4}{4} \quad (\text{Eq. 8})[17]$$

Where  $d$  is the diameter of the midsection: at 28" which converts to 0.7112 m.  $A$  is equal to  $0.3923 \text{ m}^2$  so rearranging the equation to find velocity  $V$  yields:

$$\rho V^2 A = F \quad (\text{Eq. 9})[17]$$

$$\sqrt{\frac{F}{\rho A}} = V \quad (\text{Eq. 10})[17]$$

Where  $V$  is equal to 9.165 m/s. Additionally, considering the propellers in their isolated system (without duct application), their rigid body rotation can be described by fundamental equations of motion:

$$s = r\theta \quad (\text{Eq. 11})[17]$$

where  $s$  is the position of a particle on a circular path which is described by the radius  $r$  and the angle  $\theta$ . Taking the time derivative of Equation 3 (where the radius is considered to be a constant value), Equation 5 is obtained, where  $v$  is the velocity at radius  $r$  with respect to the angular velocity  $\omega$ .

$$v = r\omega \quad (\text{Eq. 12})[17]$$

Given this rotation, the angular velocity can be utilized in Equation 5 with a radius equal to half the length of the propeller. This results in a tangential velocity at the tip of the rigid body, which is used to obtain the maximum pressure differentials at a 70% throttle, leading to the lift generated by one propeller blade at a given speed.

### 6.2.2 - Duct Introduction

The ducted system was a key feature that distinguishes the HLD from other competitors. Although the ducts add weight to the system - which in turn lowers the overall capacity for the payload, the addition of these ducts ensures a safety measure and noise reduction for the system. Lastly the most important factor for adding the ducts was to test out whether the ducts sped up the airflow leaving the propellers enough to warrant the additional weight, to verify the current information on ducted systems.

#### 6.2.2.1 - Expected Output/Modes of Failure

The failure criteria for the duct system differs from typical failure modes in most forms of analysis such as yielding or fracture. The primary metric (and thus failure criterion) for

determining the success of the duct system is whether it makes the lifting capabilities of the drone more efficient compared to a similar system with no ducts. To gain insight into how this system makes a difference, the change in thrust with the addition of the ducts is compared to the weight of the subsystem to determine whether the addition of the duct is worth the weight. For the system to be successful, the increased speed should result in a beneficial critical mass flow rate compared to a ductless iteration.

#### **6.2.2.2 - Material Selection**

The duct subsystem has a complex geometry that requires precise manufacturing and a smooth surface in order to effectively control the airflow through the system. Due to these requirements, the ducts were fabricated using 3D printing and assembled in order to ensure that the system was accurately produced. The material initially chosen for producing the ducts, as well as for the purposes of the simulated analysis of the system, is ABS polymer filament. This material was selected due to its weight being relatively low and its structural properties being quite strong. However, due to the issues with printing ABS (such as the tendency to warp during print) the material was switched to PETG because it is only slightly more dense than ABS. It is also a very rigid, accurate, and light polymer to use in the 3D printing process, making it an effective choice for this application. Aero grade sheet metal was also an option (indeed it possesses better properties than PETG), however, it cannot be easily manipulated into the shapes required for our design.

#### **6.2.2.3 - Duct Design and Iterations**

For the ducts, the primary metric used to determine a successful duct design or addition to the drone is if the increase in lifting power outweighs the duct's additional load on the chassis. As the boundary conditions in this model are assumed to be turbulent (although a laminar model is theoretically possible), many different relations were considered and are explored further on. To picture the airflow through the duct and the resulting turbulence, a rudimentary sketch of the configuration of the duct is shown in Figure 37.

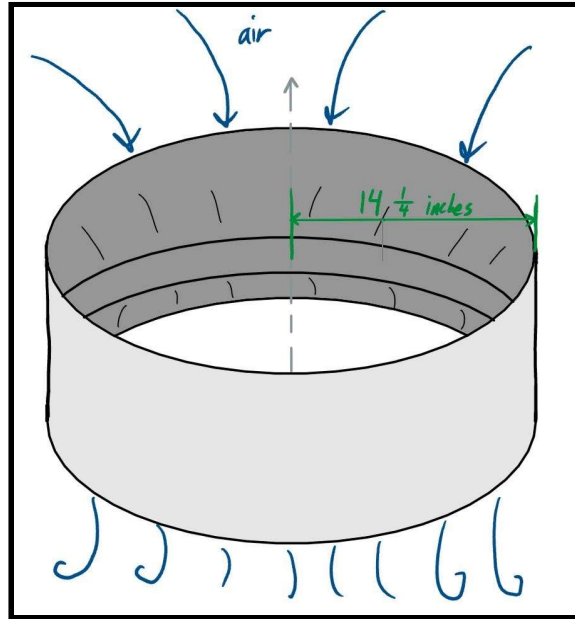


**Figure 37:** Rough sketch of the duct where air circulates through the lift efficient structure.

In developing the solidworks model for the duct, three different designs were implemented in CAD and simulated to determine which of the designs allowed for faster air flow. The first most simplified model was used for verification of the flow simulations, as presented in Figure 38.

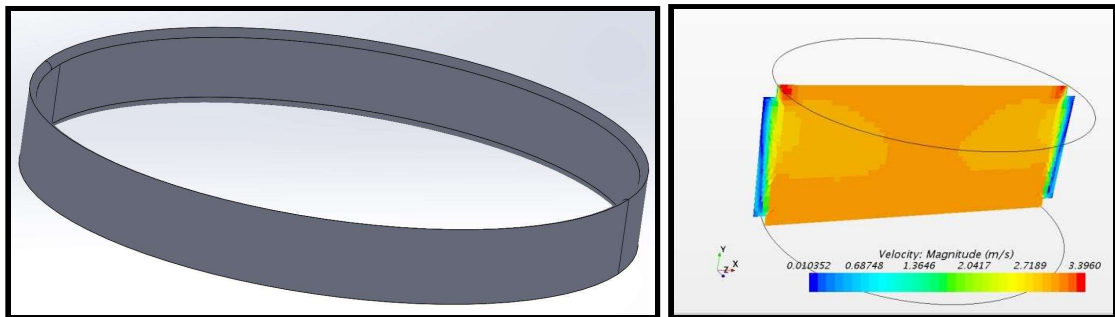


**Figure 38:** Cylindrical 29 inches in diameter duct, and the simulation done with this design.

This design showed that the presence of the walls in the system provide a boundary layer which concentrates the airflow in the center. The next designs were created to iterate on this attribute while exploring different cross sections.

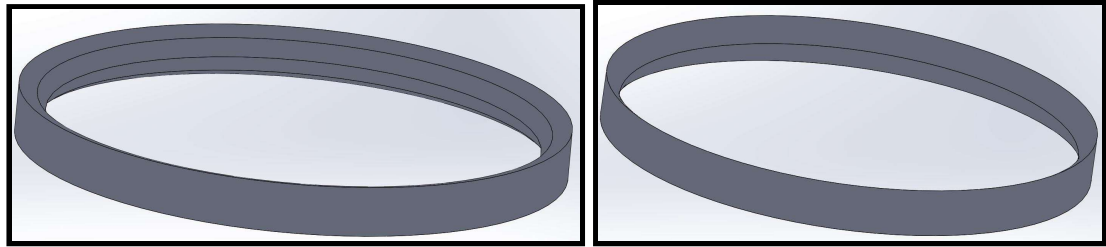


**Figure 39:** Linear converging/diverging duct of 29 inches in diameter. Parabolic converging/diverging duct of 29 inches in diameter.

When simulations were run for these two designs, the results showed that the more the ducts converge inward, the greater the flow increases in speed - due to a greater change in pressure. However, it also showed that the convergence in the parabolic duct had a smoother transition to turbulent flow before the throat than the linear duct, while the linear duct had greater flow after the “throat” in the duct. This revealed valuable insights into the duct design, and with inspiration from a Venturi Valve, the next design was created.

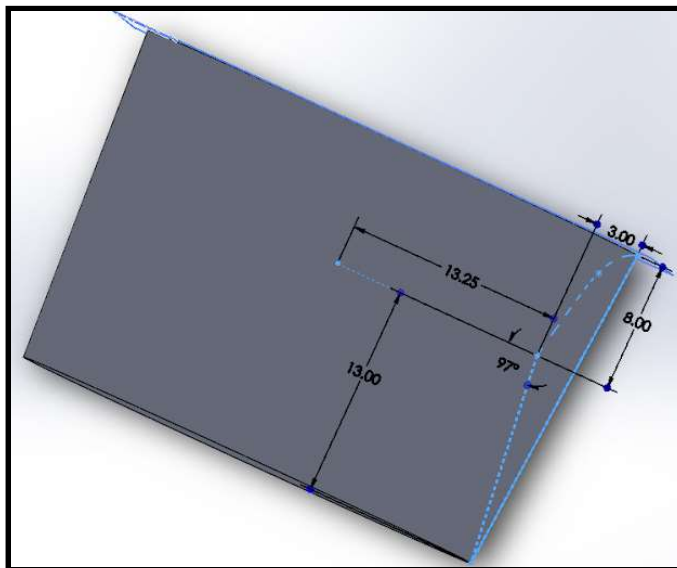


**Figure 40:** Implementation of a parabolic leading edge and a linear trailing edge for the duct cavity.

From this design a simulation was run to look at the change in velocity and see how well the increase in airflow was conducted. This was carried out STAR CCM+ where a basic velocity plot was generated.

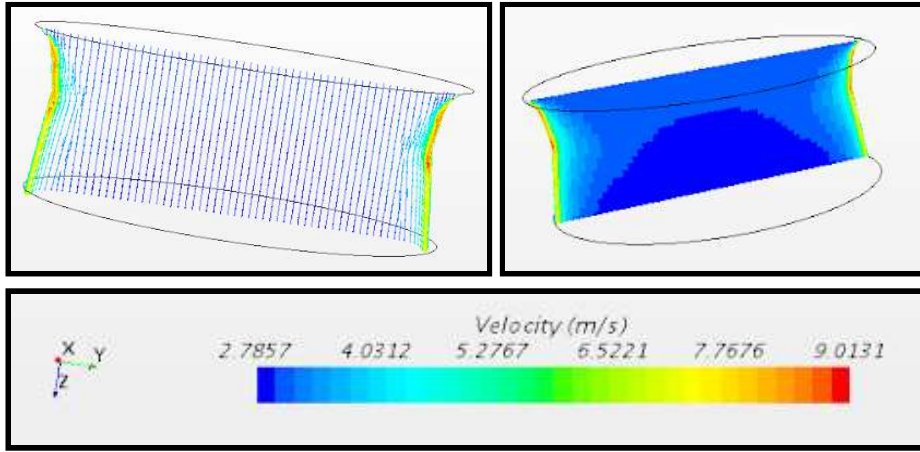


**Figure 41:** STAR CCM+ simulations of parabolic leading edge duct.

Initially simulations only needed to show that the duct, when air is flowing through its cavity, speeds up this air flow. A design would then be chosen that allowed for the greatest increase in air speed. After this, we showed that the next important measure is to determine whether the airflow was turbulent or laminar. With assistance from our fluid dynamics advisors and taking inspiration from Boeing's Turbojet engines, the next change to the system was made, which was the addition of corrugated features on the leading edges and a serrated feature on the trailing edges.

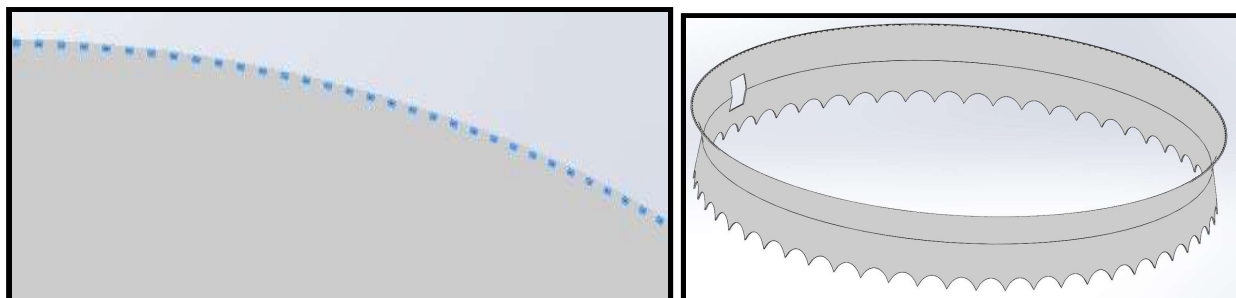


**Figure 42:** Model of a bump feature on the ducts.

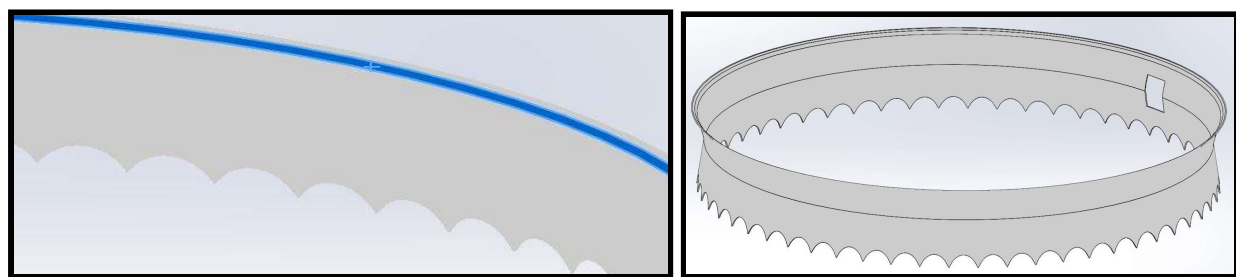


**Figure 43:** Model of a lip feature on the ducts.

Both of these ducts were developed as a proof of concept. Although the project ultimately pursued the lipped design due to the lower computation time, the other design can warrant additional simulations and exploration.

To go along with the testing and simulations of the ducts, an accurate CAD model of the 28 inch propellers (which were a recommended pairing with the U8 II motors by T-Motor) were developed in the attempt to model the rotation of the propellers and the subsequent airflow. These analyses take into account the propeller's geometry and the speed at which air is interacting with the rigid body. With the propeller rotating at a certain rate, the average velocity over the entire blade was chosen for the flow potential calculations in order to obtain maximum pressure differentials at a chosen throttle percentage. These propellers will be discussed in a later section which highlights the types of simulations that were done in order to understand how effective the ducts are and how well the aerodynamic subsystem is designed.

#### 6.2.2.4 - Final Duct System

After the duct design was finalized and support structures were implemented to improve the rigidity, several simulations were conducted, each of which added a level of complexity to the system. Seen below in Figure 44 is the Finite Element Analysis of the ducted system after a support rod was added, drastically increasing the duct's rigidity, and allowing the propeller to spin inside the duct without touching its sides.

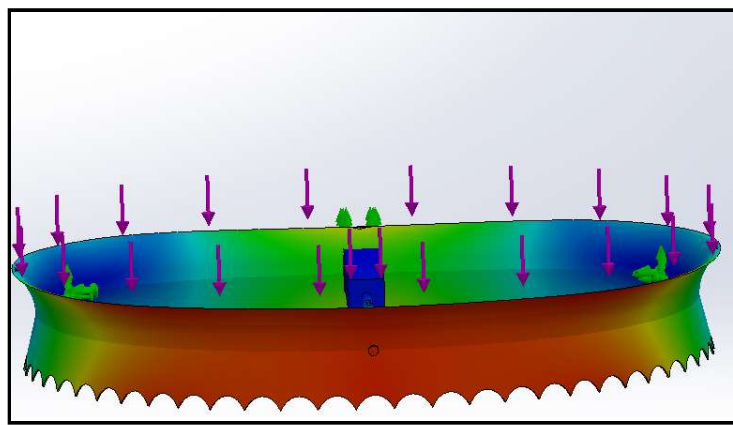


**Figure 44:** Rod Attached to Back of Duct Increases Rigidity

The duct featured in Figure 45 below shows how the duct successfully performs the purpose of speeding up airflow, although it simulates the duct independently of any attachments. After this simulation was conducted, the rest of the arm system was added to see the effects of the system. Along with that a “ground” was added to the simulation to show how ground effect changes the behavior of the airflow.

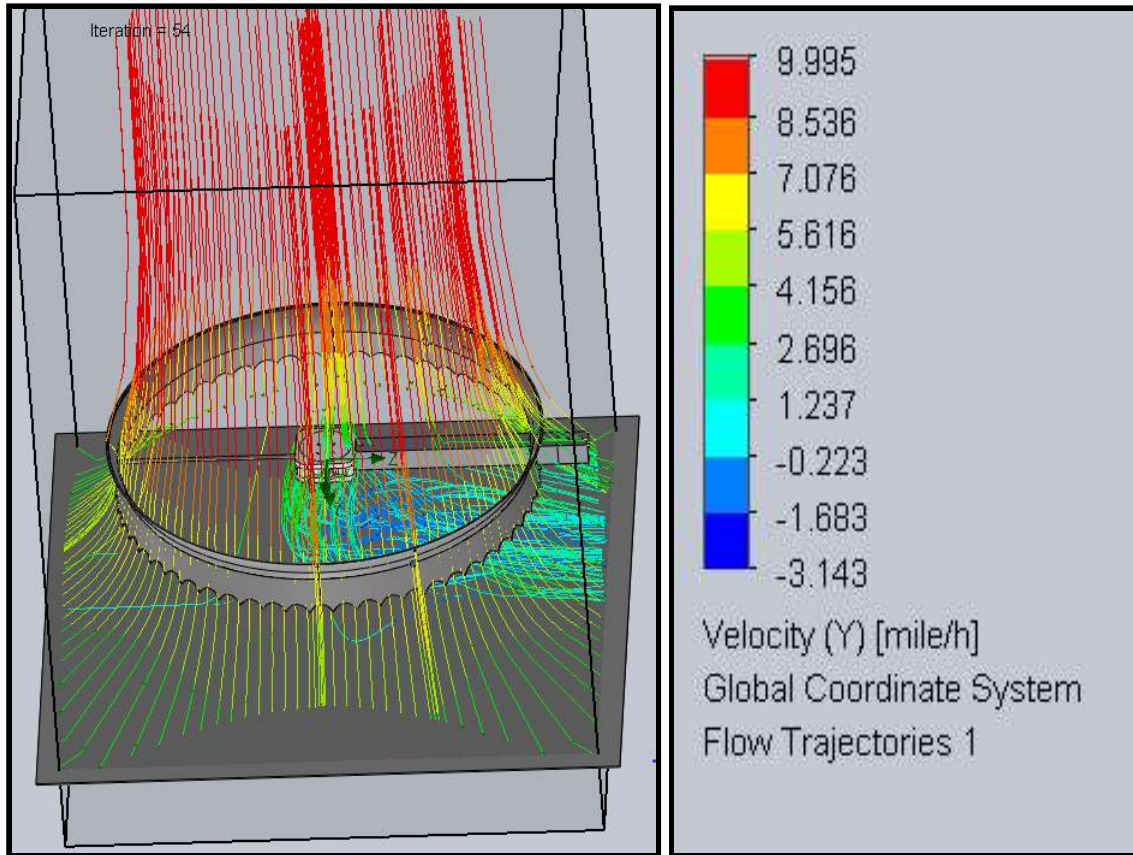


**Figure 45:** Simulated duct and arm system undergoing a 10 mph airflow.

From the many simulations shown, it was observed that as the smallest inner diameter decreases, compared to the largest inner diameter, the air flow speeds up. It was also found that the local shear on the edges produced larger velocities in the control volume. There are proposed pathways to making further iterations such as radius, spline equation, and different designs for the corrugated edges and serrated edges (including different depths and widths of the troughs and peaks). If more changes were to occur in this duct design (for future iterations of this project), such as duct thickness and shape, more simulations will be needed to produce an accurate motion and fluid study (including the propellers, not just the duct). The current model of the duct

incorporates a parabolic airfoil composed of a serrated trailing edge and a corrugated trough on the leading edge seen in Figure 43. Future designs would benefit from incorporating another ring of corrugated bumps on the lip of the leading edge.

From Figures 41, 44, and 45, it was observed that a pressure differential exists when a flow interacts with a physical object. This difference generates a low pressure zone above the propeller and a high pressure zone below, causing lift in the system. This simulation serves as a basic representation of what is occurring in the propulsive system. By doubling the lift value found in this simulation (for each blade on the propeller), the total lift of the propeller could be estimated. Indeed, in further analyses in which the entire ducted system was analyzed, this was confirmed to be true. Furthermore, if this resulting value is doubled again to accommodate the contra rotating propeller below, an estimated lift magnitude for each arm can be found.

### **6.2.3 - Propellers**

The propellers are the source of thrust used by the system to take off successfully, as well as to fly around in different directions. Although traditional set ups offer a single motor-propeller combination for each arm in a given configuration, this system supports a contra rotating version where two propellers are present for each arm. This features propellers spinning in opposite rotational directions from one another, mixing the air, thus increasing airflow, and causing more thrust to be generated. Modeling this specific characteristic for our system reveals insight on how to optimize the system and predict its behavior.

#### **6.2.3.1- Expected Output/Modes of Failure**

The primary metric for determining the success of the propellers in the aero subsystem is if they provided sufficient lift to allow the HLD to take flight. The propellers were modeled with accuracy in mind, while maintaining some simplicity for computational purposes. Initially, a singular propeller was designed and subjected to a flow simulation analysis to verify the specifications outlined by the manufacturer of the motor-propeller combination T-Motor (see Figure 46). Once this was observed, the second propeller, which completed the contra rotating system, was implemented and evaluated, and a duct was later used to envelop the subassembly. Later, a comparison was made to validate the presence of the ducts in the system, proving that

they serve their initially proposed purpose, which was to increase the overall system lift. Failure criteria such as impact to the propellers from a foreign object was not explored though that may be an area of interest for further exploration. If the ducted system performed less efficiently in terms of velocity compared to a ductless system, then it would confirm that the ducts were not worth their additional mass to the system. The duct flow simulations in Figure 44 show that this is not the case, however.

#### 6.2.3.2 - Material Selection

As explained in Section 2.2, the propellers were chosen primarily as a complement to the motor choice. T-Motor, the manufacturer of the motors, highly recommended pairing them with the propellers we chose. These 28 inch diameter propellers are shown below in Figure 46 where they are made of carbon fiber allowing light weight properties to be coupled with high strength.



*Figure 46: T-Motor's 28 Inch Carbon Fiber Propeller.*

The choice of a carbon fiber based propeller instead of a plastic one was partially justified by evaluating a scenario in which it was to undergo an accidental collision with a foreign object. Knowing the strength of both materials, a high velocity fragment that has been chipped off of a propeller during a failure caused by impact with an object results in a much larger safety risk for carbon fiber than plastic. This is because plastic tends to break apart and crumple compared to the much stiffer carbon fiber. This scenario is addressed further in the safety documentation section, which can be found in the Robotics System Lab's Database.

#### 6.2.3.3 - Propeller Design

In modeling the chosen propeller, significant attention was directed towards designing the most accurate geometry that resembled the chosen propeller. Propellers are largely similar to an airfoil in design, with much more twist along their long axis, resulting in a curved body. An initial attempt was modeled alike to a non-concave airfoil, similar to an ellipse with pointed edges on the semi major axis. This simplified design served the purpose of understanding the

basic look of airfoils while building up to a much more accurate model. With more precise propellers changing in cross sectional shape and size along the long axis of the body, the chord and its relative angle to the base were noted when measurements were taken on the physical model similar to the previous figure. The resulting design was imported into Solidworks as an assortment of cross sectional areas lofting from the base to the wing tip and is shown below in Figure 47.

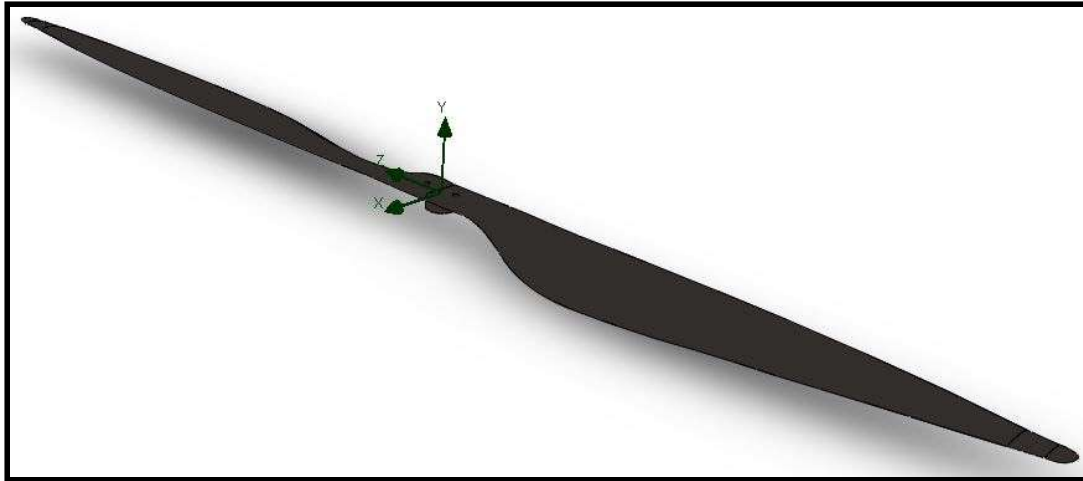


**Figure 47:** More Accurate Propeller Design.

This was achieved by arrays of x and y coordinates at specific locations along the length of the blade, that mapped out the multiple station's cross sections of interest, which were imported from MS Excel to Solidworks. As shown in Figure 47 above, the design achieved the level of accuracy needed for modeling the aero body accurately while still ensuring a simplistic approach to the complex geometry.

#### **6.2.3.4 - Propeller System Analysis**

With the detailed design shown previously, analysis concerning the modified airfoil could be carried out with specific behaviors in mind. As discussed in the beginning of the aerodynamics section concerning calculations, each propeller-arm assembly is to achieve a certain level of thrust in order to elevate it from the ground. Looking into a flow field would yield resulting velocities around the system, similar to calculations in Section 6.2.1, and they would allow for the thrust to be found. Computationally, Solidworks can solve for drag and

lifting forces as well, although the primary interest in the HLD's case was the increased velocity as a result of the inclusion of the ducts.

Integration of the propeller to the arm subassembly was initially carried out in order to model the local control volume accurately. Afterwards, a computational domain was set up as the control volume where the fluid simulation solver can utilize these boundaries for finding local velocities. Typical sea-level characteristics were included in the study as the drone would most likely be operating at STP (standard temperature and pressure) conditions. Looking back at Figure 36, one can see that takeoff would occur around the 70% throttle range for a dodecacopter system. Since this system takes advantage of a contra rotating propeller layout, an estimation of a 20% benefit is granted to the system compared to a twelve armed system without contra rotating elements. With that 20% increase in lift efficiency, the rotation of the propellers is associated with the 50% throttle percentage value equating to around 2000 rotations per minute (rpm). That 2000 rpm rotation is approximated to a 210 radian per second (rad/s) angular velocity which was assigned to the propeller as a sweeping area during computational modelling. This ensures that elements within this rotating region follow the prescribed angular velocity characteristics, thus simulating a rotating propeller. The global velocity was set to near zero in order to simulate a near static environment where some flow in the y-direction was applied. This was done in order to compare to real world examples/tests where airspeed around an object is not necessarily zero due to changes in temperature, pressure, or external flow factors. These boundary conditions and system parameters were applied to three models that progressively increased in complexity so that basic evaluations could be performed, while also understanding how the system behaved in a fundamental manner.

As stated before, a single propeller model was first evaluated with the given boundary conditions and attributes above. Figure 48 below shows the model before the computation - post processing including a cut plot is provided in Figure 49.

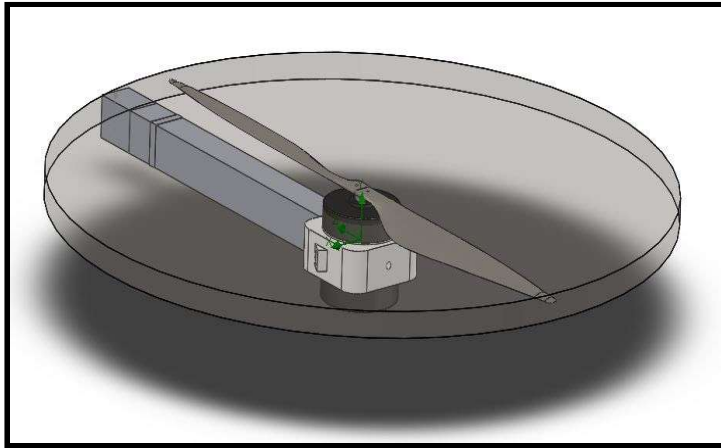


**Figure 48:** Single Propeller Model.

After computation, a cut plot of the flow was made in order to locate velocity magnitudes at contour regions of interest while also mapping a vector plot on top of that to display the flow. This result is shown in Figure 49 below where instability is evident in the model. The flow is depicted as a negative value due to the flow trending downward in the negative direction for the coordinate system.

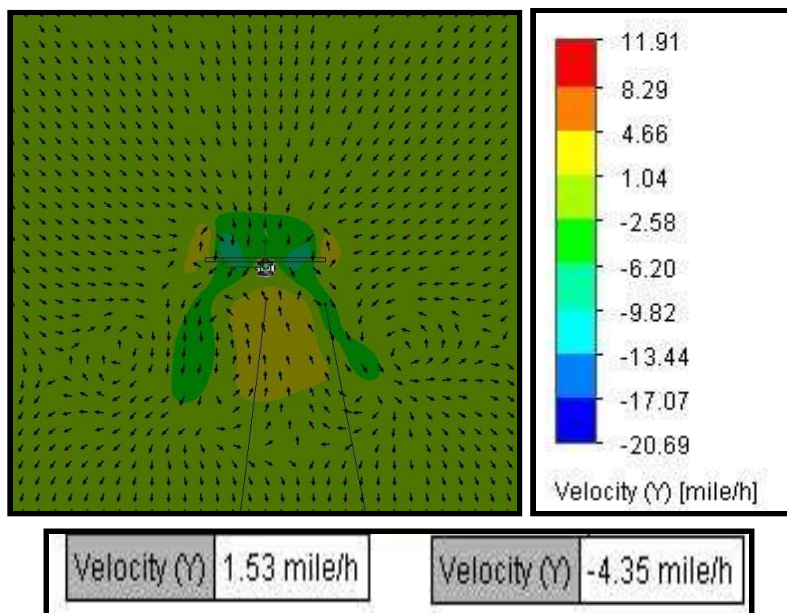


**Figure 49:** Single Propeller Cut Plot.

Along with instability, the velocity at two locations of interest, being directly below the bottom motor and the downward directed flow about a foot below the subsystem, are noted and

can be used to compare with other models. It can be seen that a 4.35 mph velocity is being generated by this subsystem in the downward directed flow region.

Moving onward to a more complex system, the contra rotating propeller was added to the bottom motor as seen in Figure 50 in order to model the subassembly without a duct. This model served as a direct comparison to the final version being the ducted subassembly in order to verify the positive effects of a ducted system. If the system experiences more drag and less benefit from the added aero surface, then a redesign of the duct would be recommended.

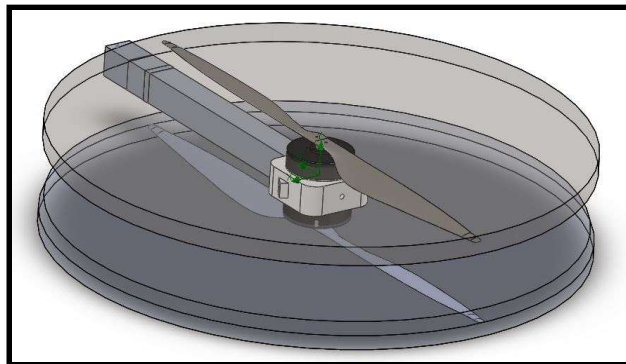


*Figure 50: Contra Rotating Propellers Model.*

From this model, the previously described boundary conditions and parameters were applied to the subsystem and resulted in a few models of interest. These models, being a cut plot shown in Figure 51 and a particle flow plot shown in Figure 52, describe the flow around the system in 2D and 3D space, making its behavior under operation more easily observed.

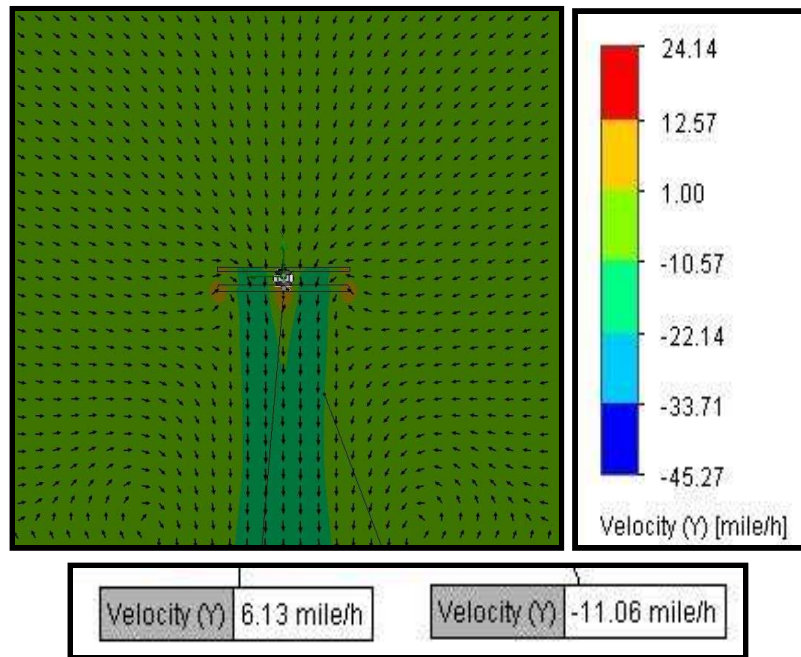


**Figure 51:** Contra Rotating Propellers Cut Plot.

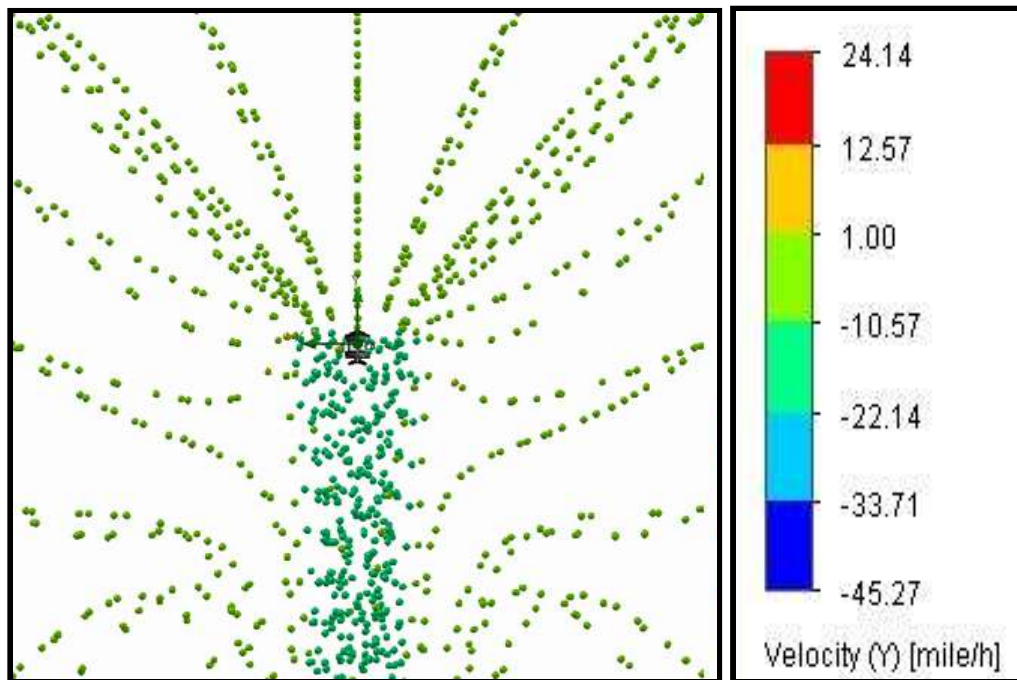


**Figure 52:** Contra Rotating Propellers Particle Flow Plot.

As seen in Figure 52 above, and in the cut plot for the ductless contra rotating propeller, the magnitude for both the upward velocity under the motors and the downward directed region

are much larger than the single propeller model, verifying the assumption that a contra rotating system outputs much higher velocities in the relatively same occupied space. In addition to that, a 154% increase in flow is displayed which is very much evident in the particle flow plot, with simulated air particles contracting into a jet-like shape. If the computational domain was increased for this model, turbulent-like vortices weakly evident in the single propeller cut plot are expected to be observable. In addition to that, this model does not display the theorized cyclical pattern where outlet particles would travel around the system and back to the top to only go through the system again. This cyclical behavior accelerates the flow through the propeller system enough to increase the efficiency of the system as it does not have to put in more power to drive air downward. At a local level, this is what is occurring for the second propeller where it is outputting less work due to the accelerated air particles entering above it from the first propeller's local outlet.

A duct was then introduced to the system, as modeled in the previous section, where the first propeller sits above the curved aero body and the second sits below the center but above the serrated cuts. This is more accurately depicted in Figure 53 below where, as a reminder, the disks represent the sweeping area that the propellers rotated about.

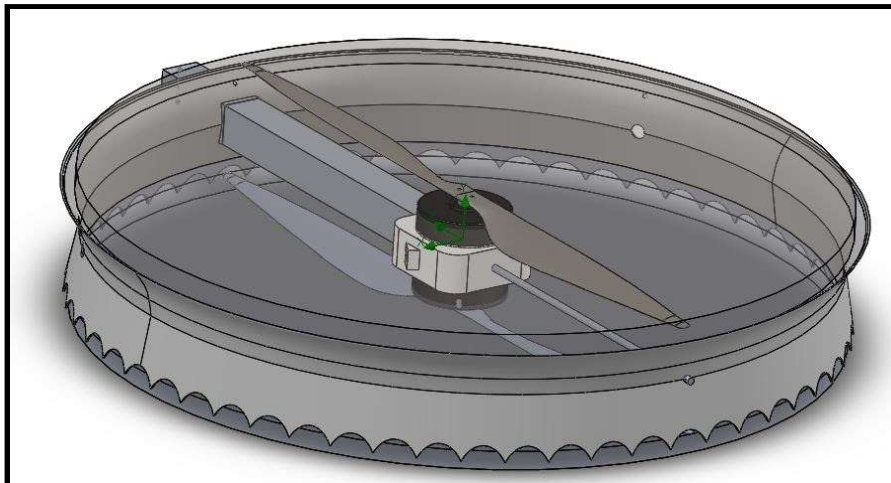


**Figure 53:** Ducted Contra Rotating Propellers Model.

As done previously, the subsystem was subjected to the same boundary conditions and system parameters, where similar outputs to the non-ducted subsystem were observed. These plots are cut plots, with contours and vectors shown, alongside a particle flow plot. These were

formulated in order to compare these results with the previous subsystem. Such results are seen in Figure 54 and Figure 55.

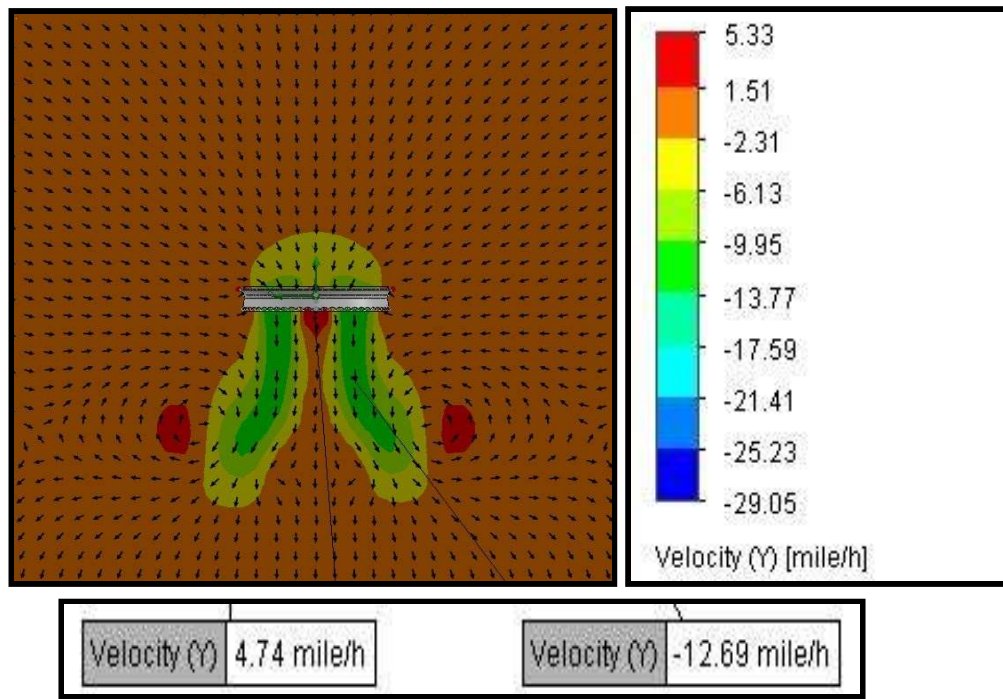


*Figure 54: Ducted Contra Rotating Propellers Cut Plot.*

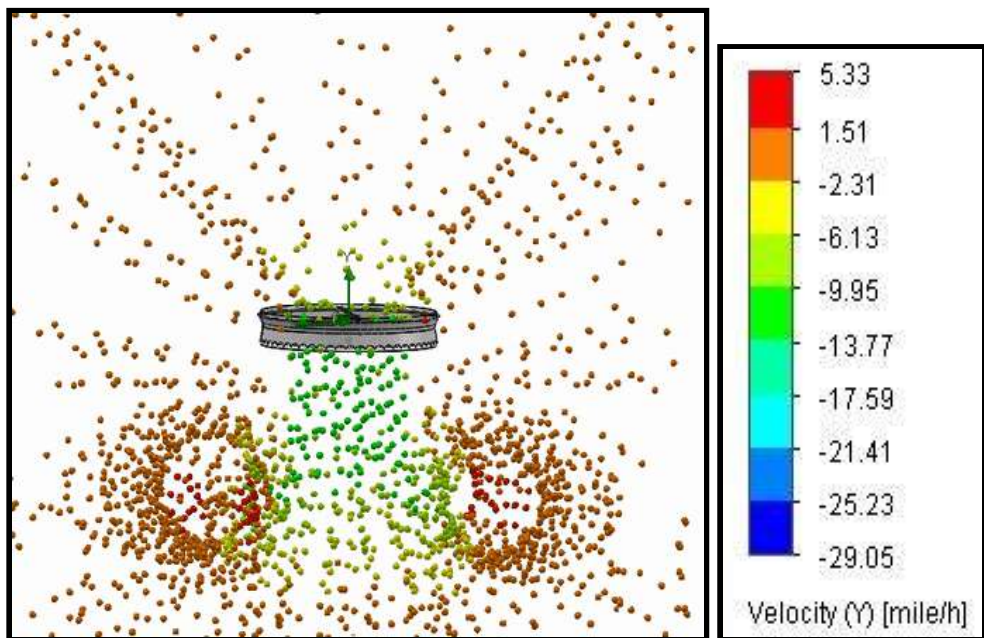


*Figure 55: Ducted Contra Rotating Propellers Particle Flow Plot.*

From these results we can observe that the downward velocity increased while the upward velocity region below the bottom motor decreased. This 14.7% increase in flow compared to the ductless model in the downward directed flow region verifies the duct's ability to increase lift via concentrating the airflow more effectively. The effectiveness of the propeller and ducted system achieves its goal, though further tests are needed along with evaluation of lifting and drag forces. Additionally, the particle flow plot for the ducted subsystem displays the large turbulent vortices generated by the system which propels air particles back upward toward the top of the system. Though many recirculate in the vortex, some eventually cycle back, ensuring a more lift efficient system. Again, a much larger computational domain would display the surrounding behavior of the flow field, but computation issues related to COVID-19 (mentioned in later sections) halted further evaluation.

Along with that progress being halted, a fully ducted system, which was to be evaluated in order to analyze the entire system under the same conditions as the last three models, as shown in Figure 56, was prepared but not computed. Further analysis for the fluid mechanics of the system would verify the flow characteristics around the system along with lift and drag details when comparing a ductless system to a ducted version.

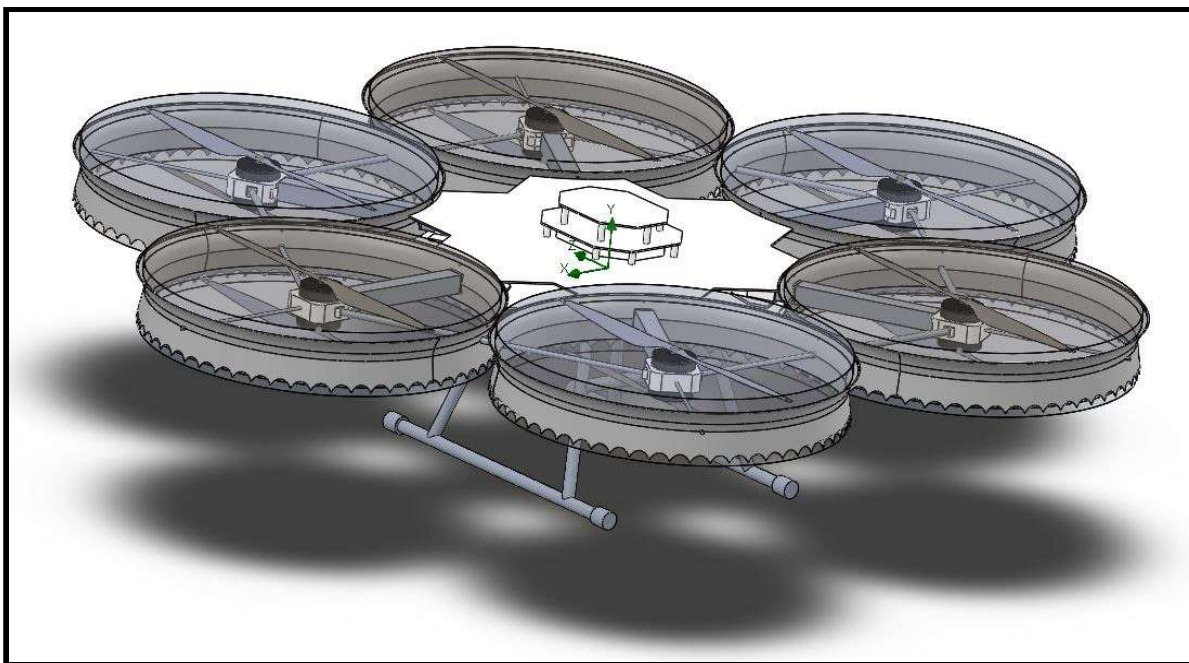


**Figure 56:** Complete Ducted Contra Rotating Propeller Model.

#### **6.2.4 - Interpretation of Modeled Results**

The process of developing simulations for the many complex systems of this project was challenging, especially during the process of analyzing the duct and conducting propeller fluid simulations.

Another issue that arose concerned the exit velocity of the ducted system. In Equation 4, the exit velocity of the ducted system was difficult to calculate. This was because the change in velocity (for the second term) in terms of time still needed to be determined, and due to the nature of the problem, comparisons were not easily made between theory and the simulations shown in Figure 41, Figure 44 and Figure 45, Figures 51 through Figure 55.

This was reflected in the Star-CCM+ models, where shearing at the edges skewed the results of what was accurately occurring in the system. For further simulation iterations regarding Star-CCM+, the control volume was increased in order to analyze the flow outside of the object while obtaining accurate values for the inner sides of the ducts.

#### **6.2.5 Aerodynamics Analysis Summary**

The progress accomplished in the aerodynamics subsystem was quite substantial. Originally the goal was to test out the ducts by themselves while modeling them in a computational simulation. However, the model was then combined with propellers and more realistic simulations were attained. This gave insight into how the ducts impact the system as well as how they compare to a system without them. This is extremely important for justifying the inclusion of them on the drone and validating current duct theory.

For the team expanding upon the project, a suggestion would be to include more iterations to be conducted for both the arm/ducts system and for the entire drone, something that has been set up, but not executed. Another useful venture is the implementation of a simulation that operates in different scenarios (laminar) as well as changing the design to allow an increase in airflow compared to the current (parabolic design) version. This may mean that aside from changes in the diameter lengths of the duct, certain shapes (like additional steps and serrated edges) can be implemented, changing the fluid dynamics of the system.

## 6.3 Mechanical Subsystem

### 6.3.1 - Arm Substructure

For the arm substructure, an analysis was conducted by approximating the members as a cantilever beam. The construction of this system features a hollow 20 inch aluminum beam, where the motors are mounted on the plates at the end. The load is assumed to be applied in the center of the circular section of the mount plate. This assumption was based on a dynamics calculation using Newton's 2nd Law in order to determine the weight. This relationship determined that each arm should withstand about 45 N (or 9.25 lbf) in order to accelerate the entire drone at  $1.25 \text{ m/s}^2$ .

The next assumption for this calculation concerned the fixture at the other end of the arm. In the full drone assembly, the arm attaches to the chassis in a bracket that encloses the arm and secures it with bolts. In the hand calculations and the simulated results, this attachment is fixed as a simple face of support to hold the arm in place.

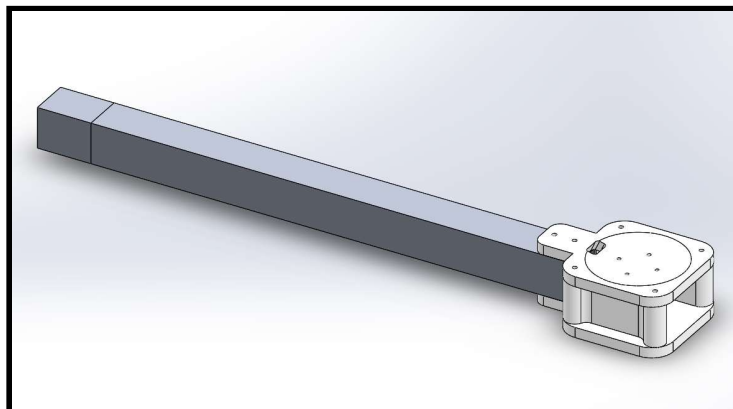


**Figure 57:** Subassembly configuration for arm created in Solidworks featuring aluminum beam, motor mounts, and spacers.

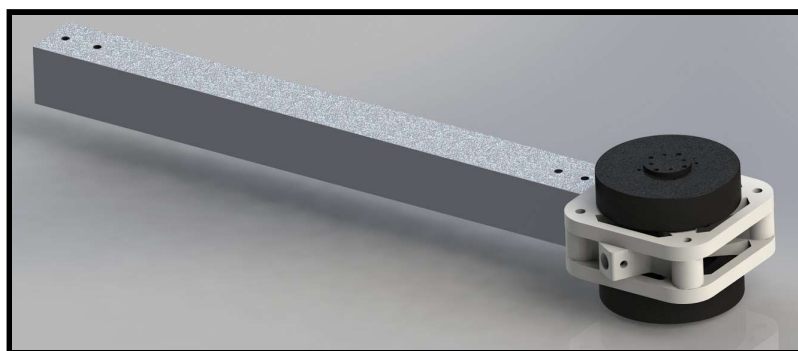


**Figure 58:** Updated subassembly configuration for the arm created in Solidworks featuring updated spacers and mounts which are less weight and add support structures for the arms.

### 6.3.1.1 - Free Body Diagrams

During take off and landing, each arm is expected to take around 10 lbs of loading, making them the primary concern in the system as they could succumb to shearing or bending. Studies concerning these modes of failure, exhibited in Beer's *Mechanics of Materials* [18], are shown in Figure 59 below where bending of the arms is the primary concern. The factor of safety for these analyses is assumed to be 2.5 to ensure that the drone is always operating well underneath the failure threshold for any circumstance.

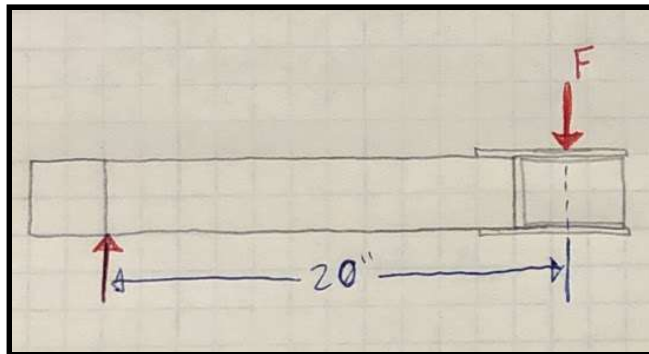


**Figure 59:** Free body diagram for the loading on the arm where  $F = 50 \text{ N}$  and the member is assumed to be fixed at the other end.

### 6.3.1.2 - Material Selection

The arm is an assembly of two main components, the aluminum tubing making up the length of the arm, and the 3D printed fixture to mount the two motors to its end. For this assembly, the tubing was selected from a metal manufacturer that makes a variety of sheet metal and aluminum fixtures. The tubing for the arm was selected to be a  $1\frac{1}{2}''$  square tube made from  $\frac{1}{8}''$  an alloy of 6063-T Aluminum. The 3D printed fixtures were manufactured from ABS in order to allow for them to accurately and securely mount the motors in place. These fixtures were attached to the arm using two bolts that prevented them from sliding or rotating.

### 6.3.1.3 - Expected Output/Modes of Failure

The primary reason for failure in this assembly would be due to the stress in the arms when bending from the 55 lbs load of the system distributed through each arm. The primary mode of failure would occur via stress concentrations in the location where the arms attach to the chassis. This attachment utilizes a bracket with multiple bolts through the aluminum of the arm to hold it in place, so there is a risk for stress concentration in the location of these bolts. The

bolts that will be used to secure the arm to the chassis as well as the motor mounts have not been included in the CAD model in order to examine the behavior of the overall subassembly.

Although this was not covered in analysis for this project, future calculations and simulations for these bolts are important considerations to ensure that stress concentrations will not cause greater issues or risk failure for the system.

### 6.3.1.4 - Calculations

Hand calculations were conducted in order to compare the results to the findings of the FEA for the load applied on the arm. These hand calculations were conducted using the previously described assumptions in which the load is applied at the center of the motor holder while the arm is fixed at the other end. This arm can be approximated as a cantilever beam, which enables the stress to be determined through the calculations shown in Figure 60 below.

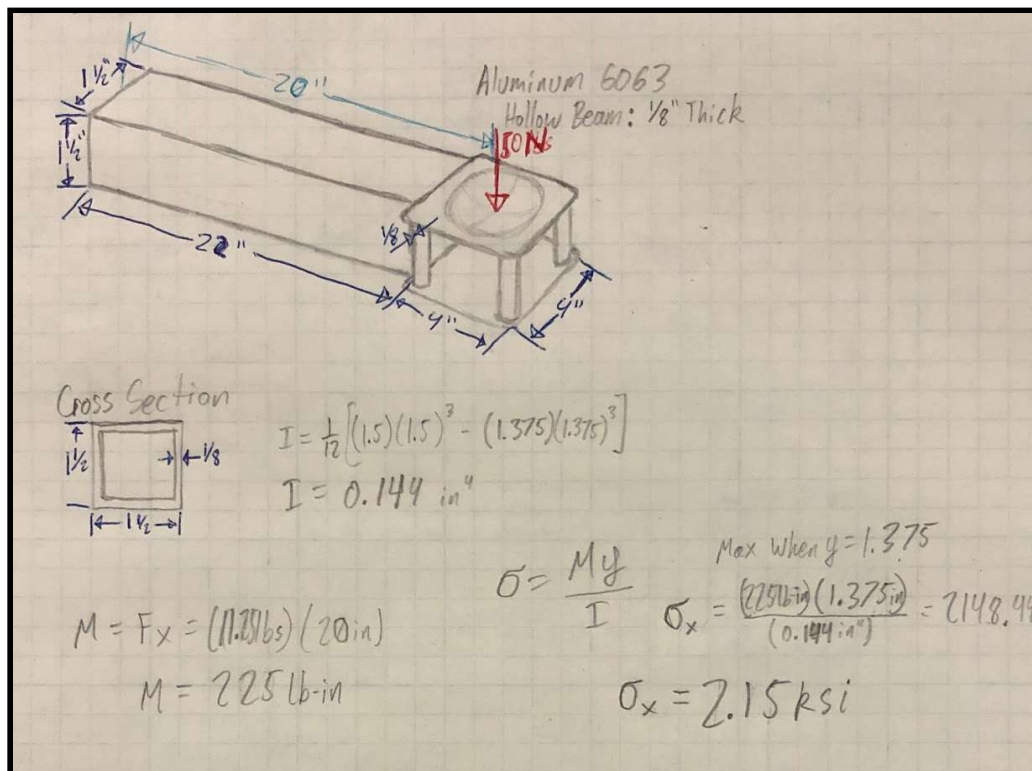


**Figure 60:** Hand calculations for the stress in the subassembly of the arm.

### 6.3.1.5 - Results of Arms Analysis

This analysis of the arm subassembly has shown that we are well within the factor of safety for our material. The yield stress for 6063-T5 Aluminum is 21 ksi, and the maximum

stress determined in the aluminum beam is 2.1 ksi - resulting in a factor of safety of 10. The construction of this arm subassembly was proven to be adequate to function under the loading conditions predicted for regular use of the drone. It is also important to note that the hand calculations agree with the Finite Element Analysis results.

**Table 13: Comparison of Hand Calculations to FEA for Arm Analysis**

	<b>Hand Calculations</b>	<b>FEA</b>	<b>% Difference</b>
<b>Maximum Stress (ksi)</b>	2.15	2.02	6.0 %

### 6.3.1.6 Interpretation of Modeled Analysis

The arm subassembly was analyzed using FEA methods in solidworks. In Figure 61, the Von Mises stress is determined in the assembly following the loading conditions previously described. The assembly was secured on the left end of the beam, and the load was applied to the center of the motor mount. The highlighted location in the FEA presents the greatest stress concentration in the system which occurs at the boundary where the beam is secured.

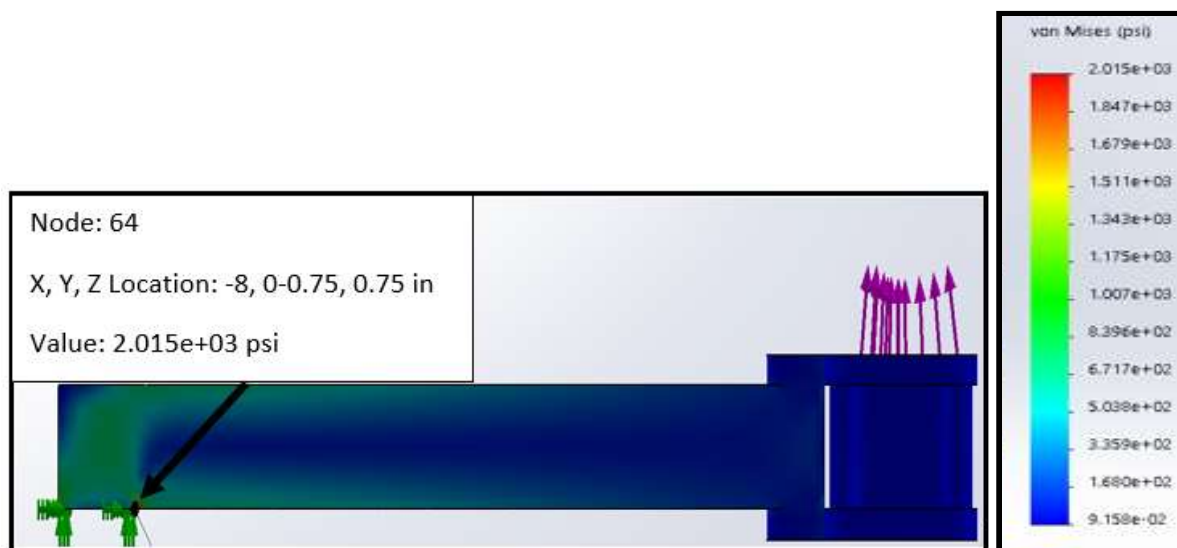


**Figure 61:** FEA for the arm in bending recording the stress in the arm with the load applied to the center of the motor mount.

## 6.3.2 Undercarriage Subassembly

### 6.3.2.1 - System Description

One system of interest for the analysis of the drone is the behavior of the undercarriage when it undergoes a shock. This would be characterized by a drop test, such as in the scenario where the drone undergoes a rough landing and it falls from a short height, landing on the undercarriage with a sudden load. Through FEA we aimed to perform design verification to ensure that our proposed materials and design would be acceptable and able to withstand a certain amount of load in a drop test. The configuration of the undercarriage is presented in Figure 62 below, and further represented in the drop test simulation.



*Figure 62: Subassembly configuration of the undercarriage created in solidworks featuring hollow 6063 Aluminum members with 3D printed fixtures.*

In order to simulate these conditions, we created a simulation in which the undercarriage would undergo a shock during a drop test from 18 inches. The system is ideally assumed to land evenly on the bottom surface of the legs, however an off balanced landing might be realistically expected as well. This choice was made to get an illustration for the expected behavior of the drone if it were to drop from a worst case scenario, while landing in the best case position.

### 6.3.2.2 - Model Simplifications

In this model, the subassembly of the legs was simplified for the sake of computational requirements in Solidworks. The original design shown in Figure 62 features eight separate aluminum members and sixteen 3D printed fixtures to make up the full assembly. In order to make this model less computationally intensive, it was simplified to just one coherent Solidworks part as shown in Figure 63 below. This part was made fully from 6063 aluminum as this was the most structurally critical material in the subassembly.

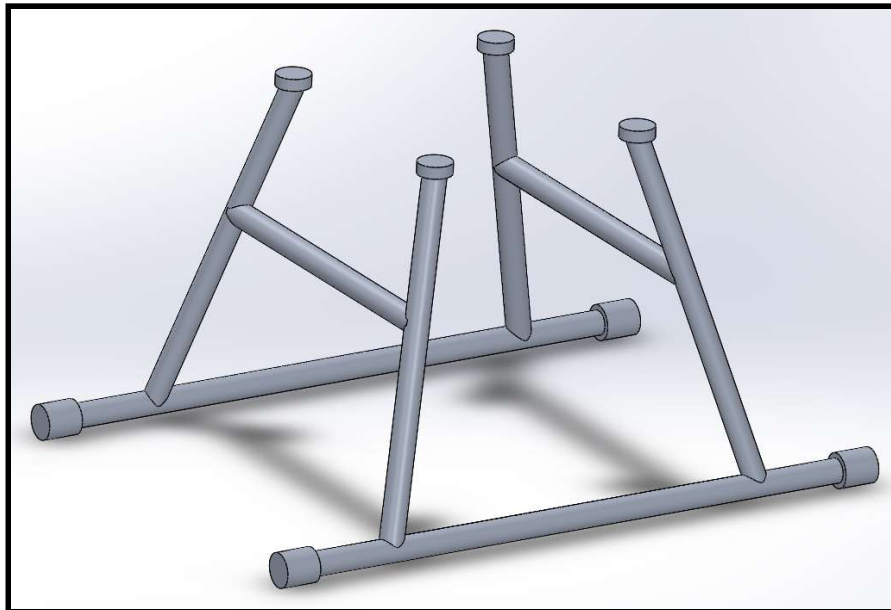


**Figure 63:** Simplified configuration of the undercarriage created in solidworks, made of 6063 Aluminum.

### 6.3.2.3 - Simulation Results

The results of this simulation showed the Von Mises stress in the legs across 0.5 seconds following the drop test of the undercarriage from 18 inches. The system underwent a maximum stress 13.3 ksi, which has an acceptable factor of safety of 1.6 for the yield strength of this aluminum. The results of this simulation are presented in Figure 64 below, which shows the Von Mises stress at the highest instance following the drop test.

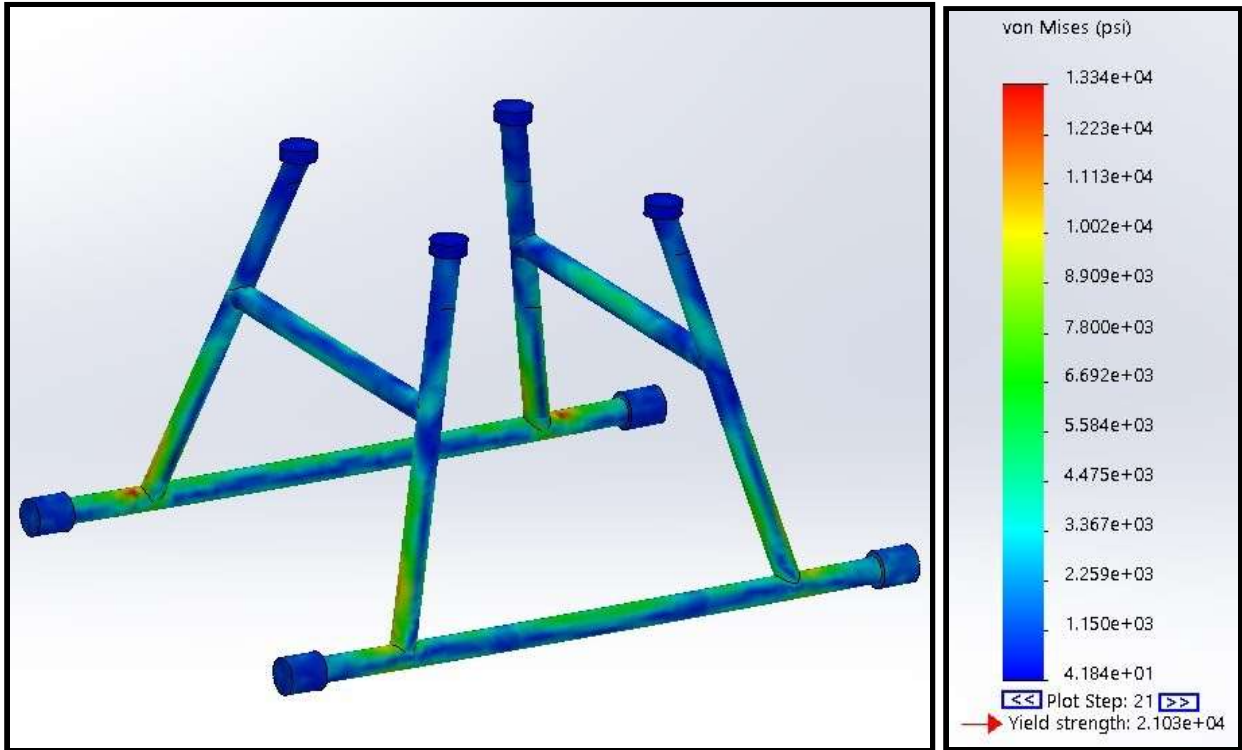


**Figure 64:** FEA results for the undercarriage during a drop test in which the system was dropped from a height of 18 inches.

### 6.3.3 - Mechanical Subsystem Analysis Summary

In this section, the main subassemblies of the structural design were analyzed in order to inform the iterations of the design and verify that it would perform well under expected loading conditions. In some of the analysis presented in this chapter, the behavior of the arm and the undercarriage were studied in order to confirm that they would both be in acceptable limits when subjected to the expected conditions of the drone's working conditions. The results of these simulations have shown that the intended designs perform successfully.

Additional analysis was conducted on some components such as the motor mounts which attach to the end of the arms. This analysis was conducted to perform weight optimization on the 3D printed part and improve the airflow around the motor to prevent it from heating. The results of these analyses are presented in Appendix F.1 and Appendix F.2.

## **7. Electrical Subsystem**

### **7.1 Propulsion Substructure**

In order to have the drone fly, there needs to be a control system implemented specifically for flight. For this, the electrical section can be broken into several smaller sections: Communications and Propulsion. This enables a greater ease of debugging and refining. The following section goes into the details of providing the thrust of the drone and the necessary components that the HLD used to reach the goal outlined at the beginning of this thesis.

#### **7.1.1 - Description**

The purpose of the propulsion substructure is to generate enough thrust to lift the drone and its payload. To meet that goal this project opted for a dodecacopter configuration with 12 motors and 12 propellers. As previously stated the FAA enforces a weight limitation of 55 pounds on drones classified as Unmanned Aerial Systems (UAS). This constraint affected the design choices made to meet this requirement. Alongside the goal of generating the thrust to lift the drone, the propulsion substructure was also responsible for providing power and an environment for the control system to properly function - to house all the onboard electronics, and lastly to not impact the mechanical and aerodynamics subsystems.

#### **7.1.2 - Requirements and Component Selection**

The first component selected was the motor. The reason this component was selected first was because this component, along with its propeller, was responsible for generating the necessary amount of lift in order for the drone to fly. Santa Clara University Environmental Health and Safety enforced a voltage limit of 24V on our system which influenced the motor that was selected. The initial selection of motors was limited to manufacturers that provided voltage, current, and thrust data. Several motors that operated with 24V were chosen as potential solutions. Section 5.2.1 outlines the aerodynamic motivations and criteria for motor selection along with the selection process. Ultimately, T-Motor's U8II KV190 motor was chosen as the system's motor and is pictured in Figure 65 below. The constant voltage value, or KV value, denotes the RPM number when 1V is applied to the motor with no load attached.



*Figure 65: U8 II motor that the HLD used.*

An ESC is needed to control the speed of the motor; to pick out the best ESC for the HLD, the primary constraint for ESC selection was the current required by the motor. The maximum peak current of the motor was used in order to maintain a good margin of safety when selecting the ESC. Reaching the maximum peak current is not anticipated during regular operation of the drone, but this threshold could be reached in emergency circumstances. The maximum peak current of the U8II was 43.7A so it was decided that picking a speed controller from T-Motor would minimize potential integration issues with the motor and ease logistical organization. T-Motor offered two speed controllers that could handle the maximum peak current needed by the motor. One speed controller used Field Oriented Control (FOC) while the other speed controller used the more traditional trapezoidal control. Understanding how components work is essential to creating a reliable system and is necessary for effective debugging when problems arise. Because of this, the learning curve involved in FOC control, and the time constraints of the project, the ESC using trapezoidal control was chosen. The T-Motor Flame 60A HV ESC, pictured in Figure 66 below, was selected as the speed controller for the system. Using FOC control should be explored in the future because it could decrease the operating temperature of the ESCs and increase motor efficiency.

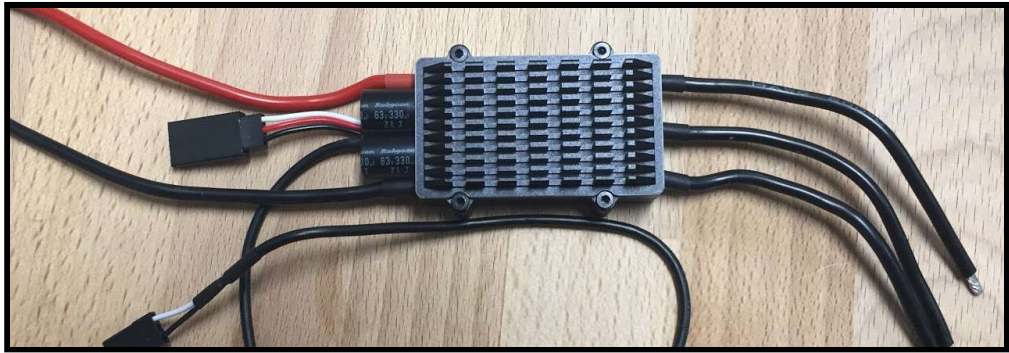


**Figure 66:** ESC that the HLD used.

The Power Distribution Board (PDB) takes in the power from the power source, in this case a battery, and spreads it to the rest of the system. The dodecacopter uses 12 motors and having all 12 motors connected to one PDB would require the PDB to handle a very high current. Because each motor's maximum peak current requires 43.7A, 12 motors would require 524.3A. This high current introduces the issue of having a PDB that can handle such a high current and selecting a battery with a sufficient discharge rate. It was decided that two PDBs would be used in the system and each PDB would power six motors. By powering six motors each PDB would need to be able to withstand 262.2A. This number was still large but more manageable. At the time there was only one PDB on the market that could take a current this high: the Tarot TL2996 Power Distribution Management Module. This PDB could handle 480A and was created for large drones used in agricultural settings. The other option for a PDB was to create a custom board capable of handling high current. Due to the low cost and availability of the Tarot board, it was chosen as the PDB for the drone. Another benefit of the Tarot board is that it has several plugs that can power other electronic devices.

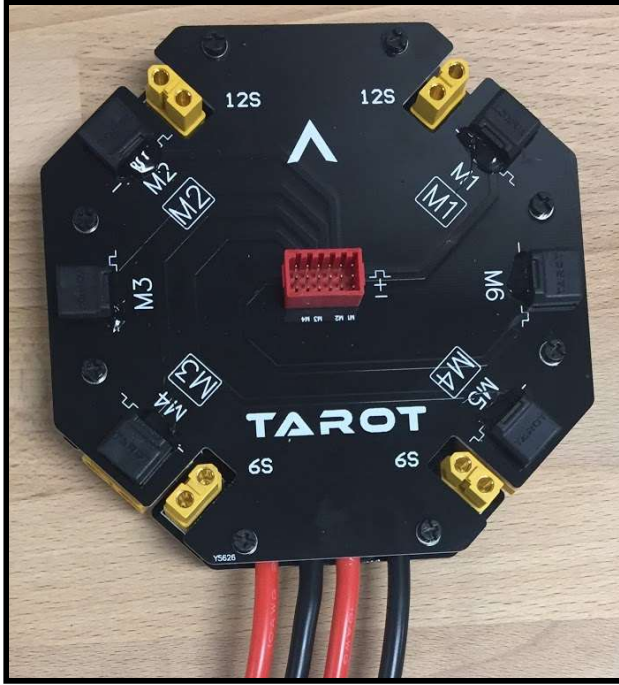


*Figure 67: PDB that the HLD used.*

The power supply provides the necessary power to the drone and any peripherals that also need power. Drones typically use lithium polymer (LiPo) batteries due to their high energy densities and high discharge rates. The motors selected needed 6S LiPo batteries which have a nominal voltage of 22.2V. The battery selected also needed to have a sufficient capacity to last for a long time. The battery selected also needed to have a discharge rate that could handle the demands of the motors. Having all 12 motors sharing a single battery source would have demanded a high discharge rate and capacity combination that did not exist on the market. It was decided that two batteries would be used for the system and each battery would power six motors. The Tattu 22000mAh 25C 6S LiPo battery was chosen for its large capacity and safe discharge rate. This battery is also used for large multirotors and other large electromechanical devices.



**Figure 68:** Tattu LiPo battery that the dodecacopter system uses as an energy source.

It should also be noted that the flight controller came with a buck converter called the Holybro PM02 Power Module. This buck converter can be connected to a LiPo battery with up to 10 cells and has a max current sensing of 120A where it outputs 5.2V and a max of 3A. This component allows the battery to power the flight controller.

These components make up the propulsion system that the HLD used. The following sections will go into the design of the propulsion system and afterwards the physical implementation with regards to the HLD.

## 7.2 - Communication and Control Substructure

### 7.2.1 - Description

The communication and control substructure is responsible for providing communication between the ground elements and the drone. It is also responsible for controlling the drone. It is made up of the transmitter-receiver pair and the flight controller in its most basic state. This becomes more complex as the various components are incorporated onto the drone, but the main purpose of it does not change. The various components work together to send a signal from the transmitter to the flight controller and then adjustments are based on that input.

### 7.2.2 - Requirements and Component Selection

The flight controller is responsible for translating the inputs from the pilot into the correct motor control outputs to the speed controllers. The flight controller for the drone needed to be able to control 12 motors. It also needed to be able to support other peripherals like the IR

camera being used for this project. There were many flight controllers on the market but not many could support 12 motors. A notable flight controller that can support 12 motors is the Pixhawk 4. The Robotic Research Lab (RSL) has worked with the Pixhawk platform in the past and choosing the Pixhawk 4 would allow some support. The Pixhawk 4 also had 16 PWM outputs which allowed it to interface with different peripherals like cameras, scanners, or external sensors. For all these reasons the Pixhawk 4, picture below in Figure 69, was chosen as the flight controller for the drone.



**Figure 69:** The Pixhawk 4 flight controller.

The GPS module is important for the HLD because without it autonomous flight would not be impossible. The GPS module used for the drone was made specifically for the Pixhawk 4. When coupled with the Pixhawk 4, the GPS allows the drone to have recognition of where it is located in proximity to the flight path and describes the tilt of the drone if the system is unbalanced. It accomplishes this by utilizing the Neo-M8 GPS module and the IST8310 3-axis digital magnetometer sensor.



**Figure 70:** Pixhawk 4 GPS module

The transmitter is used by the pilot to send commands to the drone during semi-autonomous flight. It was necessary to select a transmitter with 5 channels. Four channels are mapped to the throttle, yaw, roll, and pitch. The fifth channel is mapped to a switch that can arm and disarm the drone before and after a flight. Figure 71, below, is a picture of the Flysky FS-i6X transmitter that the HLD used for testing purposes.



**Figure 71:** The Flysky FS-i6X transmitter that the pilot uses to control the drone during semi-autonomous flight. The numbers on the transmitter correspond to the channels each switch is connected to.

The receiver is a device that takes the signal sent from the transmitter and processes it into a signal that the drone is able to take in as input. The number of channels of the receiver needed to be equal to or greater than that of the transmitter. The Flysky FS-iA6B receiver had 6

channels and came with the FS-i6X transmitter, making it a good selection for the drone's receiver. The receiver then sends the signal to the PPM encoder which then sends a PPM signal to the other electrical components. The following figures show these components:



**Figure 72:** Flysky FS-iA6B 6-channel receiver

Each channel of the receiver outputs a PWM signal but the Pixhawk 4 can only read one PPM signal. A PPM encoder was used to encode the PWM signals from the receiver into one PPM signal that goes into the Pixhawk 4.



**Figure 73:** Pulse Position Modulation (PPM) Encoder. This PPM encoder can accept up to 10 channels and encode these signals into one PPM signal.

The telemetry kit is responsible for providing live data to the ground control station and providing a way to change drone parameters mid-flight. It is also used for autonomous flight. There was only one kit that was compatible with the Pixhawk 4 so it was selected. The Holybro 915MHz Transceiver Telemetry Radio Set is pictured below, in Figure 74.



**Figure 74:** Holybro Telemetry Kit

The ground control station is composed of a laptop, software, and one of the telemetry modules from Figure 75. There were many software solutions to choose for the ground control station. QGroundControl was selected for its ease of use and user friendly interface especially when it came to using Pixhawk 4 which functioned more reliably under QGroundControl.



**Figure 75:** QGroundControl Drone Overview.

## 7.3 - Subsystem Design and Implementation

### 7.3.1 - Propulsion

With the electrical component block diagram seen at the end of Chapter 3 outlining many substructures, the next stage of interest consists of how the propulsion substructure is integrated with a control substructure (which is covered in section 7.3.2). To design a proper propulsion

substructure, the following diagram outlines the overall structure of which components interact with one another. Two 6S LiPo batteries power the dodecacopter system through two PDBs. The PDBs were originally meant to support two 6S LiPo batteries in series each, so a simple modification to the input wires was needed. One of these 6S LiPo batteries powers the flight controller with a buck converter to step down the voltage. The flight controller provides the command signals that go through PDB then to the ESCs. The ESCs convert the signals to a sequence of voltages that drive the motors. The PDB also provides power to the ESCs. One PDB assembly is composed of the top set of motors and the other PDB assembly is composed of the bottom set of motors.

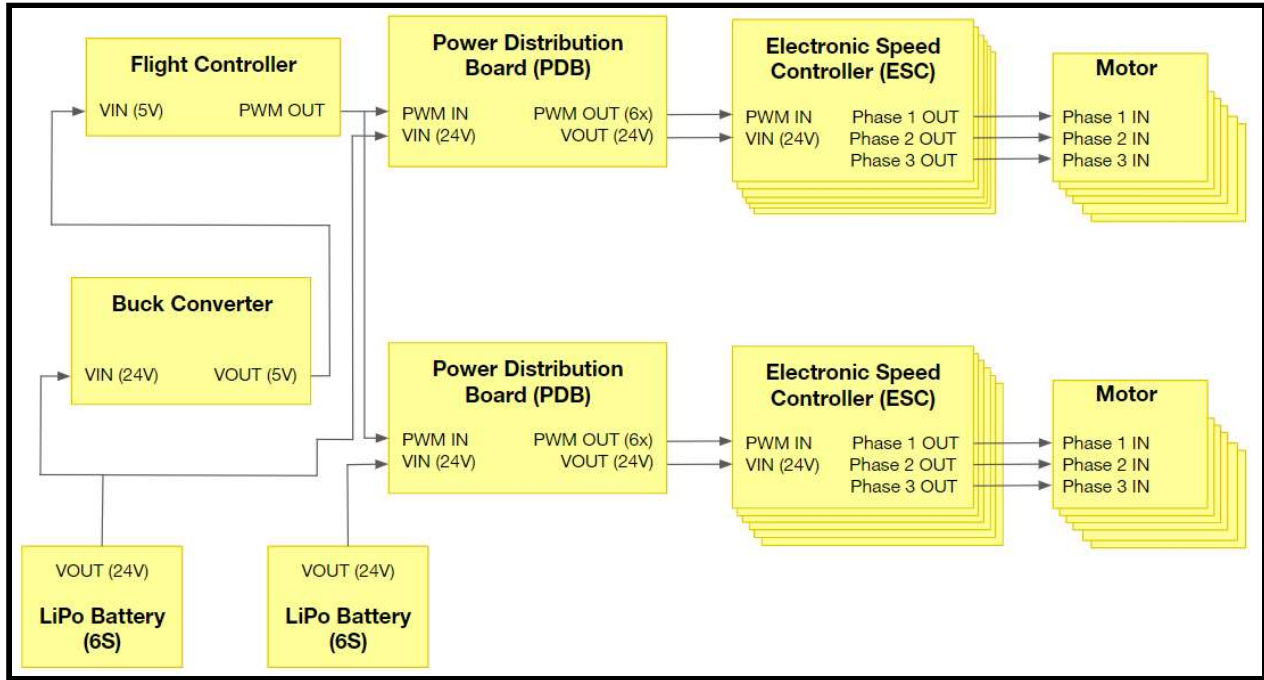


**Figure 76:** Propulsion System Component Block Diagram.

Following this model for the overarching electrical system, the physical implementation was broken down into smaller sections to make component testing far easier for the team to conduct. Figure 77 shows the primary components required to drive the propeller.

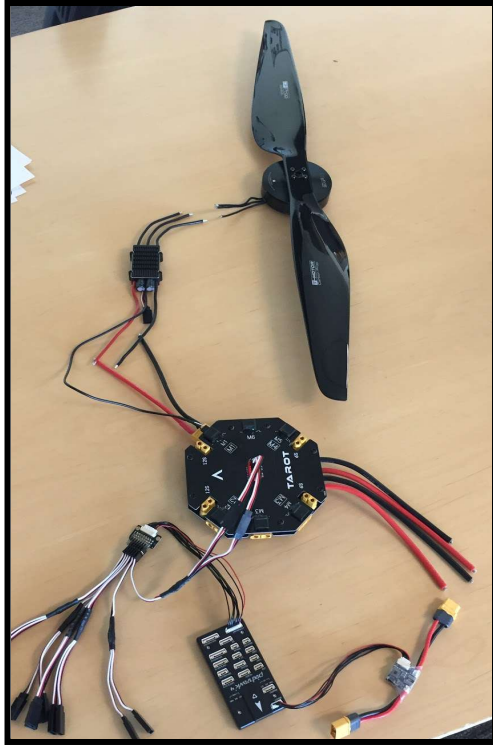


**Figure 77: Propulsion Substructure Showing Utilized Electronics.**

The propeller and motor are controlled by an ESC which receives power from the PBD and a PWM signal from the Pixhawk. The PWM signal travels through the PDB first but the PWM signal can bypass the PDB and still function correctly.

### 7.3.2 - Communication and Control

Designing the communication and control substructure required preliminary research into what the substructure was responsible for, the role of the components, and how those components worked together. Semi-Autonomous flight needs a transmitter and a receiver but there are different communication protocols that the Pixhawk 4 can understand. This includes PPM, serial bus (SBUS), and digital system multiplexer (DSM). All three of these protocols were explored but PPM was the easiest to implement and proved to work reliably.

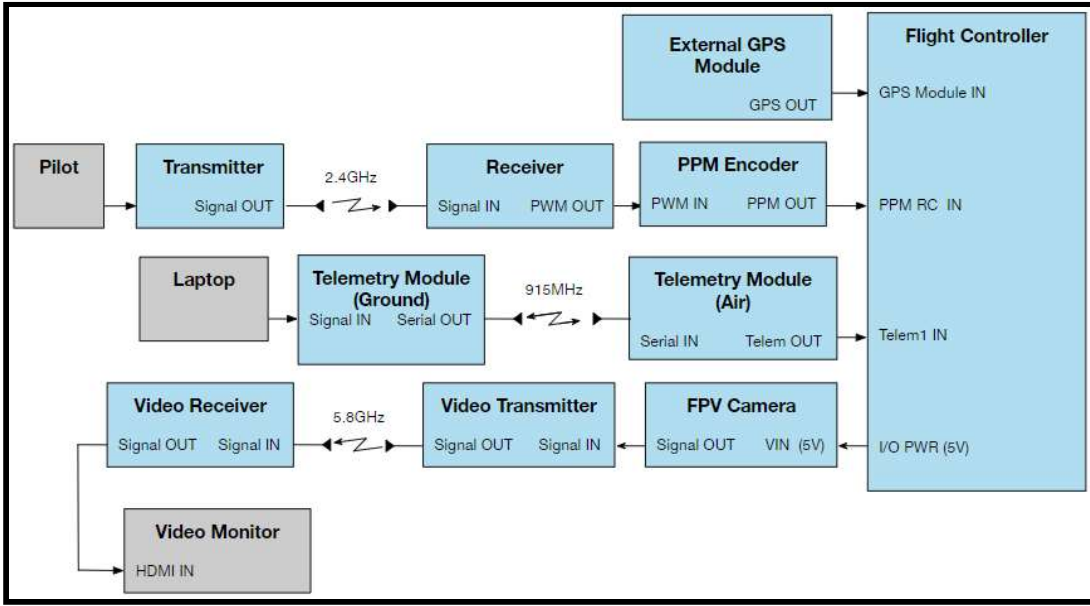


**Figure 78:** Communications Component Block Diagram.

The components for semi-autonomous flight include the PPM encoder, receiver, and transmitter. The PPM encoder is connected to the PPM RC port of the Pixhawk 4 through a special Pixhawk cable. Solid core wires connect the servo cables of the PPM encoder and the special Pixhawk cable. The PWM cables of the receiver connect to the PPM encoder. The transmitter communicates with the receiver wirelessly. The signals and components for semi-autonomous flight are shown in the second row of Figure 78. The physical components are shown in Figure 79.

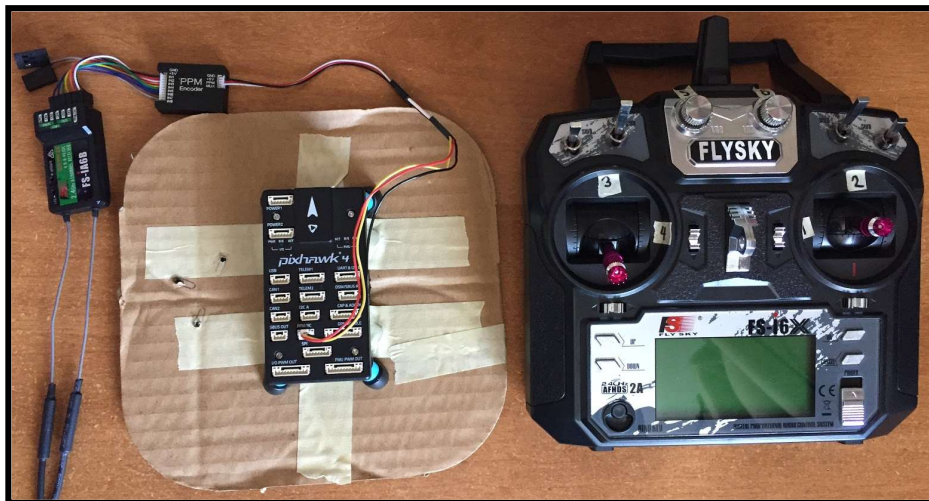


**Figure 79:** Main components necessary for semi-autonomous flight. The components, from left to right, are the receiver, PPM encoder, Pixhawk 4 flight controller, and the transmitter.

The components for autonomous flight, shown in the third row of Figure 78, include the telemetry modules and the ground control station laptop. The physical components are shown in Figure 80.



**Figure 80:** Main components necessary for autonomous flight. The components, from left to right, are the ground telemetry module, GPS module, Pixhawk 4 flight controller, and the air telemetry module.

The air telemetry module connects to the Pixhawk 4's TELEM1 port. The ground telemetry module connects to the laptop acting as the ground control station. The GPS module connects to the Pixhawk's GPS MODULE port.

When conducting a flight it is helpful to the pilot to have a better perception of the space around the drone and to see what the drone “sees”. To achieve this, a video transmission section was added to the drone system. It is composed of a camera connected to a video transmitter that communicates with a video receiver connected to a monitor, as in Figure 81.

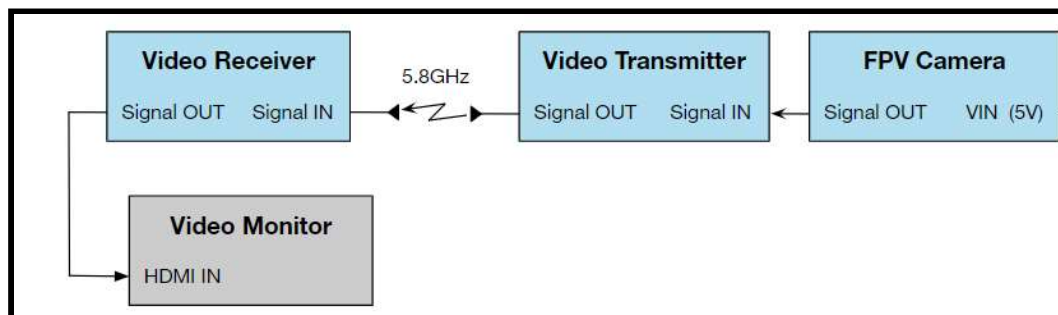


**Figure 81:** Video Assistance Component Block Diagram for the flight operator.

The components receive power from the propulsion substructure. This addition assists the pilot when flying the drone in semi-autonomous flight. In the future, this video communication feature can be used to enable collision avoidance software developed for the Pixhawk 4. While the video transmission portion of the drone is depicted as part of the communications and control substructure, it is a stand alone system whose components do not directly interact with the rest of the subsystem.

To achieve this system, there was not a significant change in the overall configuration of the communication system due to the stand alone nature of this “branch.” Figure 82 and Figure 83 show the components needed to allow this system to be added onto the drone.

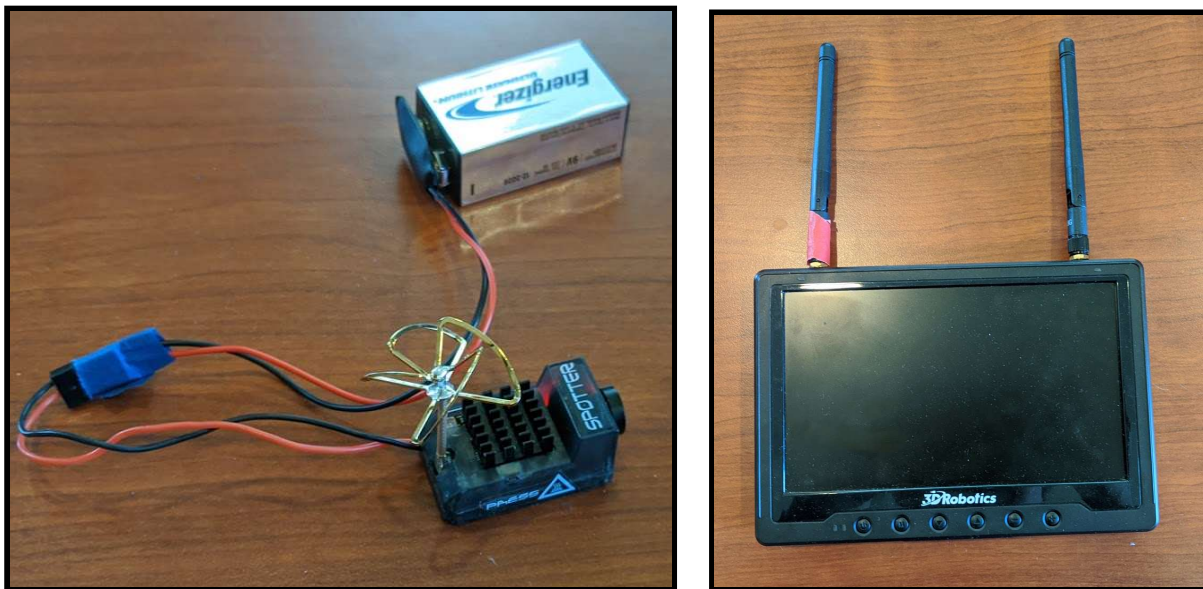


*Figure 82: Camera and Monitor with integrated 5.8 GHz transmitter and receiver.*

These two components essentially act as a means of providing video feed from the drone for the pilot. What the pilot can do in response to the video feed is make manual adjustments to the drone's orientation, and make control changes to the path should an obstacle be in the path of the drone. After establishing how all the components in the communication and control substructure work together, they were combined to form the final conglomerate of components.

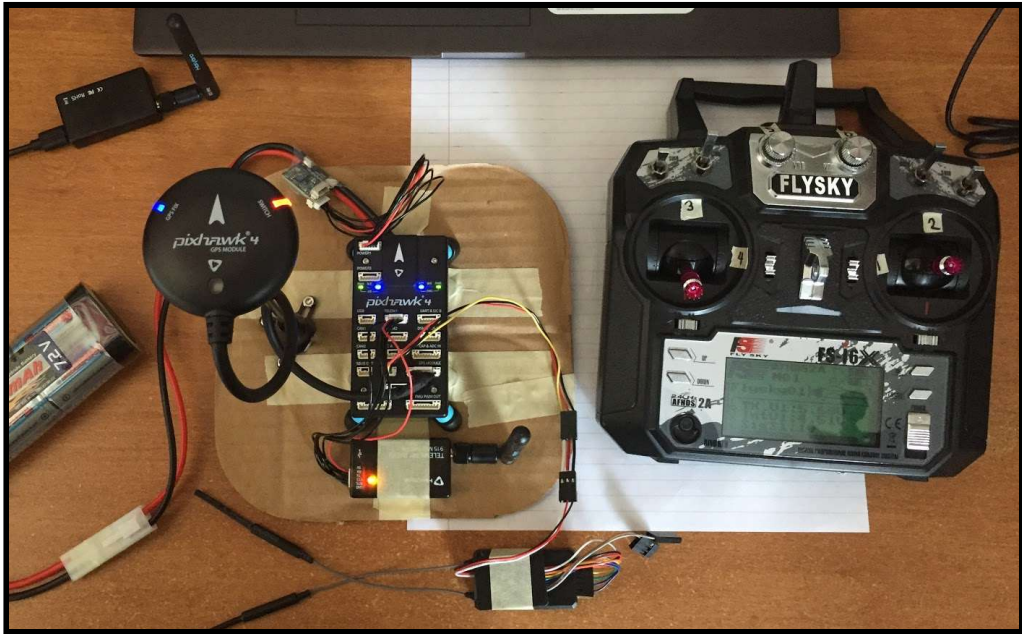


**Figure 83:** Various Electronic Components of the Communication Substructure.

### 7.3.3 - Payload: The Flir Duo R Thermal Camera

The Pixhawk 4 flight controller is capable of sending signals to the Flir Duo R to take a photo when visiting each waypoint in the drone's flight path during autonomous flight. The port normally used for this, FMU PWM OUT, is not available with the current dodecacopter configuration. A modified cable was made to allow an Arduino to externally read data from the Pixhawk 4's TELE2 port and obtain the signals for the Flir Duo R. The Arduino contains a C program that reads the data stream of the Pixhawk 4 from the TELE2 port to look for a successful waypoint visit. At each waypoint, the Arduino will forward the signal to capture an image to the PWM pins on the FLIR Duo R. The wire used for the TELE2 port is split into digital pins on the Arduino. These pins can be configured to be any pins on the Arduino. In addition, two pins are used to send a signal back to the FLIR Duo R through a cable that was provided by FLIR. After a flight, the images taken by the FLIR Duo R go through a post processing phase and the photos of the region are stitched together. This photo stitching process and post-flight image analysis are discussed in further detail in Section 8.2.



*Figure 84: Prototype of the camera trigger Arduino-Pixhawk system.*

## 7.4 - Integration, Testing, and Validation

### 7.4.1 - Motor Control of a Hobby Quadcopter

The complete implementation of the electrical subsystem was first tested in a quadcopter setup using hobby-sized components, where this test served as a proof of concept for the motor control using the transmitter. Several wires and plugs were soldered onto several motors, ESCs, and the quadcopter frame, and the configuration on QGroundControl was set to quadcopter and the Pixhawk's sensors were recalibrated. All the components were connected together and a 4S LiPo battery was used to power the system. Once the Pixhawk was armed, the throttle on the transmitter was changed and the test could begin.

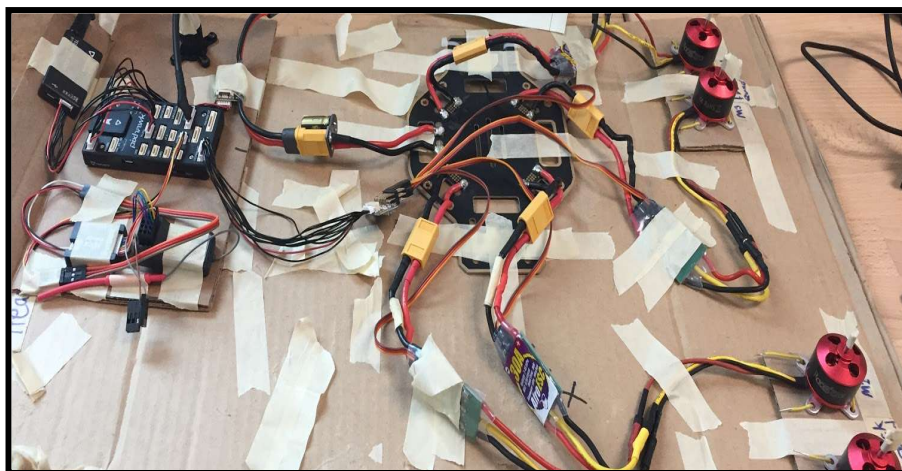


*Figure 85: Prototype of the electrical subsystem for the initial quadcopter build.*

When the transmitter changes its position, it can increase or decrease the throttle. In reaction, the rotational velocity of the motor directly increased and decreased linearly with the throttle. Roll and pitch were increased and decreased causing the motors to change speed relative to the command; for example, increasing the pitch caused the front motors to slow down and the rear motors to speed up. This makes sense since this response from the motors would cause the quadcopter to move forward if it were flying. Increasing the roll forced the motors on the right to speed up and the motors on the left to slow down, which would cause the drone to drift to the left. Reversing the direction of the roll inverted the reactions of the right and left motors. This caused the drone to drift to the right. The results from varying yaw yielded the expected results as well. Successful control of the motors with the transmitter meant testing could continue for the actual components that the dodecacopter would use.

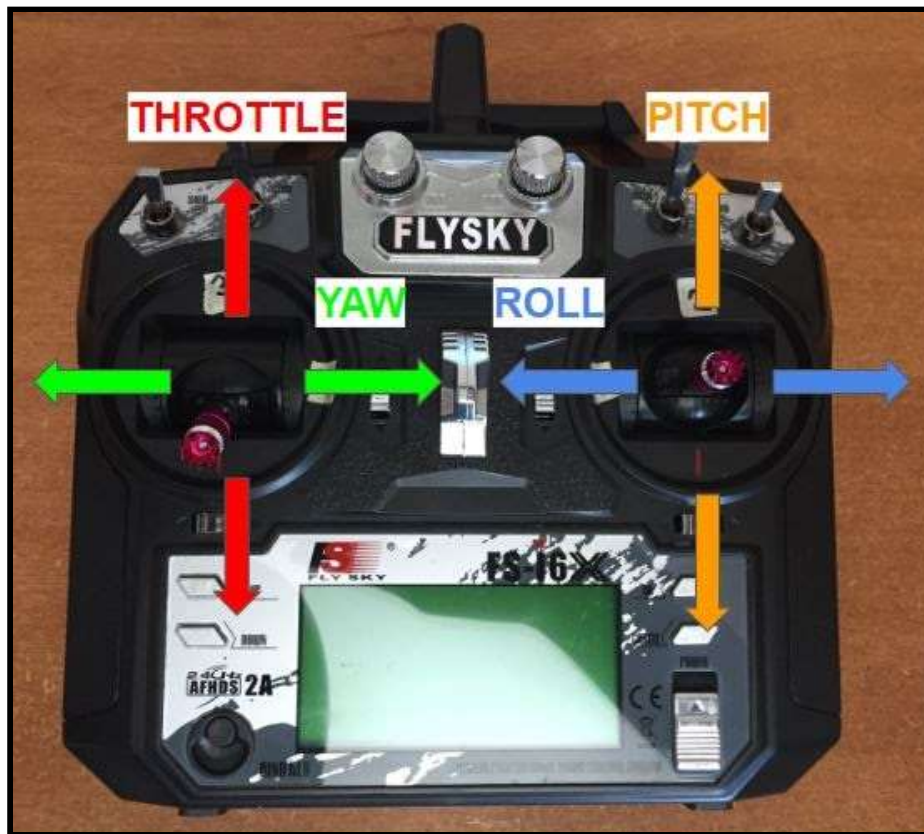


*Figure 86: Roll, Pitch, Yaw, and Throttle on the Transmitter.*

#### 7.4.2 - Motor Control of a Prototype 2x4 Quadcopter

Successful control of the hobby sized motors proved that the electrical subsystem was working as anticipated and the next step would be to try the components that would be used for

the final dodecacopter. The PDB and motor were replaced by the Tarot PDB and the T-Motor U8 motors. This required soldering many connectors onto different components. The components were mounted to a quadcopter made out of two 2x4 pieces of wood constructed by the mechanical and aerodynamics sub teams.

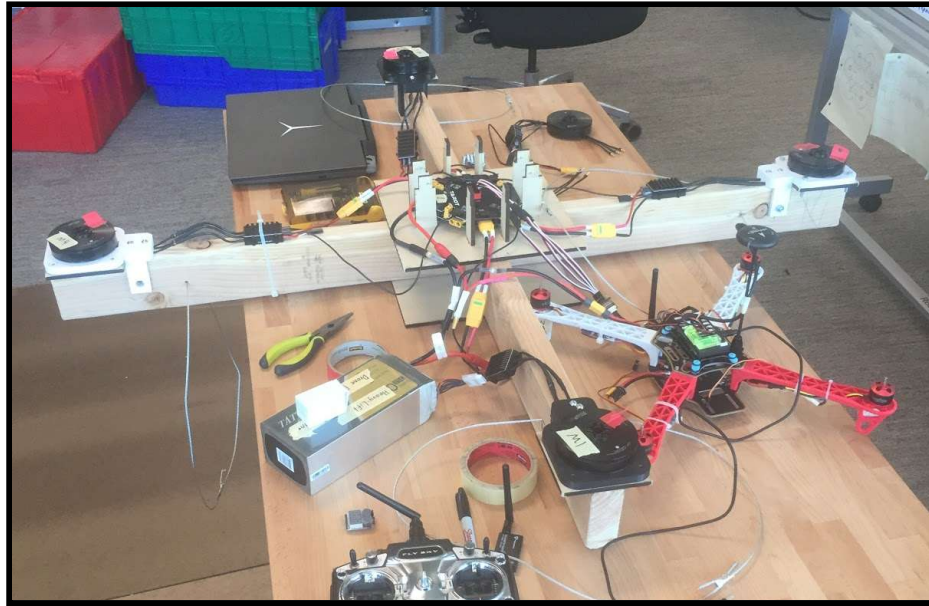


*Figure 87: Electrical system incorporated onto the quadcopter.*

The physical testing of the motor control was a very rigorous process. Many different aspects of the motors and the control system were tested to ensure that they all worked as intended. To meet these requirements not only was the rotation speed of the motor tested, but also the reaction of the control system to changes in orientation, diverging off the flight path. Another important aspect of testing the motors was to see whether or not the motors were defective or if the electrical system scaled up correctly. The same tests in Section 7.4.1 were conducted and the results yielded similar results. In some instances some motors would stop spinning when certain commands were given. After many hours of debugging with different motors and ESCs it was determined that this behavior was due to some of the Pixhawk's sensitive internal sensors. The platform that the Pixhawk was attached to was not fully leveled which affected the control of the motors. This was determined not to be an issue when the drone is flying since the flight algorithm in the Pixhawk would make the correct adjustments to stabilize. This was seen in the quadcopter hover tests covered in Section 9.2.

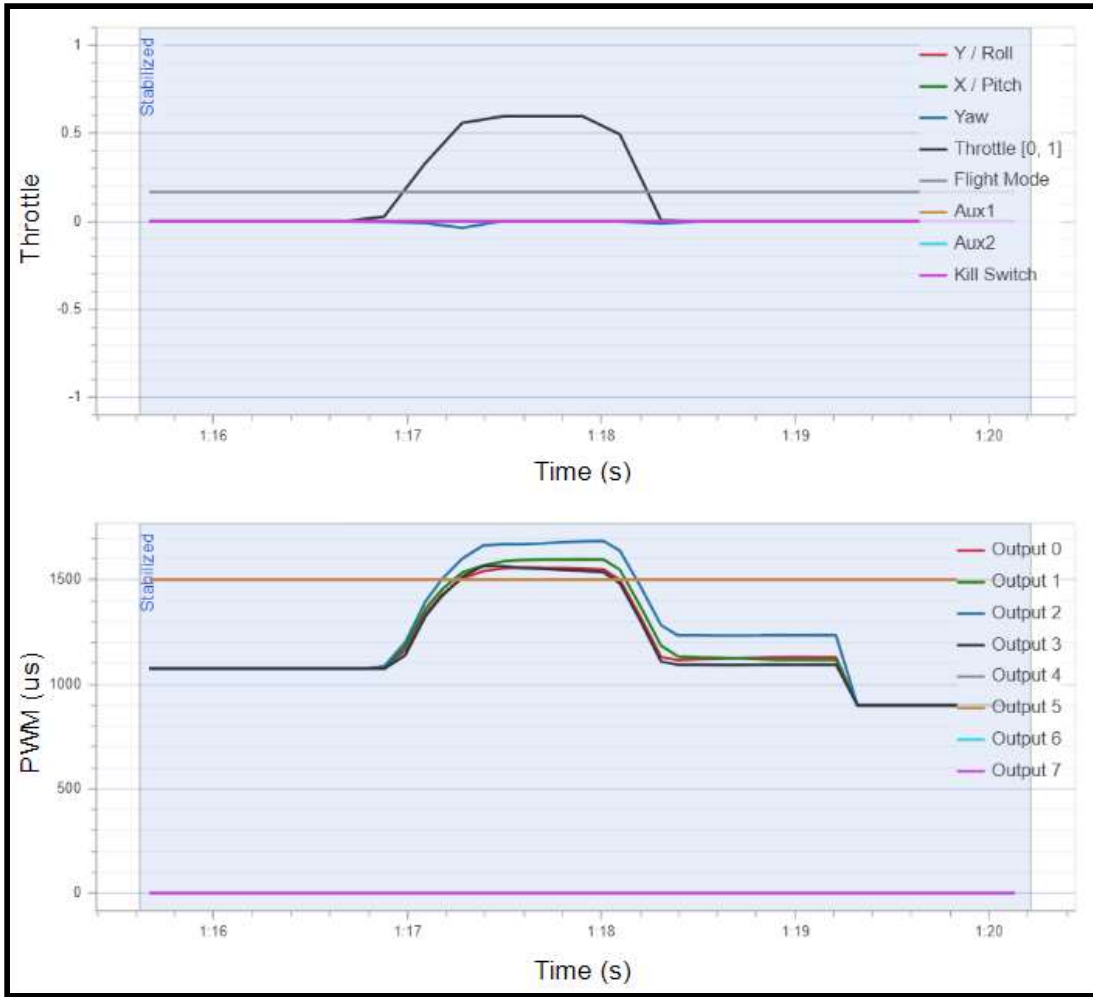


**Figure 88:** Input/Output of Transmitter-Motor Relationship, showing the output of the motors when given an input from the transmitter.

#### 7.4.3 - Preliminary Test of Autonomous Capabilities

The purpose of this test was to check the drone's ability to follow a flight path that had been mapped out through the ground control station. A flight path was mapped out in the Robotic Systems Lab's (RSL) parking lot and the drone was placed on a cart. Communication was facilitated through the telemetry modules since this was an autonomous flight test. Propellers were left off to avoid accidental takeoff and maintain safety while testing. Once the path was set the drone was armed through QGroundControl and the drone was carted along the flight path. The motors spun as if the drone were flying forward, along the flight path. After two successful non-airborne cart-flights, it was realized that the drone may be pushed off course due to environmental factors. It was decided that in the middle of a cart-flight test the drone would be

wheeled off course and we would see if the motors changed direction in such a way that would correct itself if it were actually flying. When the drone was carted off the flight path the motors indeed changed direction back toward the intended path. This preliminary test of the drone's autonomous capability was successful but airborne flight tests would need to be conducted in the future in order to know with certainty that autonomous flight works.

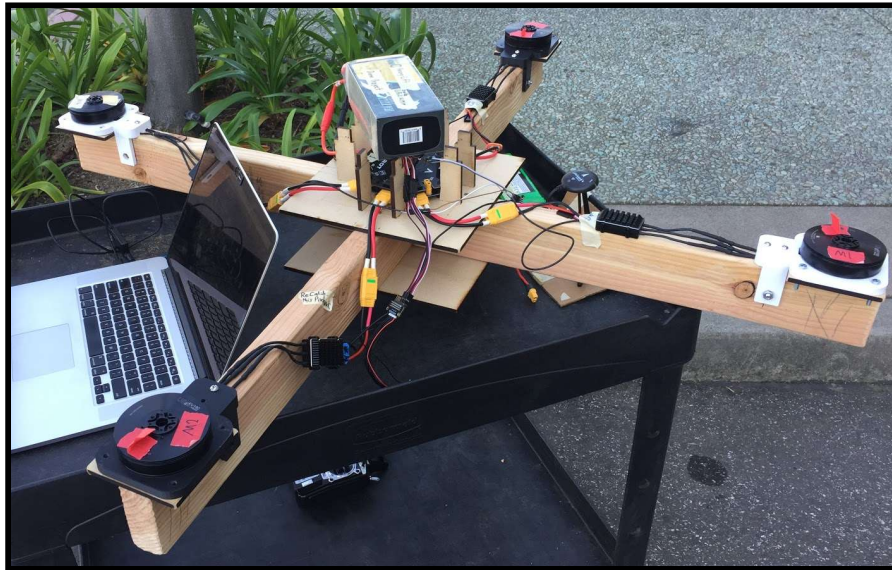


*Figure 89: Quadcopter during autonomous flight path test.*

#### 7.4.4 - Motor Control of a Hobby Hexacopter

The purpose of this test was to establish 6 motor control on the hobby level drone. Although a previous test was done with 4 motors, the change from 4 to 6 is substantial as the wiring changes significantly between those two modes. This is important because the dodecacopter configuration uses 12 motor control which is more similar to the 6 motor control than it is to the 4 motor control.

Several key setups were made for this test to succeed. First the communication was established between the transmitter and the receiver. Then the configuration in QGroundControl was changed to hexacopter and the Pixhawk's sensors were recalibrated. This step involved substantially less debugging than setting up the initial 4 motor control, because the team had experience with debugging by this point.

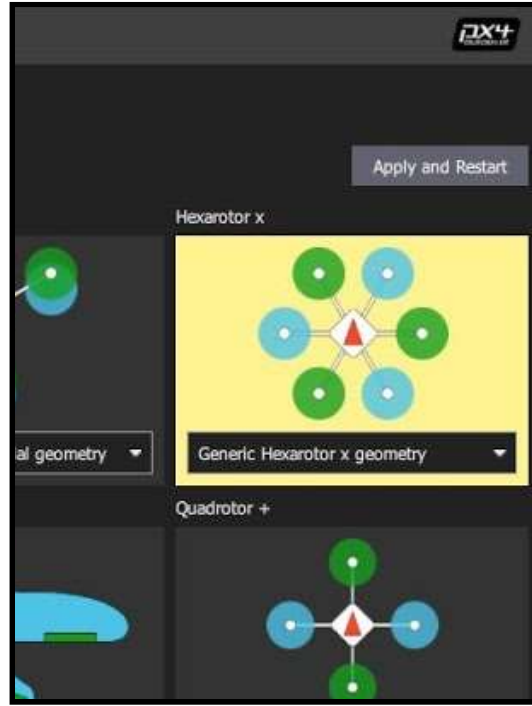


**Figure 90:** QGroundControl drone configuration selection.

Several wires and plugs were soldered onto several motors, ESCs, and the hexacopter frame. The motors and ESCs were attached to a hexacopter body and their servo cables were attached to the Pixhawk. After the Pixhawk was armed the throttle, yaw, pitch, and roll were tested. The tests resulted in results very similar to those seen in Sections 7.4.1 and 7.4.2. The primary difference was the reaction of the motors on the sides of the hexacopter. The velocity of these motors remained constant for pitching but followed the same reactions found in previous tests for rolling, yawing, and changing the throttle.

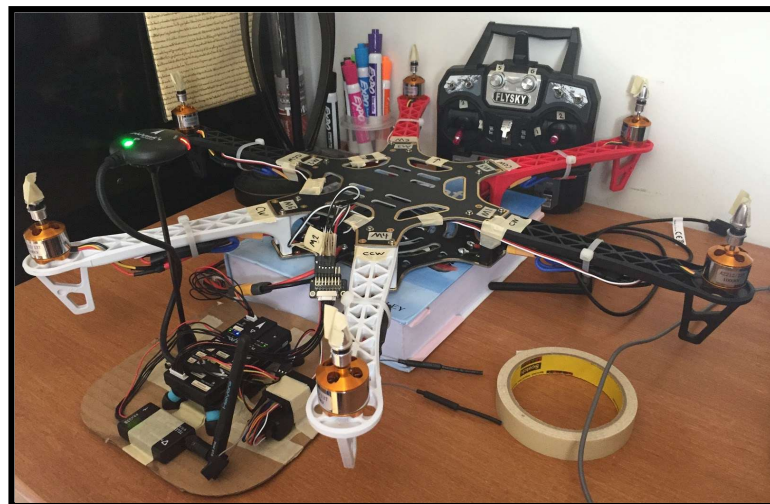


**Figure 91:** The Hexacopter Test Setup.

This test was a proof of concept for 12 motor control. There were two options for controlling 12 motors. The first option was to use the dodecacopter configuration on the PX4 firmware through QGroundControl, whereas the other option was to use the hexacopter configuration and split each control signal to control twelve motors. Future testing would need to determine the best option for control. The final dodecacopter electrical subsystem was not constructed because the team had not yet reached that phase of testing. The quadcopter prototype was the only system physically connected and tested.

## 8. Software Subsystem

### 8.1 - Generation of Mow-the-Lawn Flight Plans

#### 8.1.1 - Algorithm

The Mow-the-lawn approach is a method of sweeping an area for aerial imagery. It was originally inspired by the Mow-the-lawn approach used for underwater mapping in a previous research project by a student at Santa Clara University [19]. Given a selected region, a zig-zag flight path can be applied where images can be taken at specific points along the path. The Pixhawk utilizes a waypoint-based flight path system, where at each waypoint a photo by the drone would be taken by the FLIR Duo R. The images can then be stitched to create a larger singular image of that selected region. The Mow-the-lawn approach emphasizes image overlap, which results in higher quality image stitching and is particularly effective for agricultural use cases.

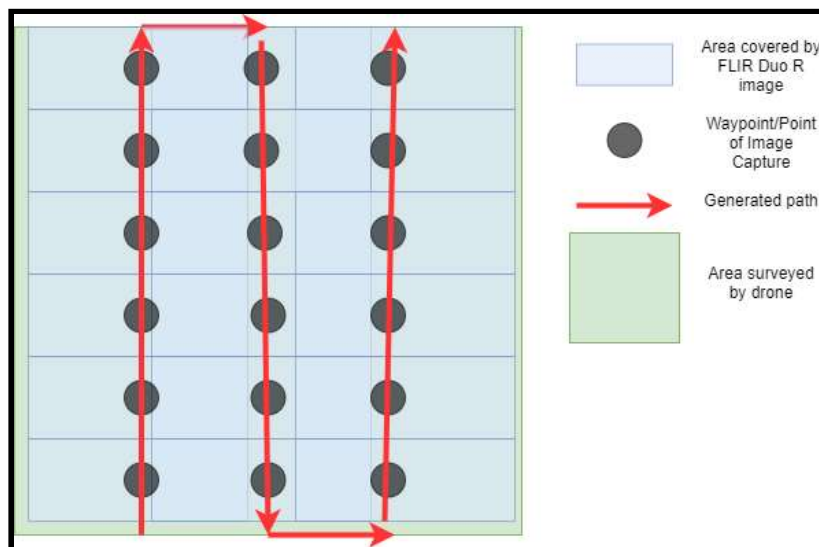


*Figure 92: Mow-the-Lawn approach.*

Each image taken by the FLIR Duo R covers a specific area of the selected region surveyed by the drone. The area overall increases as the altitude of the drone increases. The area of coverage can be interpreted as a rectangular pyramid.

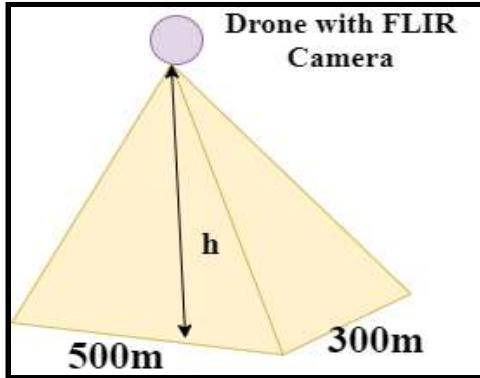


**Figure 93:** How a single image can cover a calculated area.

The slant height is first calculated using an interior triangle inside of the rectangular pyramid and Pythagorean Theorem. The slant height is the hypotenuse of this interior triangle. The slant height splits the faces of each side of the rectangular pyramid. Using the Field of View values given by FLIR in the longitudinal (xFOV) and latitudinal (yFOV) direction and the slant height, the length of each side of the rectangular base can be calculated. Overlap between images is defined as placing one image over another. The distance between two edges of overlapped images in either the latitudinal (overlapY) or longitudinal (overlapX) direction is the distance that waypoints are shifted in that direction.

$$\begin{aligned}
 sh &= \sqrt{h^2 + (h * \tan(fov))^2} \\
 arealength &= 2 * sh * \tan(yfov) \\
 areawidth &= 2 * sh * \tan(xfov) \\
 overlapy &= areaheight - (areaheight * OverlapPercentage/100) \\
 overlapx &= areawidth - (areawidth * OverlapPercentage/100)
 \end{aligned}$$

**Figure 94:** Calculation for the area of coverage.

### 8.1.2 - Implementations

The Mow-the-lawn approach was implemented with two interfaces: a web application and as a feature of QGroundControl. The web application is a custom-built piece of code aimed to make it easy for a user to select a region for the drone to survey using the FLIR Duo R. QGroundControl has this feature built in, but it did not have the proper configurations for the FLIR Duo R. Instead, a custom configuration was added to allow QGroundControl to utilize the area selection tool using configurations meant for the FLIR Duo R.

### **8.1.3 - Web Application**

The web application allows a user to interactively define a region on a map, specify parameters for a flight operation, and download a flight plan to cover the defined region with the Mow-the-lawn approach. The parameters to be configured on the website include hold time, radius, height, speed, field of view and overlaps for both horizontal and vertical. The generated flight plan can be uploaded to a drone via QGroundControl seamlessly. This custom web application was created with HTML, CSS and JavaScript.

The requirements for the website are to be able to generate a flight plan to Mow-the-lawn a rectangle, set parameters for a flight operation, and to be able to download a flight plan that can be imported to QGroundControl. Since all computations can be performed at the front-end, namely in JavaScript, there was no need for a back-end server. The web application is composed of one page that is responsive and usable on mobile devices. For the dynamic contents on the website, namely the map, Mapbox was utilized. Mapbox is “An open source mapping platform for custom designed maps” [20]. The web application comes with an intuitive drawing tool that was implemented using an open source library called “mapbox-gl-draw-assisted-rectangle-mode” [21]. Once a rectangular region is drawn on the map, points inside the region are processed to generate a flight plan.

To create the flight plan, the web application identifies the corners of the selected rectangular region. By visiting all corners with small steps determined by the overlap distance on both horizontal and vertical axes, the application can generate an ordered list of points to Mow-the-lawn the whole region. In order to accomodate the needs for rectangular shapes that are not parallel to longitude and latitude, a linear transformation of rectangular shapes is applied to the points. For example, a tilted rectangle would be transformed into a non-tilted rectangle where the edges of the rectangle would be Euclidean distances between the original points. Once the flight plan for the non-tilted, standardized rectangle is generated with the Mow-the-lawn algorithm, each point in the flight plan is converted to points in the original tilted field by applying the inverse of the linear transformation applied before applying the Mow-the-lawn algorithm.



**Figure 95:** Test area for the Mow-the-Lawn approach using the web app.

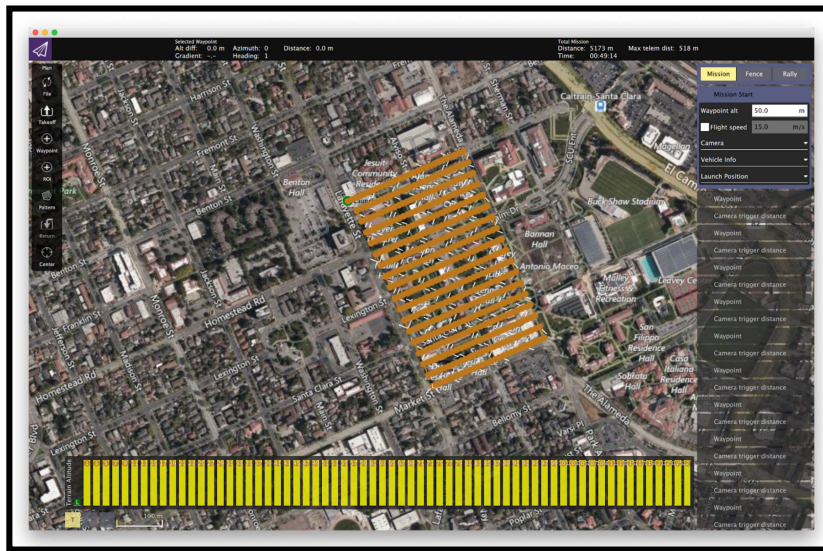


**Figure 96:** Test area for the Mow-the-Lawn approach with travel path implemented.

#### 8.1.4 - The Survey Feature of QGroundControl

Another implementation of the Mow-the-lawn approach is to utilize the survey feature of QGroundControl. This survey feature allows a user to define a region to survey and upload the flight plan to a flight controller. Initially, no support was available for the camera used in the drone's configuration, the FLIR Duo R. A configuration for the Flir Duo R was created for the survey feature on QGroundControl. The change implemented was accepted by the committees of the QGroundControl, and now the feature is available in the latest downloadable version of QGroundControl. Since QGroundControl is written in C++, the change was made in C++ by adding an instance to an existing data structure in QGroundControl's code base. The code for this change can be found in the Appendix H.

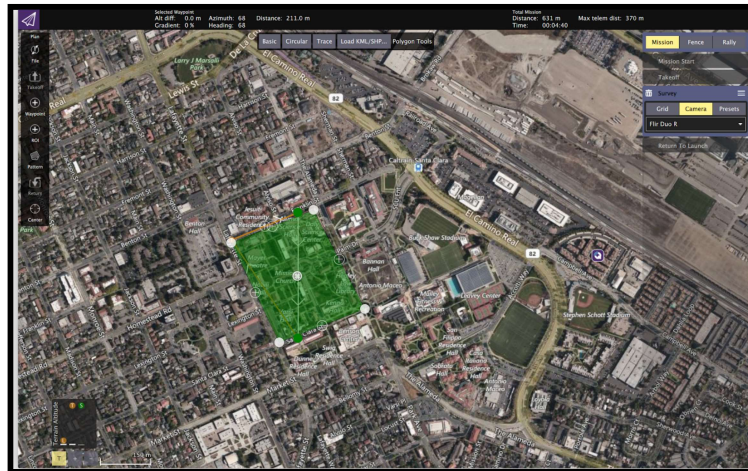


**Figure 97:** QGroundControl's survey feature with Flir Duo R configuration

## 8.2 - IR Image Analysis

### 8.2.1 - Photo Stitching

The photo stitching process involves the Agisoft Metashape software application. All photos from the FLIR Duo R camera must be imported to Agisoft Metashape. The photos aligned in the order that the photos are taken. A dense cloud is generated that marks in each individual image where there are depths and heights in the landscape with points. Once the points have been added to the image by Agisoft Metashape, a mesh is generated that creates a new model of the stitched images that includes the depths and heights of the landscape. This model can then have a detailed texture applied to it from the aerial images which is the final stitched image that the software produces and can be exported for further analysis.

To assist and speed up the process of generating a stitched photo, Agisoft Metashape contains APIs that can be used for Python scripting. A Python program has been created that utilizes the APIs to automate the process of aligning the images and stitching them to generate the final texture. The program is generic in that it can be used on any computer system that contains Agisoft Metashape. In addition to the flexibility of using this automation script, it can be modified to generate higher or lower quality stitched photos depending on the computational resources available.

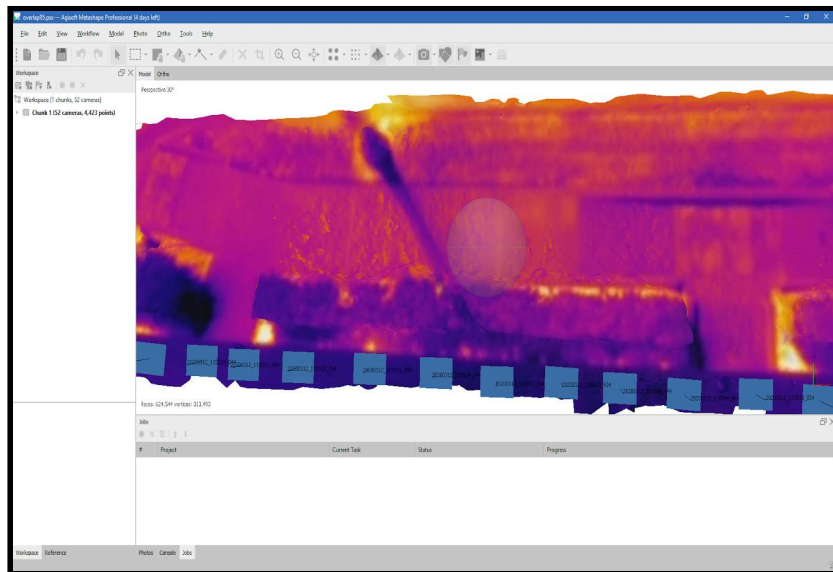


**Figure 98:** Screenshot of Agisoft Metashape with active IR stitch.

### 8.2.2 - Blob Analysis and Generation of a New Flight Plan

The image analysis process consists of four tasks and the entire process is done using Python, specifically was developed using Jupyter Notebook. An IR image stitched together must be represented as vectors in order to apply algorithms for further processing. For this task, a Python wrapper for OpenCV [21] and numpy [20] were used. Once an IR image is represented by vectors, a filter is applied to the image based on Hue-Saturation-Value (HSV) to extract regions of interest. The filter is based on color because the temperature difference of the thermal images is represented by different colors in an IR image as shown below.

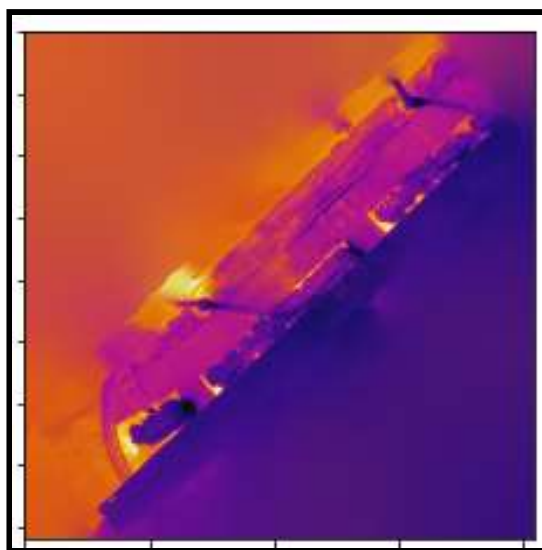


**Figure 99:** An Input IR Image (stitched together image of an area).

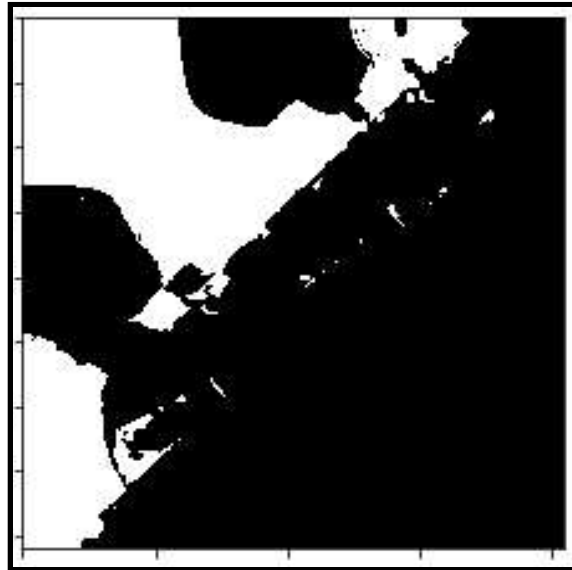


**Figure 100:** Extracted regions of interest via color filter.

Once the regions of interest are extracted, a clustering algorithm is applied to represent each region as a rectangle. The smallest unit in the new flight plan is represented to be a rectangle because the minimum unit of a photo is a rectangular shape. Since clustering is a NP-hard problem, meaning that it is computationally expensive, a heuristic algorithm called the K-means algorithm is applied to address this problem as shown in Figure 101.

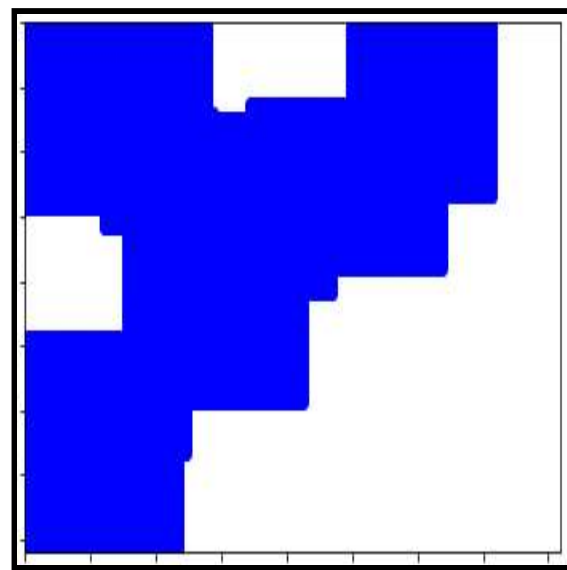


**Figure 101:** Applied K-means algorithm.

For each rectangle, the Mow-the-lawn algorithm is applied once more to derive a flight plan to cover the region. The Mow-the-lawn flight plans are connected with their closest neighbouring regions in order to generate a single flight plan to cover all regions of interest. With this software, a new flight plan to visit regions of interest can be generated automatically by giving an IR image with the flight plan used to take the photos as shown in Figure 102.



**Figure 102:** New generated flight plan from IR image.

## 9. Hardware

### 9.1 - Budget

The primary sources of funding for this design project came from the Santa Clara University School of Engineering and the Robotics System Laboratory. The most substantial costs for this project come from the electrical components such as the motors and propulsion equipment, especially the propellers. Because this drone is very large, featuring six pairs of contra-rotating propellers, these expensive components add up to a substantial investment.

*Table 14: Income for the Drone*

Source	Per Engineering Student	Contribution Total
Santa Clara University School of Engineering	\$500	\$3,000
Santa Clara University Robotic Systems Laboratory	N/A	\$10,921
<b>Sum Total:</b>		\$13,921

*Table 15: Expenses for the Drone*

Part	Product Name	Sub Assembly	Source	Quantity	Price Per	Total Price
Motor	U8 II KV190	Electrical	T-Motor	14	\$310	\$4340
ESC	FLAME 60A HV	Electrical	T-Motor	14	\$100	\$1400
Propellers	G28*9.2 Prop 2pcs	Aerodynamics	T-Motor	8	\$311	\$2488
Controller	Pixhawk 4 + GPS	Electrical	GetFPV	2	\$196	\$392
Battery	Tattu 22000 mAh 6S 25C LiPo	Electrical	GetFPV	4	\$478	\$1912
PDB	Tarot TL2996 12S 480A	Electrical	Amazon	3	\$46	\$138
Transceiver	HolyBro Transceiver Radio	Electrical	GetFPV	2	\$42	\$84
Arms	Square Tubing 1.5 inch width $\frac{1}{8}$ inch wall	Mechanical	Metals4U	2	\$27	\$54
Legs	Circular Tubing 1 inch diameter $\frac{1}{8}$ inch wall	Mechanical	Metals4U	2	\$19	\$38
Prototype Body	2x4	Mechanical	Home Depot	1	\$10	\$10
Ducts	3D Printed Ducts	Aerodynamics	IC3D Inc.	6	\$415	\$2490
Wire Connector	Wiring Connectors	Mechanical	Amazon	4	\$19	\$76
Battery Switches	Battery Switch Wiring	Electrical	Amazon	5	\$7	\$35

Wiring	Communications Wiring	Electrical	Amazon	2	\$13	\$26
Chassis Plates	5mm Plywood	Mechanical	Home Depot	2	\$16	\$32
Fasteners	Assortment of Fasteners	Mechanical	Home Depot	84	\$2	\$168
Motor Mounts	3D Printed Motor Mounts	Mechanical	Jinxbot 3D Print	12	\$14	\$168
Support Rods	¼ Inch Threaded Rod	Mechanical	Home Depot	5	\$6	\$30
Testing Equipment	Anemometer	Aerodynamics	Amazon	1	\$40	\$40
<b>Sum Total:</b>						\$13,921

Overall, the current prospective cost totals up to \$13,921 with contributions from the School of Engineering and Robotic Systems Laboratory matching these expenses. With COVID-19 impacting the businesses that we planned on purchasing other materials from, the cost of the system is expected to be larger in the future, especially if the previous parts, such as the chassis plates, motor spacers, and chassis mounts are substituted for the initially chosen materials.

## 9.2 - Physical Testing Accomplishments and Documentation

Due to the hazard associated with testing the drone, several documents and testing procedures were written up to act as safety instructions and for evaluating the performance and capabilities of the drone and the drone subsystems.

The thrust and velocity tests are meant to determine how accurately the Star-CCM+ simulations model the real world. For this, a test stand was constructed with the purpose of safely testing the propeller. Another stand was conceptualized for the thrust test - however, because material arrived after the quarantine was implemented for the COVID-19 pandemic, the stand was not constructed. Although further testing was largely halted for this year, the capabilities to test are all prepared and accessible via the supplementary HLD documents, most notably the safety and thrust test documents. These tests were meant to not only show a proof of concept for the propellers and control system but also meant to take data for the airflow and thrust generated by the system.

**Table 16:** The purpose and expected outcomes for implementing aerodynamic tests

Purpose	Results	Learning Outcome
To physically test the lift efficiency of the duct.	Velocity (m/s), Thrust (N)	Make a decision on how to iterate the next design.

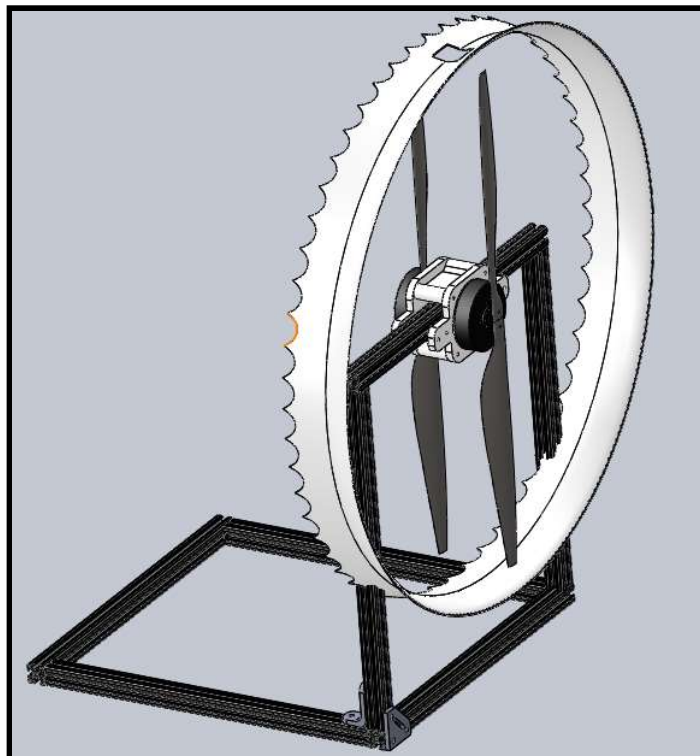


**Figure 103:** Velocity Test Stand.

This test stand is utilized in accordance with the document titled: *Velocity Test Stand Procedure*, which outlines the purpose and the reasons for conducting the test as well as the outcomes from it. This was not the only purpose of the stand as it was also used to test the electrical control system.

**Table 17:** Descriptions for the two test stands that should be used by future teams or by RSL approved personnel.

Test Stand 1	Test Stand 2
Velocity Test: Pitot tubes measure the velocity on the trailing edges of the duct.	Thrust Test: A force/spring scale measures the thrust generated by a motor and propeller.

Another important milestone was achieved before COVID-19 shut down the testing facility at NASA AMES consisting of the Hover Flight Test. This test was meant to show how the electrical layout of the drone worked for a quadcopter configuration, most notably the PID controller. It was also critical in understanding propeller behavior and lifting capability as it served as a test bed for many components.

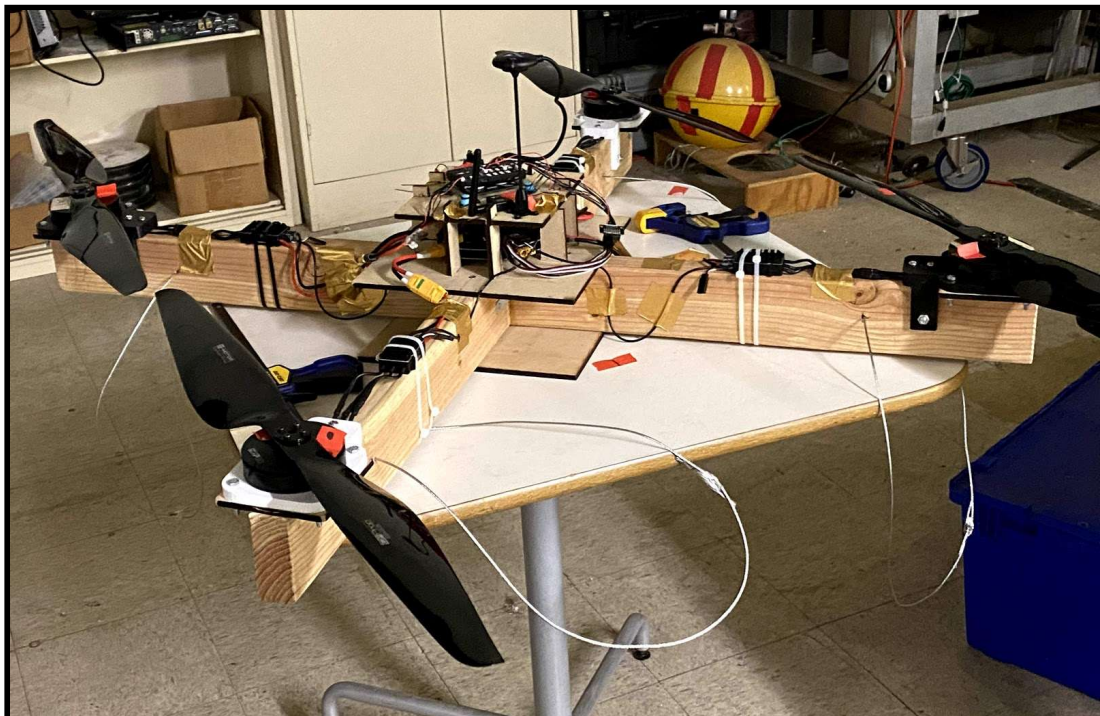


**Figure 104:** Configuration for Quadcopter Prototype equipped with propellers and electrical components.



**Figure 105:** Hover test for Quadcopter Prototype using tethers to limit hover height.

As shown in the figures above, the tethers were attached to the arms and mounted to the table so that the drone would not fly higher than a set point. After the drone performed well in the initial tests, the tethers were progressively lengthed. The last hover test was conducted March 6th which achieved a controlled 8 inch elevation.

While the Quadcopter was planned for disassembly shortly after its intended usage (serving as a test bed for components and low level flight), the system was kept intact at the end of the project so that it could support future tests. Doing this avoids unnecessary risk in damaging newly developed products and or components. Although this proof of concept is significantly smaller than the final product, all the electrical configurations as well as the code for the system can be further developed for the final dodecacopter. All of the electrical configurations can be found in Appendix G.1, and they essentially outline the physical layout for the electrical system of the drone.

Although the long term goals for this project were altered due to COVID-19, major goals that were marked at the start of this capstone project, such as various FEA, Testing Procedures and Safety Documentation, and Construction of both a working prototype and a stationary model were accomplished. All Testing Procedures have been developed - however, there may be smaller edits that may be required to ensure the most efficient test procedure and methodology. Additionally, the construction of the final drone, which was initially optimized for weight and strength, had to be altered due to COVID-19 limiting our access to certain parts and

manufacturing facilities. For instance, the final product was not given a carbon fiber plate, instead, it was made of plywood to save on fabrication feasibility and time. Reverting to the initial design of the drone is certainly doable, as all the plans, procedures, and schematics necessary for doing so are available. There may of course, be other areas for optimization if the next team wishes to change the drone's primary objective. These areas will be explored in the Future Work section of this document. The current testing procedures that have been drawn up and some drafts which have been sorted through by RSL can be found in Appendix A.7.

## **9.3 - Completed Hardware**

With the many changes that have come from the national conditions surrounding COVID-19, many changes had to be made in the manufacturing process of the drone. As discussed previously in this report, certain materials were changed and several design decisions had to be made in order to produce a structural prototype which would be feasible to manufacture with limited resources. In addition, this prototype is intended to serve as the platform for physical flight testing when it is permitted once again by the university and the Robotic Systems Lab.

### **9.3.1 - Chassis Manufacturing**

The first change that had to take place in the manufacturing of the drone was the material and process for creating the central chassis. The original design as shown in the left of Figure 106 below is the original design constructed from 4 levels of carbon fiber with 3D printed fixtures. Due to the closure of the manufacturing company and the limited access to 3D printing following the COVID-19 conditions, the material of this subassembly was changed to wood. The right side of Figure 106 shows the simplifications to the design that were made when manufacturing the physical structure of the chassis subassembly. While the original design featured multiple internal cut outs for weight reductions and airflow, these were not replicated in the simplified plywood design. In addition to the plywood sheets for the structural layers, the 3D printed brackets which fix the arms in the original design were recreated out of plywood as well.

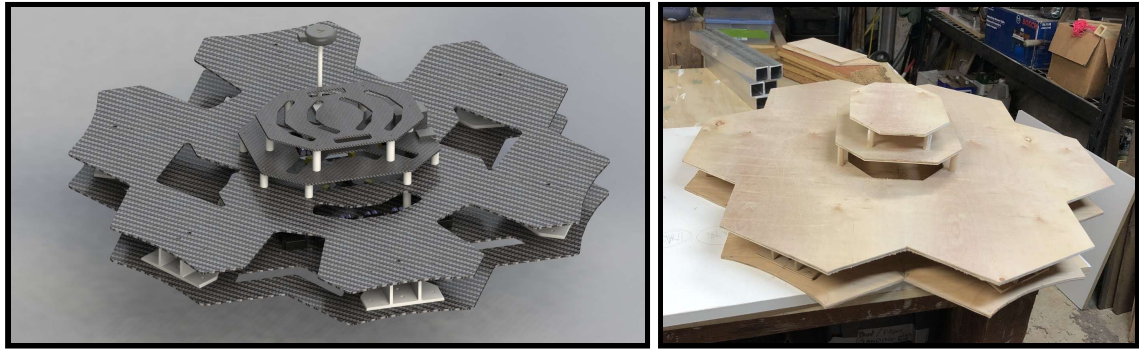


**Figure 106:** Original conceptual design (left) and the achieved design (right) for the chassis.

### 9.3.2 - Arms, Motor Mounts, and Support Fixtures

The construction of the arms subassembly went mostly unchanged from the original design, with the only alteration being the spacers between the motor mounts which were recreated from a structural foam-core as shown on the right in Figure 107 below. These components, used as spacers for the motor mounts and as the mounting point for the crossed supports which pass through the ducts, were originally designed to be three separate 3D printed fixtures. This change simplifies the construction of the subassembly and reduces the weight, but the structural integrity of the foamcore is not as strong or durable as the original design.

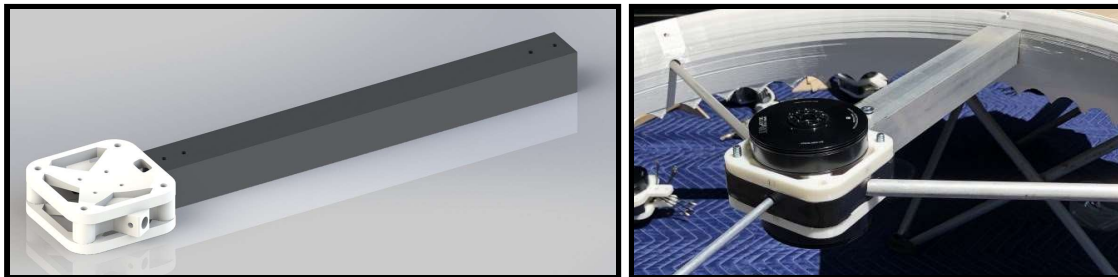


**Figure 107:** Original conceptual design (left) and the achieved design (right) for the arms.

The arm was made from the hollow aluminum tubing as initially designed and the motor mounts were successfully printed as intended. The support fixtures attach to the arms in the same configuration as the original design, and pass through the ducts according to the original design as well. These supports were constructed from the same alloy of aluminum as the arms according to the original design.

### 9.3.3 - Undercarriage Manufacturing

The construction of the undercarriage was successfully completed according to the material and components of the original design. The Aluminum tubing and 3D printed fixtures

were manufactured in accordance to the proposed design as shown in the original rendering and the finished manufactured product shown in Figure 108 below. The only change to the proposed design is the fixture at the end of the bottom most members of the undercarriage which were changed from 3D printed components to rubber end caps.



**Figure 108:** Original conceptual design (left) and the achieved design (right) for the undercarriage.

#### 9.3.4 - Final Drone Prototype Assembly

The final assembly of the physical prototype of the drone features all of the structural components of the design and can house all of the hardware and electrical components required for flight tests. Although the original prototype was not accomplished due to COVID-19, this assembly serves as the first functional prototype for the HLD system. For the time being, the only electrical components attached to the drone were the motors in order to present the completed assembly including the propellers. The original design is presented along with the completed structural prototype in Figure 109 below.



**Figure 109:** Original conceptual design (top) and the achieved design (bottom) for the full drone assembly.

While this achieved model does not have all of the completed features intended to be in the original design, it serves as a good platform for the hardware of this project. All of the structural assembly was completed in a manner that is consistent with the goals of the original design, and changes that had to take place were within acceptable limits given the circumstances. If conditions allow following the restrictions from COVID-19, the model may even be adapted to conduct preliminary flight testing in the field, but this would be the task of another group.

Although the drone would theoretically be capable of flight several checks would still need to be made to ensure that the drone would properly behave under the pilot's control and that the hardware is approved for flight. This would also include reviewing any documentation relating to the test and to the drone for safety. More so before each flight test, certain checks are necessary prior to any live testing with this model to ensure that any changes made in the modified manufacturing process would not be detrimental to the function of the drone.

## **10. Professional Issues**

### **10.1 - Ethics**

Unlike other projects which may have an explicit humanitarian or ethical purpose, the Heavy Lift Drone, combines a powerfully technical project with an indirectly anti - monopolistic framework. This drone solution bridges the gap between a drone that is light enough to operate without advanced licenses, affordable enough to be purchased by individuals, safer than existing models, while simultaneously boasting a high payload-to-weight ratio. The primary ethical purpose of our drone is to provide smaller farmers with the ability to compete with larger farming corporations, and match/exceed their standards for water usage and crop irrigation efficiency.

Economic Darwinism, is the idea that the most financially profitable individuals and corporations will survive in the market economy. This is a key phenomenon which the development of the drone aims to address. Beyond the reality that social darwinism can only provide short term benefits to society (for instance an initial reduction in prices for consumers due to more streamlined processes), it can be argued that it is simply an unethical ideology which this system is working to combat. The Markkula Center's Framework for Ethical Decision Making [22] outlines the ethical approaches that we have taken in the development of our drone. For instance, the drone combines a Utilitarian approach, which calls for the greatest balance of good over harm, with the fairness approach that argues that all humans should be treated equally. In providing a more affordable solution for smaller farmers to keep up with larger farming corporations, our drone satisfies these outlined approaches. Overall, due to the project's unique ability to fill an ethical need in society, it comes with a significant amount of risk that has been attempted to be minimized, as described below.

### **10.2 - Safety and Legal Framework**

The very nature of this project carries with it a level of risk that needs to be addressed. Being a very large drone that is seven feet across, with 12 propellers that are each 28 inches in diameter that spin rapidly, safety measures were outlined so that usage of the system does not result in injury.

The propellers were the main hazards within the system due to the rapidly spinning blades possibly coming into contact with foreign objects. To mitigate this risk, ducts that envelop each propeller were added to the system. These ducts also theoretically provided a noise dampening effect so that large magnitude sound waves that were generated by the propeller system would be reduced. Another physical safety measure that was added was an emergency stop button. This would cut power to the system when the situation became unsafe for the drone to continue flight.

Additionally, an extensive set of rules and procedures were developed for operating the drone. Some of these rules outline what conditions the drone requires for nominal flight. As an example, a large distance must be maintained between the operator/observers and the dodecacopter system when the system is active unless a barrier is present allowing that distance to be reduced. These procedures also cover different possible tests and how to perform these system validation experiments. These tests and other safety regulations are packaged with the drone system ensuring that the user must read these documents before usage.

### **10.3 - Economics and Sustainability**

As is often the case in many industries, large corporations end up squeezing out small businesses and monopolizing the market, leading to increased costs for consumers. Big industrial farms are implementing efficient irrigation and crop tending practices that smalltime farmers cannot. The Heavy Lift Drone system seeks to balance the playing field by providing a relatively affordable way for these farmers to compete. A high payload-to-weight ratio, as well as the HLD's relatively low cost help to reduce the differences between these farmers and industrial farms.

In terms of agriculture and the improvement of techniques in that industry, the HLD can scout out areas using its IR camera and detect at-risk regions of soil. This would result in the application of water and fertilizer in a localized area of need. This would lead to a significant reduction of resources needed, as well as an increase in crop production. As stated by Dr. Berezovskiy, "...the use of a drone can help increase the crop yield by 10%" [23]. In addition to that benefit, the HLD can give useful feedback on how much fertilizer should be used effectively as drones have been shown to reduce fertilizer use by 20% [23].

Besides the economic aspect of the HLD, its environmental impacts lead to a more sustainable footprint. During the design phase of the HLD, it was important to emphasize the manufacturability as well as the ability for quick disassembly and reassembly. The HLD is meant to be very lightweight, but also rigid and safe to operate. A large number of components were 3D printed, as that was the simplest and most accurate manufacturing method for small quantities. When the circumstances did not permit 3D printing, alternative manufacturing methods were employed in order to preserve the overall design of the drone while using materials and methods more readily available to the team. All of this was done without much material waste, as the extraneous material was either utilized on the system or used for another project/job.

# **11. Conclusion**

## **11.1 - Summary**

The primary purpose of the Heavy Lift Drone project was to create a drone that could lift a total system weight of 55 lbs. This drone was to be used in agriculture, specifically as a device for crop surveying. This report has documented the progress in the research, development, and design for creating the HLD. In order to identify the requirements for our project, several potential customers in multiple fields were interviewed. By considering these customer needs, a series of product requirements were developed in order to give quantifiable goals for the project - which were then developed into practical metrics that our final project could meet.

As progress into the design of the drone was made, a variety of concepts were generated to address certain aspects of the design criteria. Several of the initial concept designs were modified to account for various criteria, although the primary concern with the construction of the drone came down to balancing weight considerations with structural integrity. After the weight was reduced, there was a fusion of two designs to ensure that the frame would be rigid enough to last throughout a flight. This led to the final design of the drone and prompted material sourcing and manufacturing for the rest of that quarter.

Additionally, there was a considerable amount of Finite Element Analysis (FEA) done in both stress analysis and fluid simulations. This was to prove that the drone performed optimally for a given task, as well as to assess the dangers and liabilities if a problem arose mid flight and during takeoff and landing. It was determined through a combination of product iteration and FEA that the design choices made were close to, if not the most optimal ones. The goals and timeline of the past three quarters were then laid out, and it was determined that they were fully accomplished in Fall and Winter quarter, and partially completed in Spring.

It was found that the inclusion of the ducts (shrouds) around the propellers does indeed increase the lift of the drone by a factor of 14.7%. Additionally, the final projected cost for the drone was significantly lower than that of our direct competitors. Costing \$13,921, or nearly 8.5% lower than the nearest comparable drone available for sale, this product also featured a higher projected payload-to-weight ratio of 0.5, as opposed to 0.4 from the competition.

The functionality of the electrical subsystem was achieved through the design, implementation, and testing of the propulsion substructure and communication/control. In terms

of design, basic motor control and pilot side communication was perfected on hobby components prior to its implementation on the prototype and before testing different motor control configurations. Both of these tests succeeded - where the results of the prototype implementation were seen in successive hover tests of the quadcopter prototype. Likewise the different configurations were aptly executed for the proof of concept in dodecacopter flight.

Additionally, the several supplemental software systems aiding flight operation of the HLD are implemented correctly. The software system includes a web application built in JavaScript to generate a waypoint-based flight plan to upload to the Pixhawk 4 drone controller. An Arduino controller using a C program then triggers the camera to take an aerial thermal photo at each waypoint to collect thermal images. An automation script in Python utilizes Agisoft Metashape via APIs to stitch the thermal images into a larger singular image. Analysis of the stitched image takes place via an algorithm that identifies areas of interest with high temperatures to generate a new flight plan for further surveying and photo acquisition.

While the physical implementation of the HLD was severely impacted by COVID-19, there were still many ways that the manufacturing of the project was accomplished. Most of the finalized design was accomplished within the project timeline. These included the aluminum structure of the arms, the undercarriage, and the various support structures, in addition to the 3D printed fixtures for motors, and the undercarriage connection points. The modifications that were implemented due to COVID-19 included the plywood chassis plates instead of carbon fiber/polycarbonate version, as well as recreating or modifying many of the parts originally designed for 3D printing from various other materials and manufacturing methods. Overall the construction of the HLD changed from its original design, however, the achieved physical model is a successful representation of the system. This structure also allocates room for growth in future versions of the system.

## 11.2 - Future Work

This project was able to meet most, but not all of the original goals laid out for the Spring '20 quarter, due to many barriers met during the time period including COVID-19. Considering these setbacks, planned continuation of the project will be explored by the Robotic Systems Lab.

Further testing, design modifications, and mission implementations can be evaluated in later iterations.

Many of the early tests conducted in this process established subsystem success criteria. For example, the aeronautical and electrical systems were tested on a constructed velocity propeller test stand to determine if the wiring was configured correctly. While a procedure to test the velocity was laid out, data was not gathered for it. Other systems had similar testing done such as the mechanical, electrical, and software system, in that all of them were tested independently. This means that the system in its entirety was not rigorously tested. To ensure a fully successful drone, all these tests should be explored in further depth along with further flight testing.

Optimization of the mechanical design is also to be carried out for future iterations. Some of the parts, namely the motor mounts as well as the conceptual carbon fiber plate, had cuts in the material for reducing the system weight. Streamlining the arms of the drone for aerodynamic efficiency reasons will also increase the flight time, which is something that can be explored.

Generally, simulations were conducted to analyze whether a design was effective in accomplishing the task each part was meant to fulfill. Some simulations were not conducted, largely due to inadequate computational capabilities, as the full drone assembly was far too complex. This can be remedied in the future by generating a mesh simple enough to be analyzed, but complex enough to be realistic. Another useful simulation would be to do a thermal analysis on the drone in order to determine how the system heats up under certain throttling conditions and to ensure the integrity of the material and that the components can withstand the burden of flight. Along with thermal analysis, modal frequency evaluations are to be explored so that the vibrating system can perform its task without experiencing rapid deconstruction due to flutter or resonance.

For the electrical subsystem, the components have yet to be stress tested in order to better understand the limitations of the system and to ensure that the system can continue to safely operate during emergency maneuvers. The transmitter and receiver can be optimized in order to maximize the drone's operational range as well. Antenna selection and a review of laws regarding sending and receiving signals without special licensure, like a ham radio license, would also need to be explored.

In terms of software, additional features can be implemented into the web application that accompanies this system. This includes selecting areas to survey that are not rectangular in shape, while applying the Mow-the-lawn algorithm. Connecting the FLIR camera directly to the Pixhawk flight controller, instead of an Arduino, to gain access to GPS data and geotag aerial images would benefit the system as well. This would allow for configurable quality stitching, depending on available computational resources. This would also increase the efficiency of the analysis algorithm that generates a new flight plan within a selected region.

## References

- [1] "How Much Does It Cost to Become a Pilot?" *Pilot Institute*, 29 Apr. 2020, [pilotinstitute.com/pilot-license-cost/](http://pilotinstitute.com/pilot-license-cost/).
- [2] NASA, National Aeronautics and Space Administration. Computational Aerodynamic Modeling of Small Quadcopter Vehicles  
[https://rotorcraft.arc.nasa.gov/Publications/files/73\\_2017\\_0015.pdf](https://rotorcraft.arc.nasa.gov/Publications/files/73_2017_0015.pdf)  
[https://rotorcraft.arc.nasa.gov/Publications/files/73\\_2017\\_0015.pdf](https://rotorcraft.arc.nasa.gov/Publications/files/73_2017_0015.pdf)
- [3] Penkov and D. Aleksandrov Propeller shrouding influence on lift force of mini unmanned quadcopter  
[http://ijame.ump.edu.my/images/Volume%2014%20Issue%203%20September%202017/7\\_Penkov%20and%20Aleksandrov.pdf](http://ijame.ump.edu.my/images/Volume%2014%20Issue%203%20September%202017/7_Penkov%20and%20Aleksandrov.pdf)
- [4] Sánchez-Caja, Antonio & Rautaheimo, Patrik & Siikonen, Timo. (2000). Computation of Incompressible Viscous -Flow Around a Ducted Propeller Using a RANS Equation Solver.
- [5] Kuantama, Endowednes & Craciun, Dan & Tarca, Radu. (2016). QUADCOPTER BODY FRAME MODEL AND ANALYSIS. ANNALS OF THE ORADEA UNIVERSITY. Fascicle of Management and Technological Engineering.. Volume XXV (XV), 2016/1. 10.15660/AUOFMTE.2016-1.3205.
- [6] What is a MultiCopter and How Does it Work?. (2019). Retrieved from <http://ardupilot.org/copter/docs/what-is-a-multicopter-and-how-does-it-work.html#what-is-a-multicopter-and-how-does-it-work>.
- [7] What is Lift. National Aeronautics Space Administration (2015, May 15). Retrieved from <https://www.grc.nasa.gov/WWW/K-12/airplane/lift1.html>
- [8] Instructables. (2017, October 27). Lithium Polymer Etiquette: a Comprehensive Guide to Working With LiPo. Retrieved from <https://www.instructables.com/id/Lithium-Polymer-Etiquette/>.
- [9] Audronis, Ty. *Designing Purpose-Built Drones for Ardupilot Pixhawk 2.1: Build drones with Ardupilot*. Packt Publishing. Kindle Edition.
- [10] xFold Dragon. (n.d.). Retrieved from <http://www.xfoldrig.com/xfold-dragon/>.
- [11] Big Hexy- Heavy Lift Drone. (n.d.). Retrieved from

[https://bigdroneguy.com/products/big-hexy?variant=28313274974280&cy=&utm\\_campaign=gs-2019-05-27&utm\\_source=google&utm\\_medium=smart\\_campaign&gclid=CjwKC Ajw\\_uDsBRAMEiwAaFiHa5tYurRdkKV55mp6-d9EaRn-nhKsP-gCKOdOMDohHEbW NGw94nl8dBoCqvcQAvD\\_BwE](https://bigdroneguy.com/products/big-hexy?variant=28313274974280&cy=&utm_campaign=gs-2019-05-27&utm_source=google&utm_medium=smart_campaign&gclid=CjwKC Ajw_uDsBRAMEiwAaFiHa5tYurRdkKV55mp6-d9EaRn-nhKsP-gCKOdOMDohHEbW NGw94nl8dBoCqvcQAvD_BwE)

[12] Build your own DRONES. (n.d.). Retrieved from <https://www.scorpiondrones.com/>.

[13] AltiGator. (n.d.). OnyxStar® HYDRA-12 - Heavy-lift drone with 12Kg of payload.

Retrieved from

<https://drones.altigator.com/onyxstar-hydra12-heavylift-drone-with-12kg-of-payload-p-41854.html?zenid=t72mc08gh1jl8877mmh0esn772#options>.

[14] Aircraft - VulcanUAV. (n.d.). Retrieved from <http://vulcanuav.com/aircraft/>.

[15] Stepniewski, W. Z.. *Rotary-Wing Aerodynamics* (Dover Books on Aeronautical Engineering) . Dover Publications. Kindle Edition.

[16] NASA, National Aeronautics and Space Administration. Aeroelastic effects in multi-rotor vehicles with application to a hybrid heavy lift system. Part 1: Formulation of equations of motion

[17] Meriam, J. L., et al. *Engineering Mechanics: Dynamics*. 8th ed., Wiley, 2015.

[18] Beer, Ferdinand P., et al. *Mechanics of Materials*. 8th ed., McGraw-Hill Education, 2020.

[19] Rasal, Ketan. “Navigation & Control of an Automated SWATH Surface Vessel for Bathymetric Mapping.” Santa Clara University, Santa Clara University, 2013, pp. 23–25.

[20] Gunderson, Eric. “Mapbox” Mapbox, <https://www.mapbox.com/>.

[21] Geostarters. “Geostarters/Mapbox-Gl-Draw-Assisted-Rectangle-Mode.” GitHub, Geostarters, 12 Dec. 2019,

[22] Santa Clara University. “A Framework for Ethical Decision Making.” *Markkula Center for Applied Ethics*, Santa Clara University,  
<https://www.scu.edu/ethics/ethics-resources/ethical-decision-making/a-framework-for-ethical-decision-making/>

[23] Berezovskiy. “Reducing Fertiliser Application by 20% Using an Ebee Ag Drone.” *Youtube.com*, SenseFly, 8 Apr. 2016,  
[www.youtube.com/watch?v=p2ryvtX4Oh4&feature=youtu.be](https://www.youtube.com/watch?v=p2ryvtX4Oh4&feature=youtu.be).

# Appendix

## A - Airflight Research

This section outlines some of the aerodynamic terms and orientations that were discussed in research. Although they do not contribute substantially to the content in the thesis it is a cornerstone of how the literature review and design was executed and conceptualized.

### Aircraft Operation:

There are four main forces on an aircraft. The first, weight, is the product of the mass of the object multiplied by gravitational acceleration. Lift is the force opposing the weight which is produced by the airfoils of the aircraft such as the wings or the propellers. Air flows over the aero surface producing a difference in pressure enabling such lift to be generated. Drag is the force that opposes the movement of the aircraft which is dependent on the shape of the aircraft, the viscosity of the air, and the velocity of the aircraft. Lastly, thrust is the force that moves the aircraft forward. Typically a propeller, jet, or rocket generates the velocity necessary for forward motion. Visualizations for such topics, as well as potential drone configurations, are shown below in the following figures:

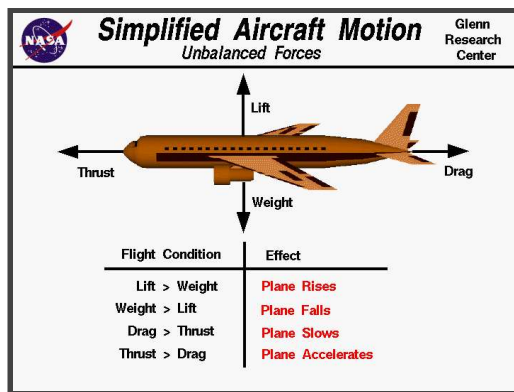


**Figure A1:** Components of Aircraft Motion [2]

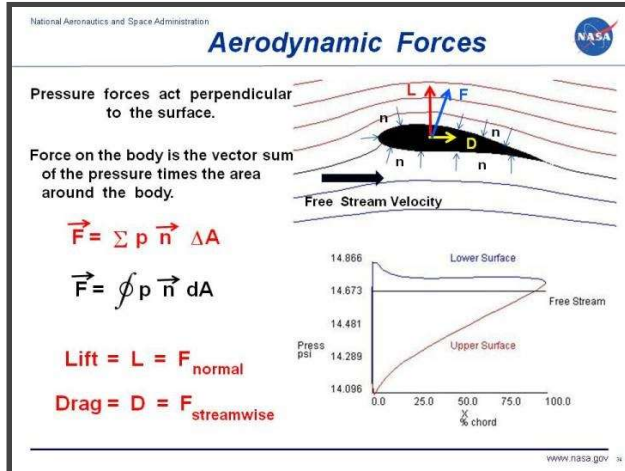


**Figure A2:** Aerodynamic forces acting on a wing [2]

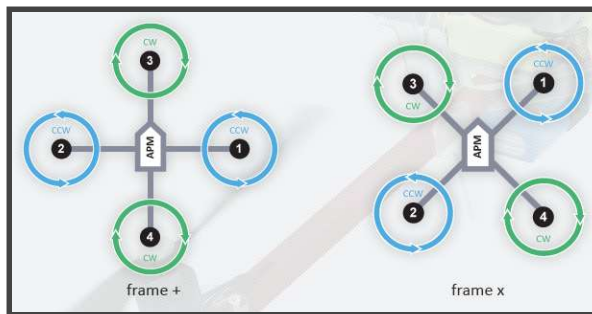


**Figure A3:** Quadcopter Configurations [6]

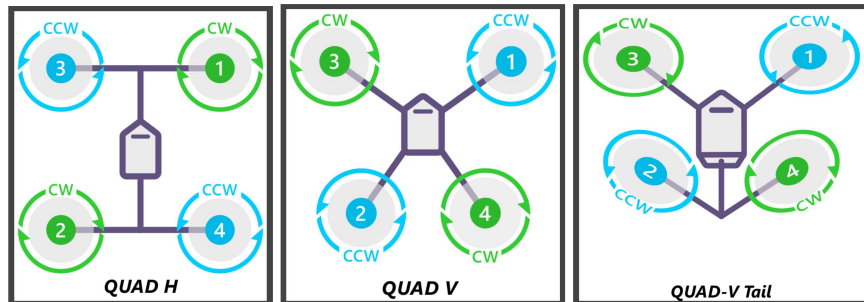


**Figure A4:** Additional Quadcopter Configurations [6]

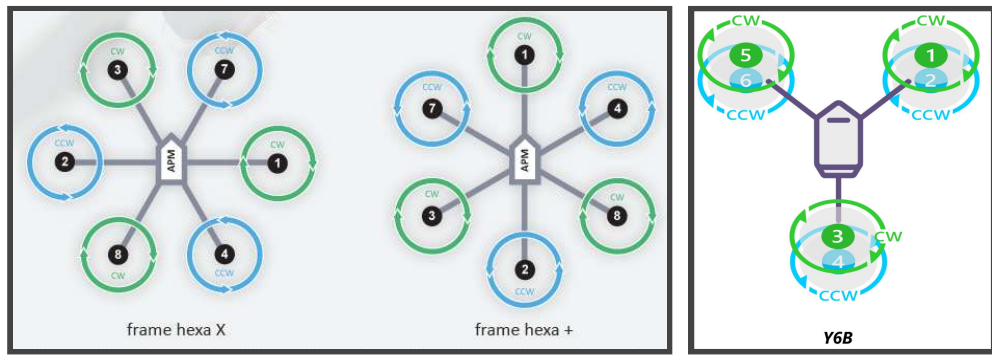


**Figure A5:** Hexacopter Configurations [6]

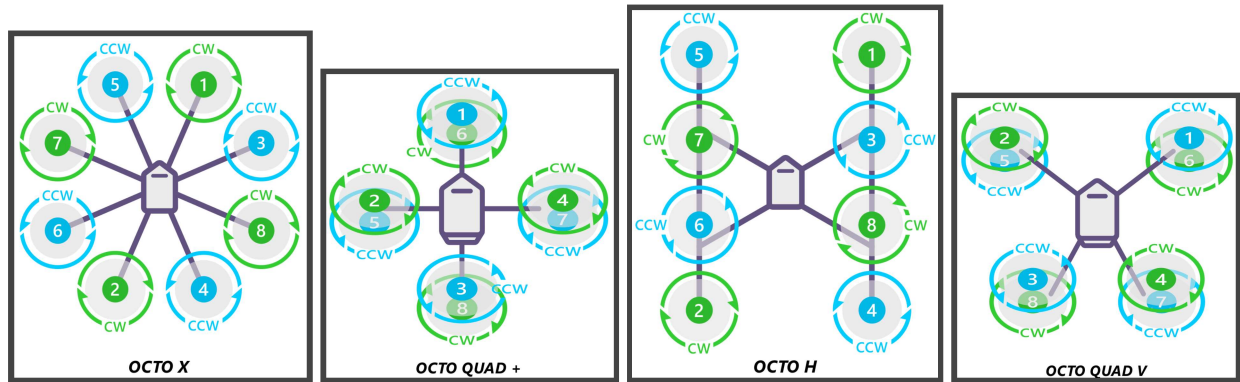


**Figure A6:** Octocopter Configurations [6]

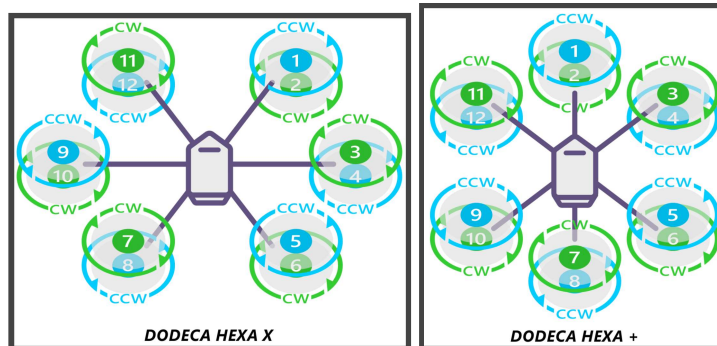


**Figure A7:** Dodecacopter Configurations [6]

## B - Customer Needs Q&A

This section outlines the potential customers that the team interviewed for insights into what this project should seek to be capable of doing. After these interviews were conducted a table was drafted that contains all of the major needs that the drone should be able to accomplish

*Interviewed Individual:* John Cugini (Packaging and delivery Director at Phoenix Controls)

*Questions/Queries:*

- Reduce physical trips by an employee who has multiple payloads to make
  - What does the drone need to be able to do?
  - Are there payloads that are physically hard to carry (outside of weight constrictions)?
  - What sort of restrictions should the drone have to ensure safety and performance are up to spec?

*Potential applications for delivery:*

- Carrying payload
  - Up a multi-storied building
  - Across a distance that a car/other vehicle can not traverse

*Answers/Responses:*

- Wants the drone to be very easy to control in flight:
  - Accurate in movement
  - Lower liability of machine
  - When it is given a load it should “be able to handle whatever it’s given”
- Needs to deliver packages faster than a worker otherwise it becomes a liability
- Be able to adapt to any environment “weather”:
  - Resistant to water and rain, snow
  - Look at how it deals with heat and the battery life with heat conditions
  - Humidity vs dry

- Safety measures for if the drone loses connection to the user:
  - Landing sequence if drone detects abnormality
  - Sensors implemented for emergency landing sequence
- Handle landing even with human error

*Interviewed Individual:* Chris Shay (Vice President of Operations at Santa Clara University)

*Questions/Queries:*

- What do you do at SCU
- SCU and Drones:
  - What has been done
  - What could be done/applied
- Process for flying drones (if he knows)
- Safety relating to drones:
  - Ideas on what safety protocols/  
actions we can implement

*Answers/Responses:* Filming has been good.

- Applying OSHA window washing to the drone system.
- Especially for Charney and STEM building.
- Amazon packaging. Ways to consolidate package flow so skateboarding
- Delivering water/fertilizer to balcony plants on STEM building
- Camera system on campus, felony's forwarded to campus safety.
- Hazard management
- Grounds people
- Solar panel/roof surveys
- Emergency: Scans, delivering medicine

*Interviewed Individual:* Nina Shami (Agricultural Developer)

*Potential Applications for agricultural use:*

- Distributing water/chemicals from above
- Multispectral imaging to detect early warning sign for plant health
- Infrared camera to identify underground irrigation patterns

*Questions/Queries:*

- How many acres of land do you need to irrigate each day?
- What methods do you use for irrigation in your fields?
- How many crops do you lose per season on average?
- Are there common plant diseases that predominantly affect your crops and can it be avoided?
  - Do such diseases spread throughout the entire crop field from a few initial plants?
- How much water does your field need per square foot per day?
- What is the maximum temperature in this area?

*Answers/Responses:*

- 50 Acres Walnuts, 3 Acres Pecans
- 20 Acres Lease to Plunasa: Raspberry's, Wheat, Strawberries, Corn
- Watered through drip irrigation
- Walnuts watered through levied flooding
- Pesticides for walnuts
- Maximum daily temperature can exceed 100 F
- Nematode, spiders, diseases are main concerns

*Interviewed Individual:* Kevin Fontana (Assistant Director to Facilities and Operations at Santa Clara University)

*Potential Applications for agricultural use:*

- Your role in athletics
  - Knowledge of drones
- Sports that could benefit from drone assistance

*Questions/Queries:*

- Duration of most sports/games/events
  - How much coverage time is needed
- Proximity of the shot
  - What sort of restrictions should the drone have to ensure safety and performance are up to spec?

*Answers/Responses:*

- Taking care of teams, equipment, maintaining equipment/upgrades. AEC (new training facility, 2 basket ball court, academic center. Transportation of local games, cross country, etc. Nike arrangements.
- Sports information department handles videography, for highlights. Freelancers come in.
- Tennis, soccer, baseball are also handled along with water polo.
- Don't have a drone and don't have too many needs.
- Average time: 2-3 hours 3.5 max 1.5 min
- Usually one photographer during the entire game. Some students use phones for social media coverage.
- Drone coverage is welcomed, just not much money for it.
- Concerns for drones in sports: interference in play (noise/distraction, physical danger)

*Interviewed Individual:* Mike Rasay (Photographer)

*Potential Applications for agricultural use:*

Potential applications for photography:

- Carrying camera

*Questions/Queries:*

- Stabilizer for flying camera footage
  - How heavy is the camera that you would like to use?
  - What areas would you be filming in?
  - What is the maximum temperature in this area?
  - How long would you film for? Typical footage time?
  - Are your subjects typically in motion or static?

*Answers/Responses:*

- Depends, Lenses are defining weight gain. ~12-15lbs
- ~5-8 lbs. Tripods are usually rated for weight of such lenses/systems.
- On market, Matrice is usually go-to for video end of operations.
- Drone isn't most useful in gyms/arenas where he usually shoots. Usually football/other sports have those applications for drones. Friends in the business have gotten pilots licenses in order to diversify and gain more opportunities. Usually the surfing world is a popular field.
- A lot of people in this business, especially landscape photographers, operate in temperate climates. Desert is a "hot" topic for such shots. Also ocean has thermal winds that push the drone around which is a tough environment. 40's is most likely lowest.
- In scheduled event, 1-3 hours of shooting is the average amount of time on the job. With art driven jobs (portraits, landscapes, etc.), can take from 5 minutes to 5 hours.
  - "How many extra camera batteries do I need? How many do I have to have in order to be safe?" For new cameras and their spec sheet, battery life isn't an issue, its quality that is focused on.

- "How convenient can I make it for myself?" Sometimes 8 extra batteries is required for a job. Mike uses 4 different cameras with different slots, but uses the same battery. Plugging in and changing battery is what is important, not how long it lasts.
- Up to an hour is spent walking and checking out shots for 10-15 min max, evaluating scope and picture. Mainly the time is invested in looking at the frame, and thinking about what is wanted.
- Repeatability is a valued asset. Driven by capability, not by infinite space. In the photography world, power consumption is usually balanced with battery life.
- Both static and dynamic shots.
- Safety of drones next to triathlon race, how to make it safer. Think about putting a safety component into the Heavy Lift Drone.

**Table B1:** Benchmarks on customer needs (where “•” represent a score between 1 and 5. For reference, “••••” is the highest score attainable.)

#	Part	Need	Importance	Vulcan	Hydra	Big Hexy	Our Drone
1	The drone	Is easy to assemble/disassemble	4	••	•	•	••••
2	The drone	Is not too noisy	2	•	•	•	•••
3	The drone	Is safe to handle and manipulate	5	••	•••	••	••••
4	The drone	Needs to move swiftly	3	•••	•••	•••	•••
5	The drone	Must be able to crash safely	4	••	•	•	••••
6	The drone	Can sustain flight for	3	••	••	••••	••••

		30 minutes					
7	The drone	Is affordable for small companies	3	••	••	••••	••••
8	The drone	Can perform tasks that humans cannot	4	••••	••••	••••	••••
9	The drone	Has a long lifespan	3	•••	•••	•••	••••
10	The drone	Can carry a large load	4	•••	•••	••••	••••
11	The drone	Takes off and lands smoothly	3	•••	•••	•••	•••••
12	The drone	Is lightweight	3	••	••	••	•••
13	The drone	Instills pride	5	••••	•••	•••••	•••••
14	The drone	Is easily cleanable	2	•••	•••	••••	•••••
15	The drone	Is controlled through an app	1	•	•	•	••••
16	The drone	Is able to operate at high temperatures	3	•••	•••	•••	•••
17	The drone	Stored in a convenient way	5	•••	•••	••	••••
18	The drone	Is less expensive than competitors	4	••••	•••	••	••••
19	The chassis	Is sturdy and does not flex too much	5	••••	••••	••	••••
20	The	Is aesthetically	3	••••	••••	•	•••••

	chassis	pleasing					
21	The chassis	Is robust and not prone to breaking	4	••••	•••	••	•••••
22	The landing gear	Is able to land on uneven surfaces	2	••	••	••	•••
23	The ducts	Protect the drone from minor collisions	4	•	•	•	•••••
24	The ducts	Prevent user contact with propellers	5	•	•	•	•••••
25	The propellers	Have a long lifespan	4	•	•	••	••••
26	The propellers	Are safely mounted and covered	5	•••	•••	•••	••••
27	The electronic s	Are easily accessible for maintenance	4	•••	•••	••••	••••
28	The electronic s	Are easily modifiable	3	••	••	•••	••••
29	The electronic s	Reliably communicate with the controller and computer	5	•••	•••	•••	••••
30	The batteries	Can be accessed and swapped easily	4	•••	••••	•••••	•••••

**Table B2: Customer Needs Matrix (5 notes the highest importance)**

#	Component	Need	Importance
1	The drone	Is easy to assemble/disassemble	4
2	The drone	Is not too noisy	2
3	The drone	Is safe to handle and manipulate	5
4	The drone	Needs to move swiftly	3
5	The drone	Must be able to crash safely	4
6	The drone	Can sustain flight for 30 minutes	3
7	The drone	Is affordable for small companies	3
8	The drone	Can perform tasks that humans cannot	4
9	The drone	Has a long lifespan	3
10	The drone	Can carry a large load	4
11	The drone	Takes off and lands smoothly	3
12	The drone	Is lightweight	3
13	The drone	Instills pride	5
14	The drone	Is easily cleanable	2
15	The drone	Is controlled through an app	1
16	The drone	Is able to operate at high temperatures	3
17	The drone	Stored in a convenient way	5
18	The drone	Is less expensive than competitors	4

19	The chassis	Is sturdy and does not flex too much	5
20	The chassis	Is aesthetically pleasing	3
21	The chassis	Is robust and not prone to breaking	4
22	The landing gear	Is able to land on uneven surfaces	2
23	The ducts	Protect the drone from minor collisions	4
24	The ducts	Prevent user contact with propellers	5
25	The ducts	Increase lifting efficiency	4
26	The propellers	Have a long lifespan	4
27	The propellers	Are safely mounted and covered	5
28	The electronics	Are easily accessible for maintenance	4
29	The electronics	Are easily modifiable	3
30	The electronics	Reliably communicate with the controller and computer	5
31	The batteries	Can be accessed and swapped easily	4

## C - Component Diagrams and Additional Concept Generation

The purpose of this section is to outline all of the conceptualization of design elements for the drone. Although some of them were not incorporated into the final design it was useful for formulating the final design and because there is more work to be done some of these designs can be used by other senior project groups.

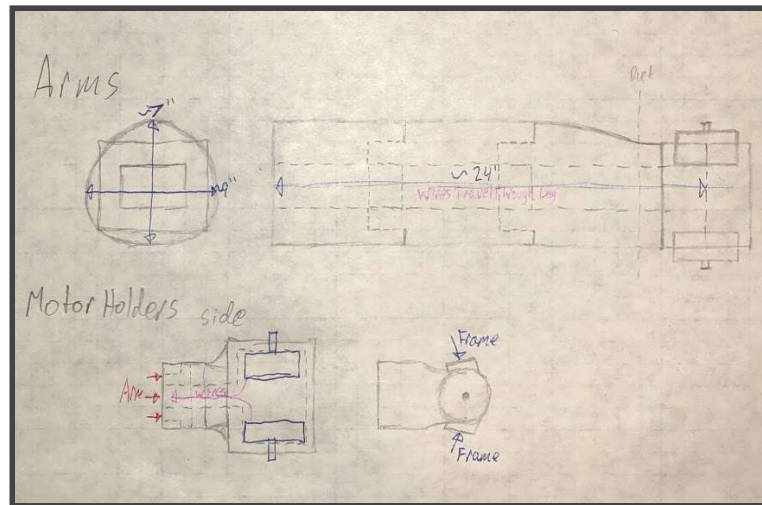


**Figure C1:** Initial Arm sketches

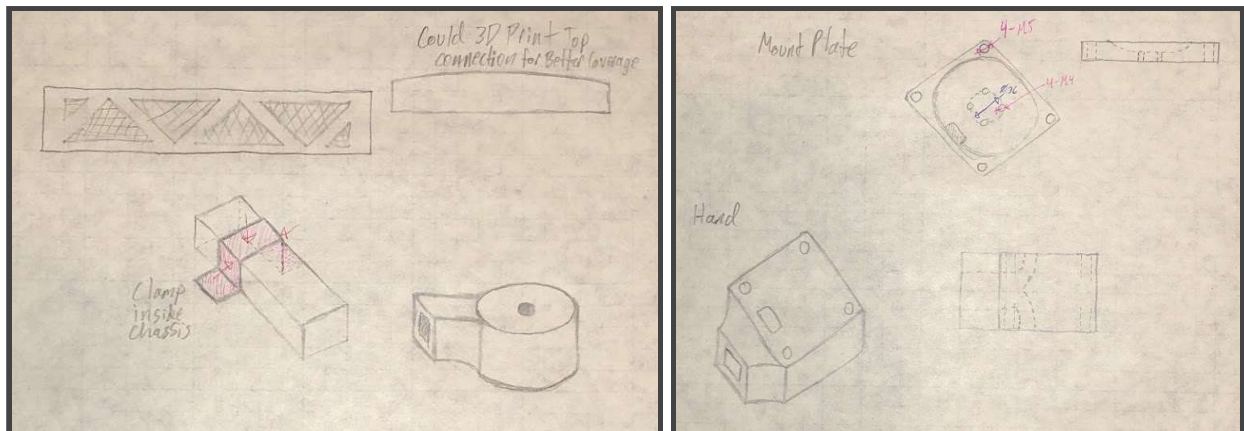


**Figure C2:** Alternate Arm sketches

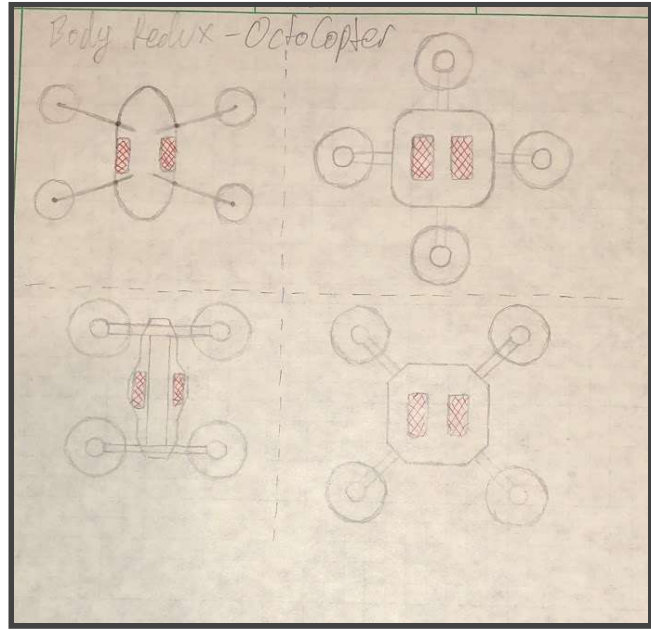


**Figure C3:** Initial concepts for the layout of the drone as an octocopter

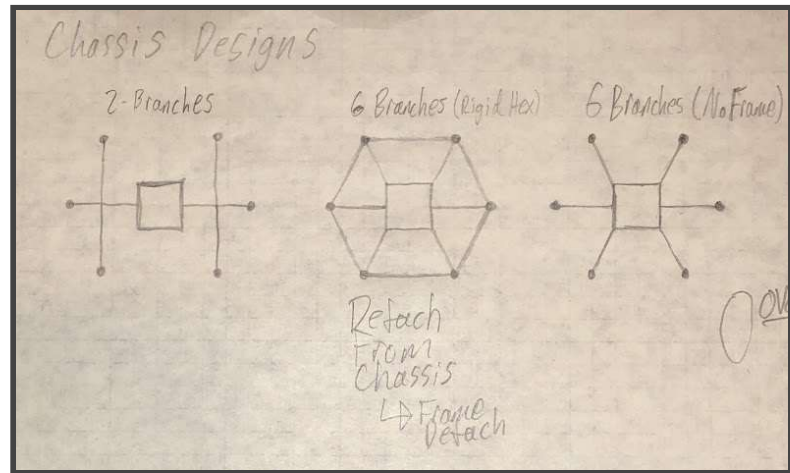


**Figure C4:** Initial concepts for the layout of the drone as a dodecacopter

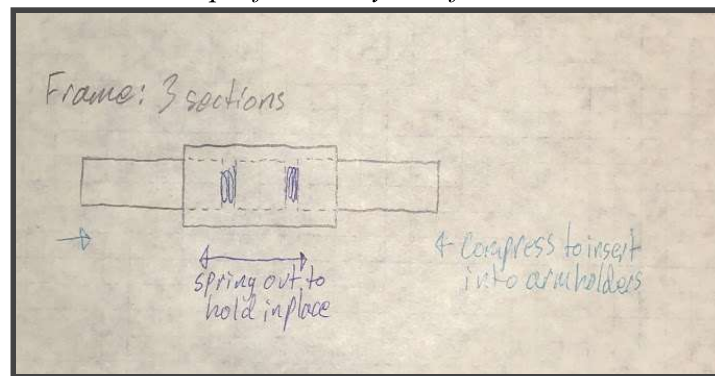


**Figure C5:** Initial concept for the frame of the drone using a telescoping design

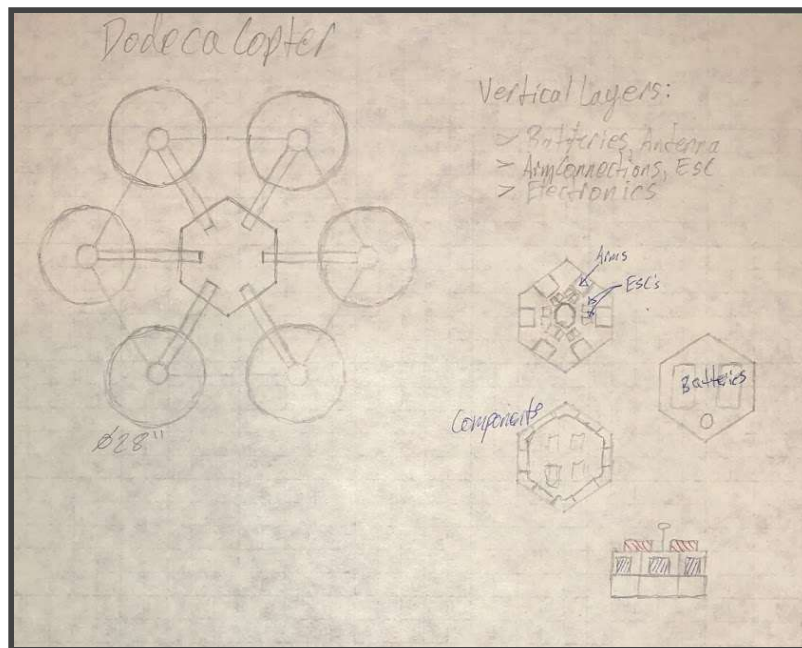


**Figure C6:** Layout for the drone and the proposed design for the chassis using layers of acrylic sheets

In the next section, the full collection of component diagrams for the structural assembly of the drone are presented. The next 38 pages include detailed, dimensioned drawings for the major subassemblies and the individual components which make up the construction of the Heavy Lift Drone.

8

7

6

5

4

3

2

1

F

F

E

E

D

D

C

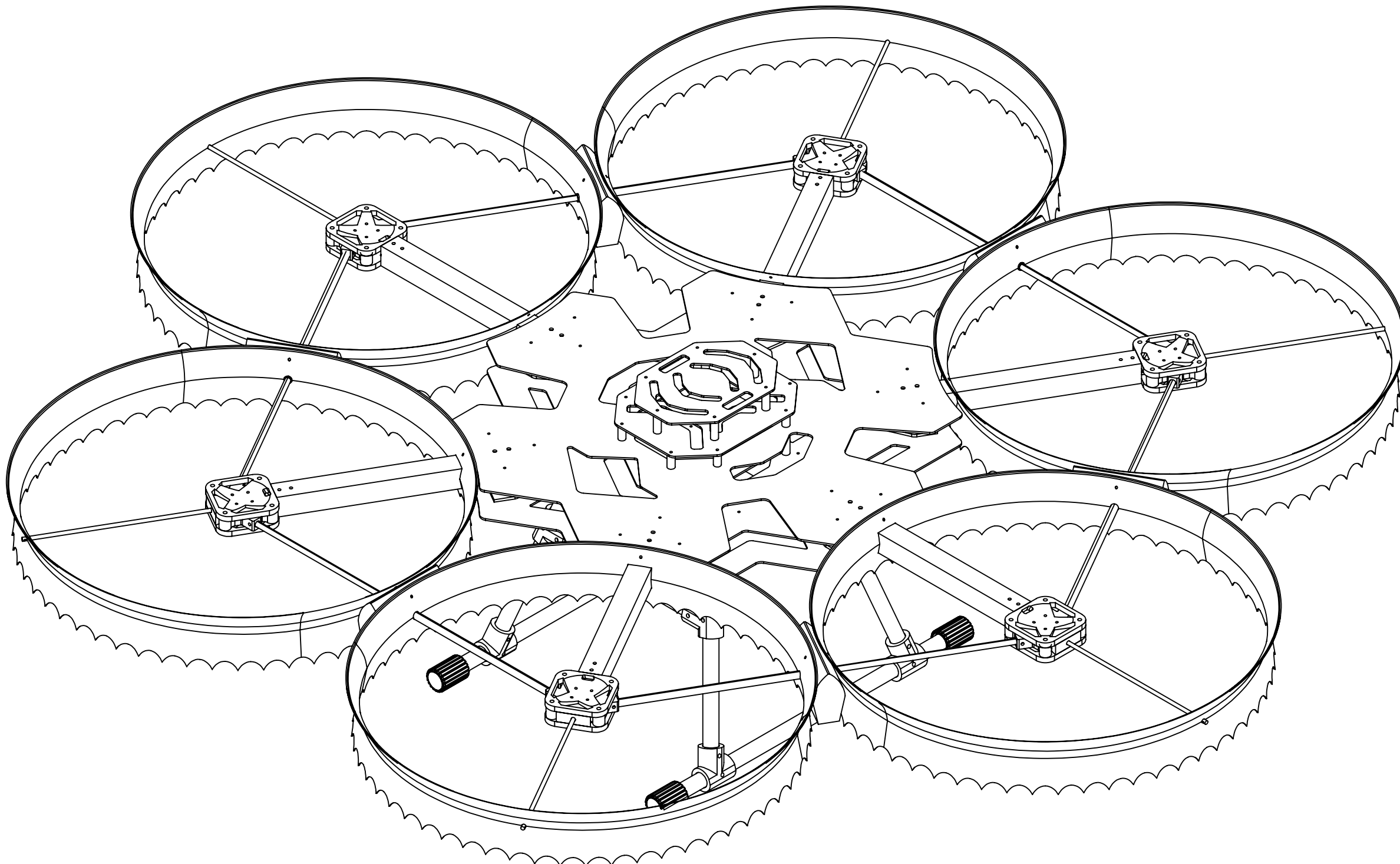
C

B

B

A

A



Group 5:  
Sam Carhart  
David Cooper  
Michael Kaliterna  
Sami Lama  
  
Santa Clara University  
Mechanical Engineering

**Heavy Lift  
Drone**

Material:  
Mixed  
Assembly

Assembly:  
Drone

Part Quantity:  
1

Part ID:  
HLD-A1

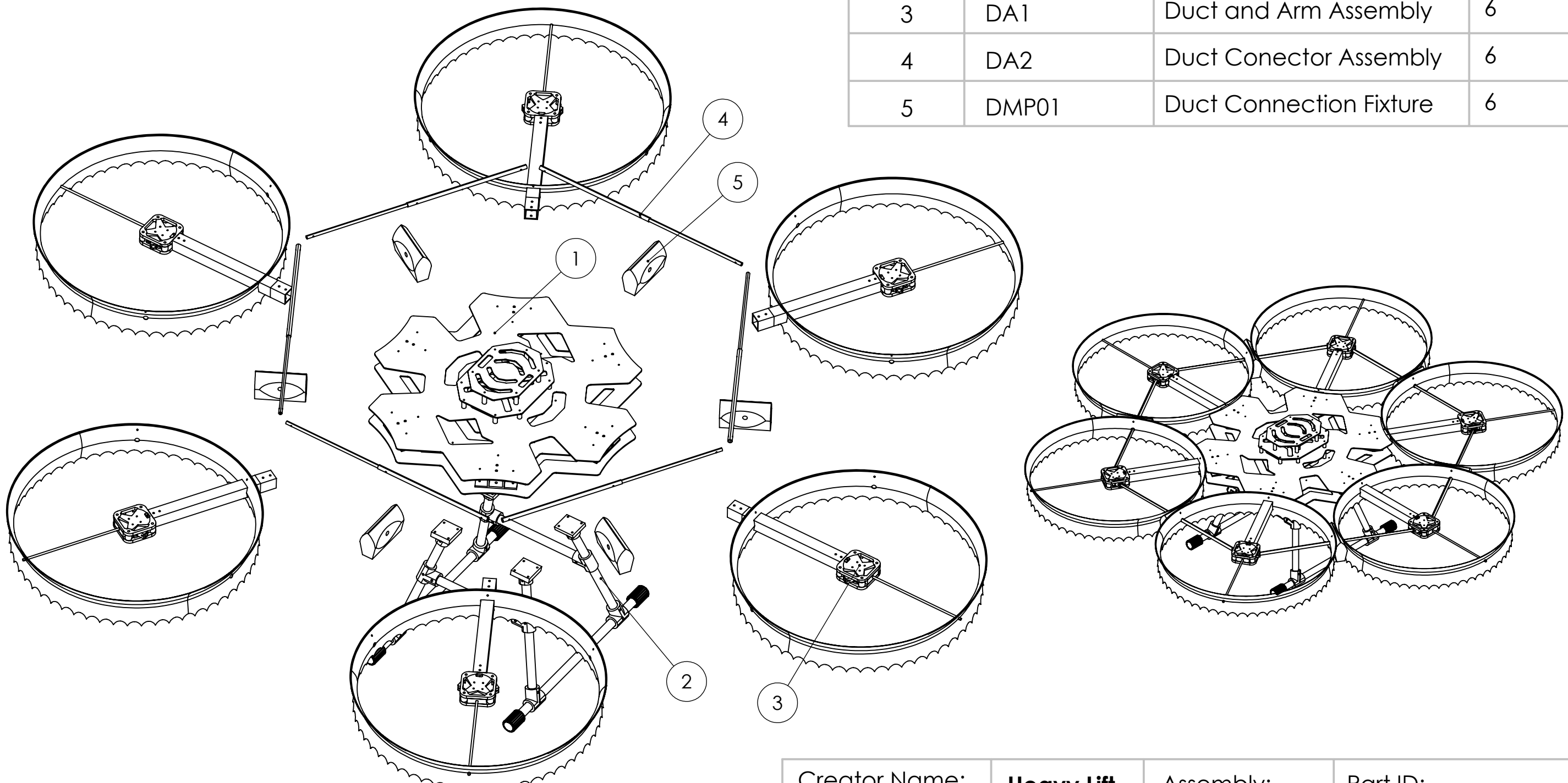
Description:  
Drone Structural  
Assembly

SCALE:1:7

SHEET 1 OF 3

8 7 6 5 4 3 2 1

Item No.	Part ID	Description	Qty
1	CA1	Chassis Assembly	1
2	LA1	Undercarriage Assembly	1
3	DA1	Duct and Arm Assembly	6
4	DA2	Duct Conector Assembly	6
5	DMP01	Duct Connection Fixture	6



Creator Name: Sam Carhart	<b>Heavy Lift Drone</b>	Assembly: Drone	Part ID: HLD-A1
TOLERANCES: 0.X = $\pm 0.05$ 0.XX = $\pm 0.005$ 0.XXX = $\pm 0.0005$	Material: Mixed Assembly	Part Quantity: 1	Description: Drone Structural Assembly

8 7 6 5 4 3 2 1

8

7

6

5

4

3

2

1

F

F

E

E

D

D

C

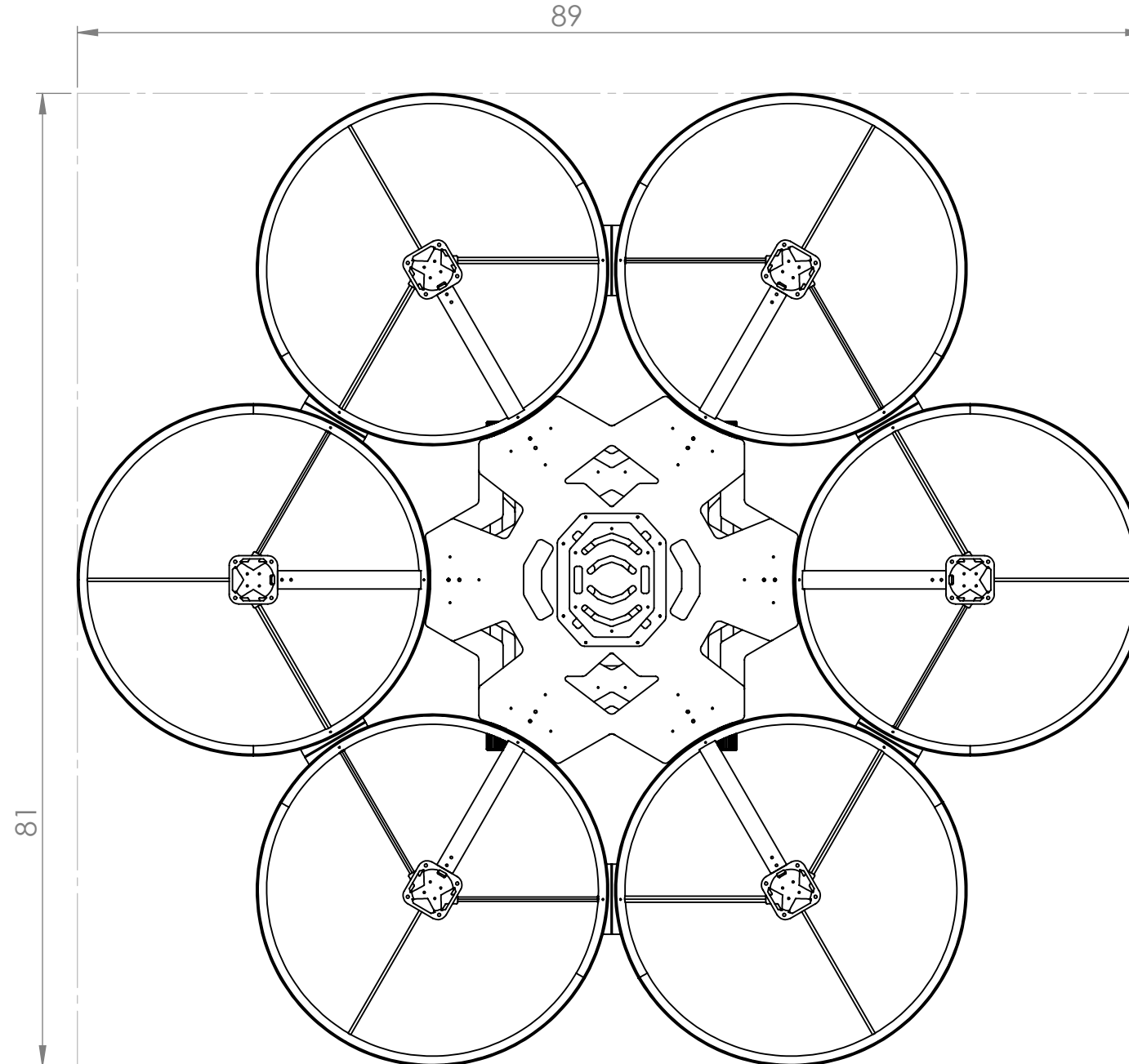
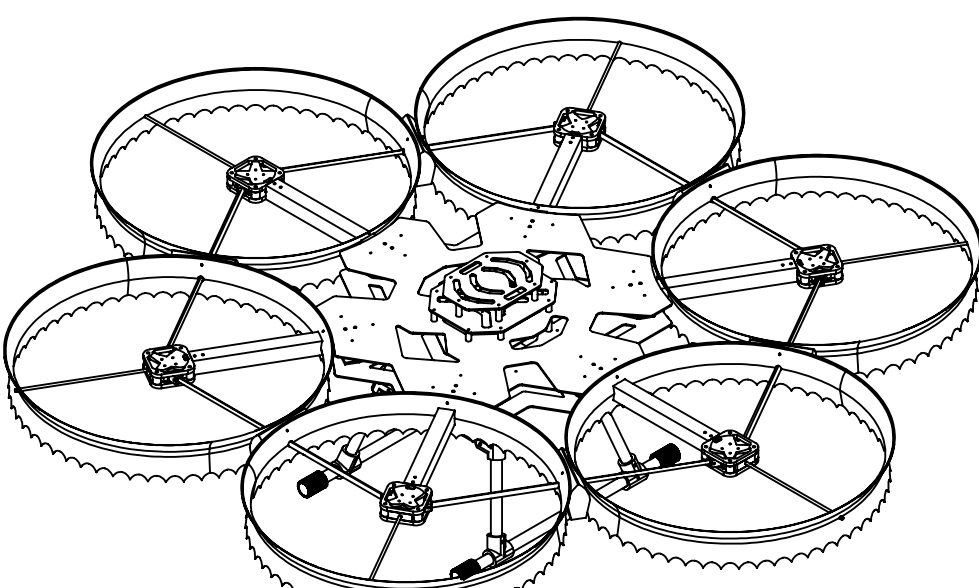
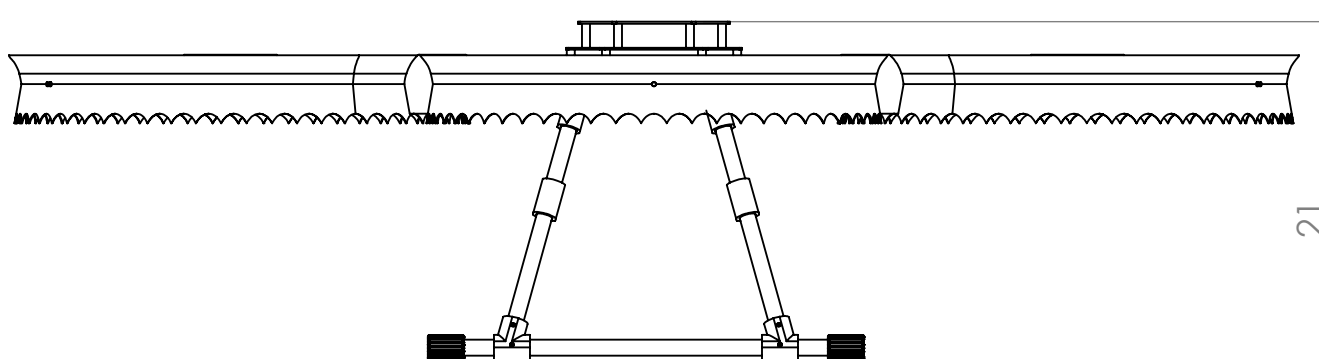
C

B

B

A

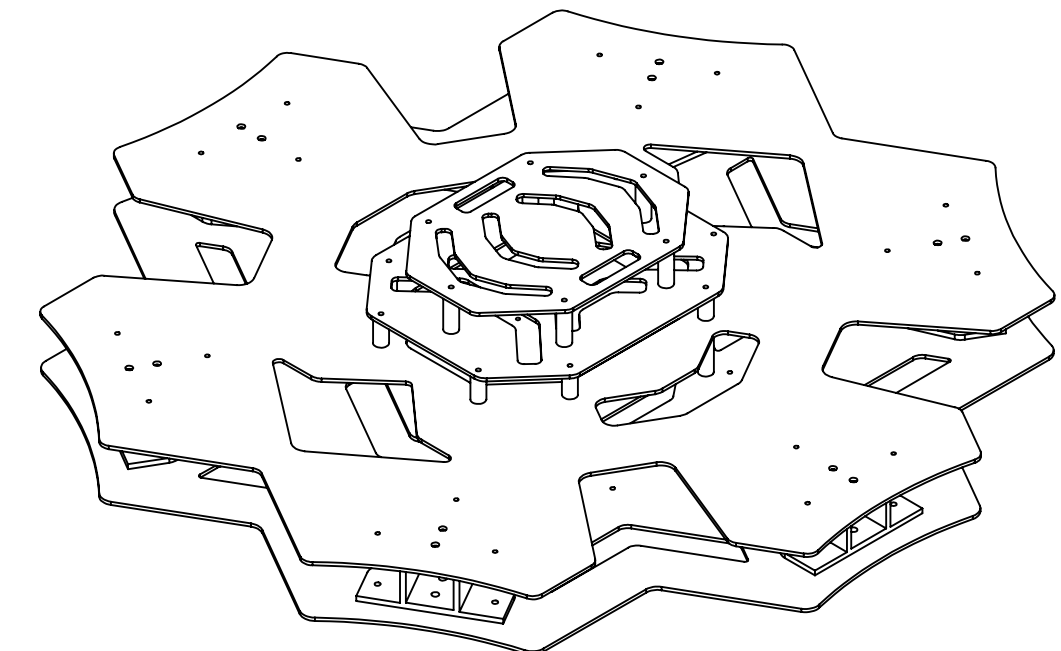
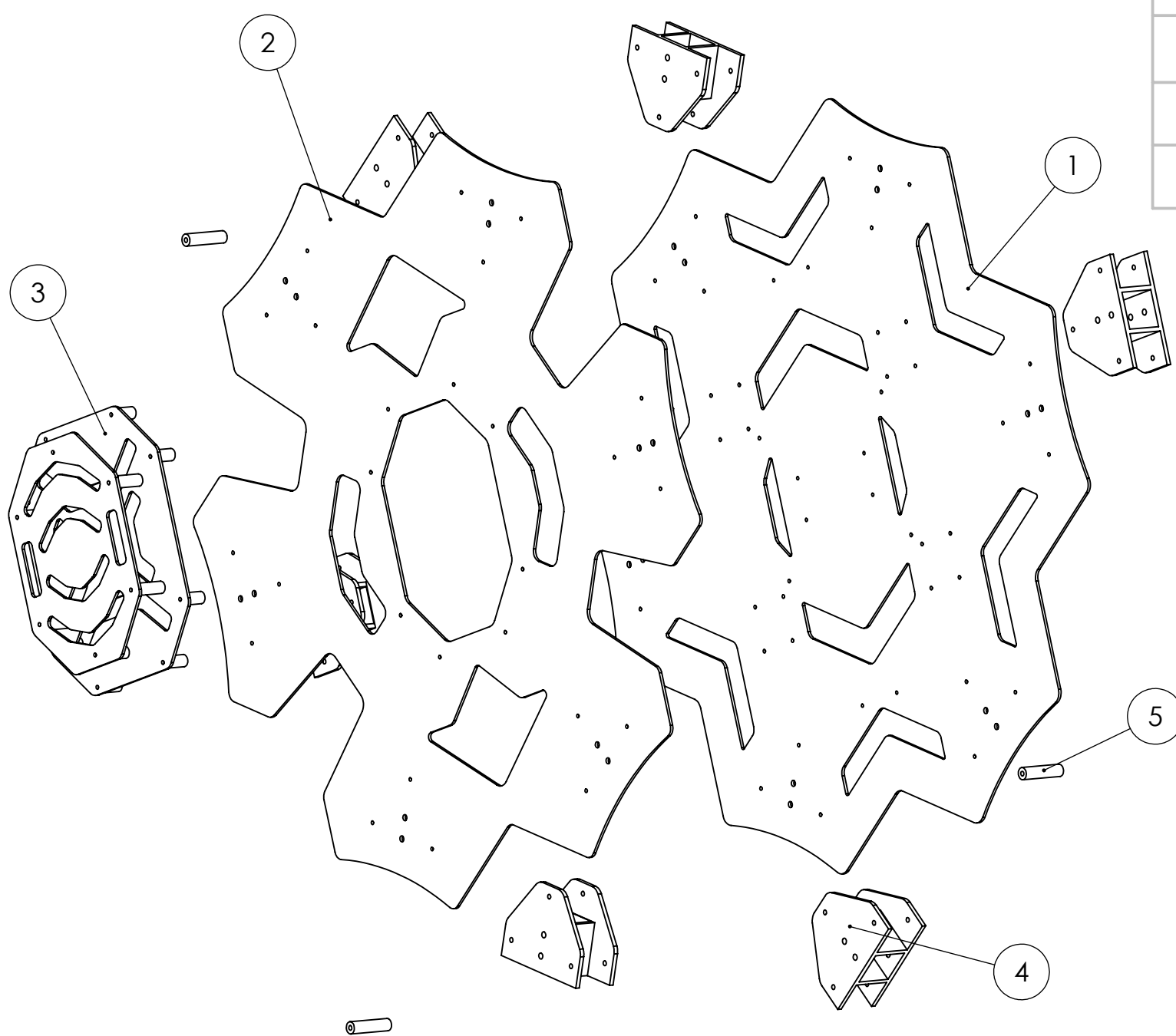
A



Creator Name: Sam Carhart	<b>Heavy Lift Drone</b>	Assembly: Drone	Part ID: HLD-A1
TOLERANCES: 0.X = $\pm 0.05$ 0.XX = $\pm 0.005$ 0.XXX = $\pm 0.0005$	Material: Mixed Assembly	Part Quantity: 1	Description: Drone Structural Assembly

8 7 6 5 4 3 2 1

Item No.	Part ID	Description	Qty
1	CMB01	Chassis Bottom Plate	1
2	CMB02	Chassis Top Plate	1
3	CA2	Chassis Riser Assembly	1
4	CMP01	Chassis Arm Bracket	6
5	CMP02-C	Chassis Layer Spacer - 2"	4



Creator Name: Sam Carhart	<b>Heavy Lift Drone</b>	Subassembly: Chassis	Part ID: CA1
TOLERANCES: 0.X = $\pm 0.05$ 0.XX = $\pm 0.005$ 0.XXX = $\pm 0.0005$	Material: Mixed Assembly	Part Quantity: 1	Description: Chassis Assembly

8 7 6 5 4 3 2 1

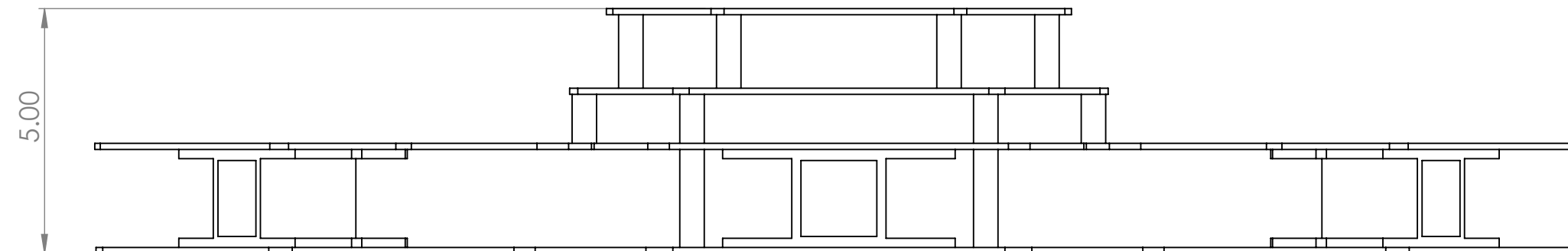
8 7 6 5 4 3 2 1

F

F

E

E

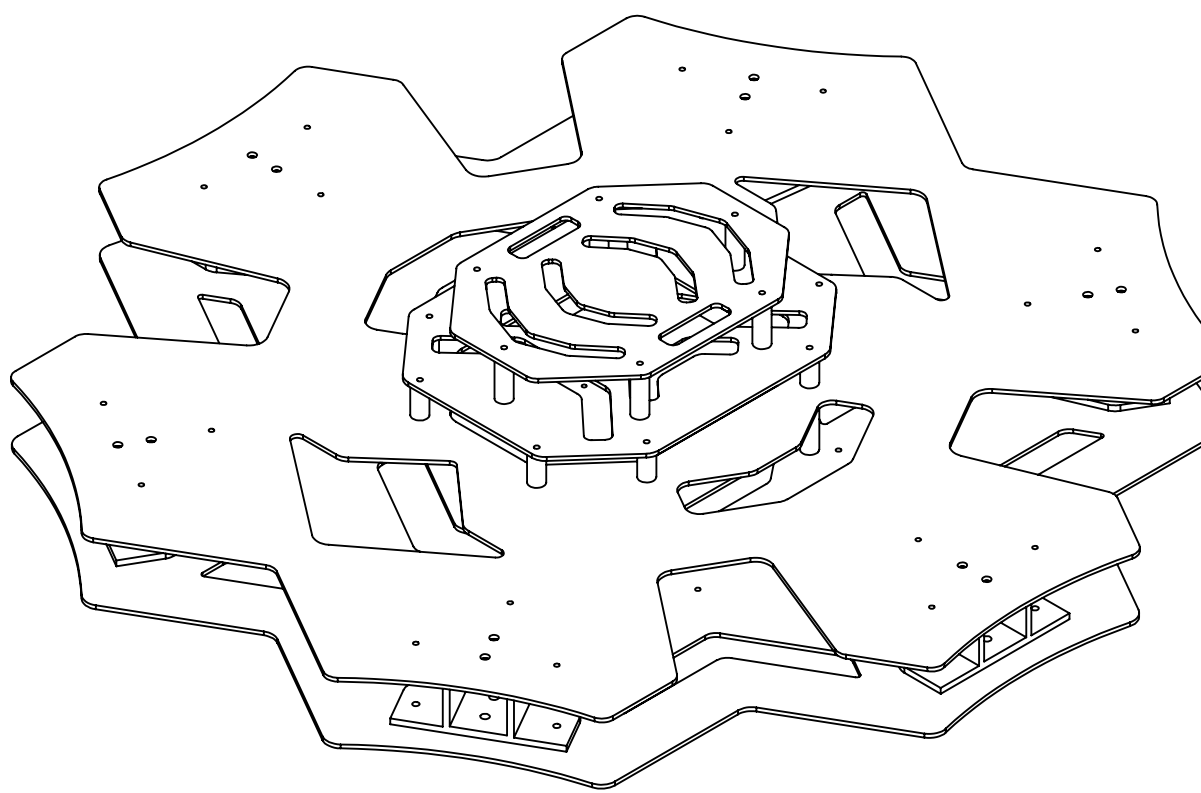


D

D

C

C



B

B

A

A

Creator Name:  
Sam Carhart

**Heavy Lift  
Drone**

Subassembly:  
Chassis

Part ID:  
CA1

TOLERANCES:  
0.X =  $\pm 0.05$   
0.XX =  $\pm 0.005$   
0.XXX =  $\pm 0.0005$

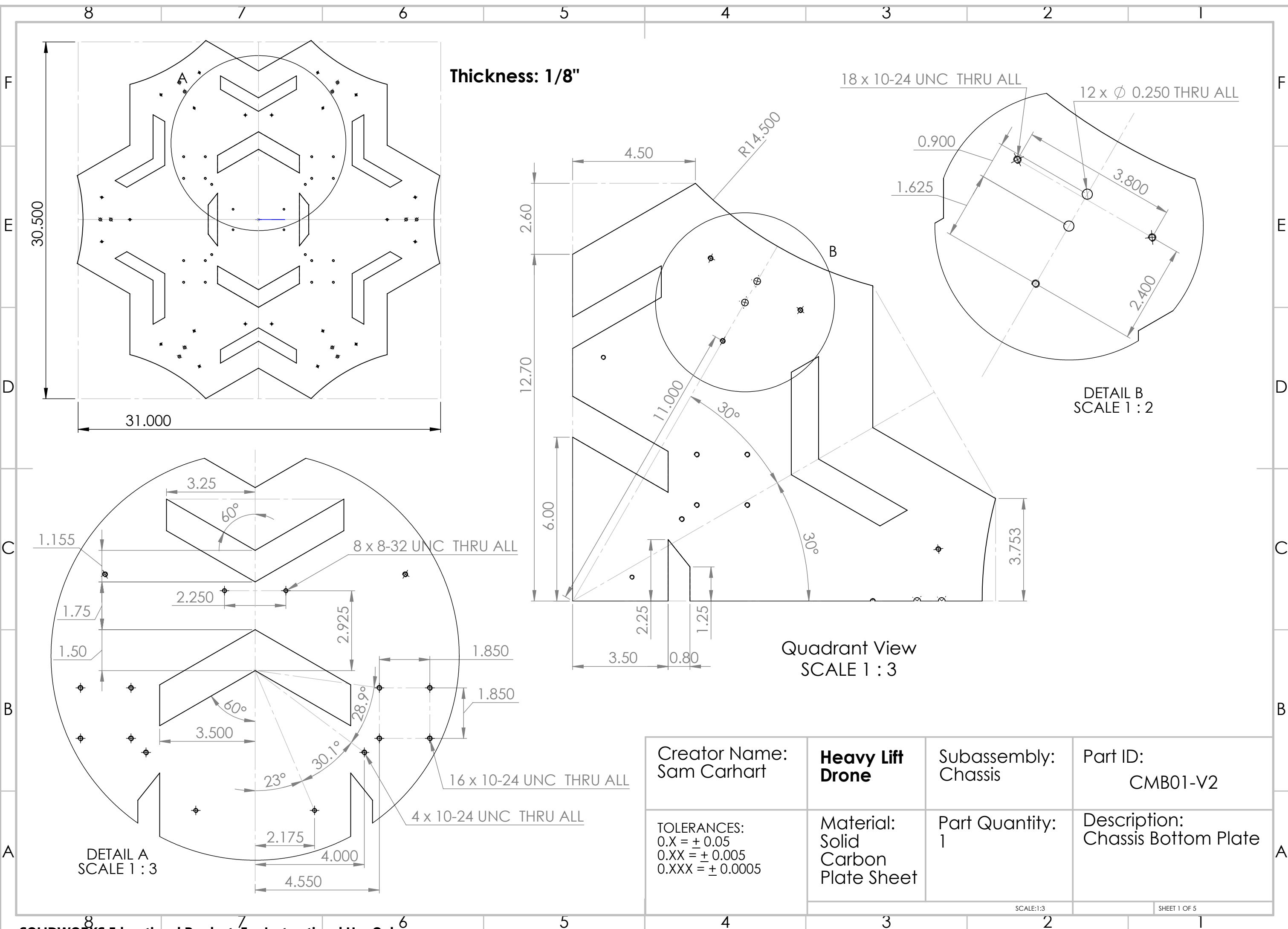
Material:  
Mixed  
Assembly

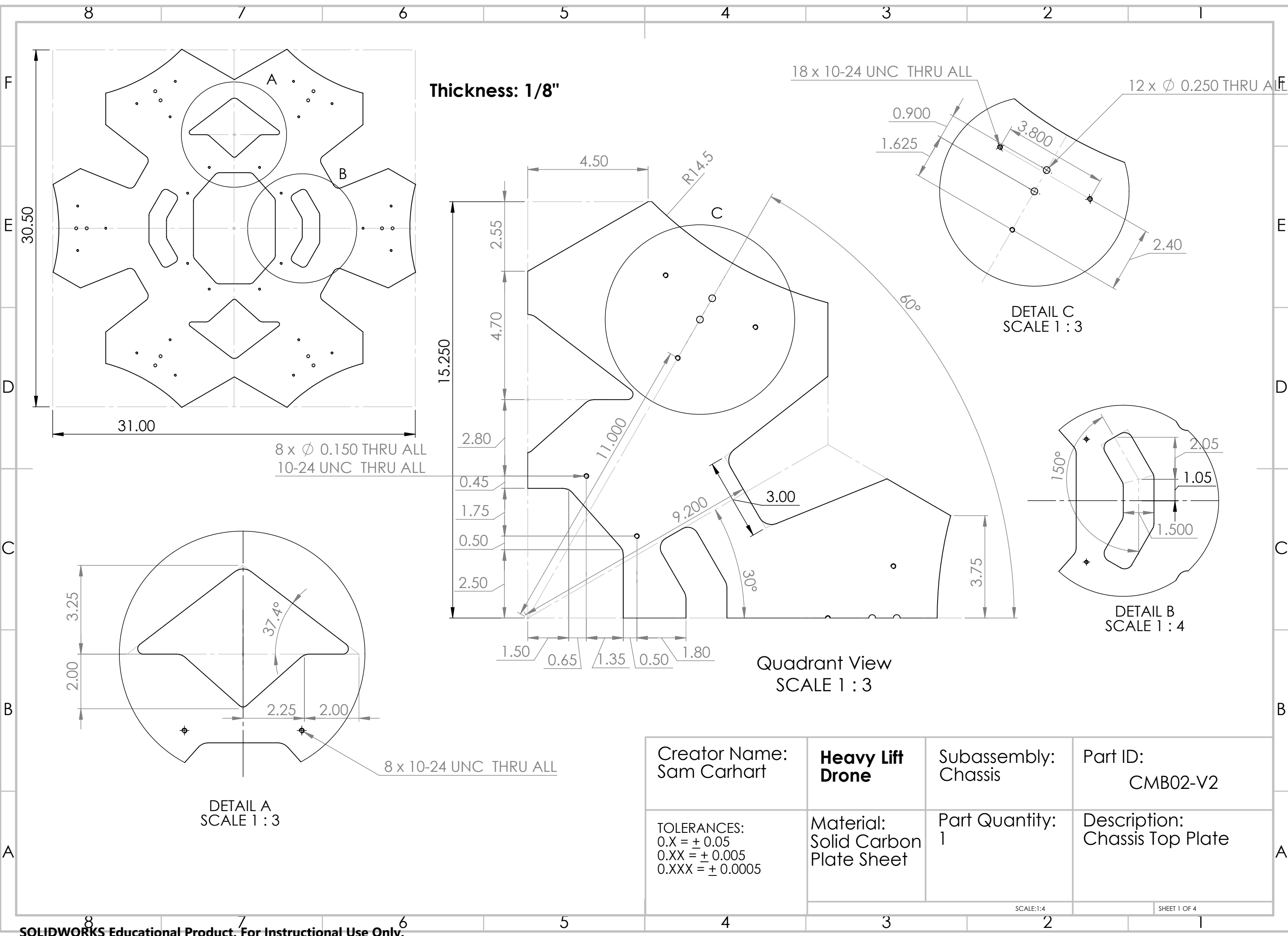
Part Quantity:  
1

Description:  
Chassis Assembly

SCALE:1:7

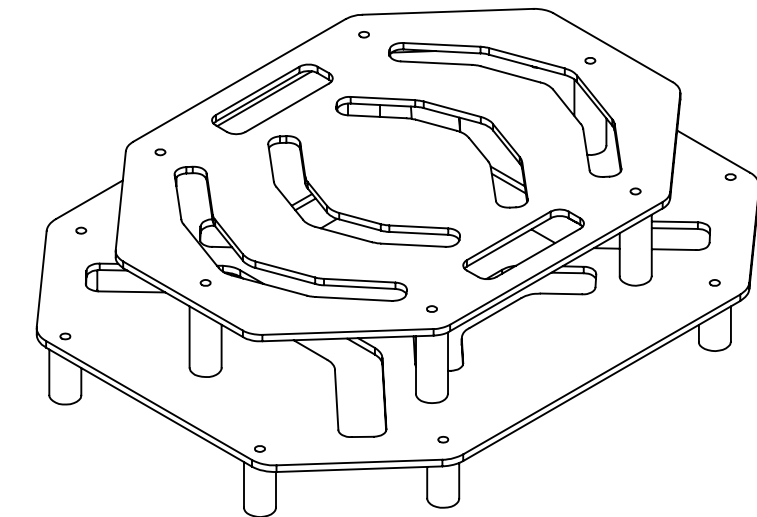
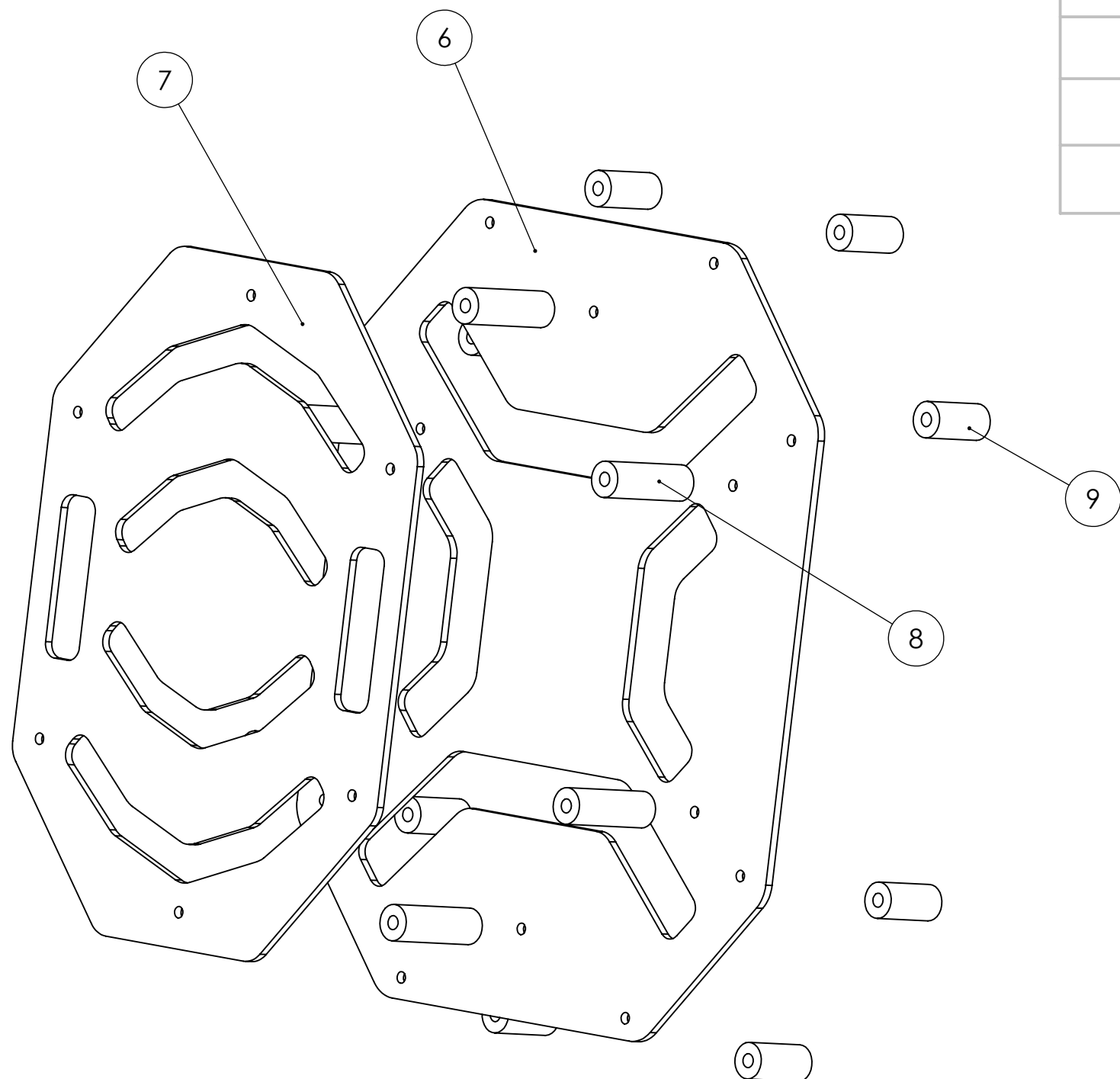
SHEET 2 OF 3





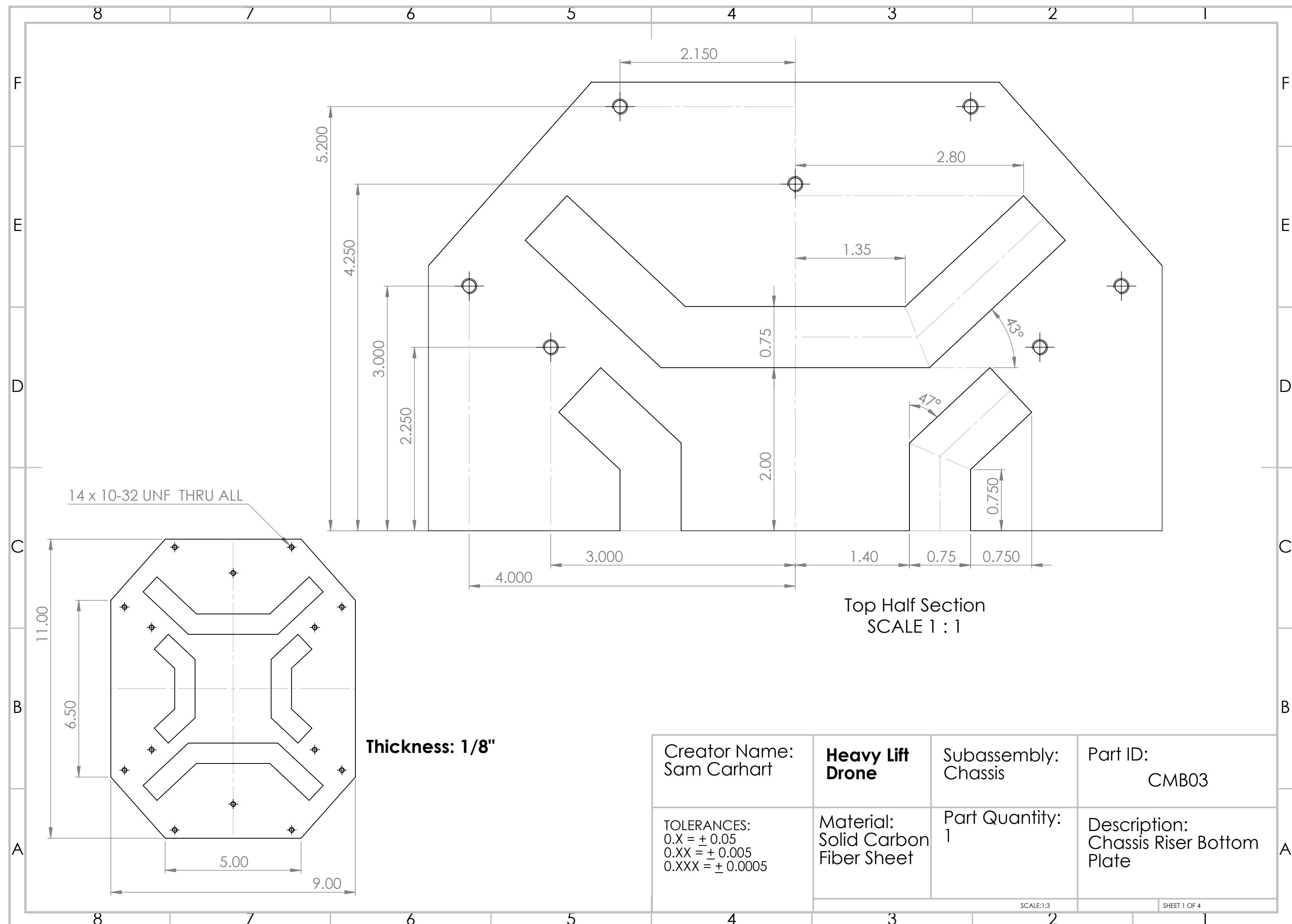
8 7 6 5 4 3 2 1

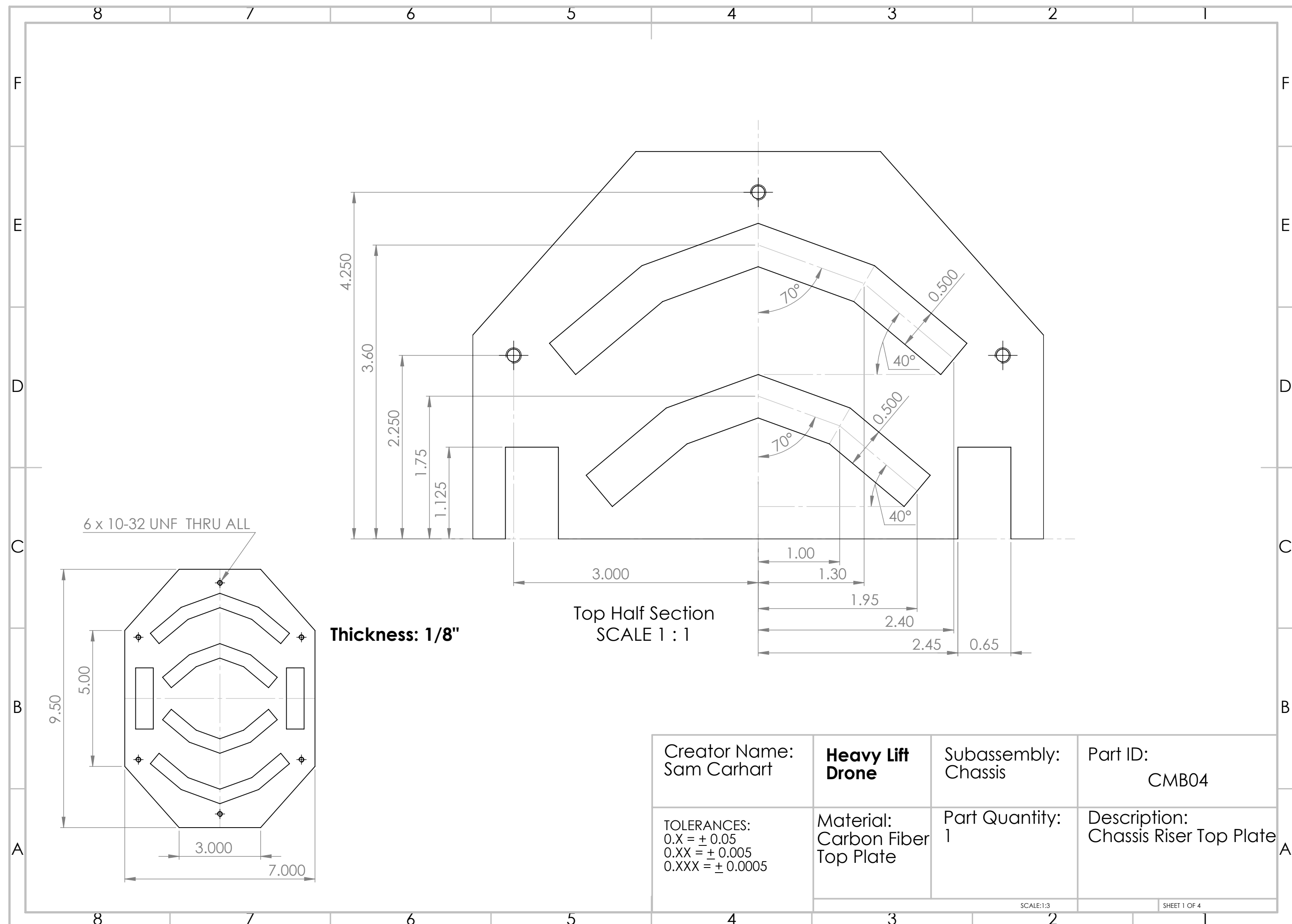
Item No.	Part ID	Description	Qty
6	CMB02	Chassis Riser Bottom	1
7	CMB03	Chassis Riser Top	1
8	CMP02-B	Chassis Layer Spacer - 1.5"	6
9	CMP02-A	Chassis Layer Spacer - 1"	8

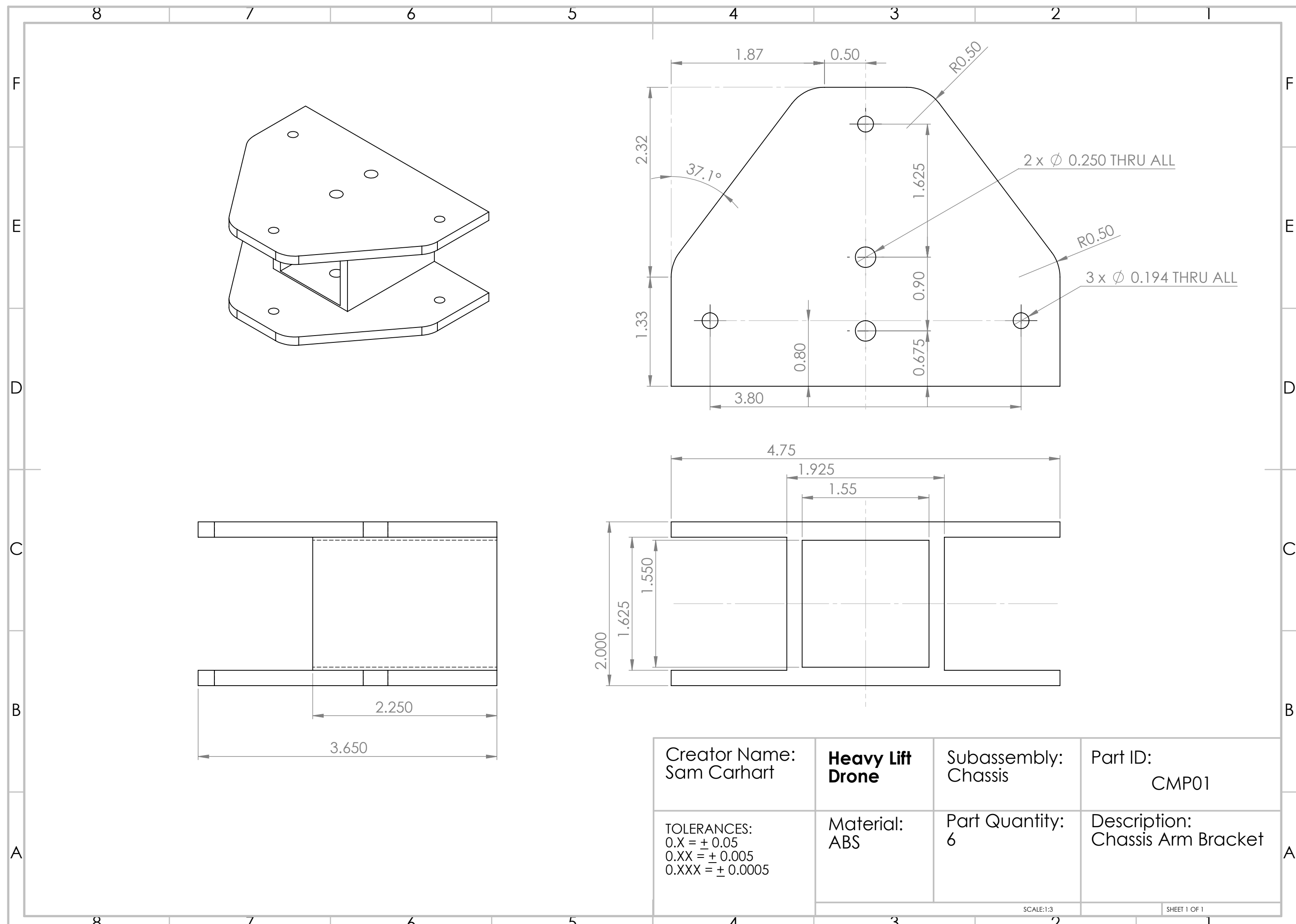


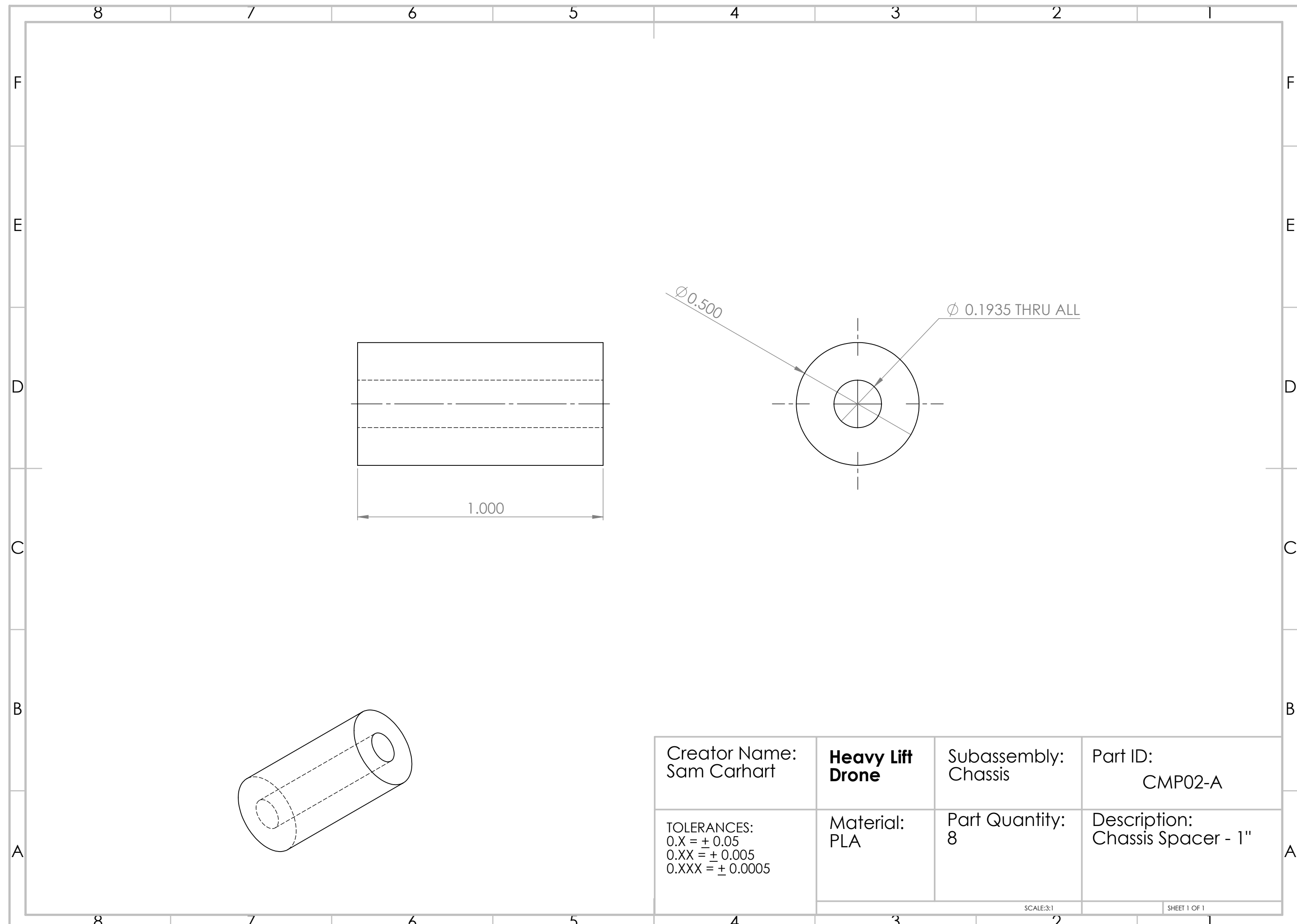
Creator Name: Sam Carhart	<b>Heavy Lift Drone</b>	Subassembly: Chassis	Part ID: CA1
TOLERANCES: 0.X = $\pm 0.05$ 0.XX = $\pm 0.005$ 0.XXX = $\pm 0.0005$	Material: Mixed Assembly	Part Quantity: 1	Description: Chassis Assembly

8 7 6 5 4 3 2 1









8

7

6

5

4

3

2

1

F

F

E

E

D

D

C

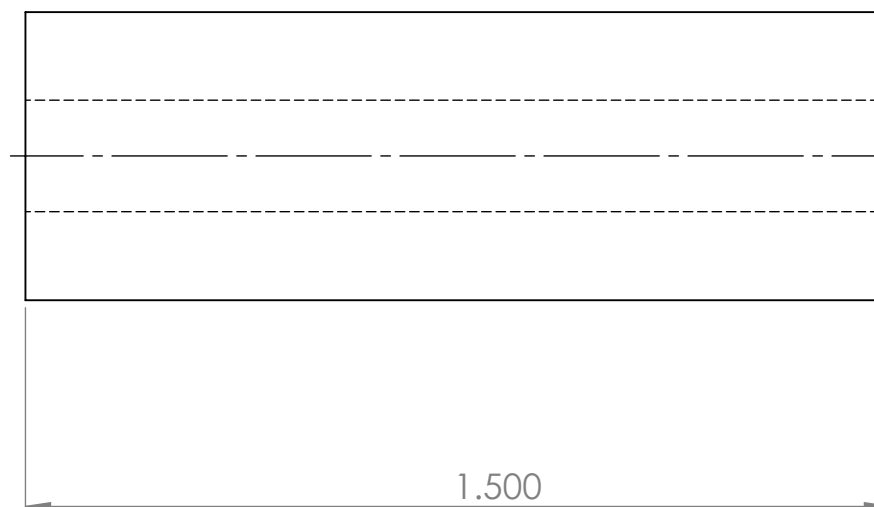
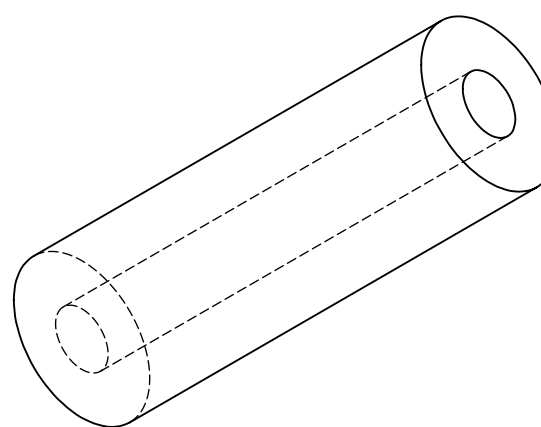
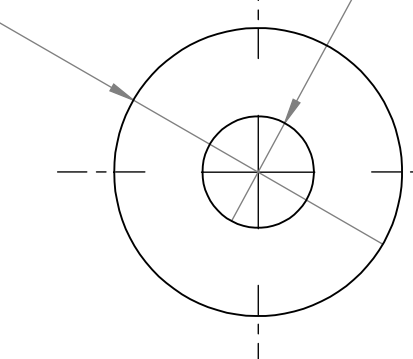
C

B

B

A

A

 $\phi 0.500$  $\phi 0.1935$  THRU ALLCreator Name:  
Sam Carhart**Heavy Lift  
Drone**Subassembly:  
ChassisPart ID:  
CMP02-BTOLERANCES:  
 $0.X = \pm 0.05$   
 $0.XX = \pm 0.005$   
 $0.XXX = \pm 0.0005$ Material:  
PLAPart Quantity:  
6Description:  
Chassis Spacer - 1.5"

SCALE:3:1

SHEET 1 OF 1

8 7 6 5 4 3 2 1

F

F

E

E

D

D

C

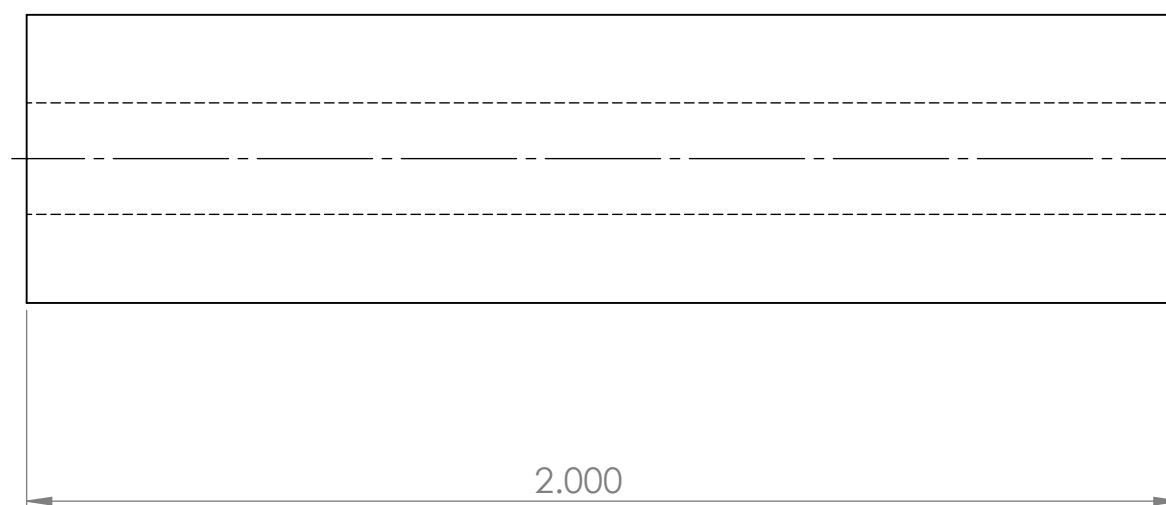
C

B

B

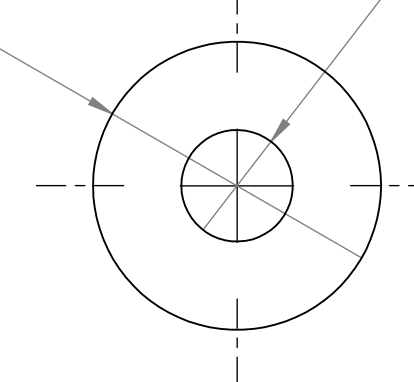
A

A



$\phi 0.500$

$\phi 0.1935$  THRU ALL



Creator Name:  
Sam Carhart

**Heavy Lift  
Drone**

Subassembly:  
Chassis

Part ID:  
CMP02-C

TOLERANCES:  
 $0.X = \pm 0.05$   
 $0.XX = \pm 0.005$   
 $0.XXX = \pm 0.0005$

Material:  
PLA

Part Quantity:  
4

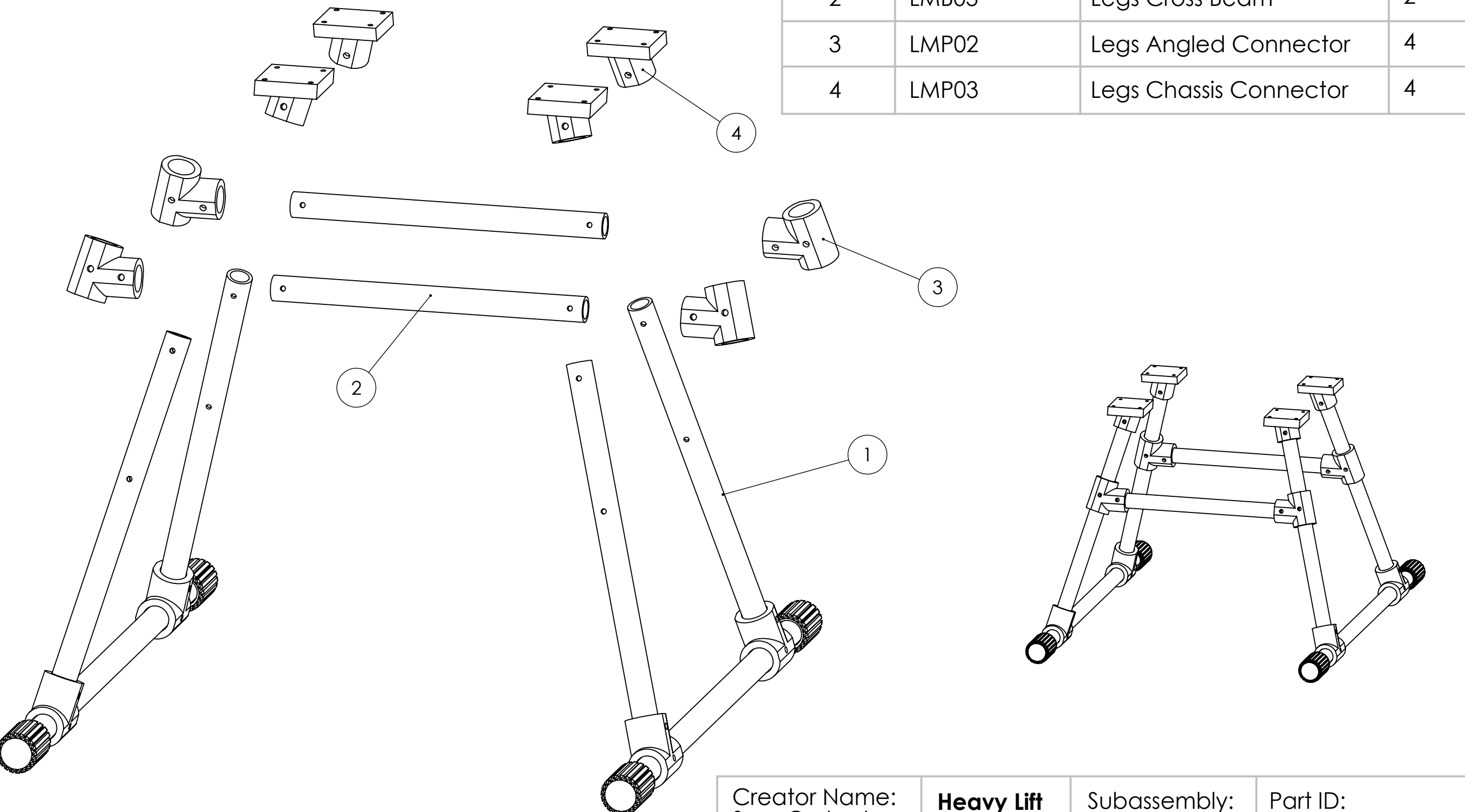
Description:  
Chassis Spacer - 2"

SCALE:3:1

SHEET 1 OF 1

8 7 6 5 4 3 2 1

Item No.	Part ID	Description	Qty
1	LA2	Legs Side Assembly	2
2	LMB03	Legs Cross Beam	2
3	LMP02	Legs Angled Connector	4
4	LMP03	Legs Chassis Connector	4

Creator Name:  
Sam Carhart**Heavy Lift  
Drone**Subassembly:  
LegsPart ID:  
LA1TOLERANCES:  
0.X =  $\pm 0.05$   
0.XX =  $\pm 0.005$   
0.XXX =  $\pm 0.0005$ Material:  
Mixed  
AssemblyPart Quantity:  
1Description:  
Legs Assembly

8 7 6 5 4 3 2 1

8 7 6 5 4 3 2 1

F

F

E

E

D

D

C

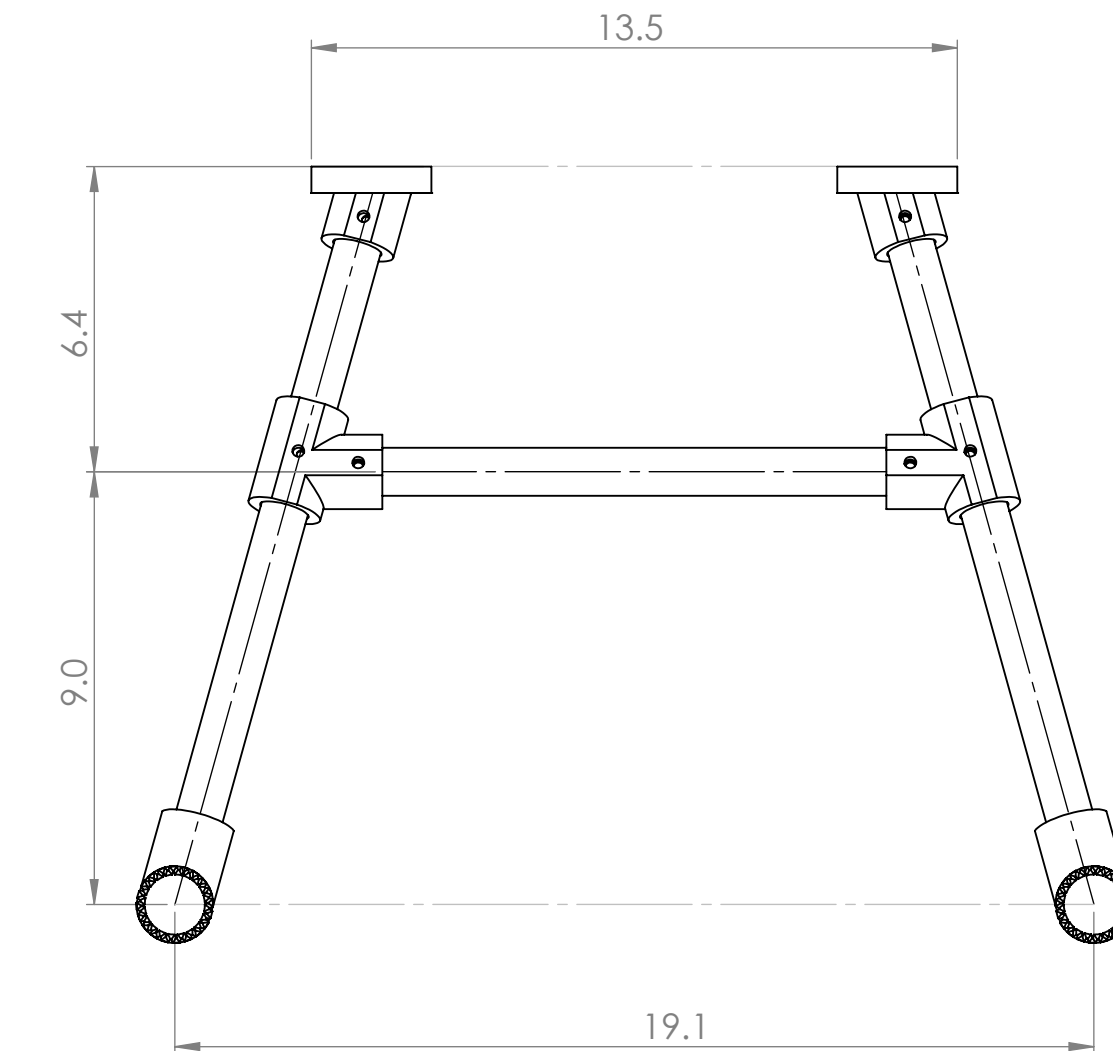
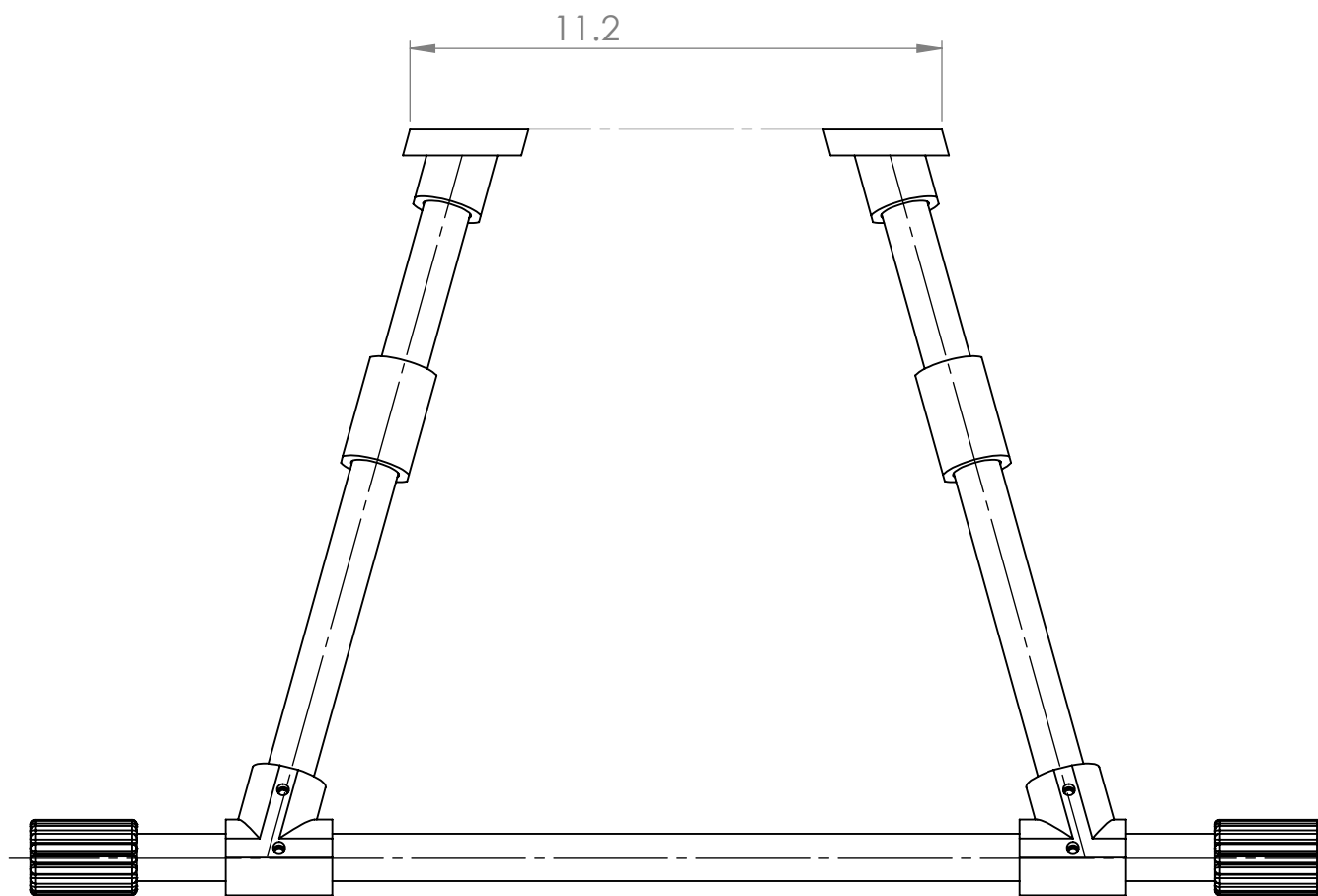
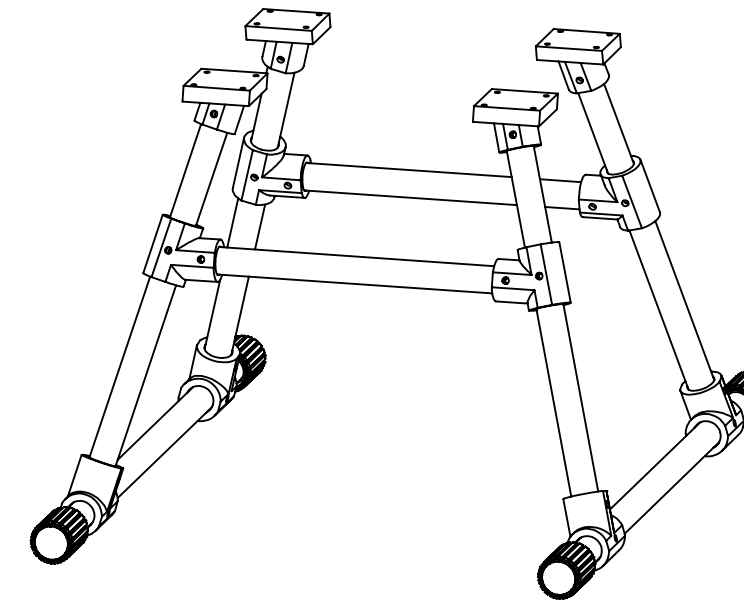
C

B

B

A

A



Creator Name: Sam Carhart	<b>Heavy Lift Drone</b>	Subassembly: Legs	Part ID: LA1
TOLERANCES: $0.X = \pm 0.05$ $0.XX = \pm 0.005$ $0.XXX = \pm 0.0005$	Material: Mixed Assembly	Part Quantity: 1	Description: Legs Assembly

8 7 6 5 4 3 2 1

Item No.	Part ID	Description	Qty
5	LMB01	Legs Lower Beam	1
3	LMP02	Legs Angled Connector	2
6	LMB02	Legs Vertical Beam	2
7	LMP01	Legs End Cap	2

F

E

D

C

B

A

F

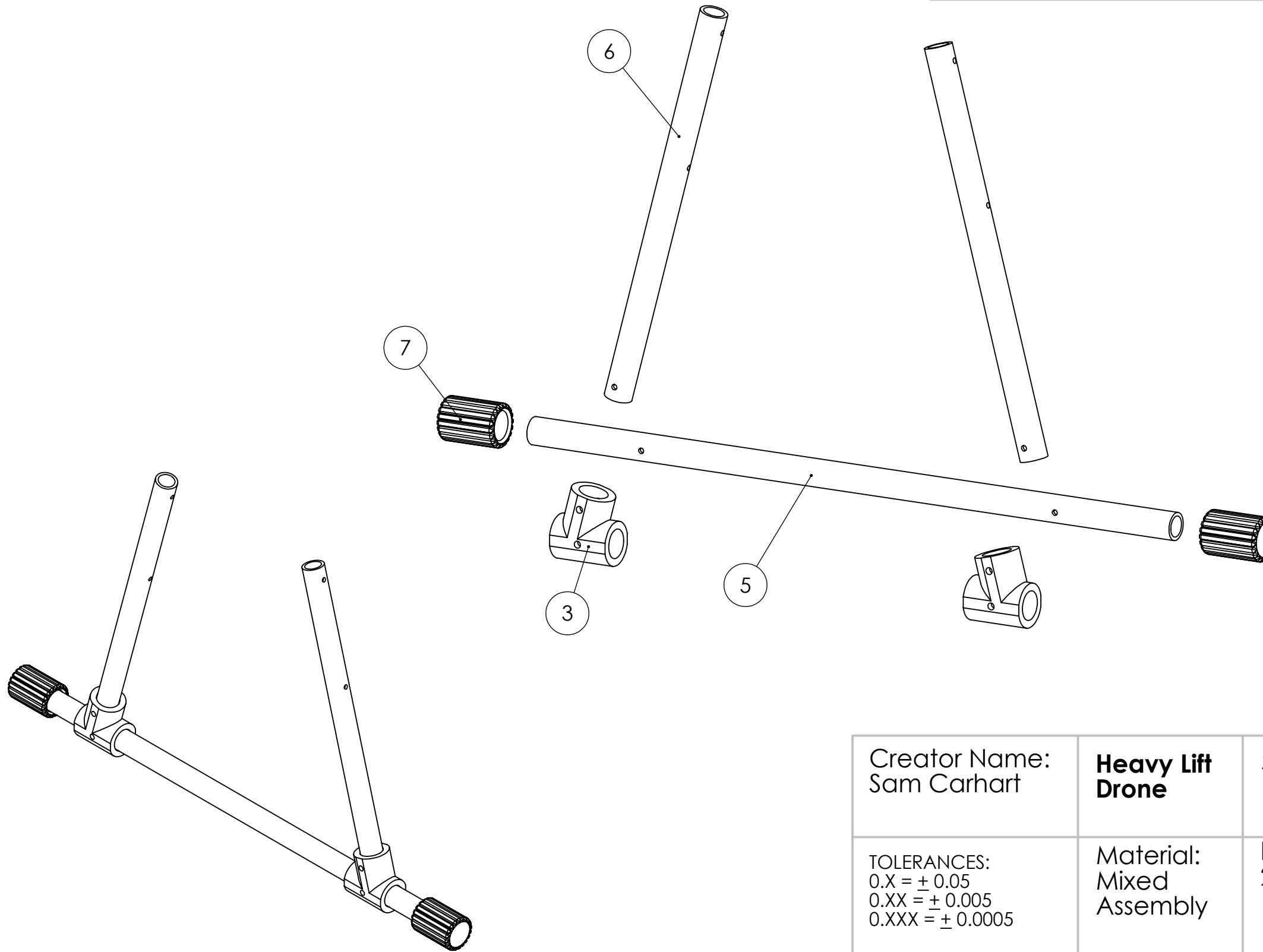
E

D

C

B

A



Creator Name:  
Sam Carhart

**Heavy Lift  
Drone**

Subassembly:  
Legs

Part ID:  
LA2

TOLERANCES:  
0.X =  $\pm 0.05$   
0.XX =  $\pm 0.005$   
0.XXX =  $\pm 0.0005$

Material:  
Mixed  
Assembly

Part Quantity:  
2

Description:  
Legs Side Assembly

SCALE:1:4

SHEET 3 OF 4

8 7 6 5 4 3 2 1

F

F

E

E

D

D

C

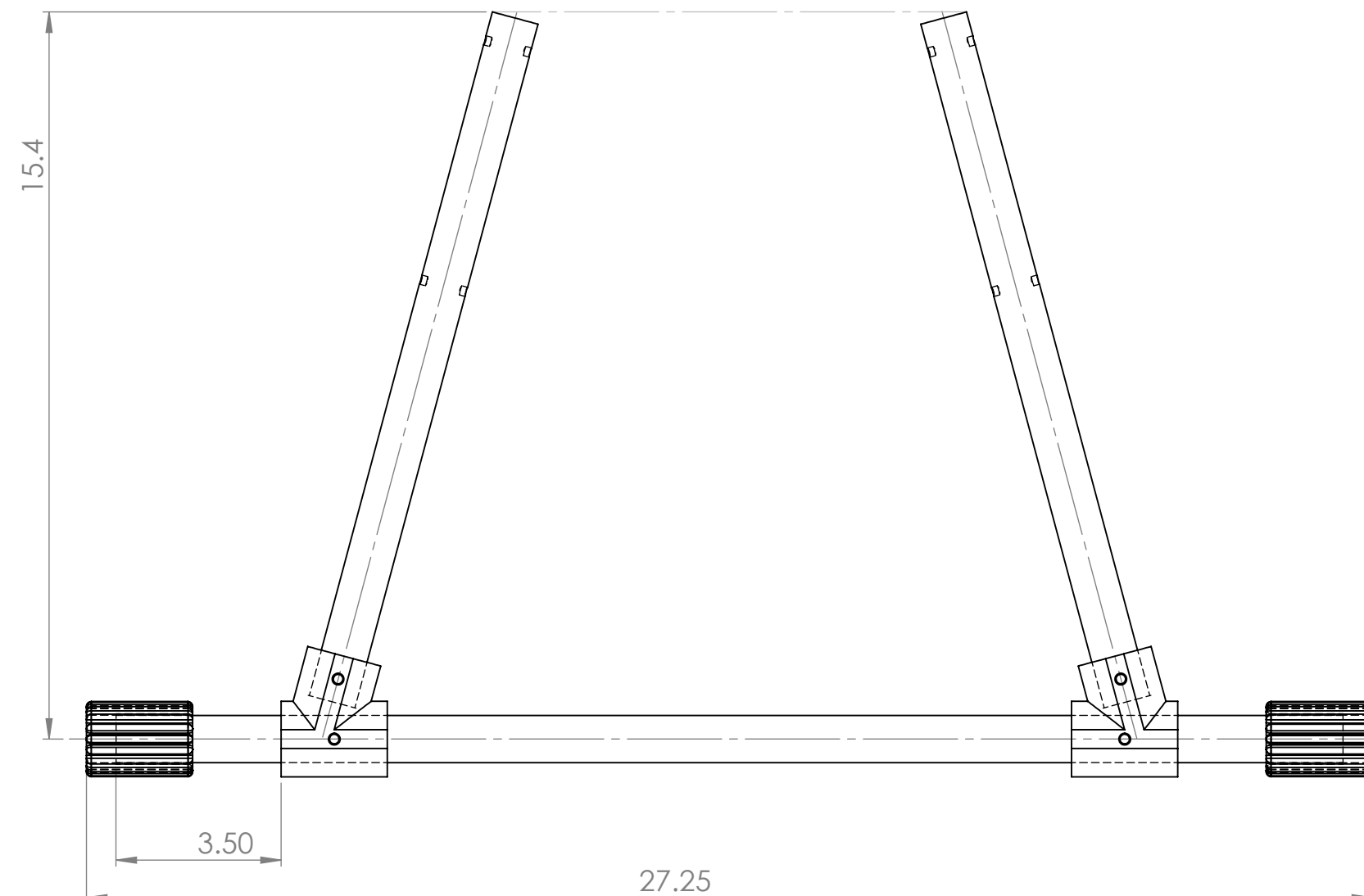
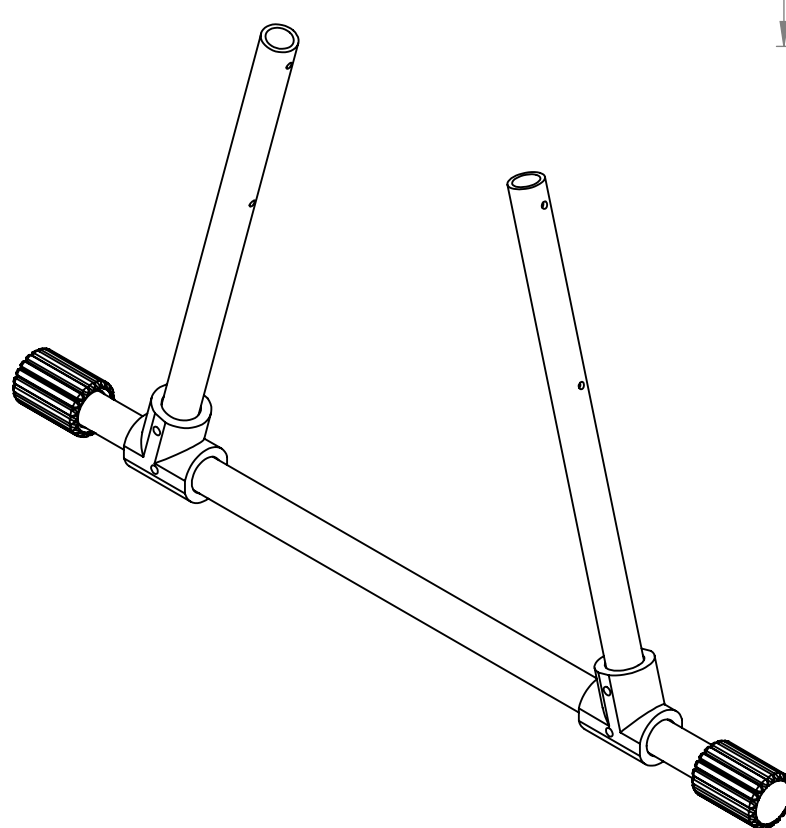
C

B

B

A

A



Creator Name:  
Sam Carhart

**Heavy Lift  
Drone**

Subassembly:  
Legs

Part ID:  
LA2

TOLERANCES:  
 $0.X = \pm 0.05$   
 $0.XX = \pm 0.005$   
 $0.XXX = \pm 0.0005$

Material:  
Mixed  
Assembly

Part Quantity:  
2

Description:  
Legs Side Assembly

SCALE:1:4

SHEET 4 OF 4

8 7 6 5 4 3 2 1

1

8 7 6 5 4 3 2 1

F

F

E

E

D

D

C

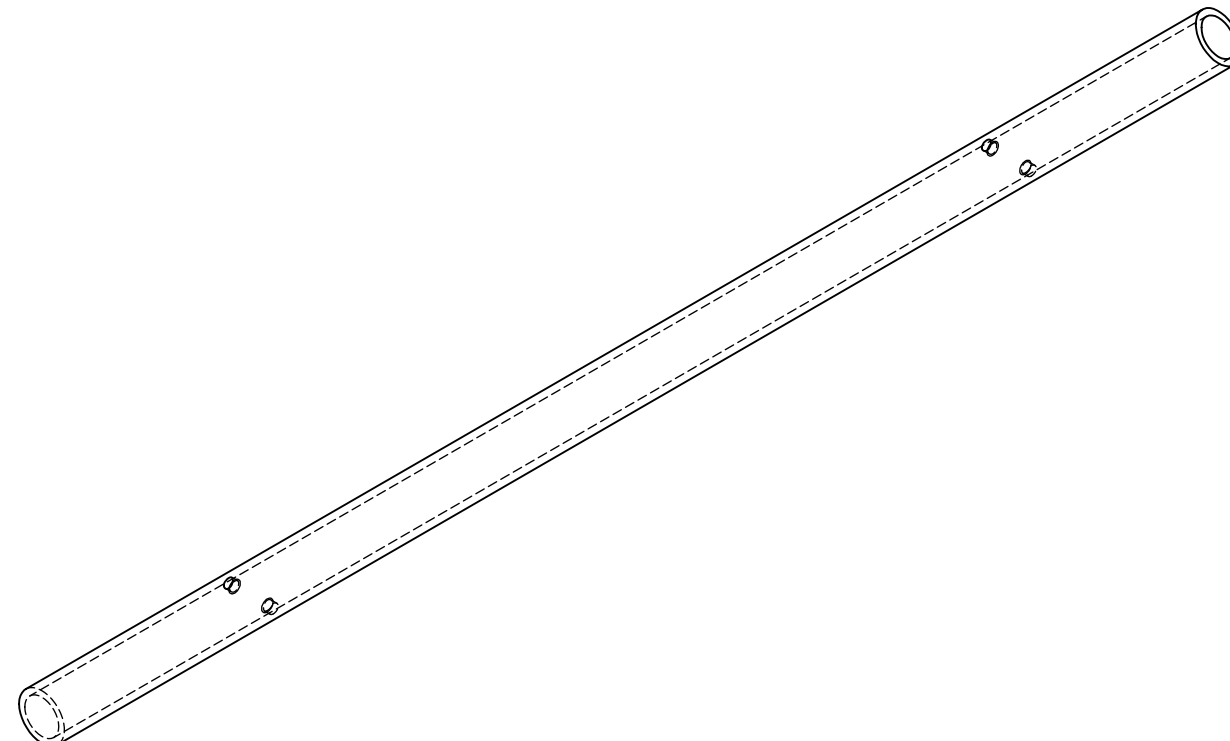
C

B

B

A

A



Creator Name:  
Sam Carhart

**Heavy Lift  
Drone**

Subassembly:  
Legs

Part ID:  
LMB01

TOLERANCES:  
 $0.X = \pm 0.05$   
 $0.XX = \pm 0.005$   
 $0.XXX = \pm 0.0005$

Material:  
6063  
Aluminum

Part Quantity:  
2

Description:  
Legs Lower Beam

SCALE:1:3

SHEET 1 OF 1

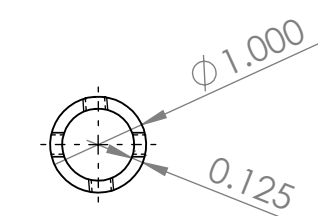
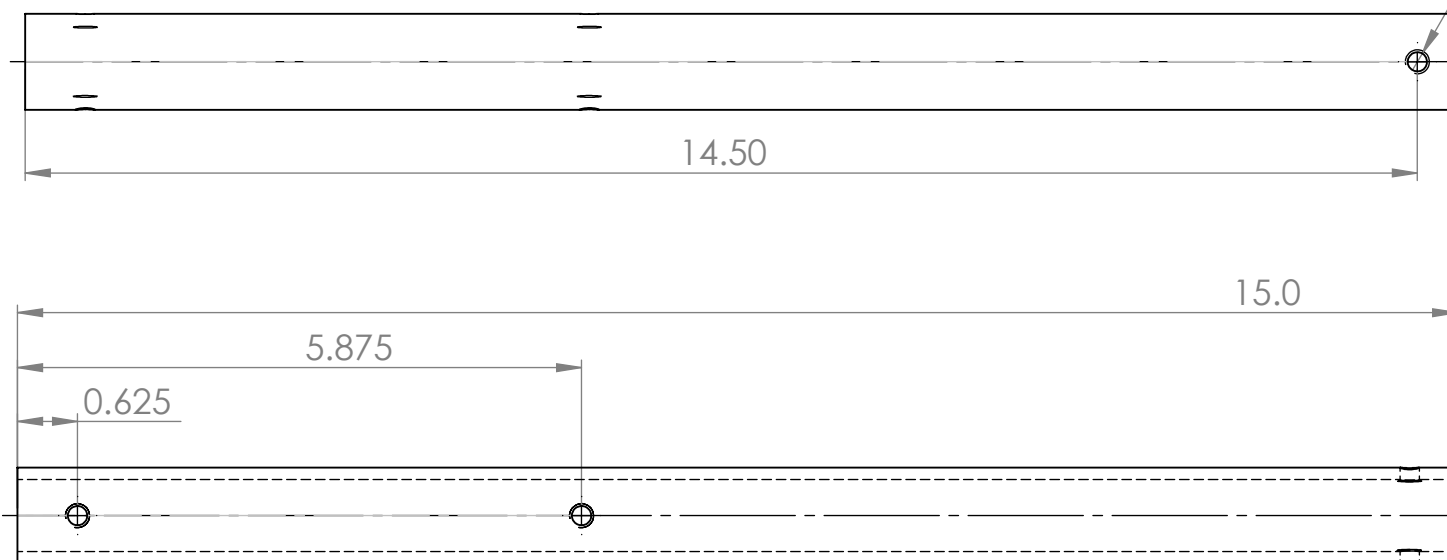
8 7 6 5 4 3 2 1

F

F

E

3 x 1/4-20 UNC THRU ALL



D

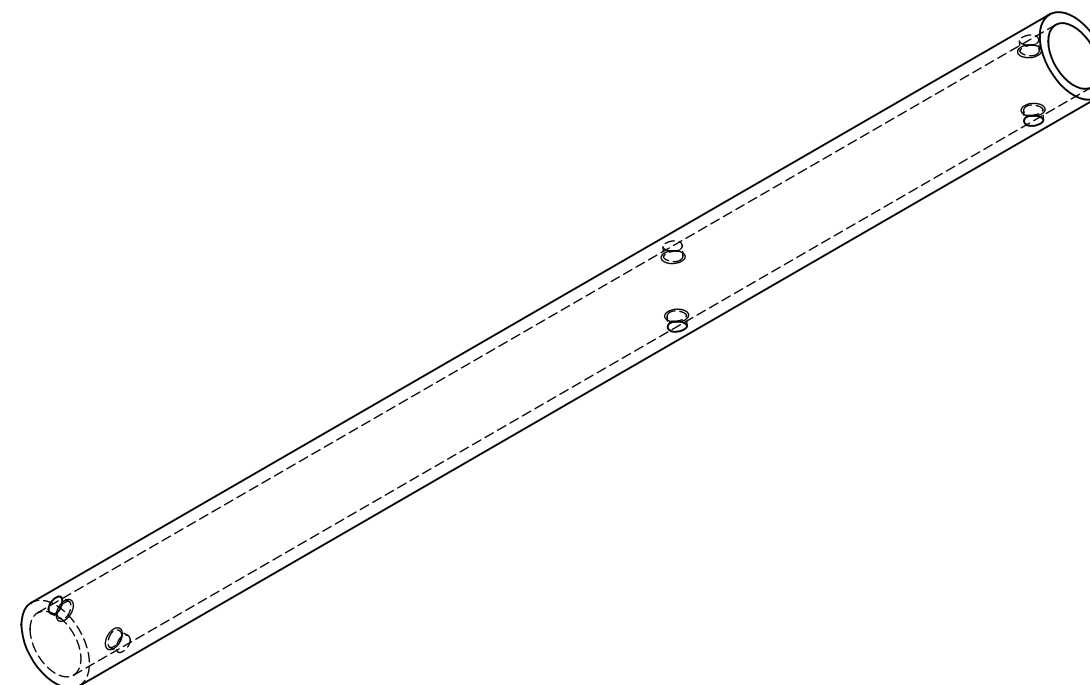
15.0

5.875

0.625

C

B



A

Creator Name:  
Sam Carhart

**Heavy Lift  
Drone**

Subassembly:  
Legs - LA2

Part ID:  
LMB02

TOLERANCES:  
 $0.X = \pm 0.05$   
 $0.XX = \pm 0.005$   
 $0.XXX = \pm 0.0005$

Material:  
6063  
Aluminum

Part Quantity:  
2 per  
Subassembly  
4 Total

Description:  
Legs Vertical Beam

SCALE:1:3

SHEET 1 OF 1

8 7 6 5 4 3 2 1

F

F

E

E

D

D

C

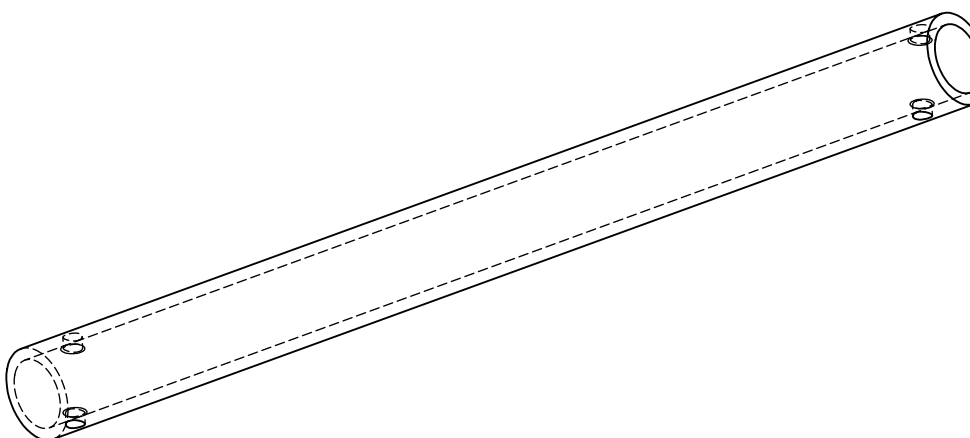
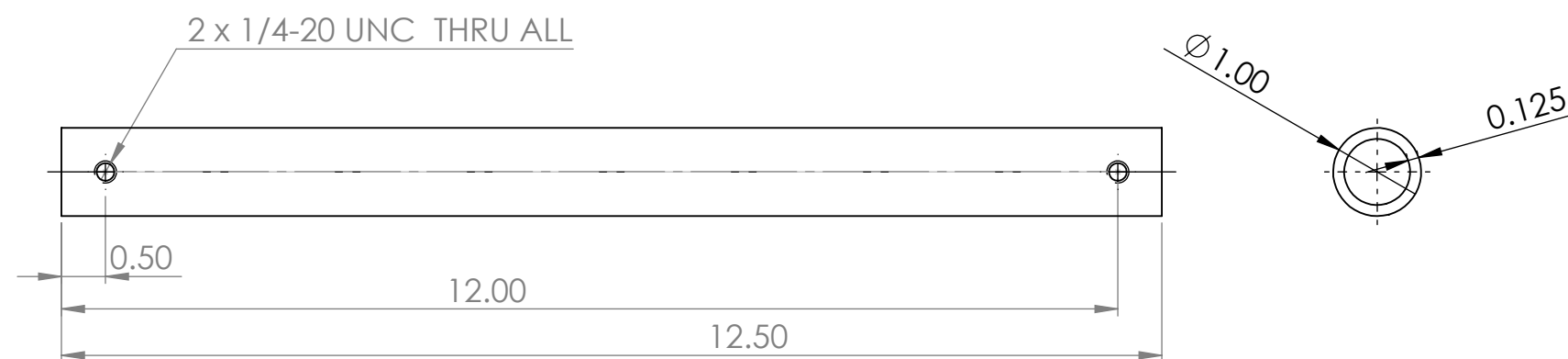
C

B

B

A

A



Creator Name:  
Sam Carhart

**Heavy Lift  
Drone**

Subassembly:  
Legs

Part ID:  
LMB03

TOLERANCES:  
 $0.X = \pm 0.05$   
 $0.XX = \pm 0.005$   
 $0.XXX = \pm 0.0005$

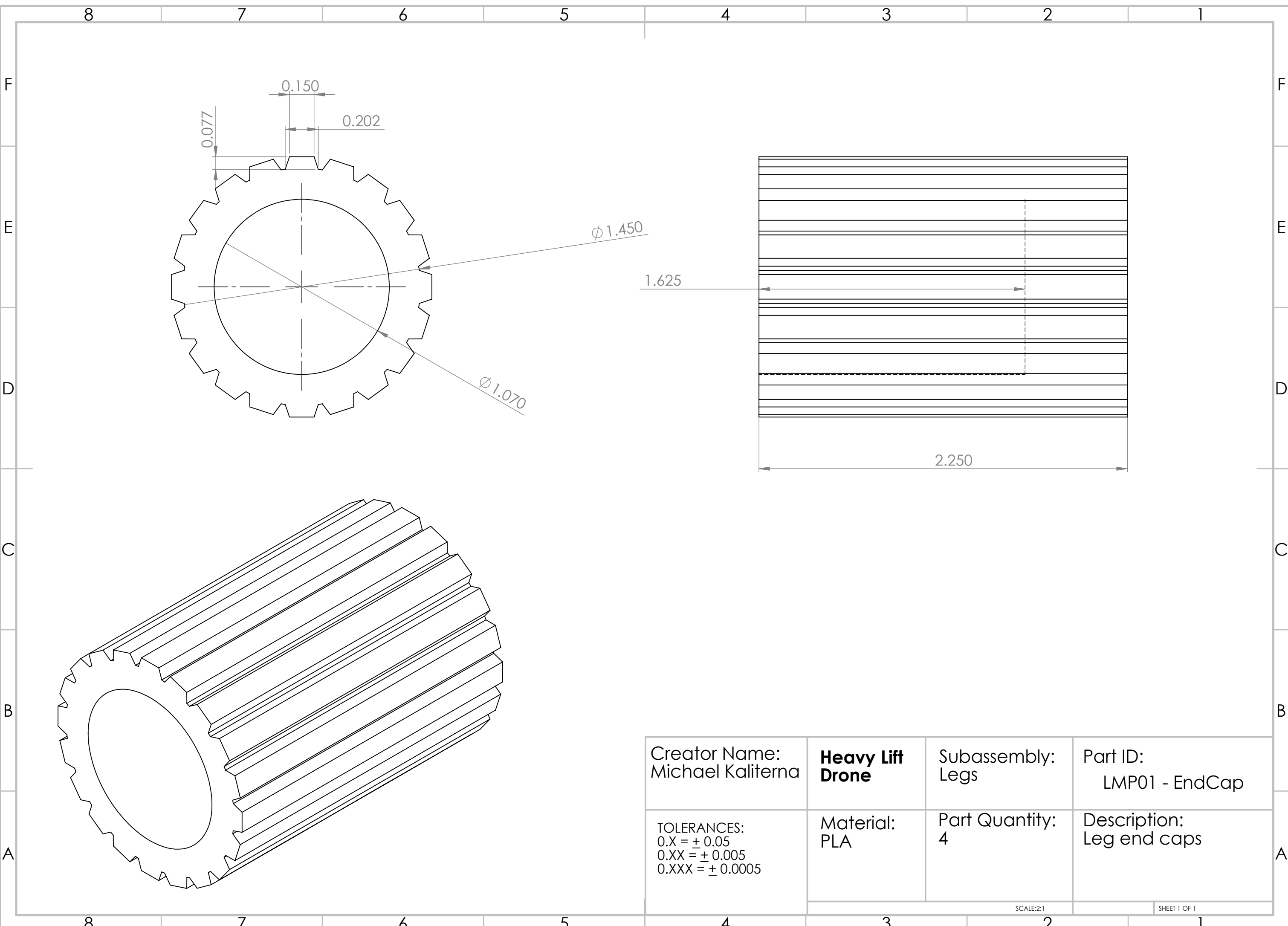
Material:  
6063  
Aluminum

Part Quantity:  
2

Description:  
Legs Cross Beam

SCALE:1:2

SHEET 1 OF 1



8

7

6

5

4

3

2

1

F

F

E

E

D

D

C

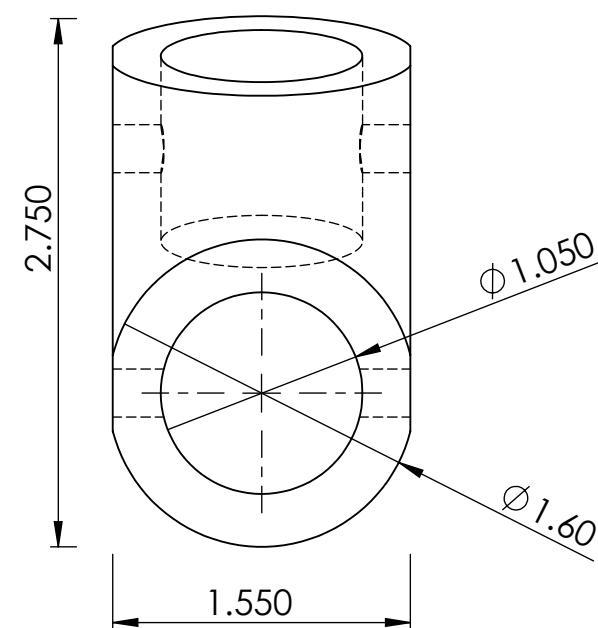
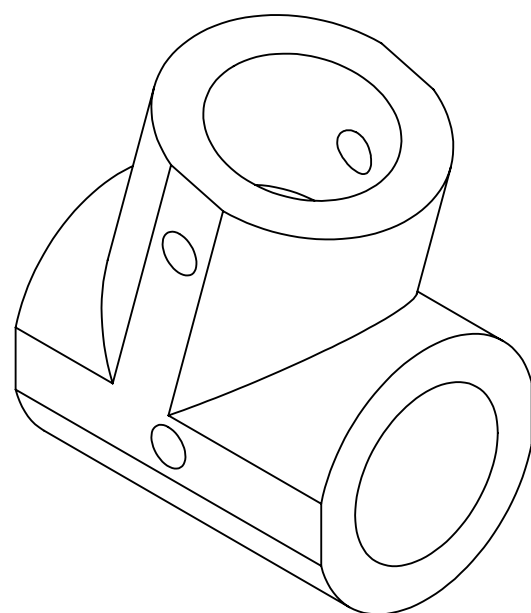
C

B

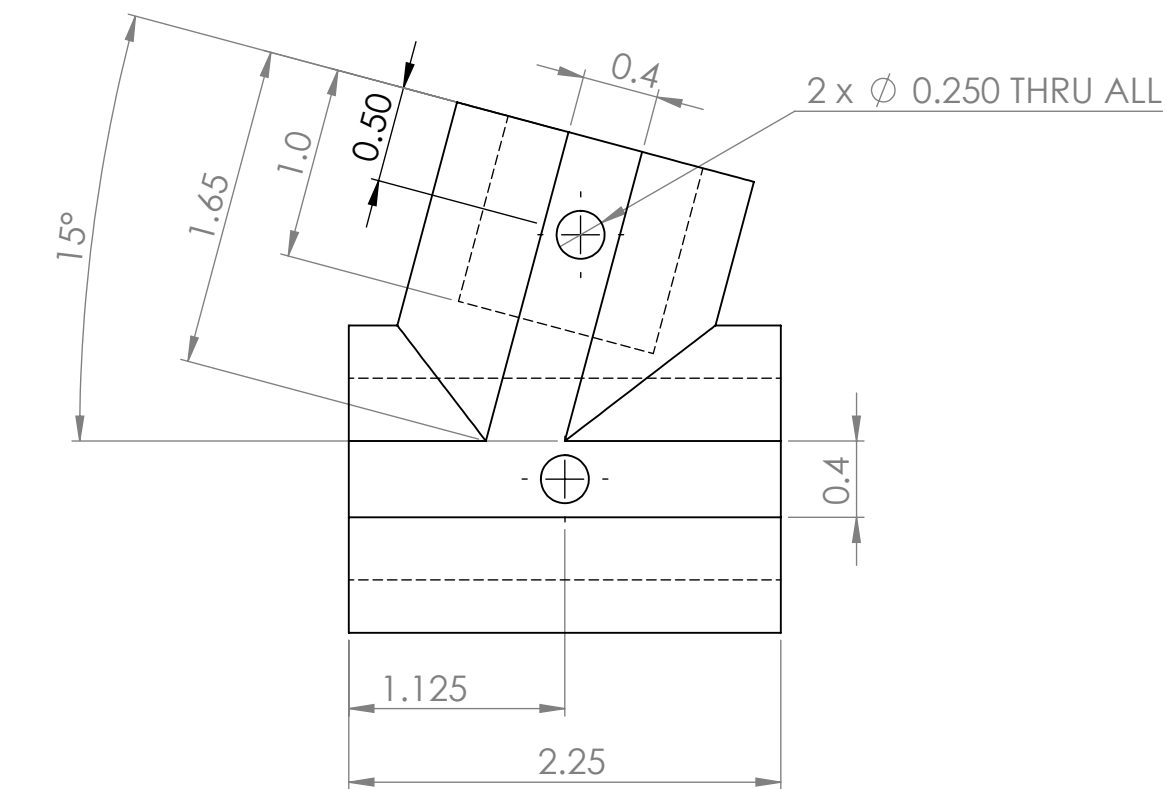
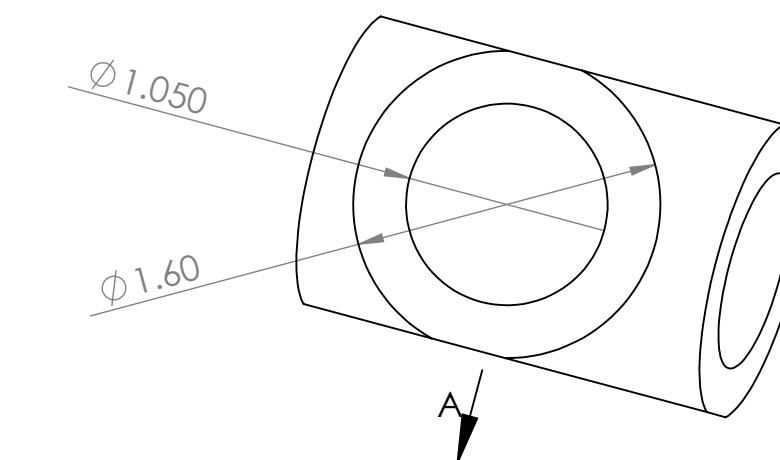
B

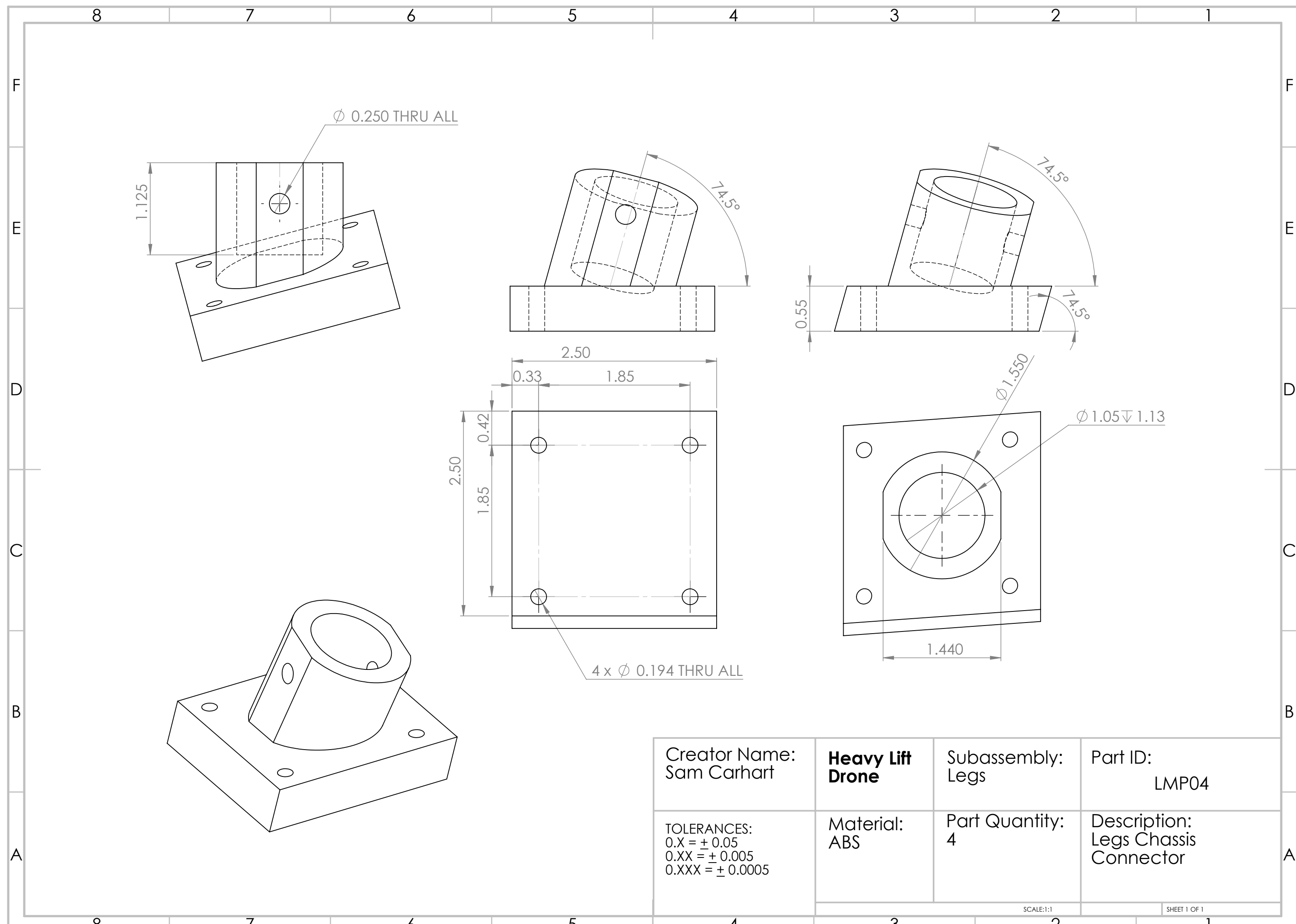
A

A



Creator Name: Sam Carhart	<b>Heavy Lift Drone</b>	Subassembly: Legs	Part ID: LMP02
TOLERANCES: $0.X = \pm 0.05$ $0.XX = \pm 0.005$ $0.XXX = \pm 0.0005$	Material: ABS	Part Quantity: 8	Description: Legs Angled Member Connector





8

7

6

5

4

3

2

1

F

E

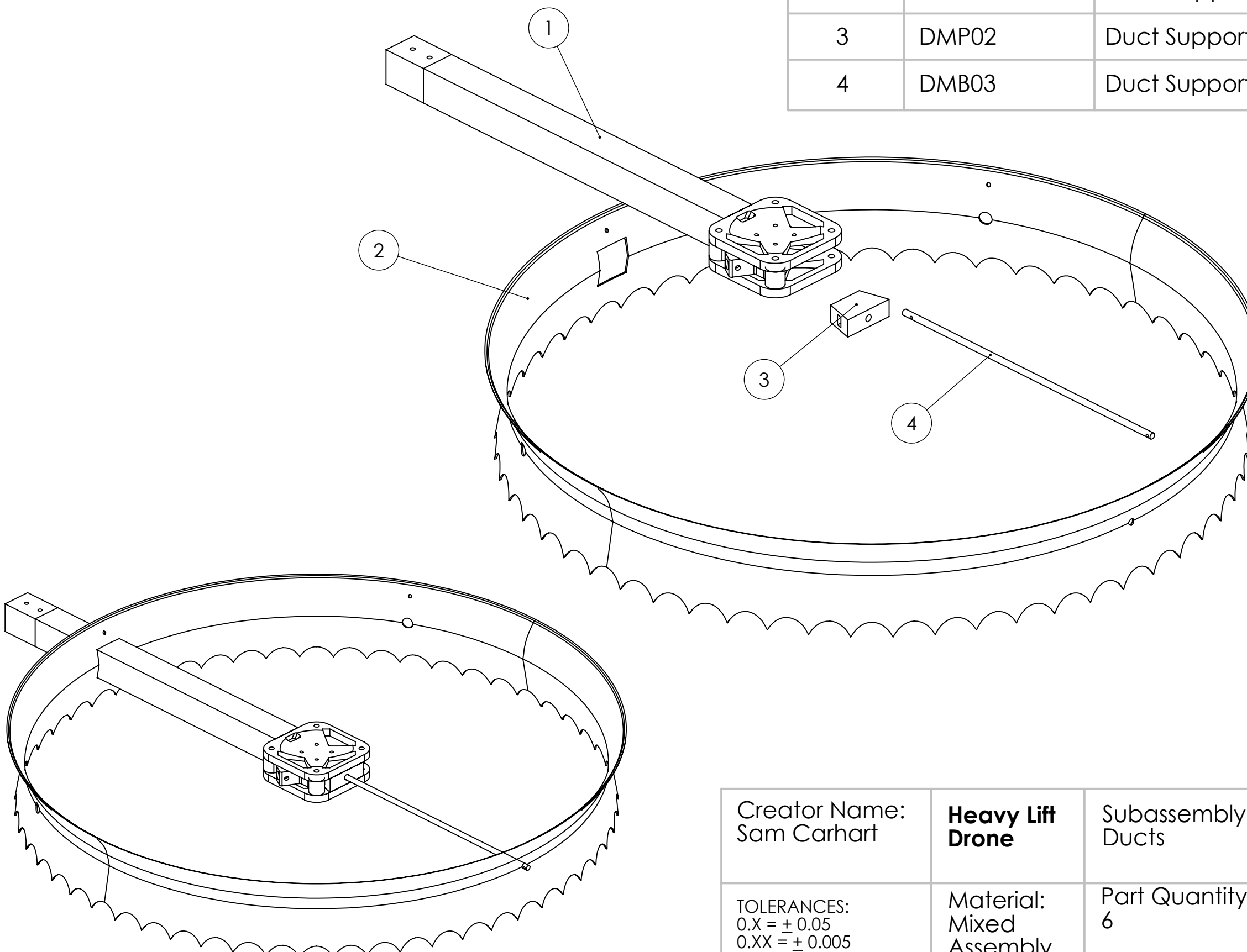
D

C

B

A

Item No.	Part ID	Description	Qty
1	AA1	Arm Assembly	1
2	DAP01	Duct - Lipped Edge	1
3	DMP02	Duct Support Rod Fixture	1
4	DMB03	Duct Support Rod	1

Creator Name:  
Sam Carhart**Heavy Lift  
Drone**Subassembly:  
DuctsPart ID:  
DA1TOLERANCES:  
0.X = ± 0.05  
0.XX = ± 0.005  
0.XXX = ± 0.0005Material:  
Mixed  
AssemblyPart Quantity:  
6Description:  
Duct Assembly with  
Arm and Support  
Rod

SCALE:1:7

SHEET 1 OF 1

8

7

6

5

4

3

2

1

F

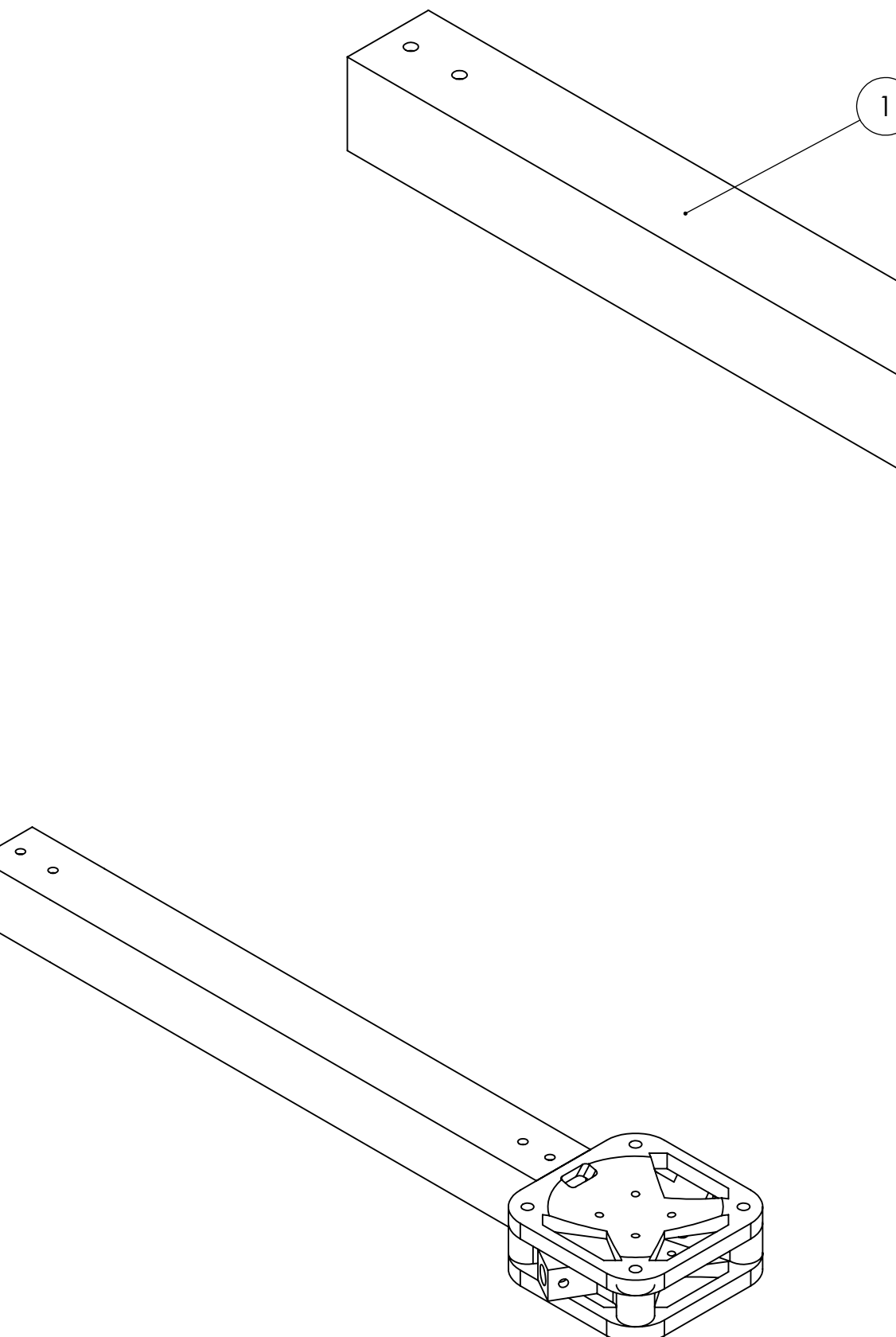
E

D

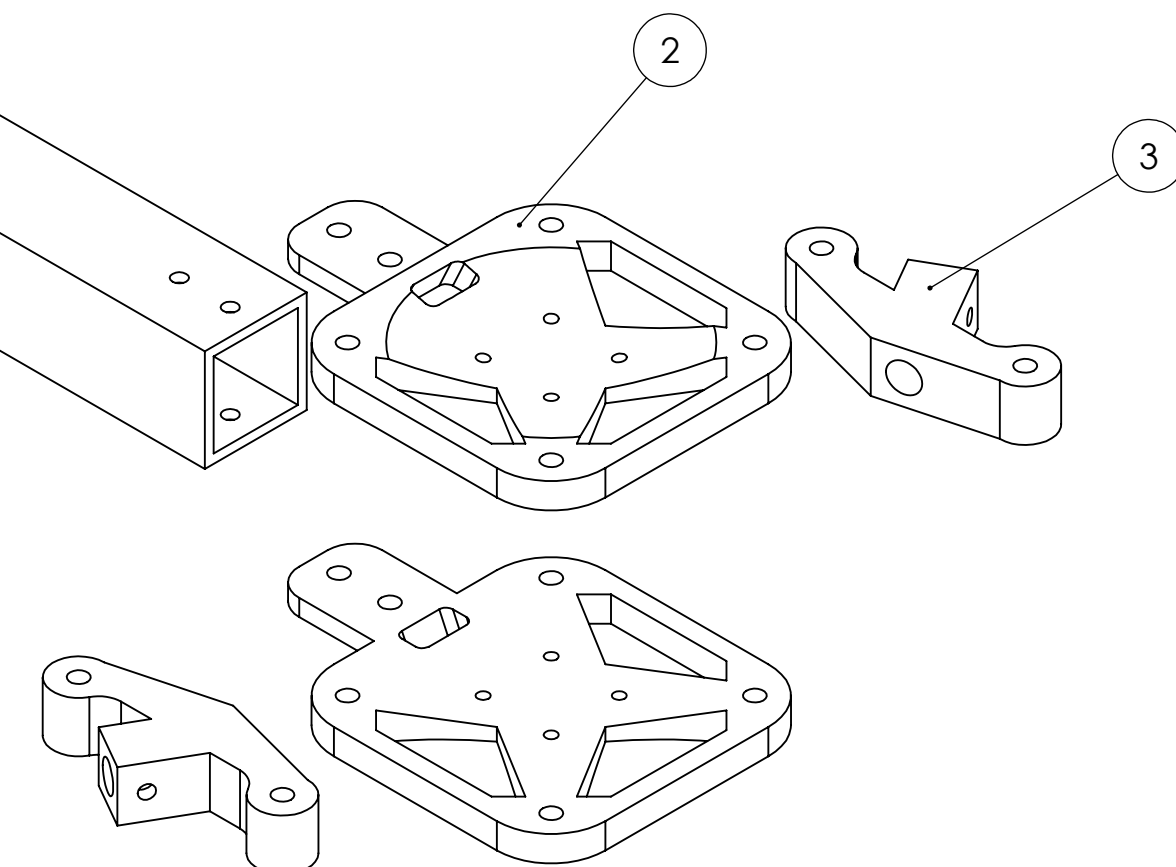
C

B

A



Item No.	Part ID	Description	Qty
1	AMB01	Arm Al Tube - 13"	1
2	AMP01	Motor Mount Plate	2
3	AMP02	Mount Plate Spacer	2



Creator Name: Sam Carhart	<b>Heavy Lift Drone</b>	Subassembly: Arm	Part ID: AA1
TOLERANCES: 0.X = $\pm 0.05$ 0.XX = $\pm 0.005$ 0.XXX = $\pm 0.0005$	Material: Mixed Assembly	Part Quantity: 6	Description: Arm Assembly

8 7 6 5 4 3 2 1

F

E

D

C

B

A

F

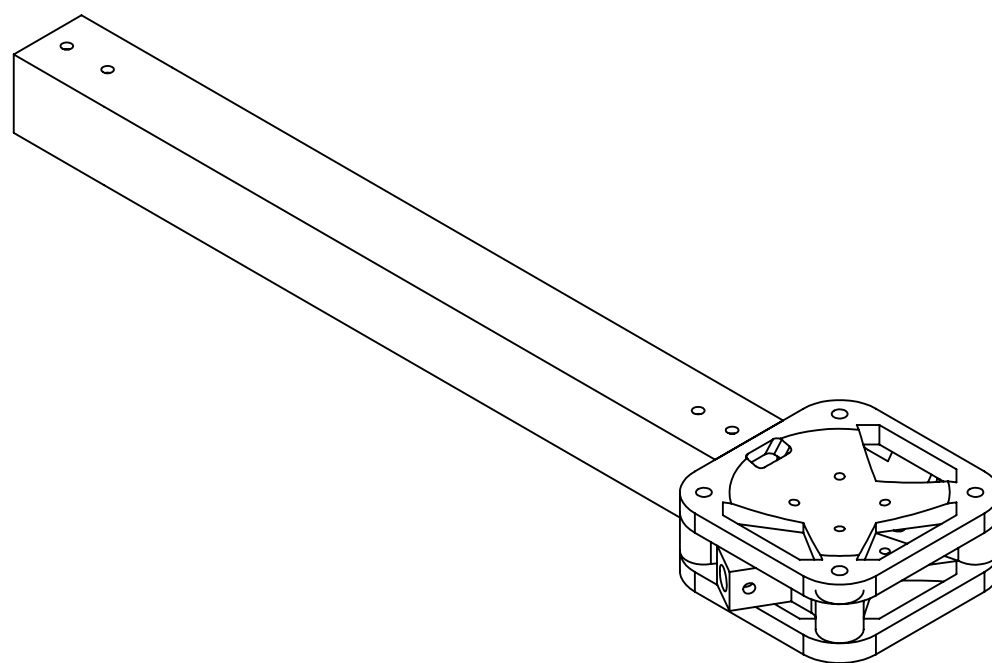
E

D

C

B

A



Creator Name: Sam Carhart	<b>Heavy Lift Drone</b>	Subassembly: Arm	Part ID: AA1
TOLERANCES: $0.X = \pm 0.05$ $0.XX = \pm 0.005$ $0.XXX = \pm 0.0005$	Material: Mixed Assembly	Part Quantity: 6	Description: Arm Assembly

SCALE:1:3

SHEET 2 OF 2

8 7 6 5 4 3 2 1

F

F

E

E

D

D

C

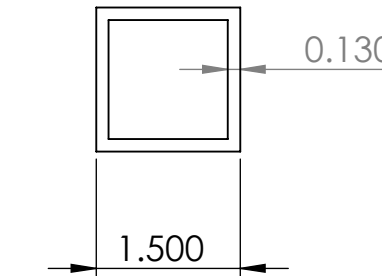
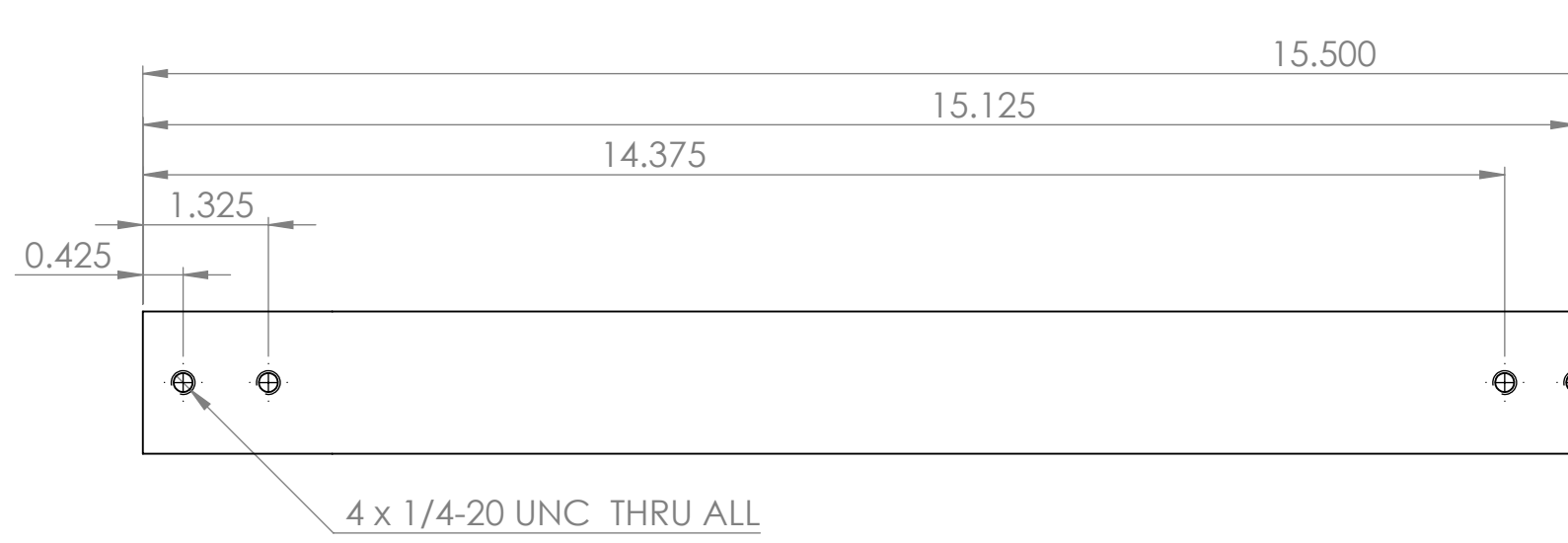
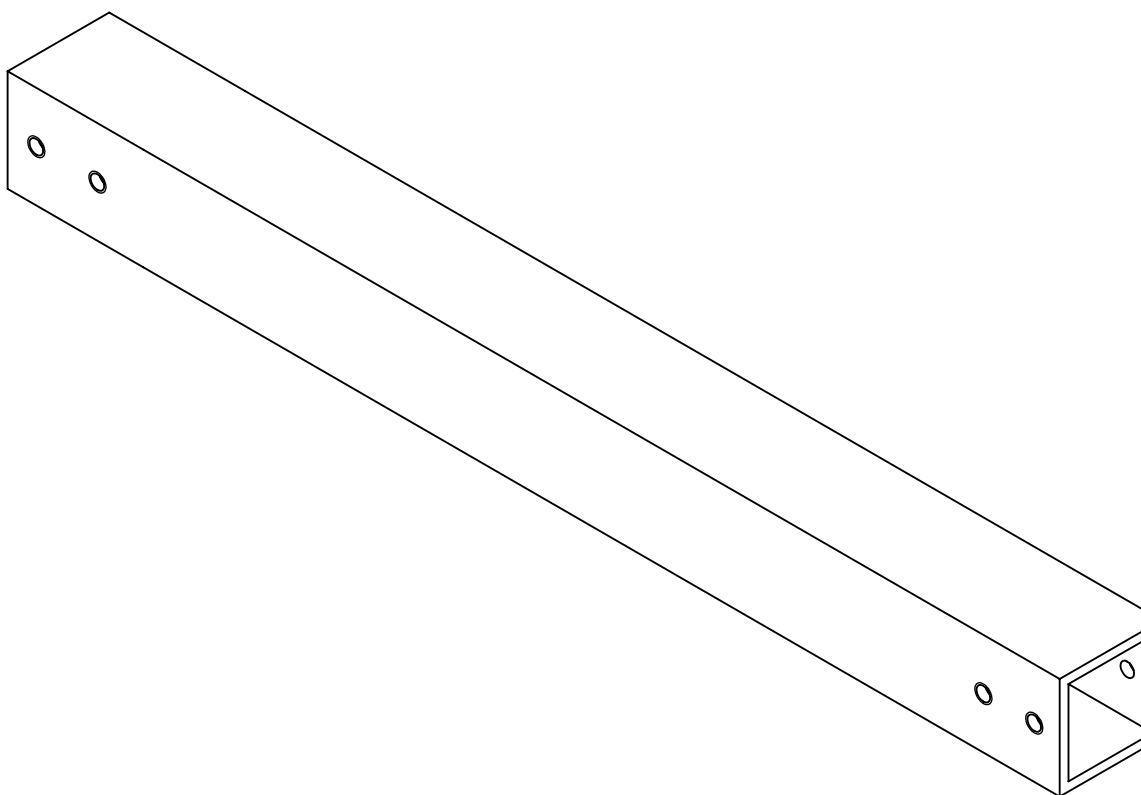
C

B

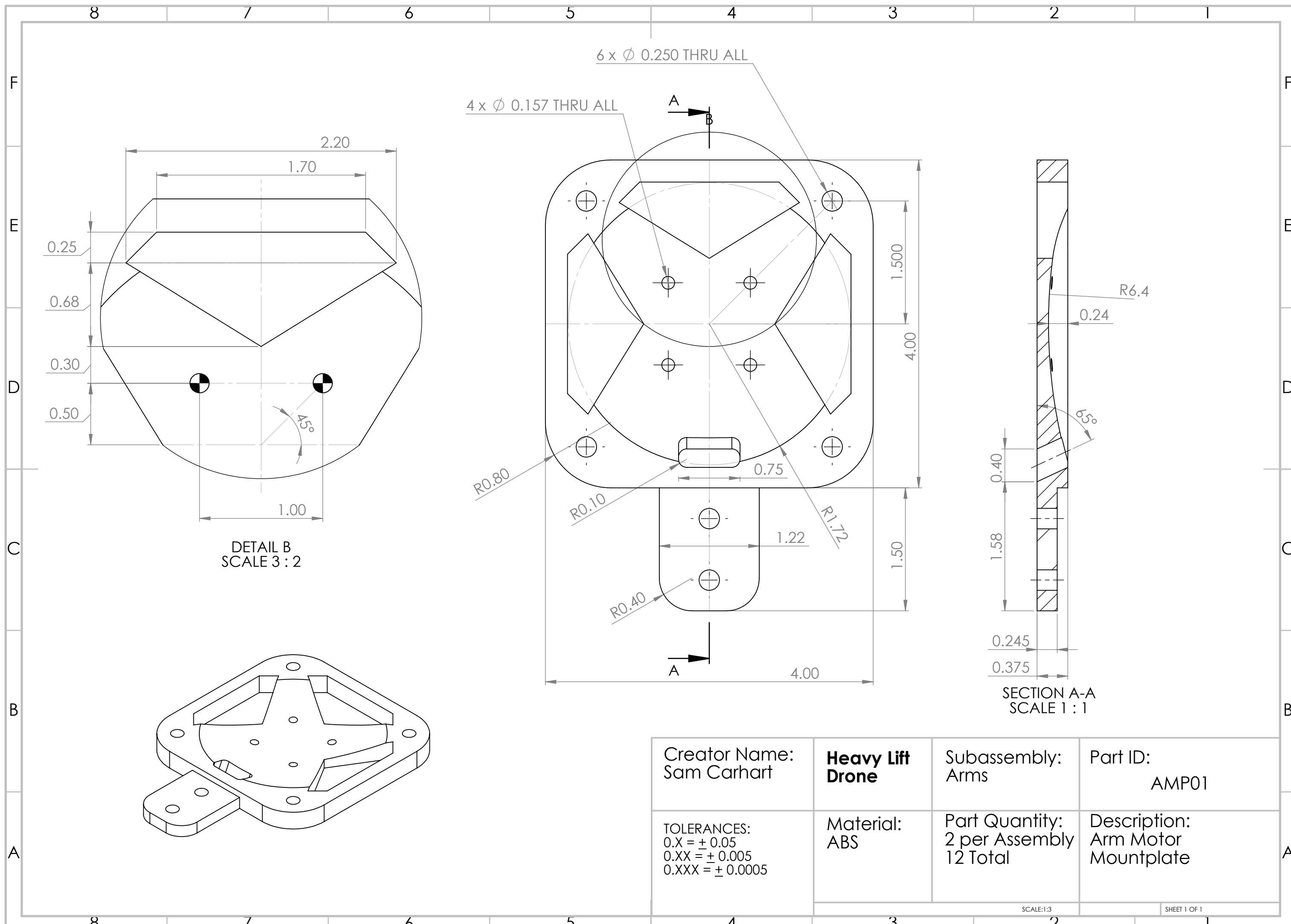
B

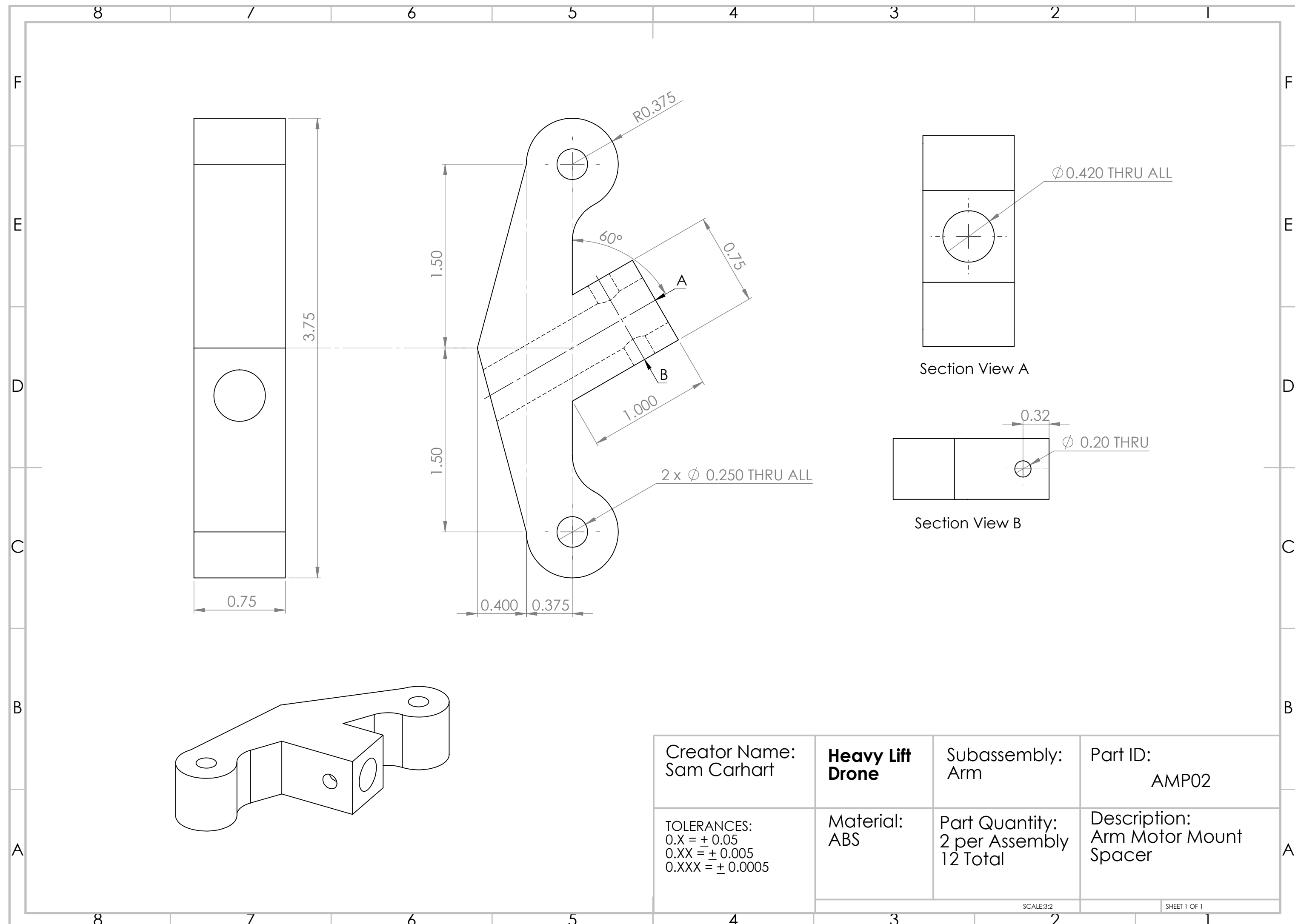
A

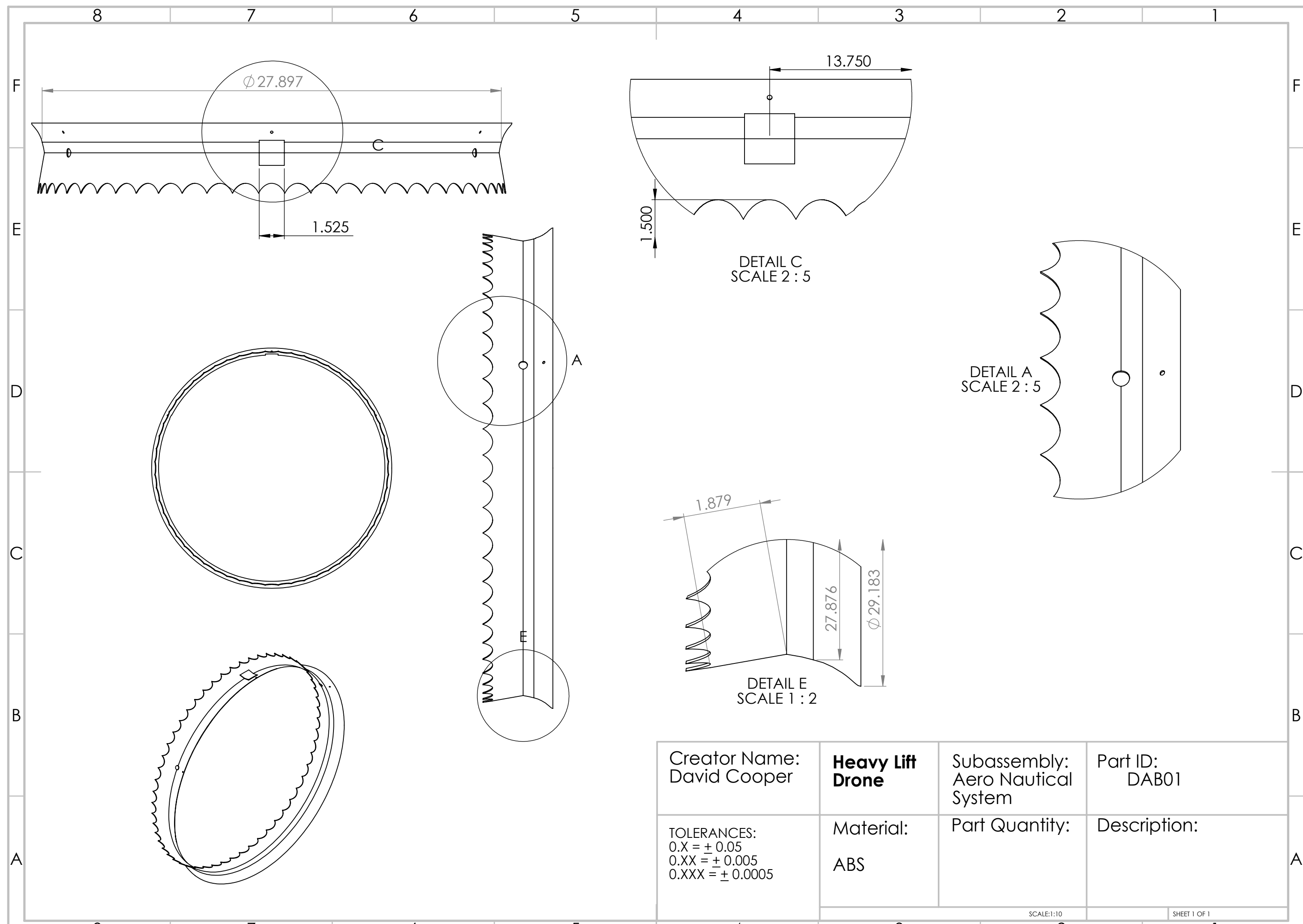
A



Creator Name: Sam Carhart	<b>Heavy Lift Drone</b>	Subassembly: Arms	Part ID: AMB01-V2
TOLERANCES: $0.X = \pm 0.05$ $0.XX = \pm 0.005$ $0.XXX = \pm 0.0005$	Material: 6063 Aluminum	Part Quantity: 1 per Assembly 6 Total	Description: Arm Al Tube - 13"







8

7

6

5

4

3

2

1

F

F

E

E

D

D

C

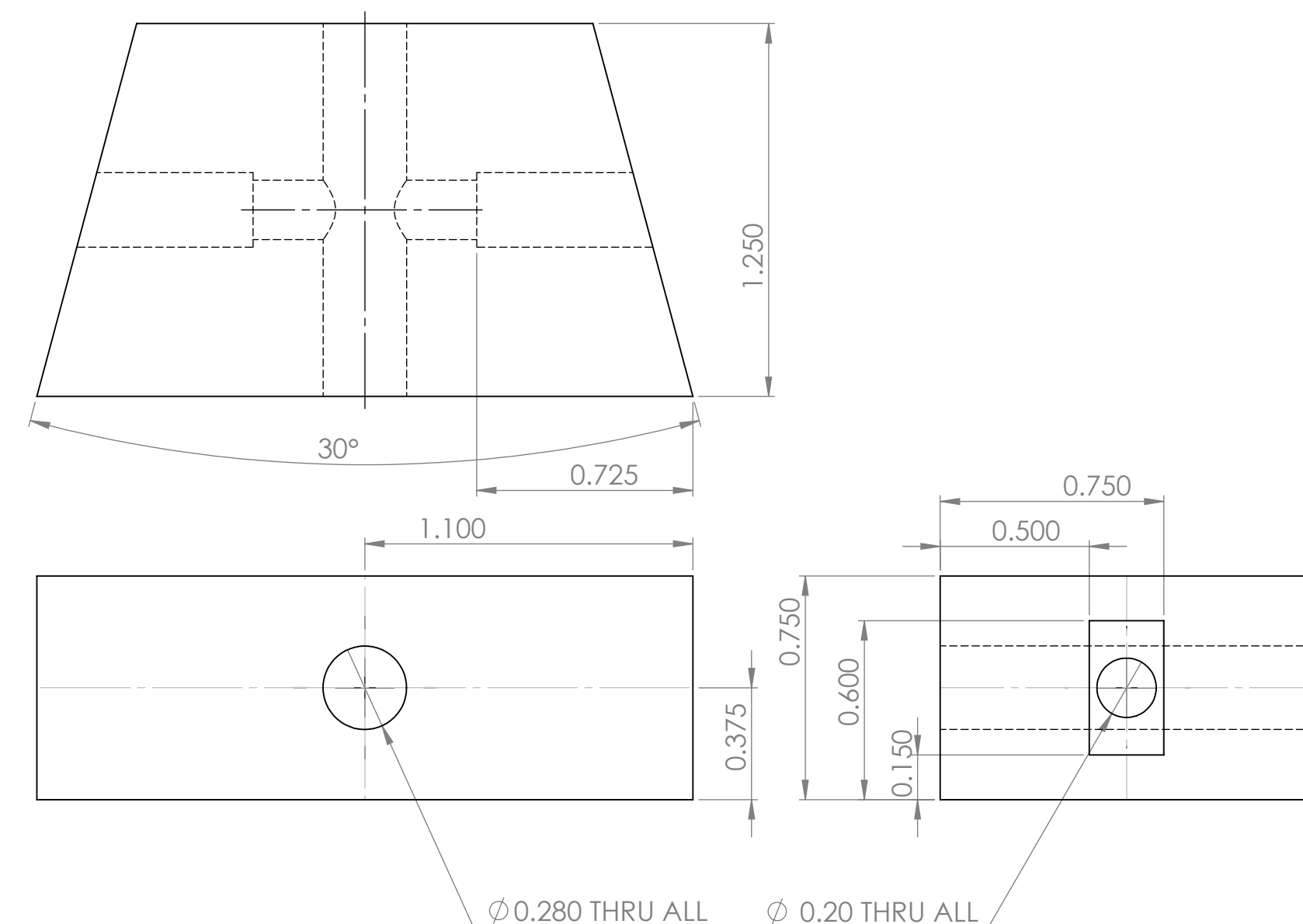
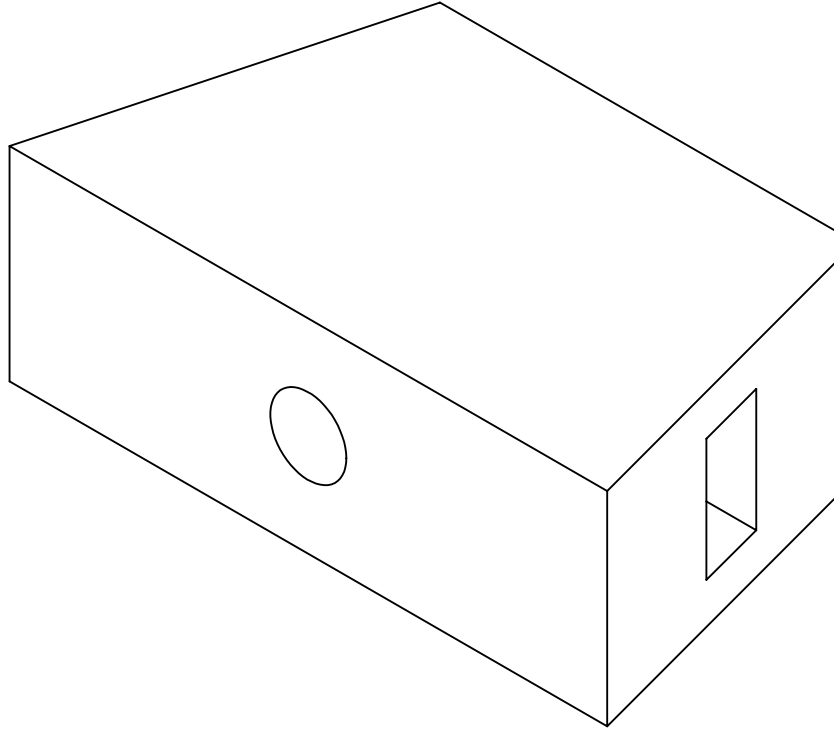
C

B

B

A

A



Creator Name:  
Sam Carhart

**Heavy Lift  
Drone**

Subassembly:  
Ducts

Part ID:  
DMP02

TOLERANCES:  
 $0.X = \pm 0.05$   
 $0.XX = \pm 0.005$   
 $0.XXX = \pm 0.0005$

Material:  
ABS

Part Quantity:  
1 per Assembly  
6 Total

Description:  
Duct Support Rod  
Fixture

SCALE:2:1

SHEET 1 OF 1

8 7 6 5 4 3 2 1

F

E

D

C

B

A

F

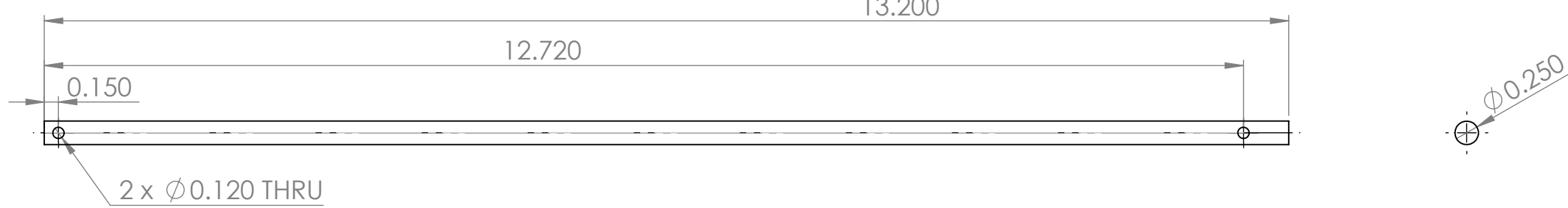
E

D

C

B

A



Creator Name: Sam Carhart	<b>Heavy Lift Drone</b>	Subassembly: Ducts	Part ID: DMB03
TOLERANCES: 0.X = $\pm$ 0.05 0.XX = $\pm$ 0.005 0.XXX = $\pm$ 0.0005	Material: 7075 Aluminum	Part Quantity: 1 per Assembly 6 Total	Description: Duct Support Rod

8

7

6

5

4

3

2

1

F

E

D

C

B

A

Item No.

Part ID

Description

Qty

1

DMB01-V2

Connector Outer Member

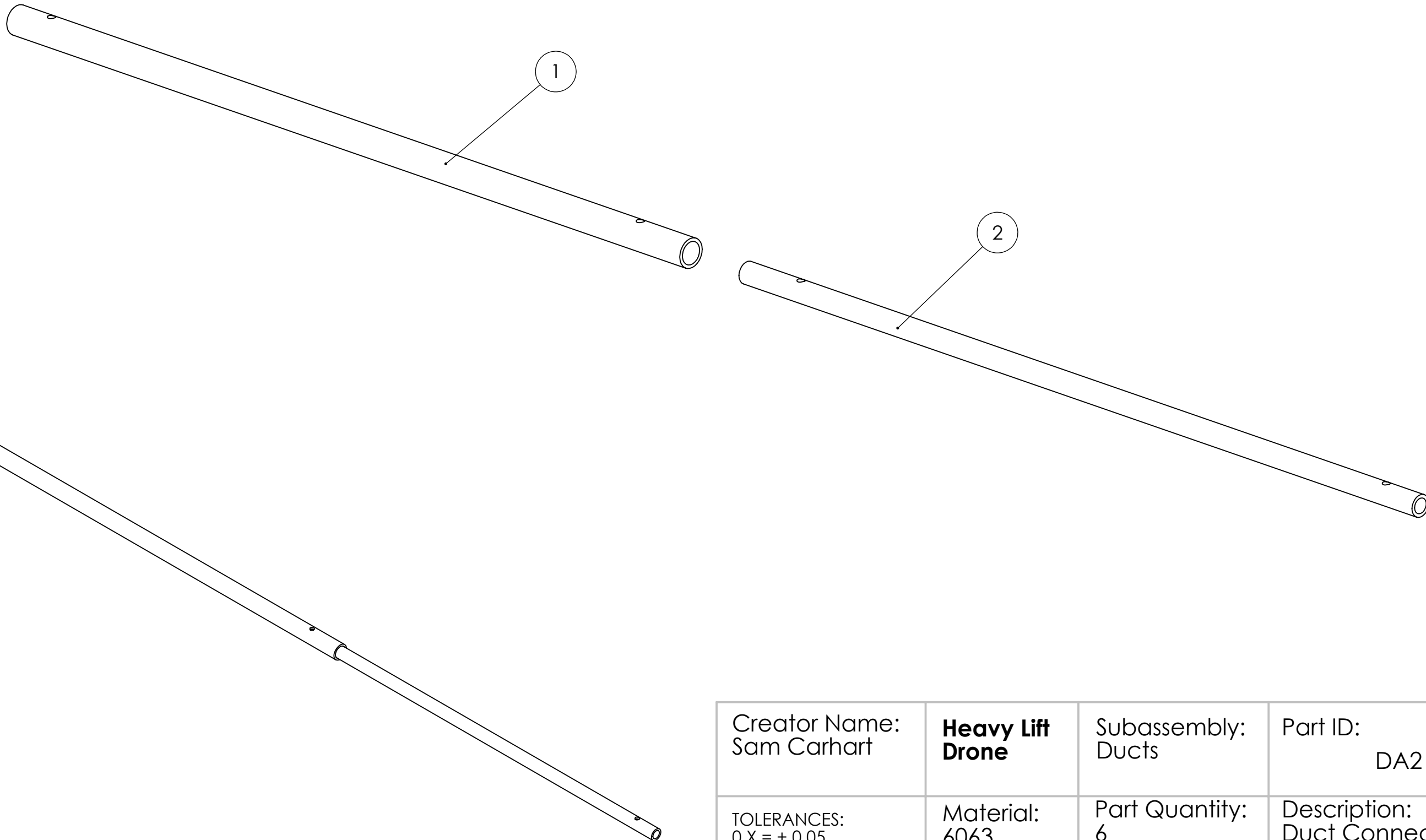
1

2

DMB02-V2

Connector Inner Member

1



Creator Name:  
Sam Carhart

**Heavy Lift  
Drone**

Subassembly:  
Ducts

Part ID:  
DA2

TOLERANCES:  
0.X =  $\pm 0.05$   
0.XX =  $\pm 0.005$   
0.XXX =  $\pm 0.0005$

Material:  
6063  
Aluminum

Part Quantity:  
6

Description:  
Duct Connector  
Assembly

SCALE:1:3

SHEET 1 OF 2

8 7 6 5 4 3 2 1

F

F

E

E

D

D

C

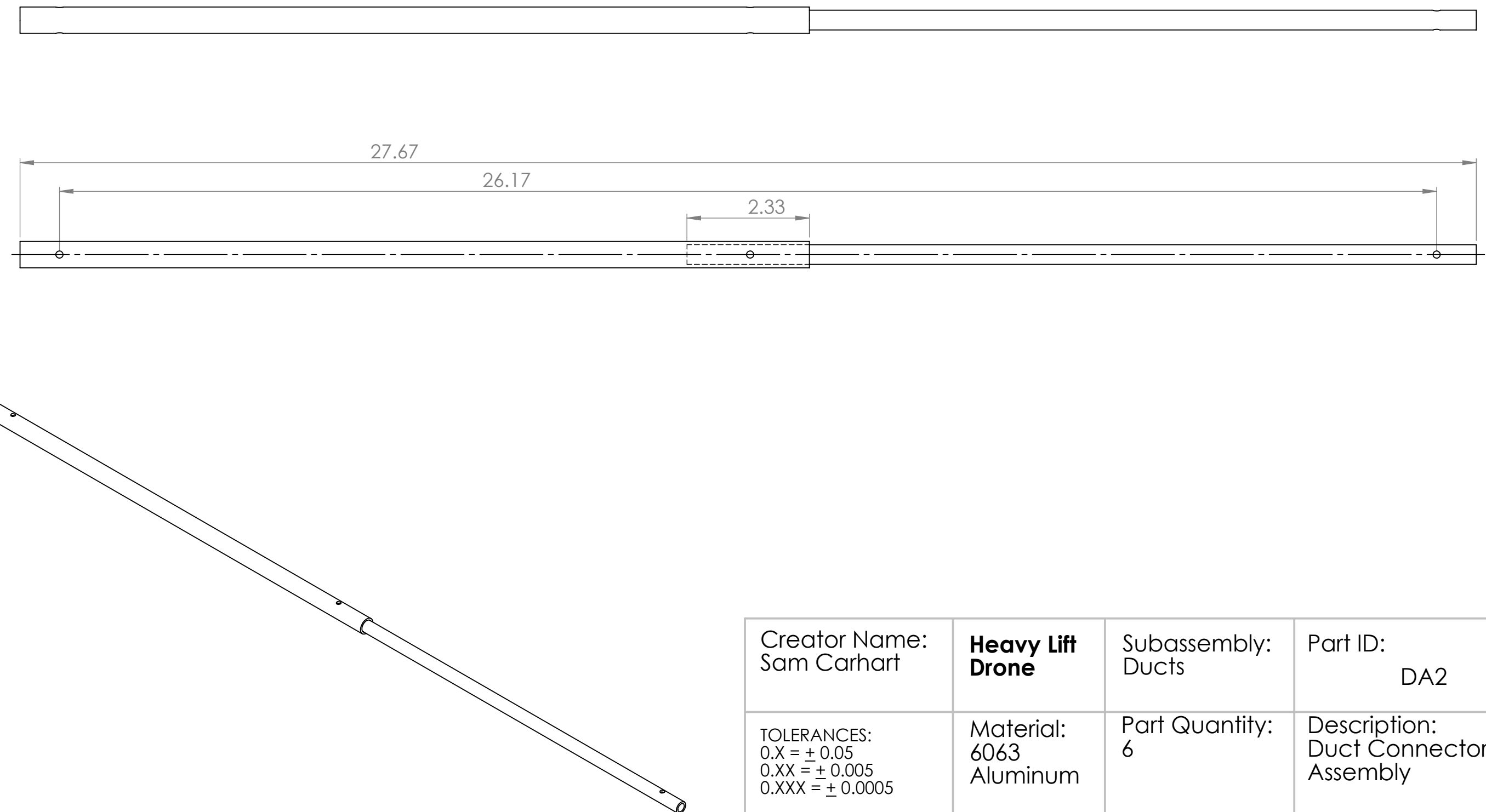
C

B

B

A

A



Creator Name:  
Sam Carhart

**Heavy Lift  
Drone**

Subassembly:  
Ducts

Part ID:  
DA2

TOLERANCES:  
0.X =  $\pm 0.05$   
0.XX =  $\pm 0.005$   
0.XXX =  $\pm 0.0005$

Material:  
6063  
Aluminum

Part Quantity:  
6

Description:  
Duct Connector  
Assembly

SCALE:1:3

SHEET 2 OF 2

8 7 6 5 4 3 2 1

F

E

D

C

B

A

F

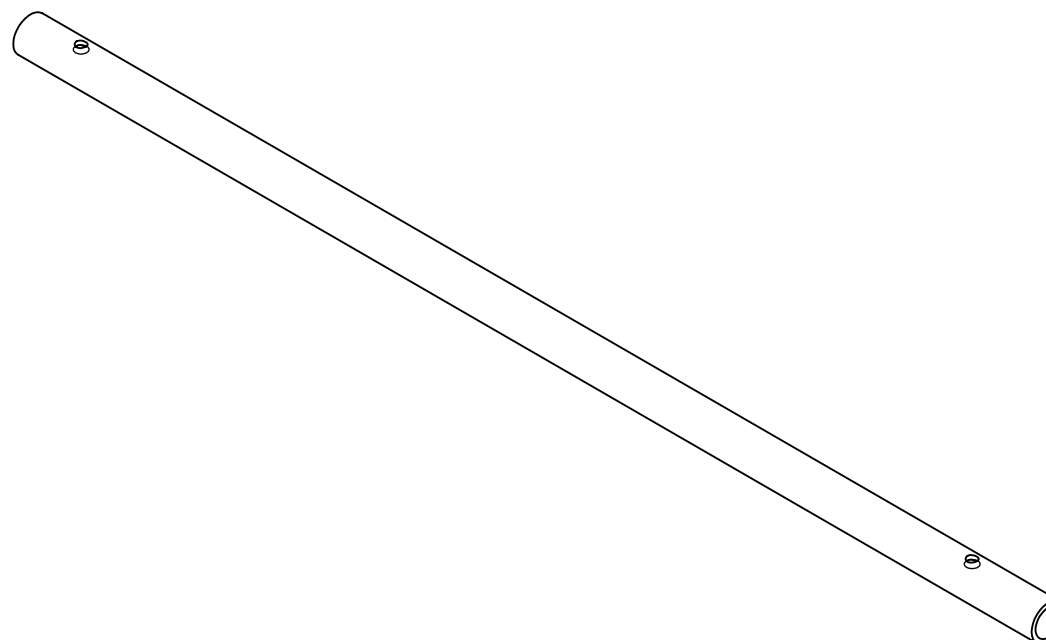
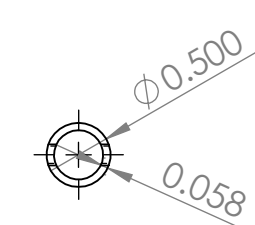
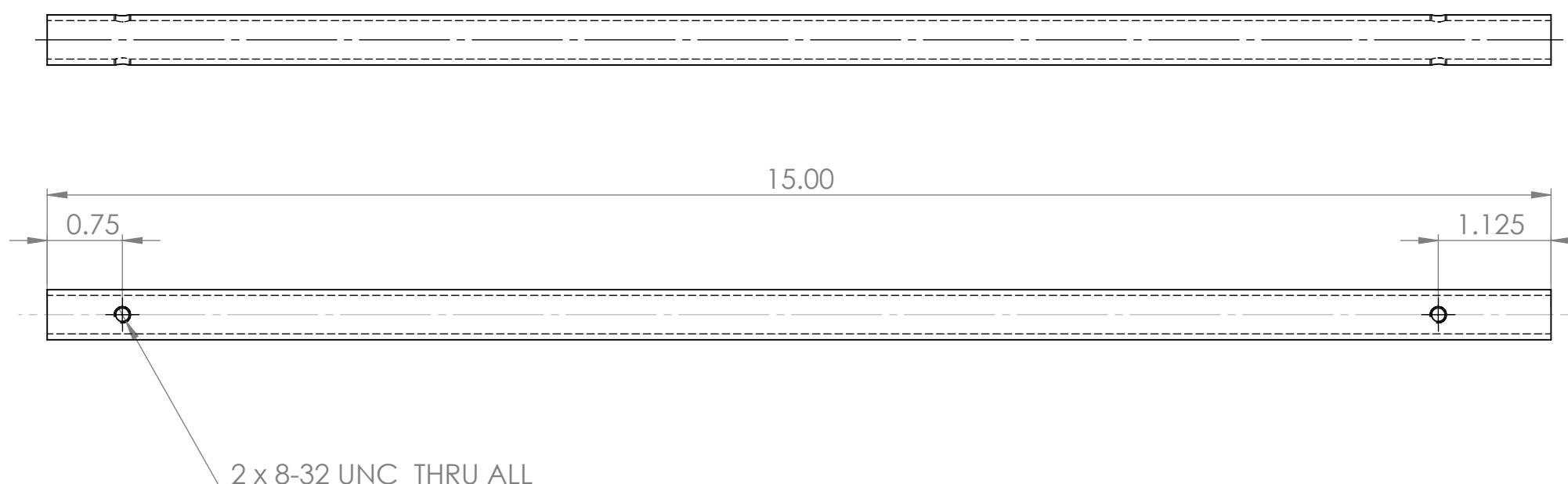
E

D

C

B

A



Creator Name: Sam Carhart	<b>Heavy Lift Drone</b>	Subassembly: Ducts	Part ID: DMB01-V2
TOLERANCES: $0.X = \pm 0.05$ $0.XX = \pm 0.005$ $0.XXX = \pm 0.0005$	Material: 6063 Aluminum	Part Quantity: 1 Per Assembly 6 Total	Description: Duct Connectors Outer Member

SCALE:1:3

SHEET 1 OF 1

8 7 6 5 4 3 2 1

F

E

D

C

B

A

F

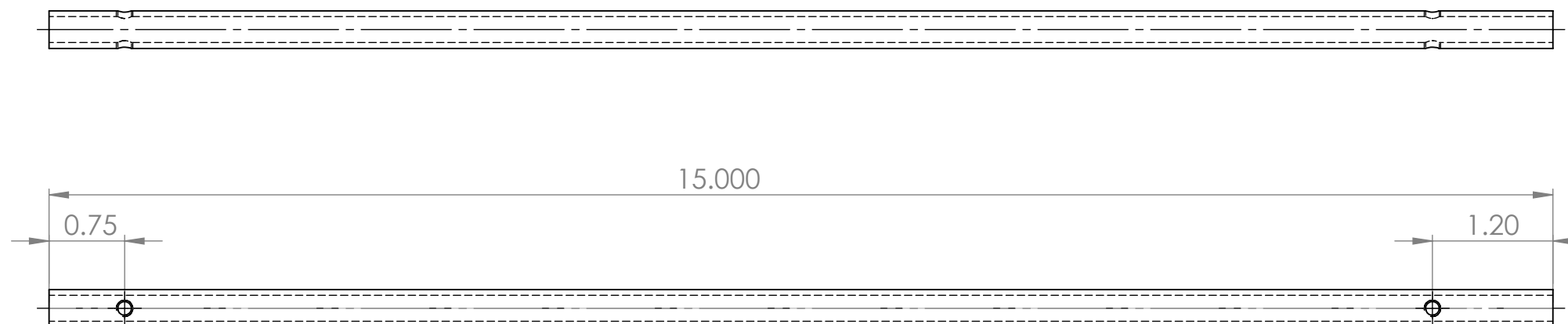
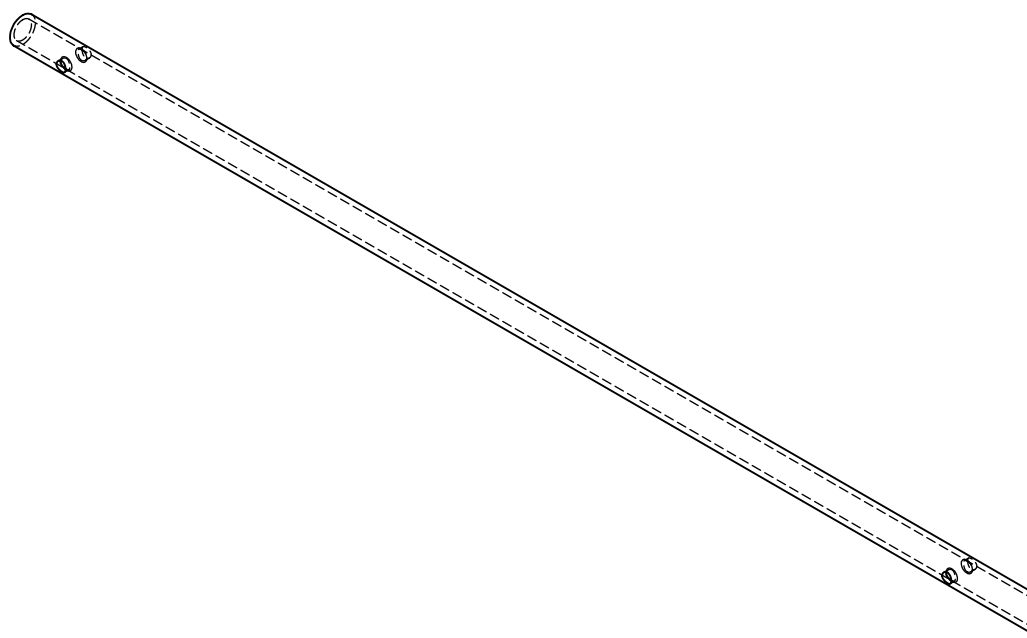
E

D

C

B

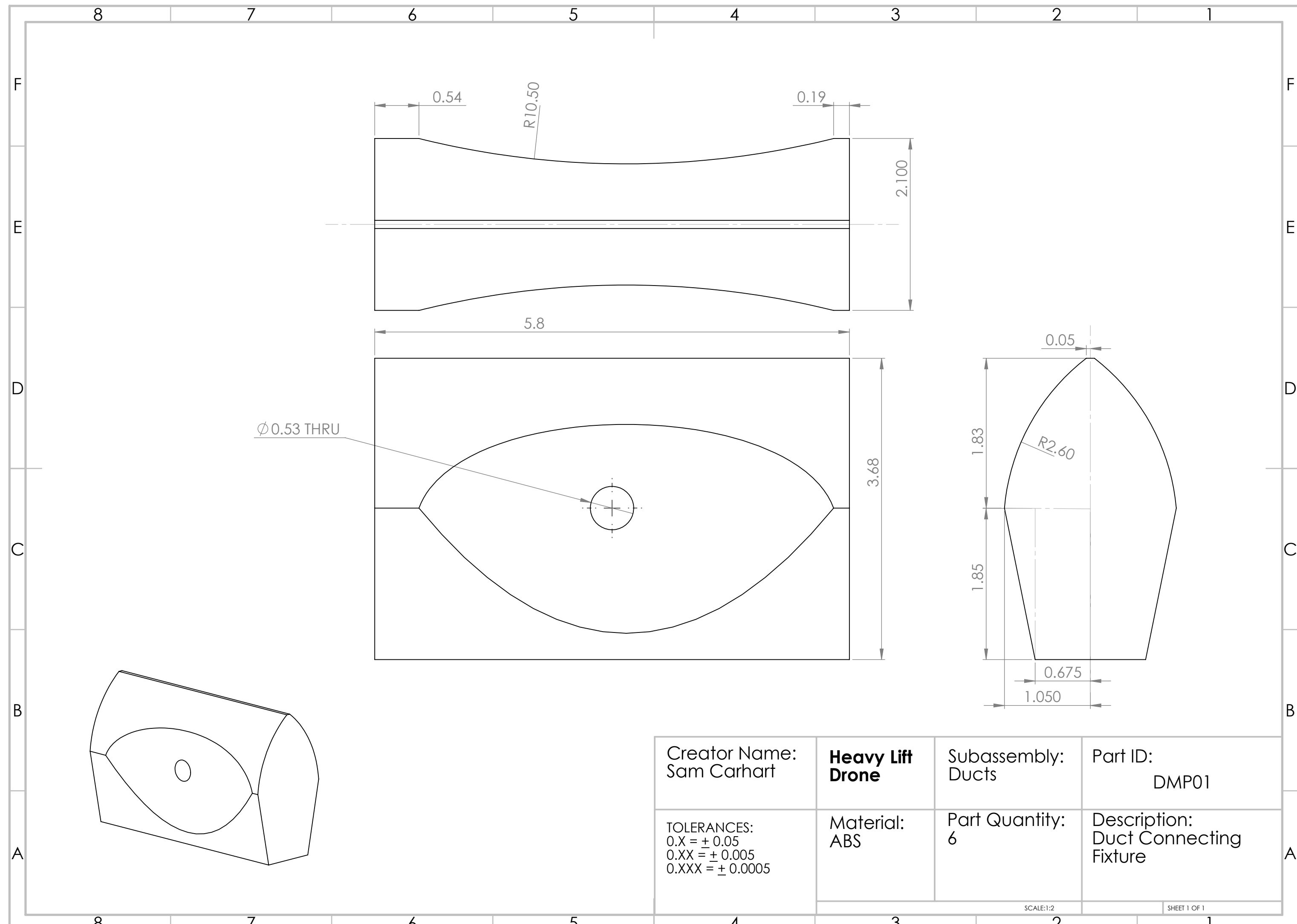
A



Creator Name: Sam Carhart	<b>Heavy Lift Drone</b>	Subassembly: Ducts	Part ID: DMB02-V2
TOLERANCES: $0.X = \pm 0.05$ $0.XX = \pm 0.005$ $0.XXX = \pm 0.0005$	Material: 6063 Aluminum	Part Quantity: 1 Per Assembly 6 Total	Description: Duct Connector Inner Member

SCALE:2:3

SHEET 1 OF 1



## D - Design Matrix Tables

The purpose of these tables were to outline the different scores each design would be given if the team pursued that option for a build. These tables appeared in graphical form in the main thesis to better illustrate the weights on scoring for each design.

**Table D.1 Scoring Matrix for Fabrication.** Colors indicate a “weight”. The darker the shade of green the more important a factor is, and thus gets multiplied by  $x1$ ,  $x2$  or  $x3$ . Higher Total  $\Rightarrow$  better performance. This table also adds the Physical Properties total to get an aggregate score for the entire design.

Rank (1-5)	Time to Fabricate	Ease of Assembly	Ease of Fabrication	Cost	Physical Total	Total (with weighting)
Design 1	1	3	4	2	27	51
Design 2	3	4	3	2	23	54
Design 3	3	4	4	3	31	66
Design 4	3	4	4	3	33	68
Design 5	4	5	4	3	35	76

**Table D.2 Scoring Matrix for Physical Properties.** Colors indicate a “weight”. The darker the shade of green the more important a factor is, and thus gets multiplied by x1, x2 or x3. Higher Total ⇒ better performance.

Rank (1-5)	Mass	Strength	Weather Resistant	Aero - dynamics	Electronics Housing	Physical Total (with weighting)
<b>Design 1</b>	1	3	4	3	4	27
<b>Design 2</b>	3	2	1	3	3	23
<b>Design 3</b>	3	3	2	4	3	31
<b>Design 4</b>	4	3	2	4	4	33
<b>Design 5</b>	3	4	2	5	5	35

## E - Material Testing Specimen Results

In these figures, the fractured state for several of the material tests are shown in order to exhibit the results and behavior of the specimen under tensile and bending conditions. The specimens were 3D printed from Carbon Fiber Filament at 20% volume infill as well as PETG filament at 20% and 50% volume infill.

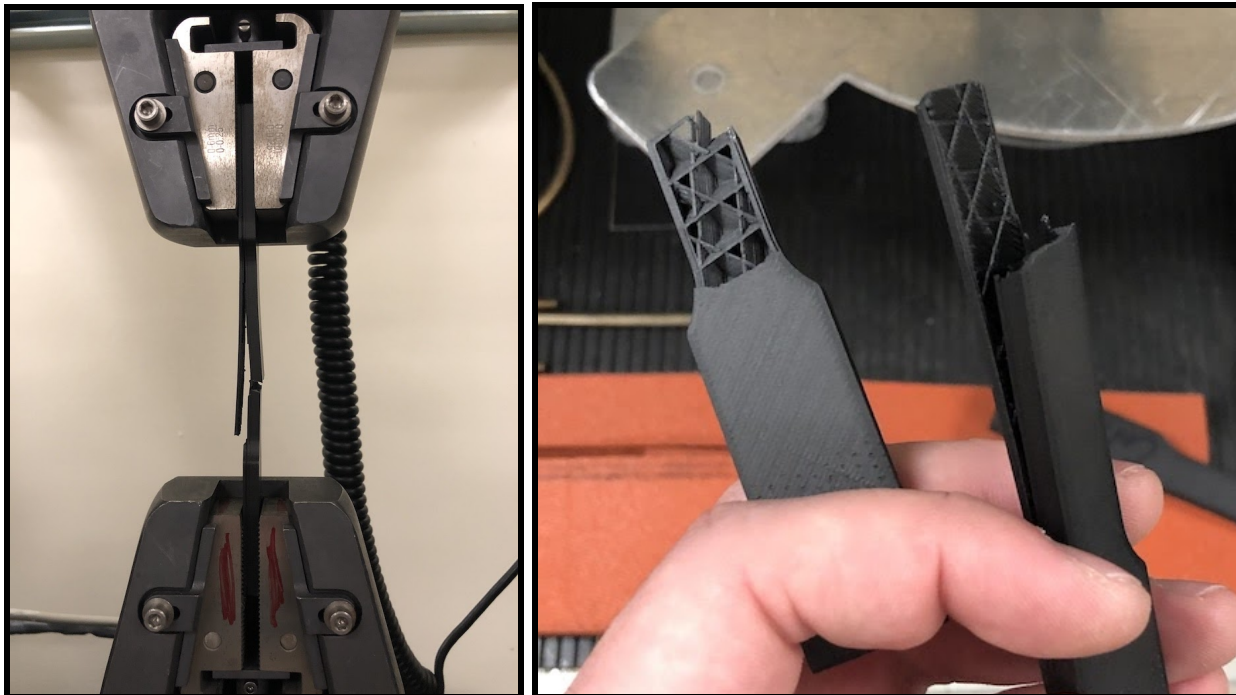


*Figure E1: Fracture State of specimen from Carbon Fiber filament with 20% infill.*



**Figure E2:** Fracture State of specimen from PETG filament with 20% infill.



**Figure E3:** Fracture State of specimen from PETG filament with 50% infill.

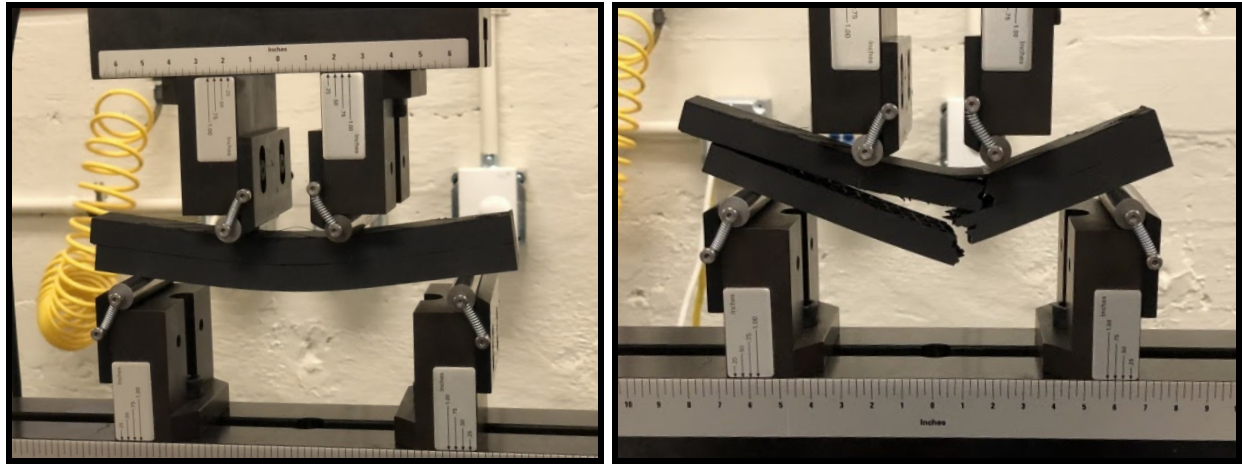


**Figure E4:** Bending failure state of specimen from Carbon Fiber filament with 20% infill.

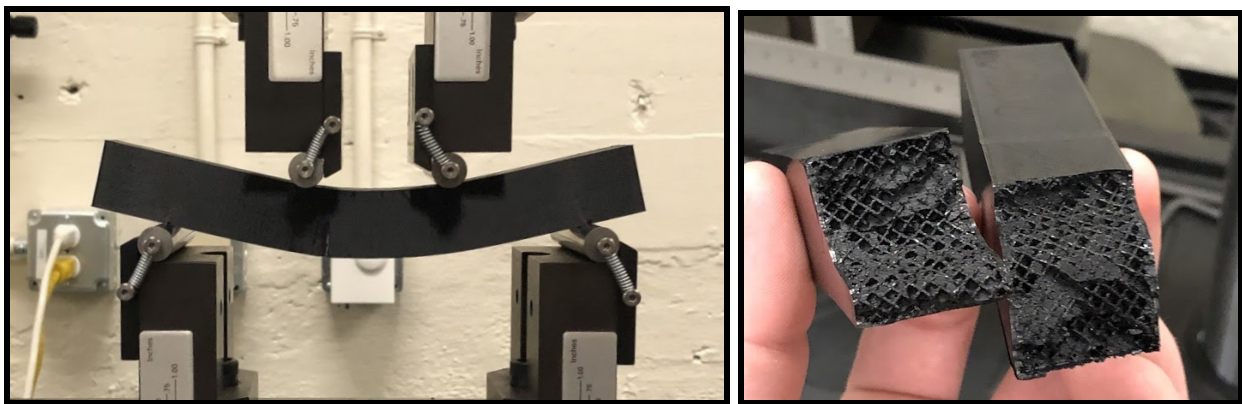


**Figure E5:** Bending failure state of specimen from PETG filament with 50% infill

## F - Additional Solidworks Simulations

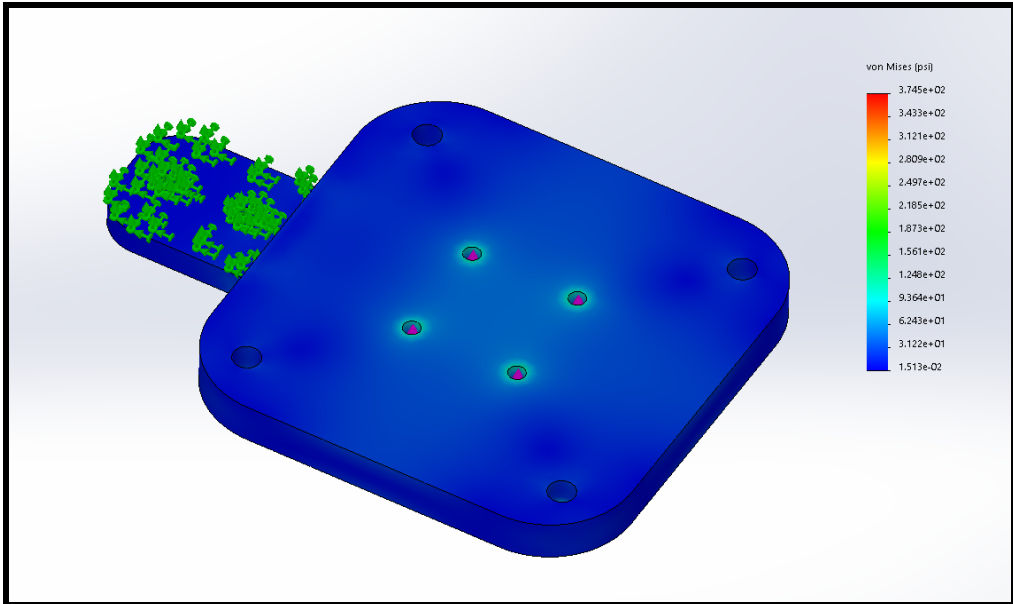


*Figure F1: Motor Mount design before weight optimization*

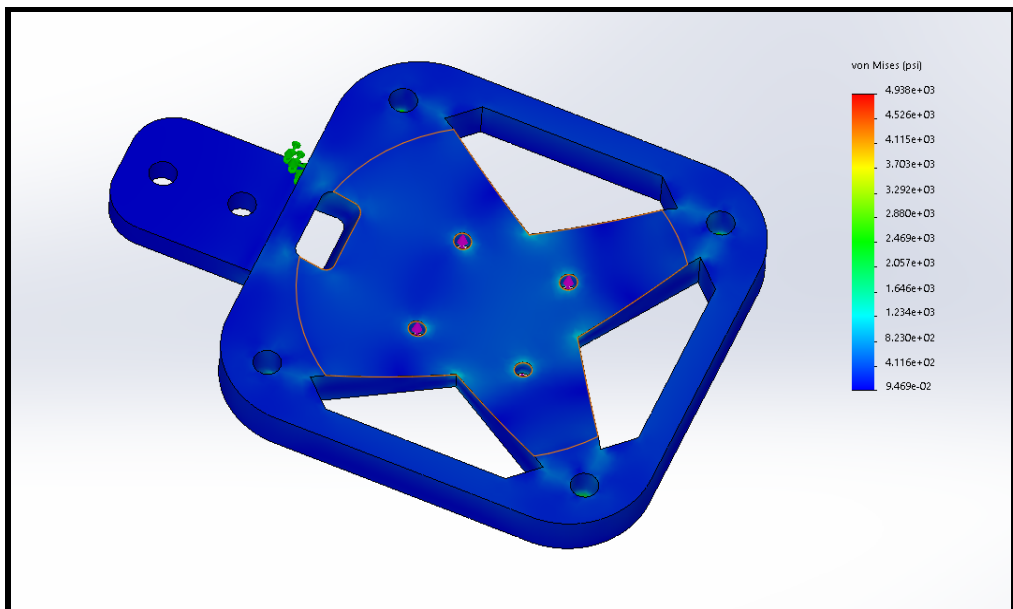


*Figure F2: Motor Mount design after optimization to reduce weight and improve airflow*

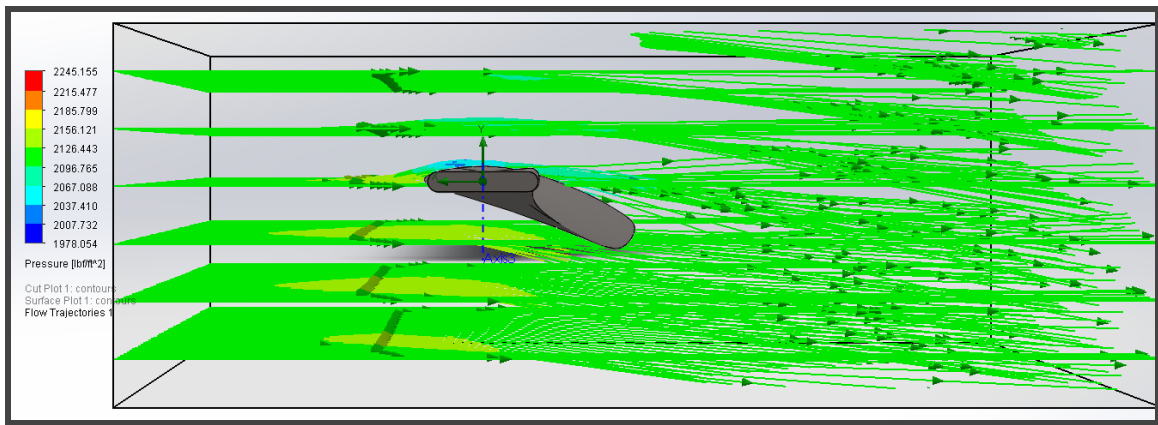


**Figure F3:** Wide View of half of the 26 inch propeller in an initial test where the cross flow of 283 ft/s

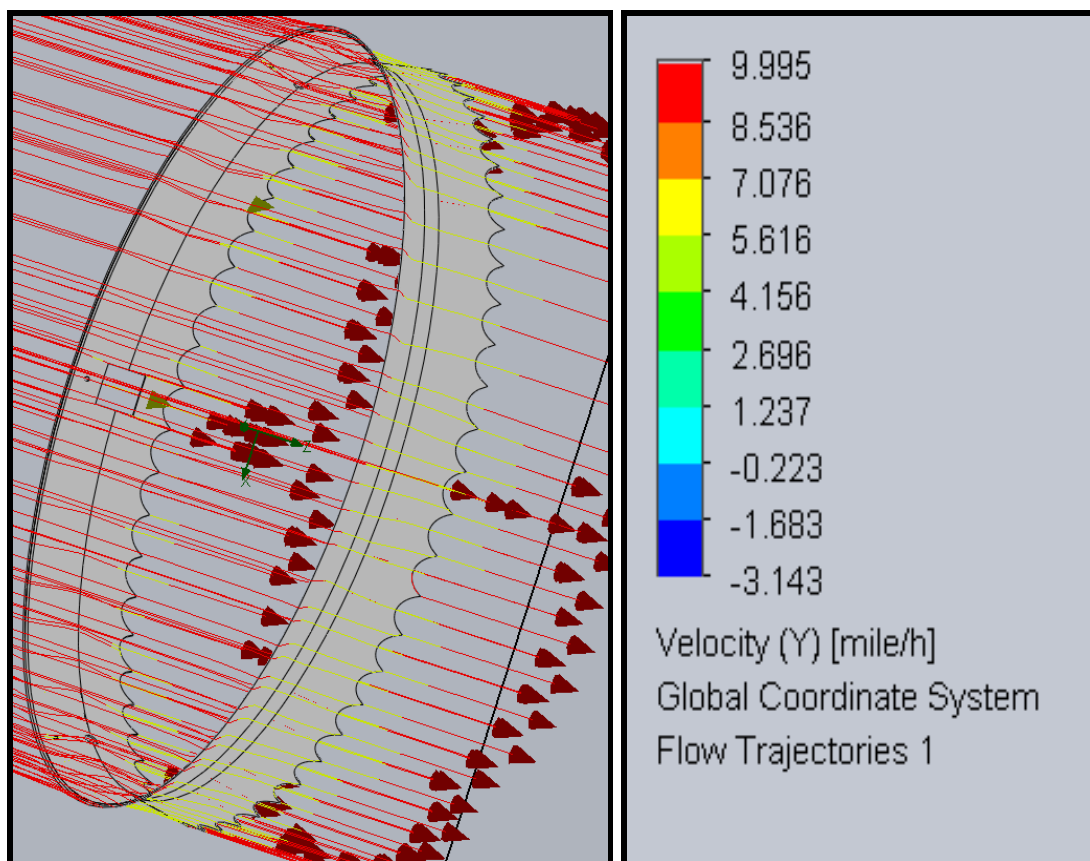


**Figure F5:** Simulated duct undergoing 10 mph of air flow

## G - Electrical

This section outlines the various designs that were implemented to create the electrical subsystem on the drone.

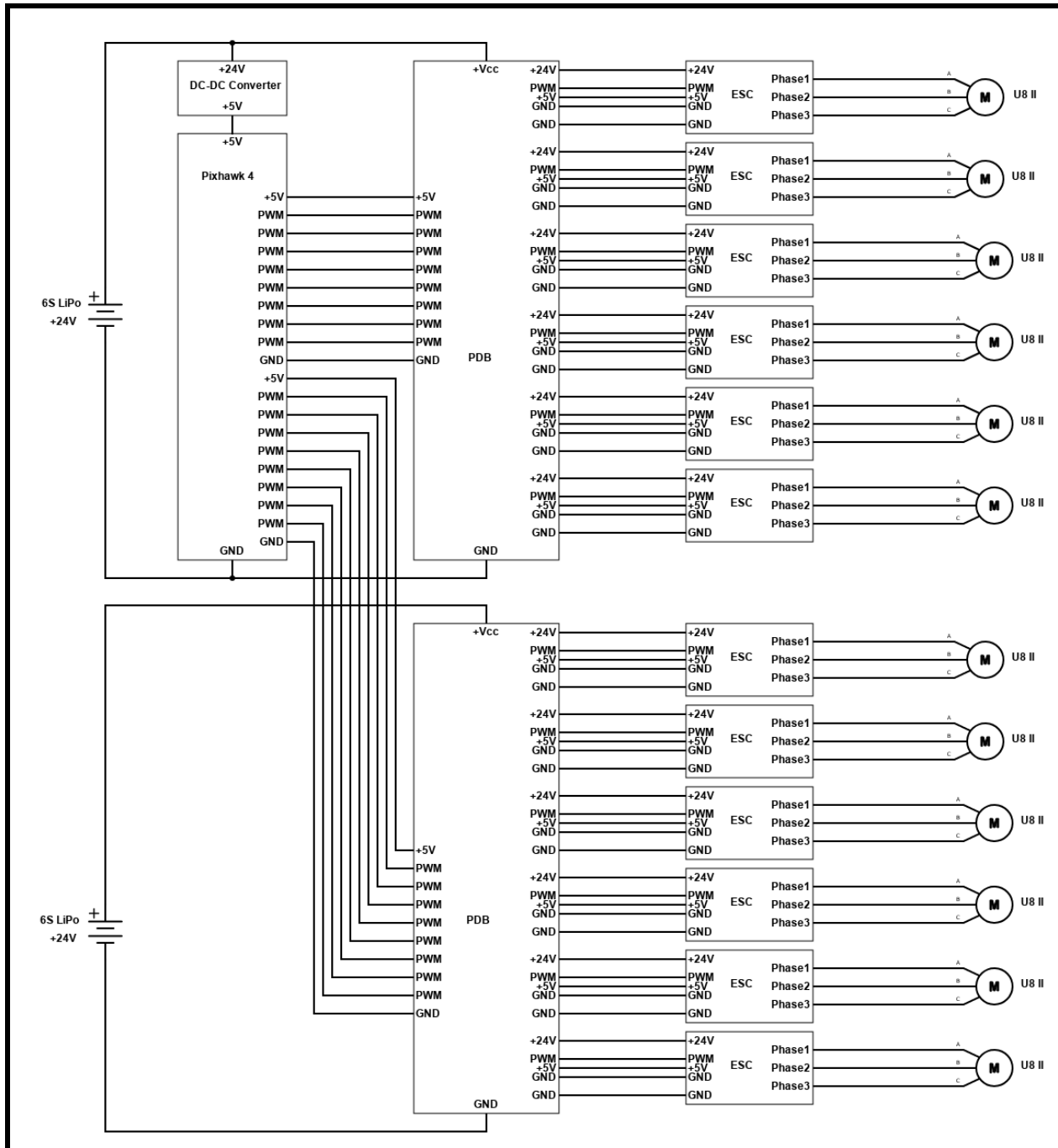


**Figure G1:** Propulsion substructure schematic.

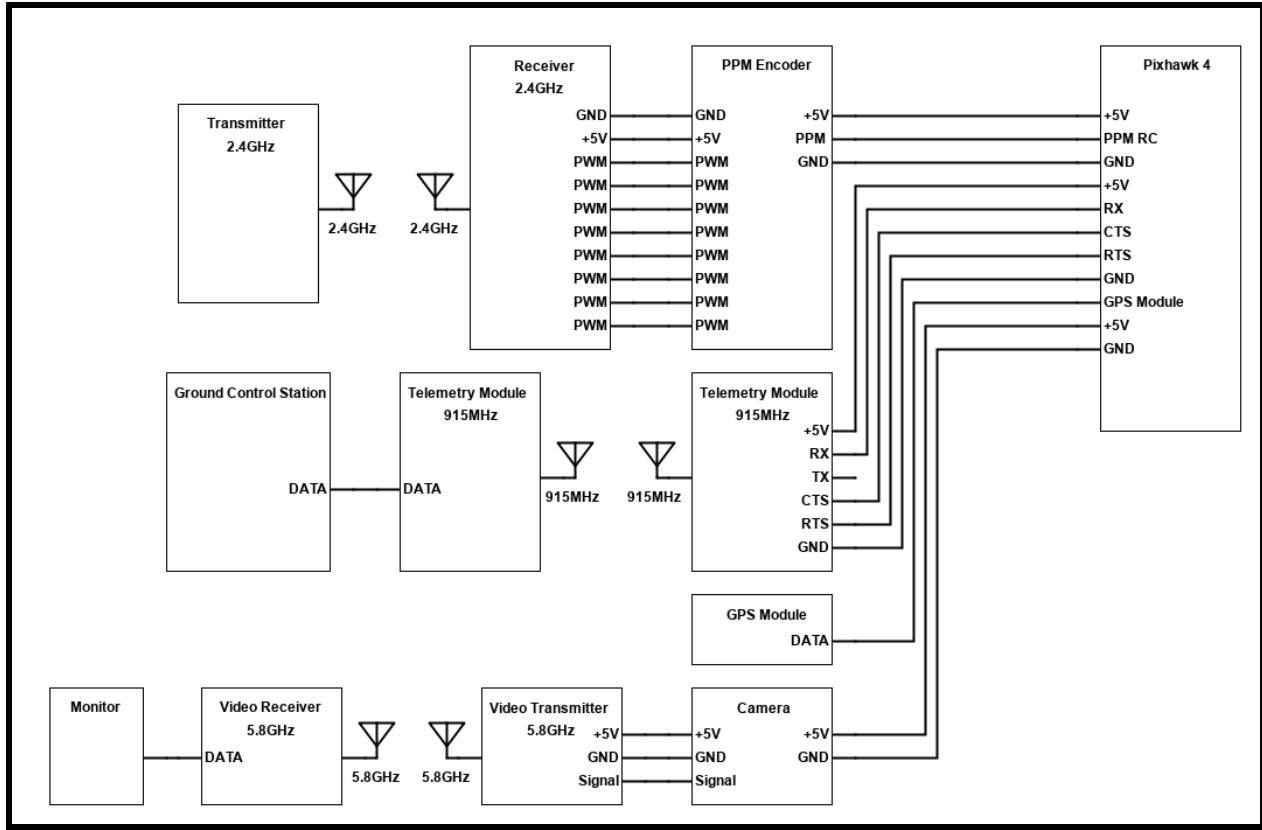


**Figure G2:** Communication and control substructure schematic.

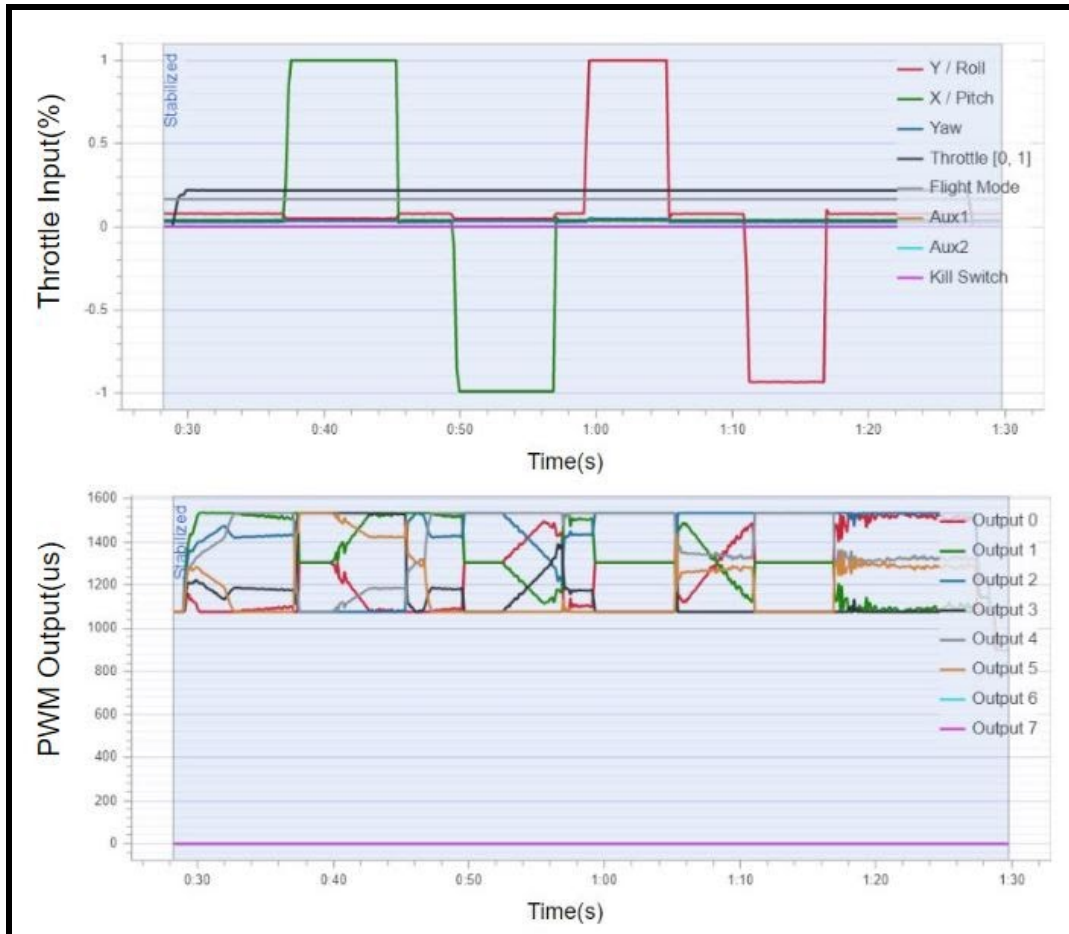


**Figure G3:** Hexacopter testing data

Item No.	Voltage (V)	Propeller	Throttle	Current (A)	Input power (W)	RPM	Torque (N·m)	Thrust (g)	Efficiency (g/W)	Operating Temperature
U8II KV190	6S (24V)	T-motor G28*9.2CF	40%	4.8	115.2	1632	0.54	1662	14.43	95°C (Ambient temperature : 27.3°C)
			42%	5.4	129.6	1709	0.58	1806	13.94	
			44%	6	144	1745	0.62	1951	13.55	
			46%	6.8	163.2	1828	0.68	2134	13.08	
			48%	7.2	172.8	1892	0.69	2254	13.04	
			50%	8.1	194.4	1953	0.75	2401	12.35	
			52%	8.9	213.6	2022	0.80	2566	12.01	
			54%	10	240	2093	0.87	2774	11.56	
			56%	10.5	252	2144	0.88	2892	11.48	
			58%	11.6	278.4	2210	0.94	3081	11.07	
			60%	12.4	297.6	2252	0.97	3208	10.78	
			62%	13.5	324	2312	1.03	3389	10.46	
			64%	14.1	338.4	2358	1.04	3502	10.35	
			66%	15	360	2394	1.08	3623	10.06	
			68%	15.8	379.2	2441	1.10	3801	10.02	
			70%	17	408	2497	1.16	3934	9.64	
			75%	19.6	470.4	2620	1.25	4376	9.30	
			80%	22.6	542.4	2776	1.36	4816	8.88	
			90%	29	696	2972	1.56	5563	7.99	
			100%	38.7	928.8	3248	1.88	6761	7.28	

**Figure G4:** T-Motor U8 II motor data (Image from tmotor.com).

**Table G1.** Propulsion substructure requirements outline.

Part	Specs Needed	Actual	Distributor
Motor	24V max	22.2V nominal, 24V max	T-Motor
ESC	43.7A peak current	60A continuous current	T-Motor
PDB	262.2A maximum current	480A maximum current	T-Motor
Battery	20 - 30 minutes flight time	30 minutes	Tattu

**Table G2.** Semi-autonomous component requirements.

Part	Specs Needed	Actual	Distributor
Transmitter	Send signal, 5CH minimum	2.4GHz, 10CH	Flysky
Receiver	Receive signal, 5CH minimum	2.4GHz with PPM encoder, 6CH	Flysky

**Table G3.** Autonomous component requirements.

Part	Specs Needed	Actual	Distributor
Flight Controller	Control 12 motors	6 motors controlled successfully	Holybro
	Support of peripherals	Multiple peripherals supported	
Telemetry Module	Send/Receive signal	915MHz	Holybro

## H - Software

This section lists codes that are not archived in SVN within the RSL.

```
673
674
675 metaData = new CameraMetaData(
676     tr("FLIR Duo R"),
677     160,           // sensorWidth
678     120,           // sensorHeight
679     1920,          // imageWidth
680     1080,          // imageHeight
681     1.9,           // focalLength
682     true,          // true: landscape orientation
683     true,          // true: camera is fixed orientation
684     0,              // minimum trigger interval
685     this);         // parent
686
687 _cameraList.append(QVariant::fromValue(metaData));
```

*Figure H1: FLIR Duo R configuration for QGroundControl in  
qgroundcontrol/src/FirmwarePlugin/FirmwarePlugin.cc*